DEVELOPMENT OF PRECAST, PRESTRESSED CONCRETE PAVEMENT TECHNOLOGY

By

NASSER M ALWEHAIDAH

Bachelor of Architectural Engineering
Oklahoma State University
Stillwater, Oklahoma
2002

Master of Architecture Engineering
Oklahoma State University
Stillwater, Oklahoma
2006

Submitted to the Faculty of the
Graduate College of the
Oklahoma State University
in partial fulfillment of
the requirements for
the Degree of
DOCTOR OF PHILOSOPHY
December, 2013

DEVELOPMENT OF PRECAST, PRESTRESSED

CONCRETE PAVEMENT

TECHNOLOGY

Dissertation Approved:

Dr. Bruce W. Russell

Dissertation Adviser

Dr. Stephen Cross

Dr. Tyler Ley

Dr. Keith Good

ACKNOWLEDGEMENTS

I would like to thank my advisor, Dr. Bruce W. Russell, for his support, inspiration, and patience during my PhD studies at Oklahoma State University. I will always be thankful to Dr. Russell for offering me this opportunity to achieve this goal and for helping me through my academic and professional careers. I would also like to express my gratitude to Dr. Stephen Cross, Dr. Keith Good, and Dr. Tyler Ley for being on my committee and for their guidance and advice.

I would like to thank the Federal Highway Administration (FHWA) for funding this research. Additionally, I would thank W&W Steel of Oklahoma City for donating the steel frame used in this testing. I would also like to thank Oklahoma State University student and personnel who assisted me during my work on this project.

I would like to thank my wife, Anwar, and my son, Bader, for their love and patience throughout my studies. I would like to thank my wonderful sisters for always being there to support my choices and decision. I would like to thank my brothers for their support and for being my best friends. Most importantly, I would like thank my father for his guidance, selflessness, and love throughout the years.

Name: NASSER M ALWEHAIDAH

Date of Degree: DECEMBER, 2013

Title of Study: DEVELOPMENT OF PRECAST, PRESTRESSED CONCRETE PAVEMENT TECHNOLOGY

Major Field: CIVIL ENGINEERING

Abstract:
Precast prestressed concrete pavement (PPCP) can provide many advantages over other pavement alternatives whether asphalt or concrete. The possible advantages are thinner pavement, faster construction, increased durability, better quality concrete, efficient use of materials, better economy by repetition, and large reductions in user costs. However, there are some disadvantages associated with precast post-tensioned concrete pavement construction including the need for more specialized and currently non-standard construction equipment, a sometimes overall decrease in ride quality, higher costs for small projects, relatively complex construction when compared to traditional rigid and flexible pavement, and different or undefined standard design procedure. Even so two of the primary benefits, reduced user costs through more rapid construction and thinner pavement, are particularly compelling in rehabilitation of urban pavements and increasing the clearance for bridges underpasses.

The general objectives of this research are to (1) investigate and analyze the current state-of-the-art, (2) examine and possibly improve the current design features, (3) perform structural analysis to evaluate pavement performance and limitations, (4) conduct laboratory tests to examine and verify proposed improvements and analysis results, (5) investigate means to make precast pavement more durable and economical.

The general objectives of this research will be achieved by using design innovations such as granular base material to reduce the overall thickness and panels with grout voids on the bottom to achieve maximum contact with the granular base. Experimental research will investigate precast prestressed concrete pavement response to static loads. Analytical research work will investigate pavement response to the effects of non-uniform subgrade support conditions and dynamic loadings. From work on dynamic loadings it is expected to develop ideas for minimum pavement thicknesses and the influence of subgrade reaction on dynamic response.

TABLE OF CONTENTS

LIST OF TABLES

LIST OF FIGURES

.

CHAPTER I

INTRODUCTION

The growing amount of traffic and the deteriorating condition of our nation's infrastructure requires new, efficient and durable methods for repairing and constructing highway pavements. Most pavements in service today were not designed to handle the current traffic counts nor the magnitude and frequency of relatively heavy loads. Traditional cast-in-place concrete pavement construction causes delays due to the time required for removal of existing pavement, rehabilitation of the base and sub-base materials for establishing grades and other preparations for casting concrete onsite, and for concrete to reach prescribed maturity or specified strength. Conversely, precast prestressed concrete pavement (PPCP) panels can require minimal site preparation and little on-site construction time. As a consequence, there can be far less disruption to the highway users, the cars and trucks that travel our highways. By using precast concrete pavement, pavement surfaces can be used intermittently as construction is staged, and in general, the roads can be opened to traffic with fewer construction delays. Further, construction with precast concrete panels can be staged where traffic ways remain open during peak periods and construction can be done intermittently during low traffic periods like nights and weekends. For these reasons, precast post-tensioned concrete pavement can be used for the construction of new pavements or rehabilitation of older pavements in high traffic areas, for bridge underpasses to increase overhead clearance, and for existing pavement repairs.

Based on an Average Daily Traffic (ADT) of 105,000 vehicles and five miles of pavement, the Users' Costs for conventional cast-in-situ concrete pavement was estimated to be $13,612,200 compared to $6,598,500 when using precast pavement systems were used (Merritt et al. 2001). Users' Costs are the costs incurred by drivers due to delays, detours, and traffic congestions caused by road construction. Precast concrete has proven to be an excellent choice for fast and durable construction in the building industry. Similarly, precast concrete pavement test projects have been successfully implemented as well. Precast pavement panels require no setting time and therefore roads can be opened to traffic immediately.

One previous research project conducted by the Joint Transportation Research Program evaluated the feasibility of using precast concrete pavement construction of pavements by the Indiana Department of Transportation. The research investigated the state-of-the-art of methods used in precast concrete pavement methods as well as conventional cast in place (CIP) concrete pavement methods. Precast concrete pavement provided many advantages such as more rapid construction, more durable pavement, more efficient use of materials, maximizing economy by repetition, and improved quality achieved by mixing concrete in a controlled environment. However, there are also some disadvantages associated with using PPCP including higher initial costs, the need for specific construction equipment, lower ride quality, more complex construction procedures.

1.1 RESEARCH OBJECTIVES

The overall objective of this research is to improve and refine precast prestressed concrete pavement technology. The specific objectives for this research are the following:

- Review and analyze the current state-of-the-art. Review the various design methods and procedures as well as the development of precast pavement construction from the earliest projects to the latest.
- Propose new precast pavement design features. New design features for this research include: 1) the use of granular base materials to reduce construction time whereas prior experimental precast pavements were placed on asphalt base materials, and; 2) the use of grouted voids on the underside of precast panels to help ensure more efficient and uniform load transfer.
- Verify the feasibility of proposed design features by fabricating, assembling, and testing full size panels. Test the panels by applying repeated and stationary loads.
- Develop three-dimensional finite element models of the precast panels with various thicknesses. Use the models to obtain stresses and deflections caused by static loads at different locations. The results from this finite element analysis were used to design the experimental test panels and to determine the prestress required for the research pavement.
- Use the finite element models to investigate the effects of non-uniform subgrade support on the pavements stresses and deflections. This was accomplished by assuming voids or gaps between the pavement and the subgrade before and after the load is applied.
- Develop generalized classic solutions for finite beams and infinite beams on elastic foundation subjected to stationary and moving loads. Investigate the effects of variables such as beam thickness and moving load speed on the stresses and deflection of the beam. Use the results to determine the minimum pavement thickness required to make pavement more durable.

- Compare the results from the full size pavement tests to verify and validate results from the finite element analysis. Determine experimentally values for subgrade reactions and to also determine whether sufficient load transfer occurred across joints.
- Compare the results from experimental testing and the FEA to solutions of the beam on elastic foundations. The results help determine whether the theory of beam on elastic foundation is accurate and can be used to predict pavement behavior. Furthermore, use the results to propose further pavement design improvement.

1.2. SUMMERY OF FINDINGS

This research demonstrated that granular base material can be used to reduce construction time and cost without affecting pavement performance. Additionally, structural analysis indicated that the use of grouted voids underneath the panels is crucial in providing uniform support to avoid damage to the pavement caused by increase in stresses. Static and dynamic analyses were performed and the results were used to establish a minimum pavement. Minimum thickness of 6 in. has been calculated for this project pavement design.

There are additional benefits and outcomes from this research that were not necessarily the focus of the research at the outset. Chief among these other outcomes are: (1) the modulus of subgrade reaction can be directly measured from test results; (2) observation that the load vs. deformation reactions remain essentially linear despite loads reaching 30,000 lbs; (3) the conclusion that the continuous precast, prestressed pavement subjected to vehicular traffic loads can be analyzed as a beam supported by an elastic foundation; and (4) that linear-elastic dynamic analyses can be performed to help with key design decisions.

CHAPTER II

LITERATURE REVIEW

Rigid pavement in the United States dates back to the first concrete pavement constructed in Bellefontaine, Ohio in 1893 (Snell and Snell 2002). Rigid pavements are built using portland cement concrete and are classified into jointed plain concrete pavement (JPCP), jointed reinforced concrete pavement (JRCP), continuous reinforced concrete pavement (CRCP), and precast prestressed concrete pavement (PPCP).

The use of prestressed concrete pavement dates back to the 1940s in Europe where it was mainly used for airport pavement. Most of the early European airport projects used post-tensioning in both directions with pavement thickness between five and half inches and eight (Klunker 1981). The first known highway applications were in France in 1945 and England in 1950s. In this literature review the focus will be on the historic and new PPCP development in the United States.

2.1 HISTORIC DEVELOPMENT

The first known application of prestressed pavement in the United Stated was in military airfields in 1953 at Patuxent River Naval Air Station, Maryland. The Maryland project was followed by two more airport projects in San Antonio, Texas and El Paso, Texas. The first prestressed concrete highway experimental project was in Pittsburgh, Pennsylvania in 1957

(Hanna 1976). The following are major projects that were built between 1960 and 1990 and are considered early attempts at developing and understanding prestressed concrete pavements.

2.1.1 BROOKINGS, SOUTH DAKOTA

In the mid-1960s, a research program by South Dakota State University and South Dakota Highway Department initiated the development of precast concrete pavement with an asphalt concrete overlay (Merritt et al. 2000). The pavement panels were six feet by 24 ft with four and half inches thick precast panels over eight inches of sand base. The panels were topped with one and half inch of asphalt concrete. After a favorable test results, a 1,000 ft test section, shown in Figure 1, was built on US 14 bypass north of Brookings, South Dakota with post-tensioning force of 400 psi (Chang et al. 2004). The main problem occurred just one month after the highway was opened in a form of reflective cracks in the asphalt overlay at the precast panel joints.

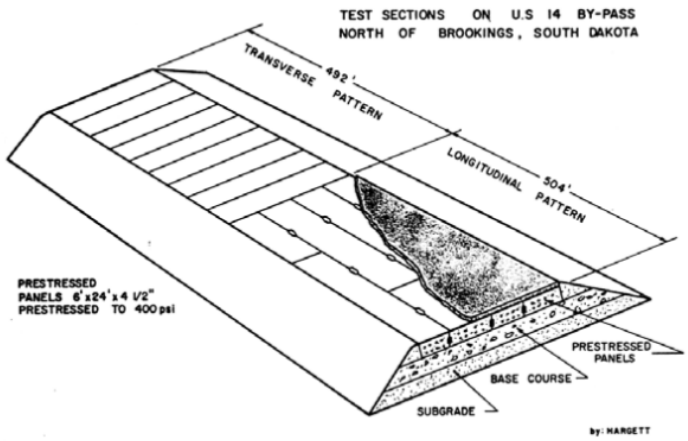

Figure 1 South Dakota 1000 Feet Section (Merritt et al. 2000)

2.1.2 HARRISBURG, PENNSYLVANIA

The one and half mile prestressed concrete pavement demonstration project was built in 1973 near Harrisburg, Pennsylvania. The projects four-lanes were constructed using 26 slabs with six inches thickness resting on six inches of asphalt base. Double layer polyethylene sheets were used to break the bond between the asphalt base and the panels. The slabs averaged 600 ft long and 24-ft wide (two lanes wide). The project used post-tensioning in the longitudinal direction with three feet gap between slabs to access the anchorage for post-tensioning. Pavements were post-tensioned to 325 psi (Tayabji et al. 2001).

2.1.3 BROOKHAVEN, MISSISSIPPI

This demonstration project was built in 1977 along a four lane section of US-84 near Brookhaven, Mississippi. The project stretches two and half miles and consists of 58 slabs that were 24 ft wide and 450 ft long. The slab thickness was six inches and rested on four inches of hot mix asphalt with double layer of polyethylene sheets to reduce friction. The slabs were post-tensioned in the transverse direction at a magnitude of 230 psi.

2.1.4 TEMPE, ARIZONA

Construction on the project was completed during in April 1977. The project was constructed along a section of the Superstition Freeway (State Route 360) in Tempe, Arizona. The project consists of 30 slabs at 31.5 ft width and 400 ft length. The slabs were six inches thick and were placed on four inches of lean concrete with double layer of polyethylene sheets in between. The pavement was post-tensioned in the transverse direction only at a magnitude of 215 psi. Gap slabs were used and they were at a dimension of eight feet in length by 10 inches in

thickness, and were conventionally reinforced. The joint was designed to accommodate maximum joint opening of two inches and a minimum joint opening of half an inch (Tayabji et al. 2001).

2.1.5 SUMMARY OF HISTORIC DEVELOPMENT

The early projects mentioned in before were an early attempts to improve and develop prestressed pavement. All of the projects featured combined slab segments of length between 300 to 760 ft, longitudinal prestress between 200 and 400 psi, longitudinal post-tensioning only, friction reducing layer, and semi-rigid base. However, the projects showed transverse cracking immediately after placement and longitudinal cracking few years later. The longitudinal cracks were attributed to temperature and shrinkage cracking and the lack of transverse prestress. Another problem was joint spalling, which in some cases was one inch deep.

2.2 NEW PRECAST PRESTRESSED CONCRETE PAVEMENT DEVELOPMENT

Following the early full scale pavement projects mentioned above, more prestressed pavement were constructed all in Texas, California, Iowa, and Missouri. The most recent project used prestressing in both directions, in most cases pretensioning in the transverse direction and post-tensioning in the longitudinal direction. The lessons learned from the early projects were valuable and helped avoid most of the issues.

2.2.1 WACO, TEXAS CAST-IN-PLACE PRESTRESSED PAVEMENT

The 1985 project by the Center for Transportation Research established several new ideas based on investigated previous projects successes and failures. The project most important

concepts were the use of central stressing, a sheet of friction reducing layer, and transverse prestressing (Chang et al. 2004).

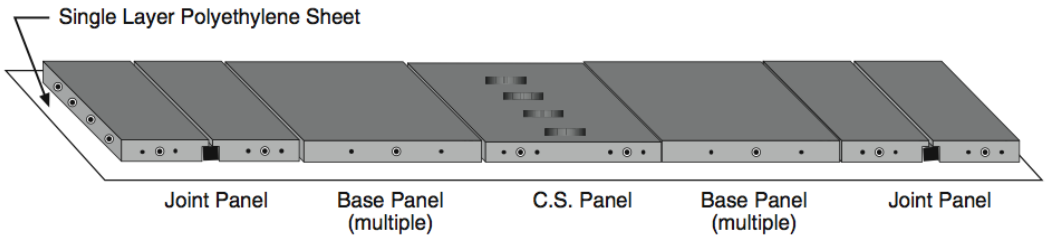

Figure 2 Assembly of Central Post-Tensioning System (Merritt et al. 2003)

Central stressing eliminated the need to access the end anchorage as shown in Figure 2 and Figure 3. Instead, the strands are anchored at the slab ends and coupled in a pocket at the middle of the panel where a jacking device can be used to post-tension the strands. This method reduced panel placement time and avoided the need for gab cast-in-situ slab between panels.

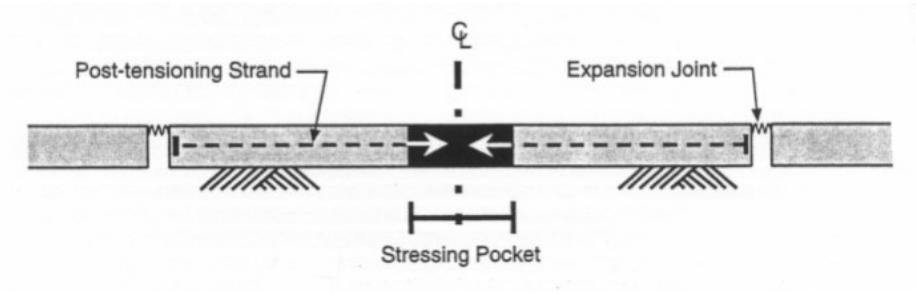

Figure 3 Central post-tensioning section view (Chang et al. 2004)

The frictional stress can develop between the precast slab and the underlying base material that can develop undesired tensile stresses and reduces durability of the precast pavement. Extensive testing concluded that one layer of polyethylene sheeting was the best solution for construction and economy. Previous precast projects encountered problems with

durability due the lack of transverse prestressing causing longitudinal cracking. Also, the use of transverse prestressing allowed for the use of wider panels.

2.2.2 IOWA HIGHWAY 60 PRECAST BRIDGE APPROACH SLAB PROJECT

Iowa highway 60 project is consists of approach slabs located on both ends of the northbound lanes of Floyd River bridge on highway 60 east of Sheldon, Iowa. The objective of this new project was to evaluate the use of precast panels in bridge approach slabs to minimize the effect of the bump at the end of the bridge and to evaluate the developed standard details for precast prestressed approach slab that can used for any precast pavement and approach slab configurations (Merritt et al. 2007).

Unlike typical precast pavement projects, the Iowa demonstration project used bi-directional post-tensioning, lane-by-lane partial width panel and an aggregate base with polyethylene sheeting (Merritt et al. 2007). The panels used in the project are full depth panels where the top surface is the actual riding surface. However, full depth panels require surface diamond grinding to be done before or after opening the road to traffic and careful base preparations. The post-tensioning tendons were grouted to provide more corrosion protection and to allow for future cut and remove repairs. Minor voids beneath the slab should be grouted before or after opening the road, and major voids before opening to traffic.

2.2.3 GEORGETOWN, TEXAS PRECAST PRESTRESSED CONCRETE PAVEMENT PROJECT

Georgetown, Texas project focused on testing and evaluating of the precast pavement techniques and methods. The pilot project was located on North I-35 frontage between Airport Road and SH-195 north of Georgetown, Texas. The location was chosen because that section of

the road can be closed for more flexible construction, contained no significant horizontal curves or super elevations, and experienced significant amount of traffic (Merritt et al. 2001).

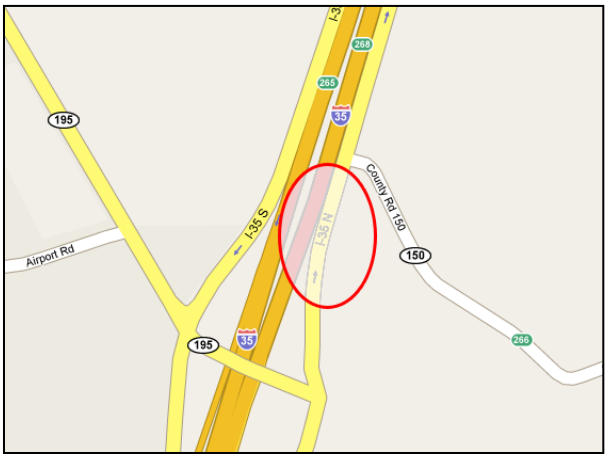

Figure 4 Location of Georgetown project on I-35

The precast pavement was 2300 ft long both sides with each side consisting of two 12 ft lanes with eight feet outside shoulder and four feet inside shoulder. Full width panels, 225 ft total length, were used on the south side of the bridge and partial width panels, 325 ft total length, were used on the north. The panels were fabricated using 400 ft casting bed producing ten full width panels or 20 partial width panels each time (Chang et al. 2004). The project utilized full depth central prestressing jointed panel method. The panels are prestressed in the transverse direction and post-tensioned in the longitudinal direction. Joint panel was placed at both ends of the slab and as many base panels as needed were placed between them with central post-tensioning panel at the center of the pavement.

The construction involved fabricating the panels, laying the leveling course, placing the precast panels, threading in the tendons, post-tensioning the tendons, and finally grout the conduits. The base was prepared using one to two inches of asphalt leveling course to support the precast prestressed pavement panels. Before placing the panels, a single layer of polyethylene

was laid to reduce post-tensioning losses and tensile stresses caused by friction (Chang et al. 2004). The strands were inserted into conduits in the panels and post-tensioned was performed at special pockets in the central panel. After achieving the required post-tensioning, the strands were grouted using non-shrink grout.

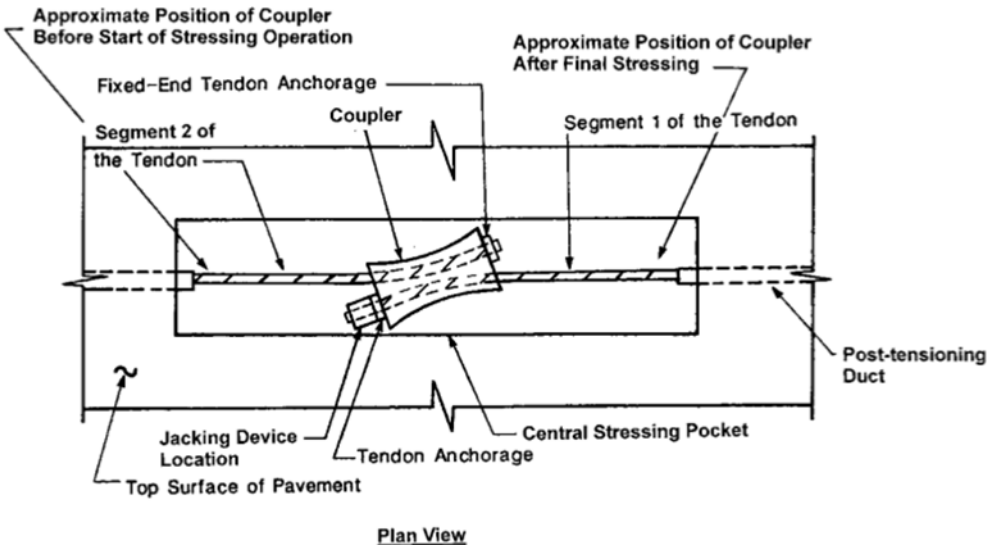

Figure 5 Prestressing Couplers System (Merritt et al. 2001)

The slab length was critical part of the design since longer slabs can have less expansion joints resulting in a reduced construction cost. However, longer slabs expand and shorten more than shorter slabs and require expansion joint to accommodate larger slab movement (Merritt et al. 2001). The project encountered challenges related to the lack of standardized design procedure and specifications for precast prestressed concrete pavement (Merritt et al. 2000). Otherwise, the project was a success and proved that precast concrete pavement is a viable solution expediting construction of concrete pavement.

2.2.4 SUMMARY OF NEW PPCP

A wide range of slab lengths has been used in projects around the United States. Pavements lengths ranging from 400 to 600 ft appear to perform well with proper prestressing for longer slabs. However, it is recommended that shorter slab lengths be used until better joint hardware is developed. There are newer projects completed during the last eight years but literature related to these projects is not yet available. The projects, which are listed in Table 1, all share the following features:

- Transverse pre-tensioning & longitudinal post-tensioning.
- Asphalt leveling base with friction reducing sheet between the asphalt & pavement.
- Night time construction where lanes were closed to traffic at the evening and opened to traffic before the morning traffic.

Project	Year	Pavement Length	Dimensions	No. of Panels	Placement Rate
El Monte, CA	2004	248 ft	8’ x 37’ x 10”~13”	31	5 panels/hr
Sikeston, MO	2005	1,000 ft	10’ x 38’ x 5.75”-11”	1,000	2 panels/hr
Newark, DE	2009	1,280 ft	24’ x 9’-10” x 8” 12’ x 9’-10” x 8”	130	2 panels/hr
Fairfax, VA	2009	1,020 ft	12’ x 10’ x 8 ¾” 27’ x 10’ x 8 ¾”	306	2 panels/hr

Table 1 Recent PPCP demonstration projects

Some specific observations regarding the design, construction, and maintenance of PCPs are (Tayabji et al. 2001):

- Shoulders, if used, should constructed monolithically with the traffic lanes and prestressed together.
- Minimum prestress levels should be at least 50 psi.
- Joint hardware design needs to be simplified and standardized.

2.3 PRECAST PAVEMENT REPAIR METHODS

In 2004, the Ministry of Transportation Ontario, Canada conducted a trial pavement repair using three methods for major highway in Toronto, ON, Canada. The three methods used were the Michigan method, and the Intermittent Super-Slab and Continuous Super-Slab methods discussed later in this report. The trial consisted of three full depth precast pavement repair for each of the Michigan and Intermittent methods using 6.6 ft by 12 ft panels with 9 in. thickness. The Continuous method trial was a 82 ft long full width lane with 9 in. thickness (Lane and Kazmierowski 2006).

2.3.1 THE MICHIGAN METHOD

The Michigan method was developed by Michigan State University and Michigan Department of Transportation. The method uses three dowels spaced 12 in. apart and placed at each wheel path. The dowels are placed in the precast panel and then inserted into precut slots in the existing pavement during placement of the precast pavement panel and grouted. However, prior to placing the precast panel the existing base must be covered with a self-leveling cementitious fill material with compressive strength of 51 psi at three days and 73 to 143 psi at 28 days (Lane and Kazmierowski 2006).

Most construction problems were related to the dimension and location of the dowels during placement of the precast panel. For the first trial, the precast panel was smaller than the removed area resulting in higher elevations at the departure end of the slab. Similarly, the other two pavements also sat higher than the existing pavement and diamond grinding was recommended. The other problem they encountered was the misaligned dowel slots in the existing pavement that raised questions related durability. However, all three pavements were installed between 10:00 P.M. and 3:00 A.M.

2.3.2 THE INTERMITTENT SUPER-SLAB METHOD

The Intermittent Super-Slab method is method patented by Fort Miller Co Inc. in 2003 as discussed later in the report. The Ontario trial project used four dowels spaced at 12 in. and placed at each wheel paths. The dowel holes are gang-drilled in the existing pavement and injected with epoxy adhesive before inserting the dowels. The new panels are slotted at based at each dowel location during fabrication. The base of removed area shall be precisely graded and crusher screenings must be placed and compacted prior to panel installation. The panels contain channels that are grouted to fill any voids beneath the slab. The only problems the contractor encountered was the slow rate of grout pumping which resulted in the delay of the final pavement grouting to the next evening.

2.3.3 THE CONTINUOUS SUPER-SLAB METHOD

Similar to the intermittent method, the continuous method is controlled by patent held by Fort Miller Co Inc. The method of installation and base preparation is similar to the intermittent method except that the cut area is 82 ft and six 13.1 ft by 12 ft panels are interlocked together. The only problem the team encountered was the oversized cut area in the existing pavement that

resulted in larger than desired gaps between panels (0.2 in. to 1.4 in.) and existing pavement (7.4 in. at one end). The trial also encountered another problem that was the 0.5 in. difference in elevation between the first and second precast panel as a result of uneven grading.

2.3.4 REPAIR METHODS SUMMARY AND RECOMMENDATIONS

The panels were tested using the nondestructive Falling Weight Deflectometer that involves applying a series of impulse loads to simulate a moving wheel. The resulted deflections are then measured using a series of sensors mounted on the pavement (Lane and Kazmierowski 2006). Results of the precast pavement is then measured and compared to the results of the existing pavement on the opposite side of the joint to calculate the Load Transfer Efficiency (LTE). Table 2 summarizes the results obtained from the tests.

Method	Slab	Left wheel path		Between wheel paths		Average for slab
		Average LTE, %	Number < 70%	Average LTE, %	Number < 70%	Average LTE, %
Michigan Method	Slab 1	90	0	66	7	78
	Slab 2	92	0	73	5	83
	Slab 3	94	0	70	6	82
	Average	92	-	70	-	81
Fort Miller Intermittent Method	Slab 1	82	0	76	2	79
	Slab 2	91	0	85	0	88
	Slab 3	83	2	76	2	80
	Average	85	-	79	-	82
Fort Miller Continuous Method	Slab 1	78	3	74	0	76
	Slab 2	86	0	84	0	85
	Slab 3	87	0	87	0	87
	Slab 4	83	0	76	1	80
	Slab 5	76	2	68	3	72
	Slab 6	92	0	90	0	90
	Average	83	-	80	-	82

Table 2 Load Transfer Efficiency (LTE) test results (Lane and Kazmierowski 2006)

The final assessment of the trials was positive. Other than the previously stated construction issues the precast pavement did not crack, spall, or rock. The trials also met the minimum 70 percent LTE required by the contract specifications. For pavement repairs, the following to be considered (Lane and Kazmierowski 2006):

- The thickness of the pavement should be accurately verified.
- In case of pavement repairs, the new panels should be thinner than existing pavement to account for grading and material under the panel.
- If dowels are used, their location should be accurately marked.
- Dowels are best to be uniformly distributed along the whole joint length instead of placing at wheel path only.
- Careful grading of the base material is key to precast pavement.
- The grouting fill needs to be carefully mixed to allow for self-leveling.
- When using grouting under panels, the aggregate base should be wet prior to placing panels to prevent water absorption from the grout.

2.4 SUMMARY

There is an increasing interest in PPCP in the United States. It has been demonstrated that PPCP is promising and feature reduction in maintenance and increase in pavement life. There are several PPCP projects being constructed in different states in the United States. It is hoped that the improved performance of previous and current will lead to improvements to PPCP design and construction methods paving the way for high performance pavements.

CHAPTER III

DESIGN METHODS & ANALYSIS FOR PRECAST PRESTRESSED CONCRETE PAVEMENTS

Rigid pavements are defined as pavement constructed of Portland cement concrete. Rigid pavements are classified as jointed plain concrete pavement (JPCP), jointed reinforced concrete pavement (JRCP), continuous reinforced concrete pavement (CRCP), or prestressed concrete pavement (PCP). Typical cross section of PPCP consists of the Portland cement concrete pavement, friction reducing membrane, asphalt leveling layer, base/subbase course, and subgrade as shown schematically in Figure 6.

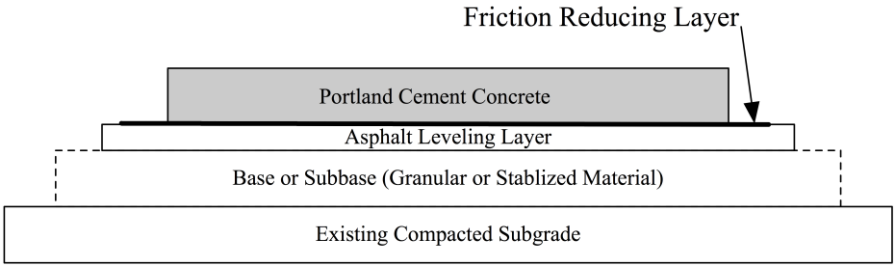

Figure 6 Typical PPCP cross section

Rigid pavement is usually analyzed using plate theory, which assumes the pavement to be a medium thick plate with planes that remain plane before and after bending. However, there are

several analytical and numerical solutions developed over the years from simple closed form equations to complex derivations. Goldbeck developed the earliest simple solution in 1919. His equation for the design of rigid pavement was based on a concentrated load applied at the corner of the slab (Goldbeck 1919).

In an extensive concrete pavement study, Westergaard developed analysis and design equations based on Winkler Foundation assuming full contacts between the pavement and base. In Winkler Foundation, the deflection of the foundation (or base) at any given point is independent of the deflection of any other point and proportional to the active pressure (Huang 2004). However, field measurements performed by Pickett (Pickett et al. 1951) found that actual corner stresses are much higher than those obtained using the Westergaard solution. Pickett developed semi-empirical formulae by assuming that the slab is not in full contact with the base. This method was used by the Portland Cement Association (PCA) until 1966 (PCA 1951) and (PCA 1966).

Recent advances in computers and software programing paved the way for more powerful finite element analysis software packages. The use of finite element method in the analysis of rigid pavement started in the early 1960s with Cheung and Zeinkiewics use of the method to analyze slabs on elastic foundation (Huang 2004). Now, there are power 3D general-purpose FEA packages that are able to simulate pavements under stationary and dynamic loading.

3.1 PPCP DESIGN CONSIDERATIONS

One of the major challenges with PPCP is the lack of standard design method or guidelines. Currently, most PPCP are designed using an equivalent pavement method. In the equivalent pavement method, the pavement is designed and analyzed as continuously reinforced concrete pavement (CRCP) using the AASHTO rigid pavement design method. Next, the CRCP

tensile stresses are calculated using the elastic layer theorem or plate theory. Finally, a series of thinner CRCP thicknesses are analyzed for tensile stresses and as the pavement gets thinner the tensile stresses get larger. Therefore, prestressing is required to counteract the stress increase and maintain the same tensile stress as in the original CRCP design.

The equivalent pavement design method does not to take into consideration the effects of thinner pavement on overall performance of the system. Furthermore,, the use of thinner pavement reduces the mass of the panel which in turn can cause increases in the dynamic response.

3.2 PPCP DESIGN FACTORS

The design factors for PPCP and conventional rigid pavement are similar. However, PPCP design factors include prestress losses. PPCP design factors are traffic loads, ambient temperature effects, moisture effects, variation in pavement temperature, subgrade friction, and prestress losses (Chang et al. 2004).

3.2.1 TRAFFIC LOADS

Traffic loads generated by moving vehicles cause tensile stresses at the bottom of pavements and compression stresses at the top, Figure 7. The controlling design parameter is usually considered flexural tension in concrete, which is usually between 10% and 15% of the compressive strength (ACI 2005).

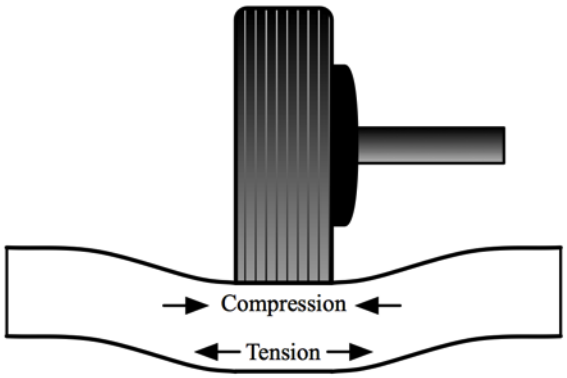

Figure 7 Top and bottom pavement stresses due to wheel load

AASHTO road tests determined that damage due to any axle load could be represented by the number of 18-kip equivalent single axle loads or ESALs (AASHTO 1993). For a given stress, concrete cracks when the number of load repetitions reaches its fatigue endurance level (Ballinger 1971). However, experiments on concrete specimens proved that more than 10 million load repetitions were achieved when the tensile stresses in concrete due to loading are below 50% of the tensile strength (Clemmer 1923) and (Huang 2004). The number of ESALs can be determined using traffic analysis data such as the annual average daily traffic (AADT), percentage of trucks, and traffic growth rate for specific highway or street.

3.2.2 TEMPERATURE CHANGES

Changes in ambient temperature and concrete temperature will cause curling and horizontal movement. Change in temperatures between summer and winter causes horizontal movement in the pavement due to expansion and contraction (Beckemeyer et al. 2002). The horizontal movement is resisted by the pavement self-weight and friction between the pavement and base. The frictional resistance in turn causes stresses at the bottom or the pavement that should be considered in prestressing and joint spacing.

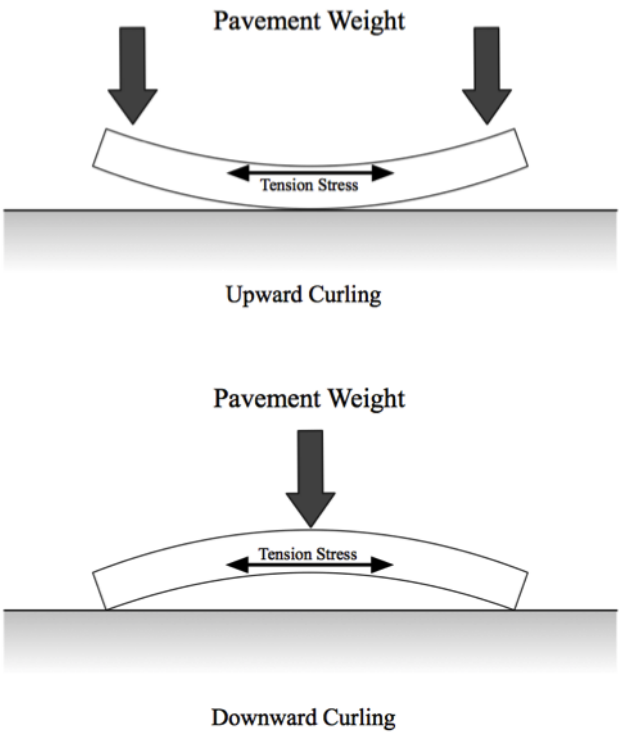

Figure 8 Curling of pavement due to temperature gradient

Temperature changes also cause curling stresses. During the day, concrete temperatures at the top surface of concrete pavement is usually elevated in comparison to temperatures at the bottom of the pavement. Higher surface temperatures cause the top to expand relative to the bottom and middle portions of the pavement. Changes in material strains caused by temperature are oftentimes offset by the self-weight of the pavement, which prevents the pavement from actually curling. However, as a result of temperature strains offset by bending caused by self-weight of pavement panels, compression and tensile stresses develop at the top and bottom, as shown in Figure 8. Conversely at nighttime, lower ambient temperatures generally cause the temperature of the top surface to cool in comparison with the bottom of the pavement causing the pavement to curl upwards at the joints. Again, the weight of the slab helps keep the edges from lifting. However, this causes tensile stresses at the top and compression stresses at bottom of the pavement.

3.2.3 MOISTURE EFFECTS

Moisture gradient between the top and bottom of the pavement have same effects as temperature gradient and would cause warping. Changes in the moisture content of the pavement depend on the environmental conditions. On dry conditions, the top of the pavement loses moisture faster than the bottom cause higher rate of shrinkage at the top. The result will be compressive stresses at the bottom and tensile stresses at the top. However, during rainy conditions most water will be trapped on the surface before making its way to the bottom causing higher moisture content in the top and therefore tensile stresses at the bottom.

3.2.4 SUBGRADE FRICTION

The seasonal and daily changes in ambient temperature cause horizontal movement in the pavement, which is resisted by the friction between the concrete and base. This is critical for PPCP where the distance between joints is between 300 ft to 500 ft since longer pavement will contract and expand more. There are three criteria for the relationship between the PPCP movement and the supporting base (Diaz 1986):

- Partially restrained movement cause by the daily change in ambient temperature.
- Unrestrained movement resulting from concrete shrinkage, creep, and swelling.
- Temporary restrained movement as a result of elastic shortening, which is countered by the applied prestressing force.

The most critical friction is a result from daily temperature changes since seasonal changes take time days to develop. Compressive stresses are developed during concrete expansion while the more critical tensile stresses develop during pavement contraction (Diaz

1986). In addition to environmental effects on friction of conventional concrete pavement, PPCP can develop additional tensile stresses during post-tensioning due to base restrains. Increased friction between the pavement and base will require higher post-tensioning force. Previous research and experiments indicated that a single layer of polyethylene sheet provide a maximum coefficient of friction between 0.57 and 0.92 and would be sufficient to reduce friction (Chia et al. 1986).

The friction resistance between the pavement and base can be calculated using the following equation (Diaz et al. 1986):

$$\sigma_F = \frac{\mu_{max} \gamma L}{288} \qquad \text{Equation 1}$$

Where,

μ_{max} = maximum coefficient of friction

γ = unit weight of concrete, pcf

L = pavement length, ft

3.2.5 PRESTRESS LOSSES

Prestressed concrete strength depends on the amount of prestressing force applied to the member. PPCP are subjected also to prestressing losses that need to be estimated to achieve the required strength. Experience in prestressed concrete have shown that prestress losses are between 15 and 20 percent of the applied prestress force (Cable et al. 1985). Common sources for prestress loss are:

- Anchorage set (this affects both pre-tensioned and post-tensioned albeit at different stages of fabrication).
- Elastic shortening of the concrete.

- Creep of the concrete.
- Shrinkage of the concrete.
- Relaxation of the tendons.
- Friction resistance between the pavement and base.
- Friction between tendons and ducts (post-tension only).

3.3 DESIGN VARIABLES

PPCP design depends on several variables that are unique to PPCP. These variables include (Chang et al. 2004):

1. Foundation properties.
2. Pavement thickness.
3. Pavement length.
4. Panel width.
5. Prestressing force

3.3.1 FOUNDATION PROPERTIES

Pavement performance is greatly affected by the supporting foundation properties that include modulus of subgrade reaction and resilience modulus. The ability of the pavement to resist fatigue loading is directly related to the foundation strength. Weaker supporting subgrade or foundation increases pavement stresses and reduces service life.

3.3.2 PAVEMENT THICKNESS

The selection of the PPCP thickness depends on several design factors such as traffic loads, curling stresses, and location of the pavement. For a given load and base, stresses in pavement increase as the thickness decrease. Since pavement design is based principally on stresses, thinner pavements will require higher prestress forces. This gives more flexibility for the designer to choose the desired thickness and corresponding prestressing magnitude to maintain certain stress level. Prestress pavement will have higher load carrying capacity than non-prestressed pavement due to lower tensile stresses due to precompression of the cross section prior to loading (ACI Committee 325 1988). There are several situations where thinner pavement is desired such as bridge underpass to increase overhead clearance.

The pavement thickness is influenced by factors such as road location, traffic loads, and environmental variables (temperature and humidity). The minimum thickness of existing PPCP thicknesses are not less 60 percent of the thickness of an equivalent CRCP (Chávez et al. 2003). Other factors limiting factor is the minimum cover that needs to be provided for reinforcement and hardware.

3.3.3 PAVEMENT LENGTH

Pavement length is governs by the amount of expansion and contraction. Longer pavement spans will increase expansion and contraction due to ambient temperature changes and therefore desired. However, longer pavement will increase the gap between joints and will decrease rise quality. Furthermore, longer pavement will require higher prestressing forces, which means an increase in cost. On the other hand, shorter pavement length will require smaller gap and less prestressing force but will decrease ride quality. Therefore, a good balance between rise quality and cost must be achieved in selecting the pavement length of PPCP. It is important to

design transverse joints to accommodate movement, transmit forces between panels, carry significant loads without significant deflection, and be composed of durable materials that can be easily repaired.

3.3.4 PANEL WIDTH

Panel length is a variable that must be considered for panel transportation, equipment requirements, and traffic management. Wider panels are heavier and therefore will require more trips to the precast plans and higher capacity lifting equipment. Traffic management could also dictate the width of PPCP panels. In high traffic volume situations it might be necessary to divert traffic to other lanes and therefore partial width panels are better choice. Either case, it is important to consider integrating the pavement shoulders with the road panels since higher stresses due to wheel loads are located near the edge of the slab.

3.3.5 PRESTRESSING FORCE

The prestressing magnitude of PPCP varies along the length of the pavement due to prestress losses as discussed earlier. The magnitude of prestress at any point along the pavement must maintain compression stresses to meet the stress limit over the pavement life. The stress at any point along the pavement length can be calculated from the following equation:

$$\sigma = \sigma_L + \sigma_C + \sigma_F + \sigma_{PE} \qquad \text{Equation 2}$$

where,

σ_L = stress cause by traffic loads

σ_C = stress cause by curling

σ_F = stress cause by friction between the pavement and subgrade

σ_{PE} = stress due to effective prestress

Since the stresses at the top and bottom are different, it is important to use the (+) for tension and (-) for compression for the stresses above. The stresses evaluated at the end and mid pavement only

CHAPTER IV

DESIGN OF PROJECT SPECIFIC PRECAST PRESTRESS CONCRETE PAVEMENTS

One of the objectives of this research is to improve the performance of PPCP. The designs from this research incorporate two techniques to help mitigate the effects of non-uniform base support:

a) The use of granular base materials that are more flexible in the final elevation as the precast elements are set in place, and;
b) Incorporating large grout voids into the precast panels to decrease the area of pavement requiring prestress and to improve the transfer of load from the pavement to the base material.

In addition, pavements may be constructed in less time and with lower user costs by not using asphalt leveling base. As a summary, the research designs feature the following with their potential benefits:

- The use of granular base material.
    - Reduce construction time.
    - Reduce construction costs.

- The use of thinner pavement panel thickness.
    - Increase bridges underpass clearance.
    - Reduce panel weight for more efficient handling and transportation.
- The use of equal magnitude of transverse prestressing and longitudinal post-tensioning.
- The use of multi-strand tendons for faster construction.
- The use of grouted voids underneath the panels.
    - To achieve full contact with the base.
    - Reduce the possibility of non-uniform base support.
    - To increase the overall mass of the pavement that reduces the dynamic effects of moving loads.

For purposes of the experimental program, the precast panels are built with a 12 ft width to match the width of one lane. The design is shown in three dimensions in Figure 9, and in plan and elevations in Figure 10, Figure 11, and Figure 12. Further, the panels are constructed in eight feet lengths segments. The "length" of the panel is defined as the length in roadway travel. The panels are pretensioned in the transverse direction during fabrication and post-tensioned in the longitudinal direction to form the pavement. The panels are connected to each other using a shear key to achieve high Load Transfer Efficiency (LTE). The depth of the panel at the wheel path (beams) and edges is greater than that at the center to give the pavement stronger section where needed the most.

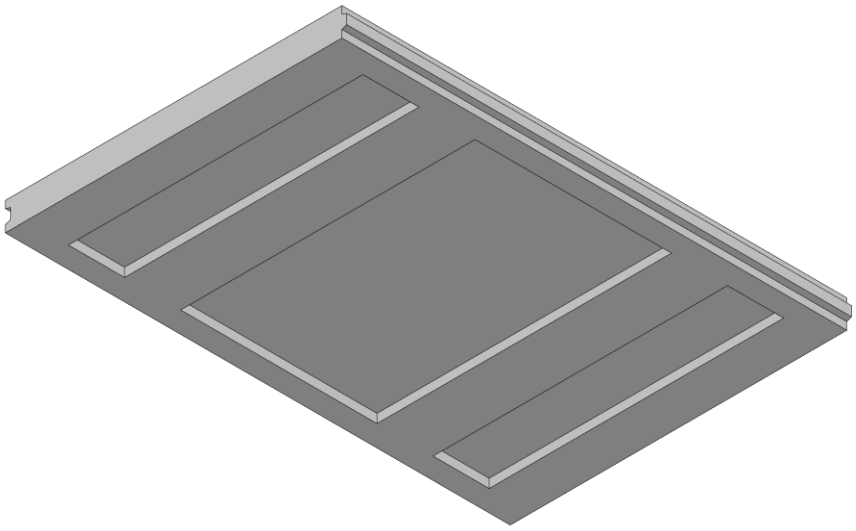

Figure 9 Three dimensional rendering of the PPCP test panels

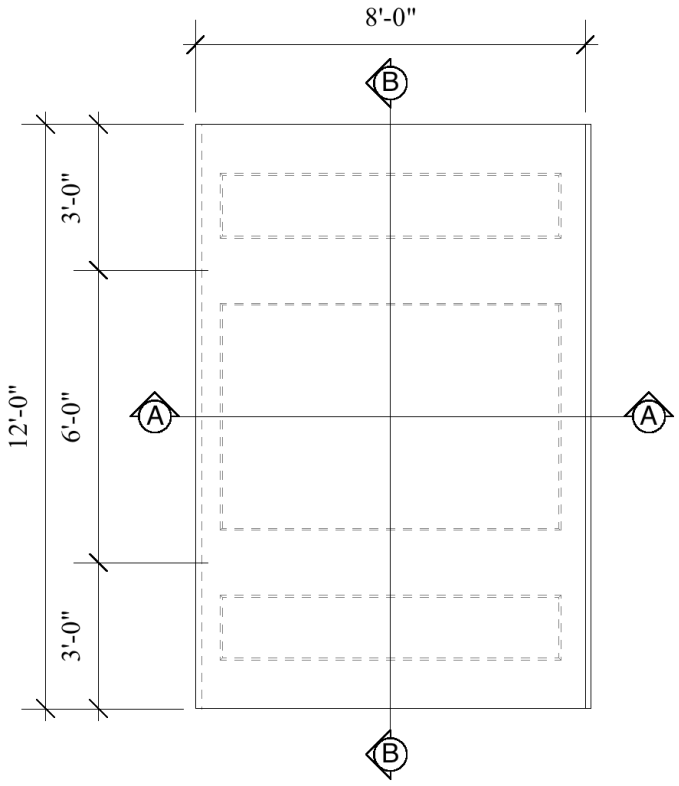

Figure 10 Plan PPCP panel plan

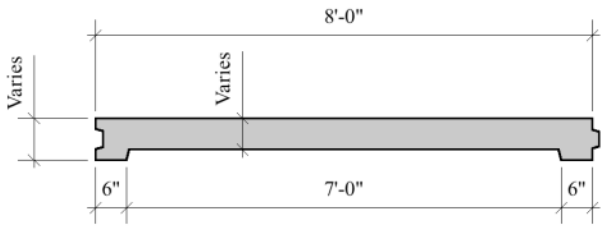

Figure 11 PPCP section A-A

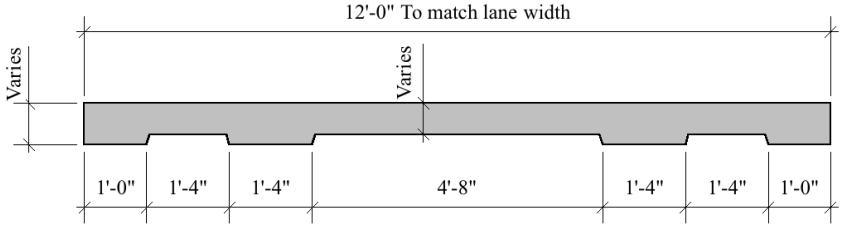

Figure 12 PPCP section B-B

4.1 PPCP DESIGN ASSUMPTIONS

The PPCP panels were analyzed for stresses and deflection using the finite element method. The concrete was assumed to have a compressive strength of 5,000 psi, modulus of rupture of 530 psi, and modulus of elasticity of 4,000,000 psi. The modulus of subgrade reaction was estimated based on existing subgrade soil and base thickness. Existing subgrade soil consisted of sand and gravel mixture with moderate amount of silt and clay giving it an estimated modulus of subgrade reaction between 120 and 170 psi/in (Huang 2004). The addition of 6 in. of untreated granular subbase improves a total subgrade reaction with new range between 130 psi/in and 200 psi/in (Huang 2004). For the purpose of this analysis, k-value of 150 psi/in was chosen.

For reference, the required CRCP thickness was calculated using AASHTO Supplemental Guild for Rigid Pavement Design for non-prestressed concrete and was found to be 13 in. The PPCP panels were designed to dimensions and thicknesses as shown in Table 3. The

thicknesses of eight inches and ten inches were chosen because they were common in most PPCP projects built lately.

Pavement	Dimensions (feet)		Panel Thickness (inches)	
	Width	Length	Beam	Slab
I	12	8	8	6
II	12	8	8	6
III	12	8	10	8

Table 3 Test pavement dimensions and thickness

4.2 FINITE ELEMENT ANALYSIS

Using software package (STAAD.Pro®), three dimensional finite element models were developed to calculate stresses caused by 18,000 lbs. single axle with tire pressure of 120 psi (two wheel loads of 9,000 lbs each separated by six feet). The elements used in the finite element were 8-noded solids with dimensions of three by three inches surface area (perpendicular to the load) and two inches in depth. The supporting foundation system was modeled as a series of linear springs with modulus of subgrade reaction (k) of 150 psi/in. Properties of the concrete was based on compressive strength of 5,000 psi and modulus of elasticity of 4,000 ksi (ACI 2005).

The two load cases were considered with an equivalent tire patch area of nine inches by nine inches for each tire and load pressure of 111 psi. The tire patch size employed in analysis was nine inches by nine inches. This helped us match the loading to the size of each to a finite element which had dimensions of three inches. The pressure could be applied only to the entire surface of the element.

The first load case (LC1) placed two tire loads spaced six feet apart at the wheel path in the middle of the panel as in Figure 13. The second load case (LC2) placed one tire load at the exterior edge of the panel and the second tire load at the center as shown in Figure 14. Summary of the finite element analysis results are shown in Table 4.

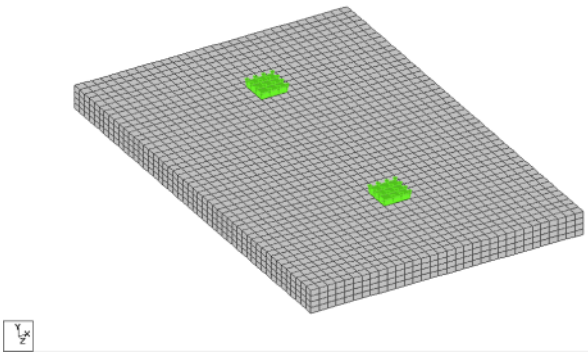

Figure 13 Finite element analysis Load Case 1 (LC1)

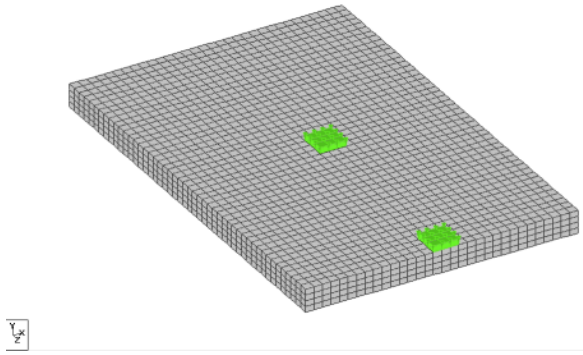

Figure 14 Finite element analysis Load Case 2 (LC2)

Pavement	Panel Thickness (in)		Maximum Transverse Stress (psi)		Maximum Longitudinal Stress (psi)	
	Beam	Slab	Compression	Tension	Compression	Tension
I & II	8	6	261 (LC2)	227 (LC2)	382 (LC2)	355 (LC2)
III	10	8	159 (LC2)	120 (LC2)	267 (LC2)	232 (LC2)

Table 4 Finite element analysis results summary

4.3 PPCP FINAL DESIGN DETAILS

The final pavement design was based on stresses obtained from the finite element analysis. The minimum prestress required was calculated based on maximum tensile stress that is 50 percent of concrete rupture strength of 530 psi. Prestressing effective "pre-compresses" the concrete making the concrete section more efficient in resisting service loads than plain or non-prestressed concrete pavements. Pavement I/II and Pavement III maximum longitudinal tensile stresses were calculated to be 355 psi and 232 psi, respectively. Post-tensioning losses were estimated to be 15 percent of the ultimate tensile strength of prestressing strand, f_{pu} of 270 ksi. The effective prestress force for 0.5" diameter strand was calculated to be 30.9 kips without losses and 26.3 kips with losses. For Pavement I/II, the required prestress was calculated by subtracting 50 percent of the tensile strength of concrete from the maximum longitudinal tensile stresses (265 psi - 355 psi = 90 psi). The minimum number of strands required to achieve 90 psi was based on the cross-section area shown previously in Figure 12 and found to be four strands for Pavement I/II. For the purpose of testing, it was decided that a total of eight strands be used for pavement I, 12 for Pavement II, and 12 for Pavement III. Transverse prestress will be used to achieve the same level of prestress as longitudinal post-tensioning.

Prestressing will be accomplished using 0.5 in. diameter low-relaxation strands. Longitudinal post-tensioning strands will be either 2-strand or 4-strand system depending on the required prestress. Testing variables include pavement thickness and amount of prestress. Two different post-tensioning layouts were chosen. Pavement I use four post-tensioning ducts with two strands per ducts located at edges and wheel paths. One the other hand, Pavement II and III use two and four strands post-tensioning ducts. The four strand post-tensioning ducts were located at the wheel paths while the two strands ducts were located at the edges. Table 5 gives prestress amount for each pavement set. The detailed construction drawings are provided in the appendix.

Pavement	Panel Thickness (inches)		Strands		Prestress Magnitude (psi)		Number of Stands per Tendons
	Beam	Slab	Count	Size (inches)	Longitudinal	Transverse (on slab)	
I	8	6	8	0.5	213	226	2-2-2-2
II	8	6	12	0.5	320	316	2-4-4-2
III	10	8	12	0.5	247	237	2-4-4-2

Table 5 Pavement design details

CHAPTER V

FABRICATION AND CONSTRUCTION OF THE PAVEMENTS

5.1 MATERIALS SPECIFICATIONS

Three PPCP test panels were fabricated and constructed in the same manner that a transportation agency would build a road. The subgrade materials were graded and compacted. Proper drainage was assured by ditches and other construction to ensure the maintenance of moisture content in the base and sub-base materials. Base materials were then brought to the jobsite, installed and leveled and then compacted. Precast Prestressed Concrete Pavement (PPCP) panels were fabricated at a precast/prestressed concrete plant and shipped to the jobsite where they were installed atop the base materials. Prestressing strands were threaded through post-tensioning ducts, and then post-tensioning was accomplished. After post-tensioning the post-tensioned tendons were grouted. Grouting was then injected into the void spaces that were cast into the underneath side of the precast panels. This completed the construction of the PPCP test panels. Upon completion each of three test pavements was 12 ft in width and 28 ft in length. This section describes the specifications of the materials used in this project.

5.1.1 BASE

In general, rigid pavements are constructed upon one or more layers of granular or stabilized material above the subgrade. The pavement base serves the following purposes:

- Provides uniform and stable support for the pavement
- Improves the modulus of subgrade reaction
- Prevents subgrade pumping, and other factors that soften or weaken subgrade response
- Provides a working platform for workers and equipment

Base materials should be uniformly graded and compacted and should have a thickness not less than 4 in. (AASHTO 1993). Furthermore sufficient drainage is required to avoid moisture accumulations which could cause changes in moisture content in the subgrade, and subsequently cause weakness and pumping in the subgrade. This research project used locally available crushed limestone granular base material with minimum base layer thickness of six inches. The selected base material conformed to ODOT specifications (OKDOT 1999) Type I aggregate subbase with 5 to 45 percent passing No. 200 seive, maximum liquid limit of 30 percent, and maximum plasticity index of 10 percent. The base was compacted in two layers to 95 percent of maximum density. Water was uniformly applied during compaction to ensure uniform texture and proper consolidation.

5.1.2 SUBGRADE

Natural soils were used as the subgrade on this project. The existing subgrade was compacted to not less than 95 percent of Standard Density and was tested in accordance with AASHTO T99.

5.1.3 NON-SHRINK GROUT FOR TENDONS AND VOID SPACES

Non-shrink grout was used to fill the post-tensioned tendon conduits and the void spaces underneath the panel. The post-tensioned tendons were grouted to help ensure a bonded reinforcement response in the event of cracking, and to help ensure durability of the tendon itself by mitigating corrosion.

For these tests, the same grout was used to fill void spaces that were intentionally located underneath the precast, prestressed panels. This construction technique is intended to affect a more uniform transfer of load between the precast panels and the base materials. The grout possess the compressive strength necessary to resist compressive stresses, and some shearing stresses, transmitted by the precast panel from wheel loading and environmental loading. Furthermore, the grout material is intended to meet the environmental durability requirements. The grout used in this research is MASTERFLOW® 1205.

5.1.4 CONCRETE

Due to traffic volume and exposure to extreme weather, high performance concrete is recommended for use in the fabrication of the precast prestressed concrete pavement (PPCP) panels. The concrete mixture was designed by the research team in collaboration with the fabricator and shown in Table 6.

5/8 in. Course Aggregate	Fine Aggregate	Cumulative	Type 3 Cement	Gal / Water	MB AE 90	Pozzolith NC 534	Glenium 7700
1855	1326	3180	564	22	6	34	59

Table 6 PPCP mixture design use for panel construction (per Cubic Yard)

5.1.5 REINFORCING STEEL AND PRESTRESSING TENDONS

The prestressing strands were specified as 0.5" diameter, Grade 270, low-relaxation strands conforming to ASTM A416/AASHTO M203. Individual strands were pretensioned and embedded within the precast panels in the transverse direction during fabrication of the precast segments in the prestressing plant. Some of the pretensioned strands were debonded to achieve the proper amount of precompression. The design details and construction drawings are found in Appendix B.

Post-tensioning tendons were installed longitudinally. During fabrication, post-tensioning tendon ducts were placed into the precast segments. Post-tensioned tendon ducts were made from polyethylene with minimum thickness 0.036 in. and conformed to ASTM D1248. Prestressing strands were placed through the ducts after the pavement segments were set atop the base materials. By definition, a "tendon" consists of the prestressing strands, the post-tensioning duct, and all hardware associated with the prestressed tendon. The post-tensioned tendons were stressed using a hydraulic jack with calibrated pressure gauge.

Mild reinforcement was also used in addition to the prestressing strands. Mild reinforcement bars were used around anchorage and perimeter of the panels. The reinforcing steel conformed to ASTM A615 with minimum yield stress of 60 ksi.

5.2 FABRICATION

The pavement panels were built at precast concrete fabrication plant and then transported to the testing location. The fabrication process started June 30, 2010 and was completed July 6, 2010. Fabrication was performed at Coreslab Structures, Oklahoma, located in Oklahoma City. The fabrication process is shown in the photographs of Figure 15, Figure 16, Figure 17, Figure 18, Figure 19, and Figure 20.

The panels were cast in three different pours on three different days. All of the casts were made in one pretensioned bed approximately 250 ft. long. A total of 12 precast pavement panels were required for this project. Figure 21 shows the layout of the panels within the precast, prestressing bed. The panels are intended for three sets of four panels each – each set was made to different thickness or prestressing amounts for three different and distinct tests.

Figure 15 Concrete formwork for Panel I-A

Figure 16 Post-tensioning hardware for 4-strand anchors

Figure 17 Concrete cast into panel form

Figure 18 Finished panel surface

Figure 19 Pressure indicators used to measure tension force in pretensioned strands

Figure 20 Shear key and the two-strand post-tensioning duct

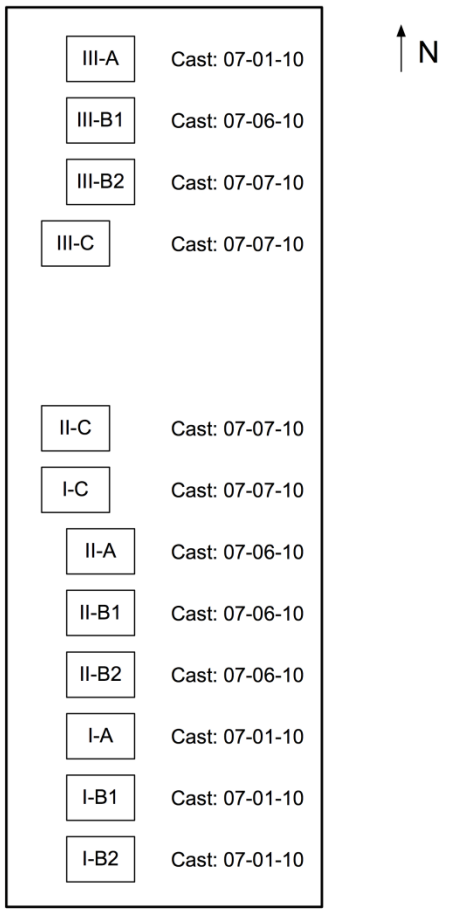

Figure 21 Fabrication bed layout and cast dates. Panels C were misaligned to achieve correct number of strands.

The panels were pre-tensioned transversely to the eventual traffic direction. The "width" or transverse dimension of each panel was made equal to a single lane width, or 12 ft. The "length" of the panels segment, running in the longitudinal direction along with traffic, was eight feet. Three eight feet long panels plus one four feet long end piece were post-tensioned longitudinally to construct test pavements with a total length of 28 ft.

During fabrication, fresh concrete properties air content, ambient temperature, concrete temperature, slump, and unit weight were measured. The results of fresh concrete properties are shown in Table 7.

Date	Slump (in.)	Air Content (%)	Unit Weight, (lb/ft^3)	Ambient Temp, ◦F	Concrete Temp, ◦F
01-Jul-10	2.5	4.0	143.8	72	90
06-Jul-10	3.5	4.2	145.2	90	91
07-Jul-10	3.0	6.6	142.2	84	86

Table 7 Fresh concrete properties

Hardened concrete properties were measured at specific time intervals and included strength, elastic modulus, and tensile strength. Compressive cylinder strength tests and modulus of elasticity tests were performed in accordance with ASTM C 39 “Test Method for Cylindrical Concrete Specimen” and ASMT C 469 “Test Method for Static Modulus of Elasticity and Poisson's Ratio of Concrete in Compression”, respectively. Furthermore, the tensile strength of concrete was measured using ASTM C 496 “Standard Test Method for Splitting Tensile Strength of Cylindrical Concrete Specimen” and was found to be 756 psi at 28 days.

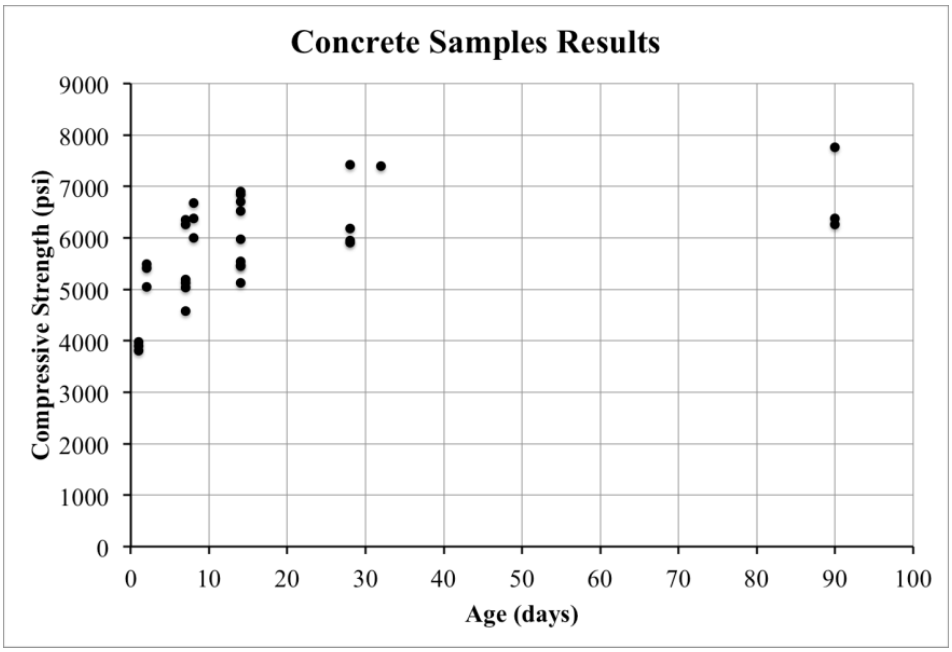

Figure 22 Concrete cylinders test results

Specimen Age	Unit Weight, lb/ft^3	Compressive Strength, psi	Measured Modulus of Elasticity, psi	ACI Modulus of Elasticity, psi
32 days	149.2	7,389	5,860,000	5,170,000

Table 8 Measurement of concrete modulus of elasticity

Specimen Age	Unit Weight, lb/ft^3	Splitting Tensile Force, lb	Measured Tensile Strength, psi
28 days	149.0	38,000	756

Table 9 Measurement of concrete tensile strength

5.3 ONSITE PAVEMENT CONSTRUCTION

Construction on the job site was performed soon after the panels were fabricated. The subgrade was graded and uniformly compacted at moisture content and density to ensure adequate support. The subgrade was compacted at minimum of 95 percent compaction at 100 percent of ASTM D 698/AASHTO T 99 density according to ODOT specifications (OKDOT 1999). Figure 23 shows preparation of the subgrade material. A stockpile of base materials are also shown in Figure 24.

Figure 23 Project site subgrade preparation


Figure 24 Aggregate base material delivered to site

A road fabric (GEOTEX® 601™) was used to separate the base and the subbase. The road fabric and its installation are shown in Figure 25 and Figure 26. The aggregate base layer was placed at the top of the compacted and graded subgrade with road fabric in between, as shown in Figure 26. The base was compacted at a density required to prevent consolidation of the granular material under heavy loads and traffic. The base was graded and compacted to 95 percent of the maximum density as per ASTM D 698/AASHTO T 99.

Figure 25 Road fabric prior to placing aggregate base

Figure 26 Base materials preparation and leveling

Figure 27 and Figure 28 show various stages during placement and compaction of the base materials. The subcontractor prepared the base course with the assistance of electronically and radar guided leveling equipment. Even so, the granular base material appeared to be subject to some un-evenness. Despite the appearance of uneven base grade, the panels once installed were both flat and level with minimal amounts of displacement at the joints. It should be noted that a French drain was constructed around the perimeter of the testing site. In this manner, rainfall and runoff is directed around the jobsite and prevents accumulation of increased moisture, and also prevents super-saturation of the subbase materials.

Figure 27 Base grading and compaction

Figure 28 Storm water drainage all around test area

5.4 PANEL INSTALLATION

The panels were delivered to the jobsite and assembled shortly after base preparation was completed. The panels were hauled to the jobsite by the fabricator and were unloaded using a five-ton rough terrain forklift. After the pavement panels were unloaded, Styrofoam® liners that were used to create the voids under the panels were removed. The process of removing the Styrofoam was completed in two days. Even so, this is one portion of the fabrication where ready-made void forms would be more easily installed and removed when compared to Styrofoam blocks. On the third day, the panels were assembled atop the base course. Two layers of bond breaker polyvinyl plastic sheeting were placed between the base course and the pavement segments. A bitumen sealant was used around the perimeter of the pavement, between the panels and the bond breaker, to prevent grout from leaking. The same sealant was used around the ducts between panels to prevent grout from leakage when grouting the ducts. Furthermore, the anchor recess formers were removed and the area around was cleaned in preparation for the strands. Placement of the pavement panels atop the base materials and placement of the polyvinyl sheeting is depicted in Figure 29 and Figure 30.

Figure 29 Panels placement on friction reducing membrane

Figure 30 Marking ducts location for alignment

Figure 31 Panels shear key at joint

Figure 32 Pavement panels assembled and ready for post-tensioning

5.5 STRAND PLACEMENT & POST-TENSIONING

Post-tensioning hardware including the ducts and the anchorages was supplied by V-Structural under contract with Oklahoma State University (OSU). Some of the end anchorages are shown in Figure 32. V-Structural was also contracted to perform the post-tensioning and grouting of the tendons and under panel voids. Initially strands and grout were delivered to the site. The post-tensioning contractor started by cleaning the ducts and anchors and cutting the strands. Next, the contractor threaded the strands through the ducts, installed anchors and anchors caps, and performed air tests to ensure the airtightness of the post-tensioning ducts. The strands were post-tensioned to 31 kips. each to achieve the required prestressing force. Lastly, the ducts and voids were grouted using special grout provided by the contractor. The conduct and completion of post-tensioning and grouting are shown in Figure 34 through Figure 40.

Figure 33 Grout being delivered to jobsite

Figure 34 Strand threaded manually through ducts for Pavement III

Figure 35 Hardware used at strands tip for better threading

Figure 36 Tendons stressing for Pavement III

Figure 37 Anchor head and grout port for two strand system

Figure 38 Sealed anchor with grouting hose for two strand system

Figure 39 Sealed four strand anchor head with grouting house for Pavement II

Figure 40 Grouting under panel pockets for Pavement III

Figure 41 Leaking grout at the middle of panel I-B1

Figure 42 Leaking grout at the joint of panel II-B2 and II-C

CHAPTER VI

EXPERIMENTAL PROGRAM AND TEST RESULTS

Three test panels were constructed as described in the previous sections. Each of the three test panels were built from four precast segments, and the overall dimensions of each test panel were 12 ft wide by 28 ft long. The 12 ft width dimension matches the width of a single traffic lane. In the longitudinal direction, or the direction of would be traffic, there were four pavement panels. Three of the panels were eight feet long and the fourth panel, or the anchor panel was only four feet long. The layout of each test panel is shown schematically in Figure 43.
The test variables for each of the test panels are outlined in Table 10. The variables were these:

(a) Slab thickness, and

(b) Compression stress in the concrete produced by prestressing.

Pavement Test Panels I and II were made with an overall thickness of eight inches. In these panels, thickened beam portions were eight inches thick and the slabs were only six inches thick. In the 10 in. panels, the beams were full depth and the slab was only eight inches thick. In accordance with the drawings and the intentions of the research, void spaces remained underneath the majority of the slab area. These voids were filled with cementitious grout after post-tensioning was completed.

Further, the amount of pre-compression stress varied as shown in Table 10. Static and repeated load testing were performed on each of the Pavement Test Panels, at each of the three were performed on each of the Pavement Test Panels, at each of the three locations shown in Figure 43.

	Panel Thicknesses (in)		**Prestressing in Concrete (psi)**	
Pavement Test Panel	Slab	Beam	Longitudinal (a) (Post-tensioning)	Transverse (b) (Pre-tensioning)
I	8.0	6.0	213	216
II	8.0	6.0	320	316
III	10.0	8.0	247	237
Notes:	a. Concrete compressive stresses in the longitudinal direction after all losses from post-tensioning tendons installed as per the design drawings with tendons initially stressed at 0.75 f_{pu}. b. Concrete compressive stresses in the transverse direction after all losses from pre-tensioned strands installed as per design drawings with 0.5 in. strands initially stressed at 0.75 f_{pu}.			

Table 10 Variables between Pavement Test Panels

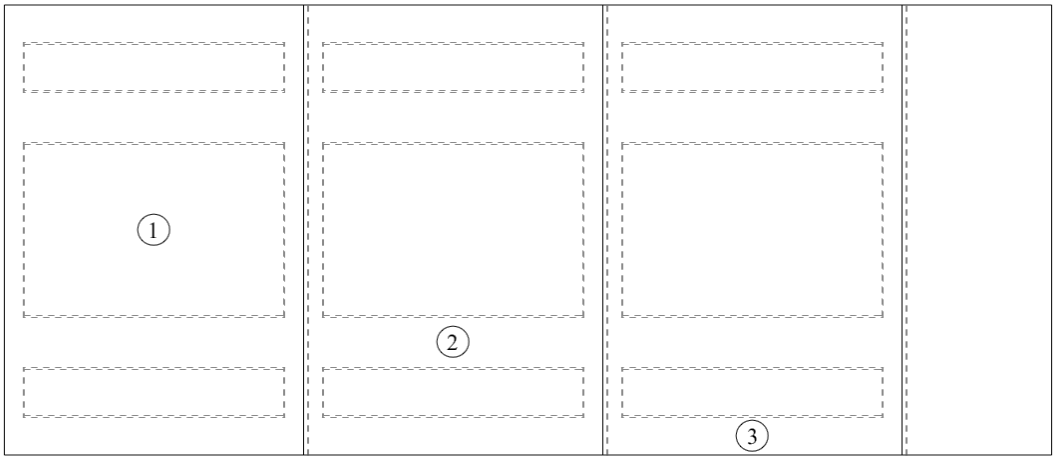

Figure 43 Static and repeated load locations

The Pavement test panels were constructed and tested on the Stillwater campus at Oklahoma State University. A testing frame was designed and fabricated to perform the testing on the Pavement Test Panels. Erection of the steel testing frame and loading ballast is depicted in Figure 44, Figure 45, Figure 46, and Figure 47. Panel III is depicted in Figure 44 where the base frame is being erected prior to testing. The testing frame consisted of structural tubing, and was designed to support grating that in turn held up to 80,000 lbs of concrete ballast. The photographs in Figure 46 and Figure 47 show the concrete blocks that were set atop the loading frame to provide ballast that resisted applied loads. The loading frame, as shown in the photographs provided sufficient strength, stiffness and ballast to allow loads up to 30,000 lb. to be applied at each individual load point. Detailed drawings of the loading frame can be found in the appendix.

Figure 44 Base frame assembled on site over Pavement III

Figure 45 Top and base frame prior to assembly

Figure 46 Concrete blocks being lifted for placement on top of the test frame

Figure 47 Final test frame assembled and ready for testing for Pavement III

6.1 INSTRUMENTATION

Instrumentation measured vertical displacement of the precast panels and load applied. Displacement of the pavement surfaces were measured at seven locations during testing using Linear Variable Differential Transformers (LVDTs). A load cell with 100 kips (100,000 lbs) capacity was used to measure the applied load. The load cell reading was cross checked with a pressure gauge on the hydraulic pump. During testing, the measured deflections and the applied load were saved to a spreadsheet using a Data Acquisition system (DaQ) running a custom LabView™ Virtual Instrument. LVDTs were attached to a tubular steel reference frame that was isolated from the test pavement and loading frame. The list of instruments can be found in Table 11. All instruments were tested and calibrated at OSU Civil Engineering Laboratory before they were used. Figure 48, Figure 50, Figure 51, and Figure 51 show the location of the LVDTs in

reference to the applied loads, and also provide photographs of the instrumentation and the reference frame that supported the LVDTs.

Description	Quantity
Laptop computer	1
National Instruments NI USB-6218 M Series Isolated Screw Terminal Data Acquisition	1
+/- 5Vdc LVDT Guided with Spring	7
Interface 100k Load Cell	1
12v Single Output Regulated Power Supply	2

Table 11 Instruments used to measure load and deflections

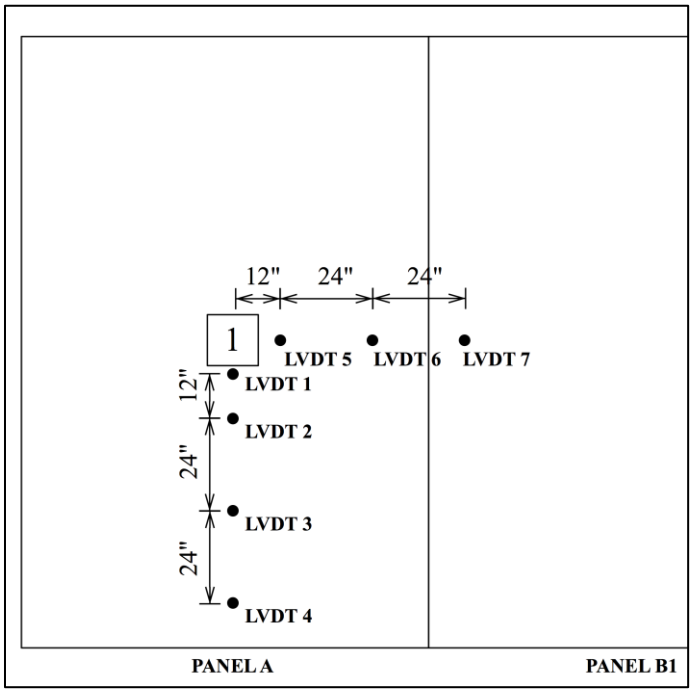

Figure 48 Instruments Layout at Test Location 1 for Test Pavement III

Figure 49 Instrumentation set for Test Location 1. Note that this test is located at the center of Panel A.

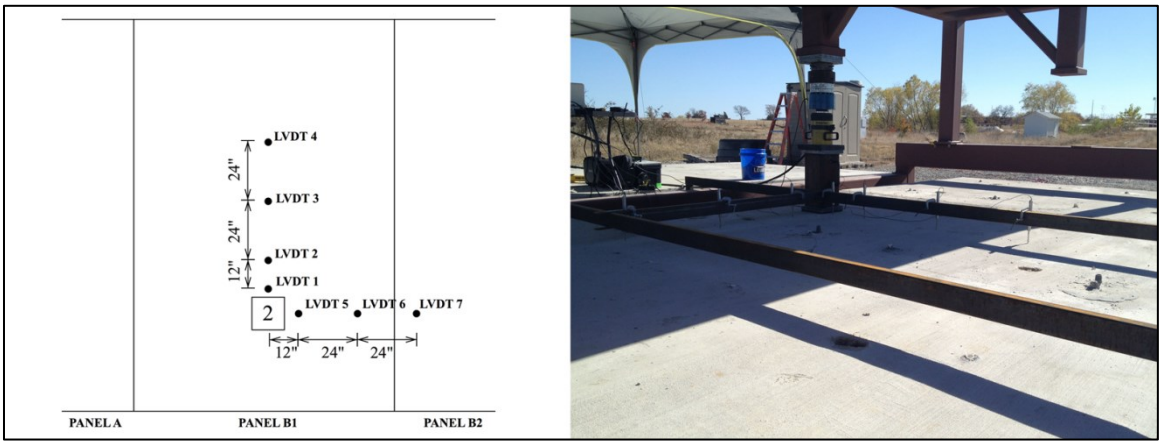

Figure 50 Instruments Layout at Test Location 2 at Test Pavement II. Test Location 2 is located over the wheel track of Panel B1, at a location supported by the thickened edge beam.

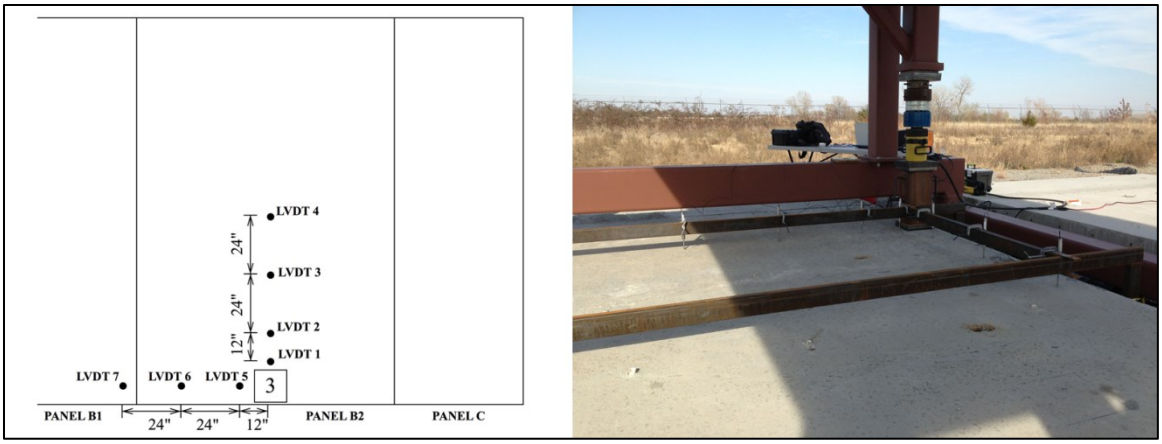

Figure 51 Instruments Layout at Test Location 3 at Panel B2. Test Location 3 is located at the edge of Panel B2, which is supported by the thickened edge beam.

Loads were applied using an hydraulic hand pump connected to an hydraulic actuator. A digital pressure gauge was used to measure pressure independently from the data acquisition system. A neoprene pad was placed at the load location between the pavement and the fabricated loading column, which can be viewed in Figure 52 along with the remaining hardware for loading. The actuator was placed on top of the column with the load cell directly above it. A spherical head was used to mitigate effects from eccentricity.

Based on 120 psi tire pressure and a total tire load of 9,000 lbs., the tire patch area was calculated to be 75 sq. in. However, for the finite element model and for the physical testing, the tire patch was represented by a nine by nine inch area (111 psi). In Figure 52, one can view the neoprene pad located between the loading column and the concrete. The base plate at the bottom of the loading column has dimensions of nine by nine inches.

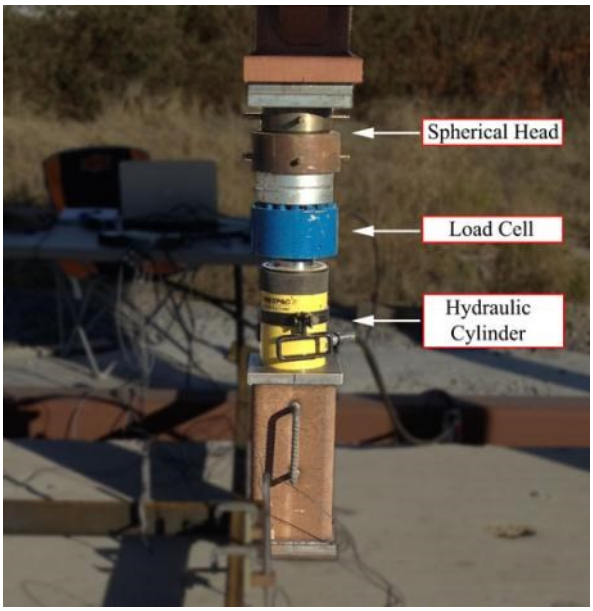

Figure 52 Loading system arrangement

6.2 LOADING PROTOCOLS

Table 12 outlines the loading protocols. For each test location, both repeated loading and a final static load was performed. The rate of loading was also controlled and the loading-time history was recorded for each test.

Number	Location	Initial Load (repeated 3 times)	2nd Load (repeated 3 times)	3rd Load (repeated 3 times)	4rd Load (repeated 3 times)	Final Load (Static)
1	Center of slab	4.5 kips	9 kips	18 kips	27 kips	30 kips
2	Beam at traffic wheel path	4.5 kips	9 kips	18 kips	27 kips	30 kips
3	Edge	4.5 kips	9 kips	18 kips	27 kips	30 kips

Table 12 Static and repeated tests loads

6.2.1 PAVEMENT REPEATED LOAD TESTS

Repeated load tests were used to measure pavement deflections and observe behavior under repetitive loads of 4,500 lbs., 9,000 lbs., 18,000 lbs., and 27,000 lbs. The repeated load test is important in verifying the linear-elastic response of the pavement. The Load vs. Time history for each Test Location is shown in Figure 53. At each load level, the peak load was repeated three times. After achieving target loads, the load was maintained for five minutes. The figure also shows the rate of loading for each loading. The loading rates were 4.5 kips per minute for repeated loads to 4.5 kips and 9.0 kips, 6.0 kips per minute for loading to 18 kips and 9.0 kips per minute for loading to 27.0 kips

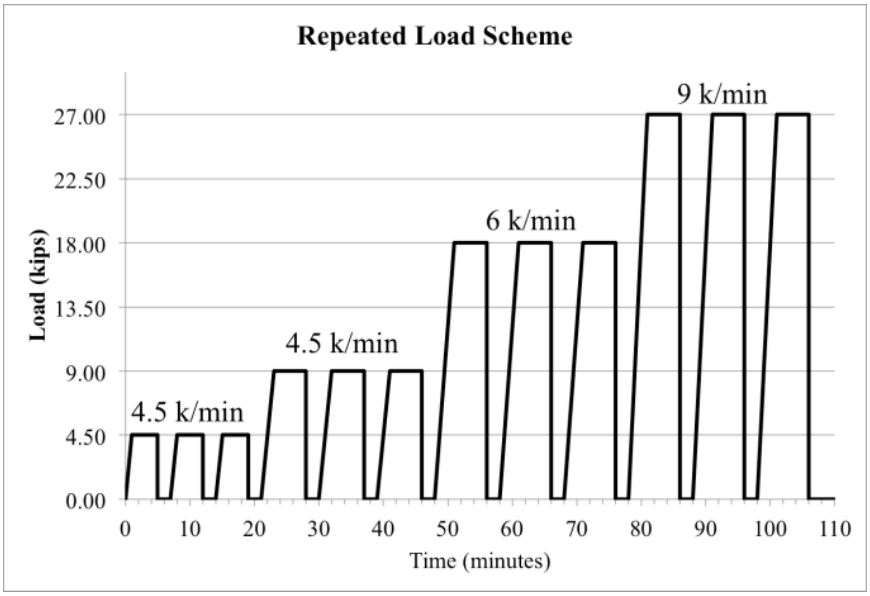

Figure 53 Repeated load scheme

As an example of testing procedures, the first test of the 4.5 kip repeated load test is described. The procedure for this test was as follow:

1. Record deflection readings before loading.
2. Increase load to the required magnitude (4.5 kips) at the prescribed rate (4.5 kips/min).

3. Immediately record deflection readings at 4.5 kips.

4. Maintain the load for five minutes.

5. Record deflection and load readings at five minutes.

6. Unload the pavement.

7. Record deflection readings after unloading.

8. Allow the system to recover without load for two minutes.

9. Repeat as per the loading chart.

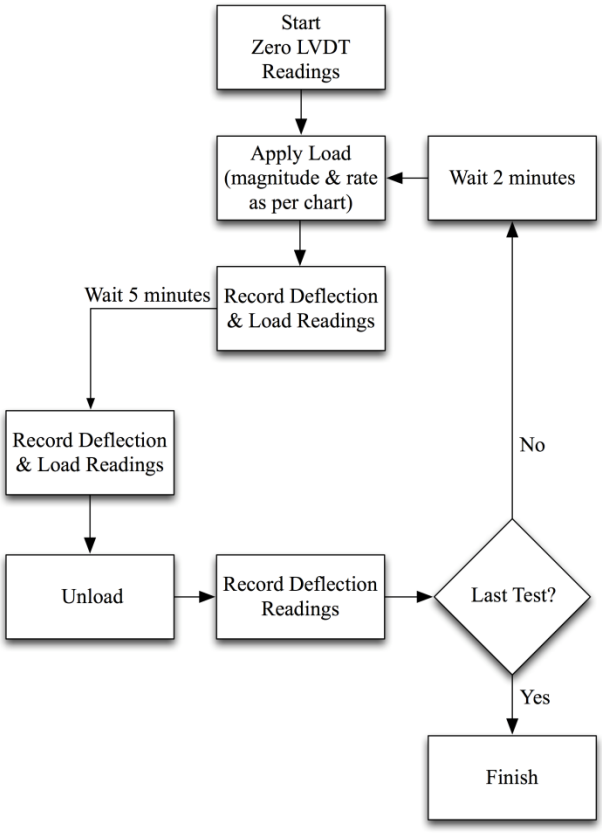

Figure 54 Repeated load test procedure for 9k, 18k and 27k loads

The load cell and LVDTs readings were taken every ten seconds and automatically recorded to a spreadsheet file. Furthermore, manual readings of deflection and hydraulic pressure

were taken during testing as a backup to electronic readings. Also, a record of visual observations was made. In addition to deflection and load measurements, ambient and pavement temperatures were recorded before and after testing.

The results from load vs. deflection readings (from LVDT 1) are shown in Table 13. LVDT 1 is the deflection measurement nearest the load point. Panel A refers to test location 1, which is located at the center of Panel A. Panel B1 refers to test location 2 where the load is at the wheel path of Panel B1. Panel B2 refers to test location 3 where the load is at the edge of Panel B2. Results indicate increasing deflections with increasing loads, as expected. In the table, positive numbers reflect downward deflections.

As an example, the displacement of LVDT1 showing the surface deflection near the load point is shown below. The deflections were all measured at the 3rd loading to 27,000 lbs. on Test Location 1, which is located at the center of Panel A for all three test pavements.

Test Panel I	(8 in. panel)	0.0313 in.
Test Panel II	(8 in. panel)	0.0240 in.
Test Panel III	(10 in. panel)	0.0218 in.

Deflection readings in Table 13 are continuous for each load test with each column in the table representing a complete repeated load test for the mentioned panel. The last reading in each column in the table indicates that a permanent deflection was recorded after the completion of each repeated load test. For an example, the permanent deflections for Test Location 1, which is located at the center of Panel A for all three test, are shown below. When viewing these results, one can conclude that the residual displacements are small, and the measured residuals do not constitute a pattern where conclusions can be drawn

Test Panel I	(8 in. panel)	0.0025 in. (downward)
Test Panel II	(8 in. panel)	0.0057 in. (upward)
Test Panel III	(10 in. panel)	0.0072 in. (downward)

Test Results, Pavement Displacements (in) at LVDT 1									
Load	**Pavement I**			**Pavement II**			**Pavement III**		
(kips)	Panel A	Panel B1	Panel B2	Panel A	Panel B1	Panel B2	Panel A	Panel B1	Panel B2
0	0.0000	0.0000	0.0000	0.0000	0.0000	0.0000	0.0000	0.0000	0.0000
4.5	0.0046	0.0040	0.0072	0.0034	0.0034	0.0079	0.0027	0.0021	0.0057
0	0.0024	0.0007	0.0014	0.0000	0.0022	0.0027	-0.0014	0.0018	0.0015
4.5	0.0071	0.0039	0.00841	0.0041	0.0042	0.0092	0.0008	0.0040	0.0070
0	0.0001	0.0006	0.0000	-0.0051	0.0017	0.0025	0.0000	0.0006	0.0009
4.5	0.0056	0.0036	0.0064	0.0012	0.0042	0.0091	0.0024	0.0020	0.0059
0	0.0024	0.0007	0.0010	-0.0015	0.0015	0.0024	0.0005	0.0017	0.0010
9	0.0112	0.0079	0.0146	0.0073	0.0051	0.0162	0.0049	0.0045	0.0116
0	0.0016	0.0030	0.0031	-0.0007	-0.0026	0.0045	0.0004	0.0012	0.0008
9	0.0109	0.0088	0.0161	0.0083	0.0022	0.0185	0.0070	0.0065	0.0121
0	0.0036	0.0037	0.0047	0.0006	0.0005	0.0057	0.0027	0.0030	0.0015
9	0.0115	0.0101	0.0176	0.0111	0.0053	0.0189	0.0082	0.0071	0.0122
0	0.0000	0.0037	0.0052	-0.0135	0.0038	0.0061	0.0040	0.0035	0.0008
18	0.0201	0.0183	0.0327	0.0054	0.0146	0.0343	0.0157	0.0115	0.0223
0	0.0018	0.0064	0.0086	-0.0098	0.0072	0.0096	0.0041	0.0020	0.0009
18	0.0226	0.0197	0.0327	0.0110	0.0181	0.0374	0.0153	0.0099	0.0227
0	0.0014	0.0063	0.0085	-0.0080	0.0095	0.0117	0.0010	-0.0006	0.0005
18	0.0221	0.0215	0.0364	0.0097	0.0188	0.0389	0.0154	0.0057	0.0223
0	0.0009	0.0081	0.0091	-0.0058	0.0104	0.0129	0.0063	-0.0046	-0.0003
27	0.0313	0.0285	0.0512	0.0207	0.0268	0.0538	0.0215	0.0064	0.0334
0	0.0018	0.0114	0.0105	-0.0064	0.0126	0.0118	0.0046	-0.0077	0.0009
27	0.0313	0.0333	0.0543	0.0203	0.0297	0.0567	0.0212	0.0042	0.0340
0	-0.0006	0.0138	0.0138	-0.0047	0.0112	0.0117	0.0050	-0.0118	-0.0001
27	0.0313	0.0348	0.0590	0.0240	0.0287	0.0593	0.0218	-0.0004	0.0346
0	0.0025	0.0127	0.0170	-0.0057	0.0140	0.0130	0.0072	-0.0132	0.0037

Table 13 Repeated load test deflections for LVDT 1 (inches)

Figure 55 provides a visual representative of the time history of the loading on Test Pavement I, at Test Location 1 on Panel A. Loading vs. time is shown in the solid line. The loading history is obtained from the physical measurements during the testing so the loading history reflects some relaxation in the applied load within the loading intervals. One can also view the slope of the line which would reveal the rate of loading.

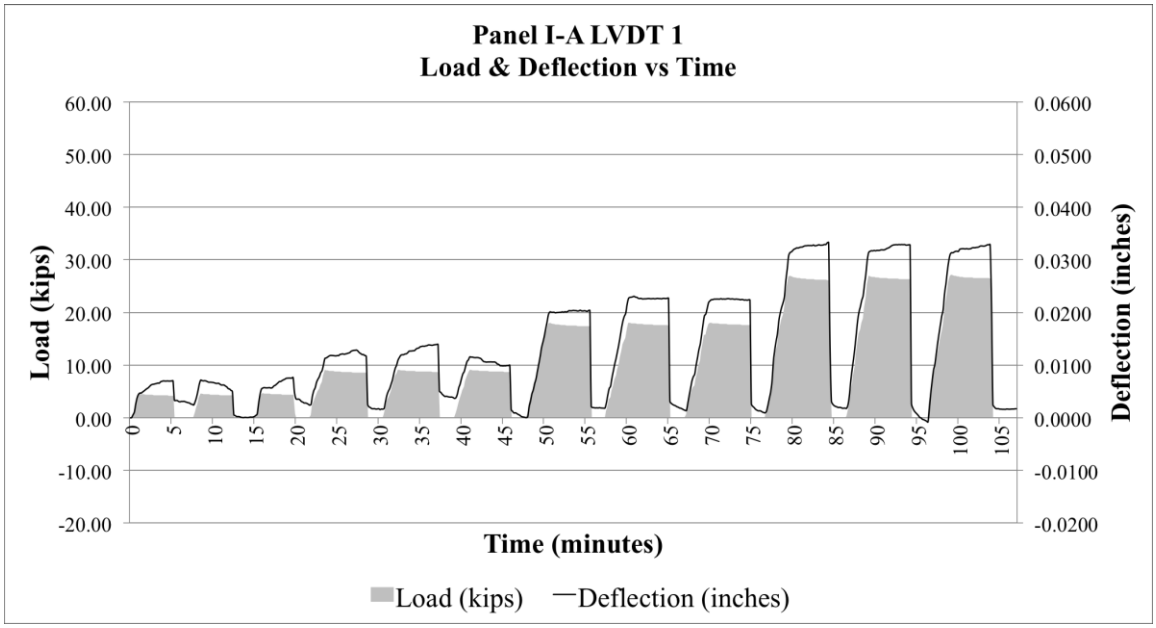

Figure 55 Repeated load & LVDT 1 deflection plotted against time for Pavement I Panel A

Figure 56 and Figure 57 represent of the time history of the loading on Test Pavement I Panels B1 and B2, respectively. Loading vs. time is shown in the solid line. The loading history is obtained from measurements during the testing. Similar to Figure 55, the loading history reflects some relaxation in the applied load within the loading intervals. The figures also reflect permanent deflections at the end of the repeated load test.

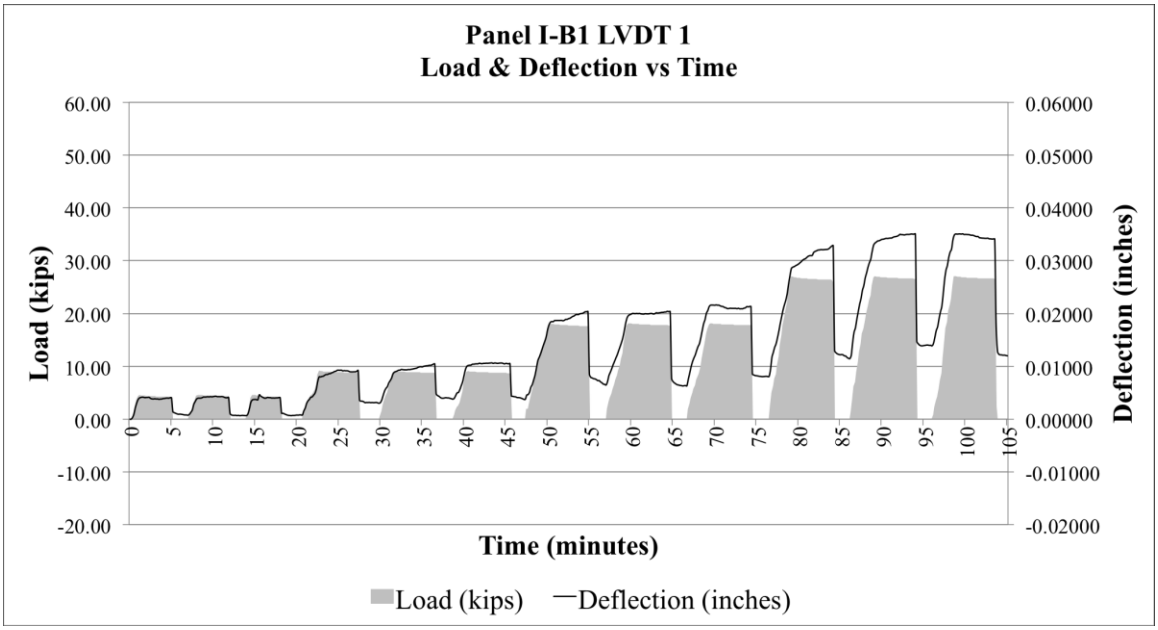

Figure 56 Repeated load & LVDT 1 deflection plotted against time for Pavement I Panel B1

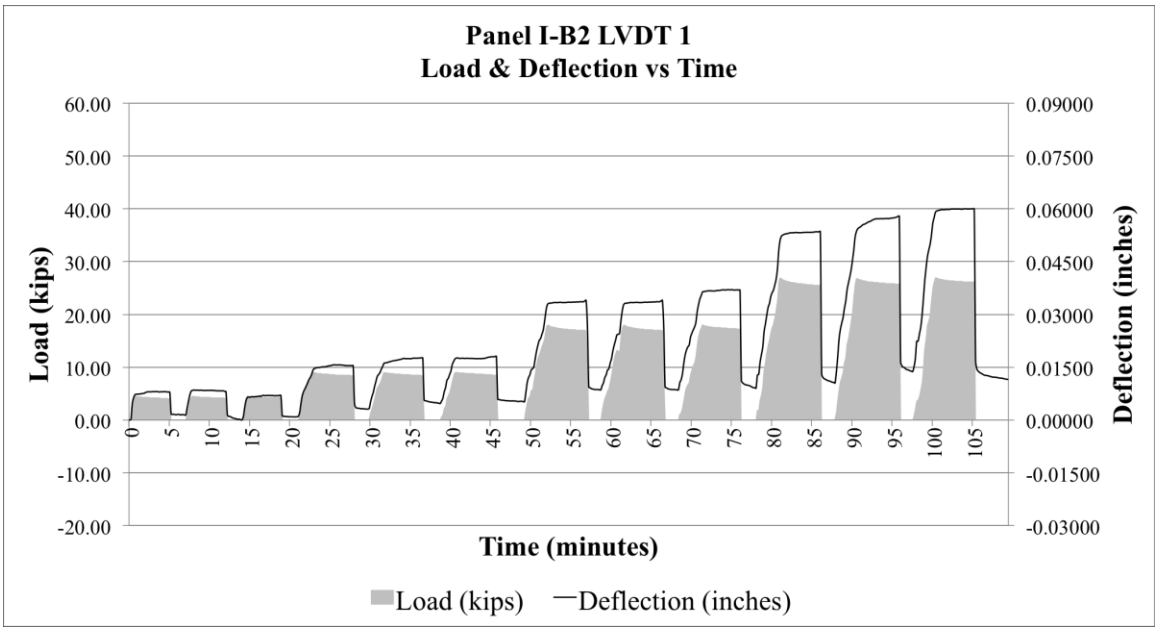

Figure 57 Repeated load & LVDT 1 deflection plotted against time for Pavement I Panel B2

It can be noted from Table 13 and previous figures that the pavement deflection did not return to zero after each load and unload cycle. Furthermore, the pavement deflection did not return to zero after the entire repeated load test was completed. This indicates that the applied

loads have compressed the subbase. However, the change in deflection before and after each load cycle of the same magnitude remained almost the same in most cases.

For example, Pavement I Panel A first 4.5k load recorded a downward deflection of 0.0046 in. at LVDT 1 and after unloading there was 0.0024 in. downward permanent deflection. When the panel was loaded again to 4.5k, the recorded pavement downward deflection was 0.0071 in. indicating that a change in pavement deflection of 0.0047 in. (0.0071 in. – 0.0024 in = 0.0047 in.), which is almost the same as the first 4.5k load deflection of 0.0046 in. In some cases, the changes in deflection between the same magnitude load cycles were different. These differences are small compared to the pavement deflection and could be due to changes in ambient and pavement surface temperatures, which could cause curling as discussed in section 3.2.2.

6.2.2 STATIC LOAD TESTS TO 30,000 LBS

Static tests were performed at the end of each repeated load test by applying a 30 kips load at the repeated test location. The load was applied at a rate of 2,000 lbs/min and maintained for a period of ten minutes. Load cell readings and deflection measurements were recorded every 10 seconds during the test. The static test procedure is as follows:

1. Zero all LVDTs readings for the current location.
2. Increase load to 30 kips at a rate of 2 k/min (15 minutes to reach 30 kips).
3. Immediately record deflection readings at 30 kips.
4. Maintain the load for five minutes.
5. Record load cell and deflection readings.
6. Continue to re-apply pressure to maintain 30 kips as necessary.
7. Maintain the load for five minutes.

8. Record deflection and load cell readings.

9. Apply pressure to re-acquire 30 kips if necessary.

10. Record deflection and load cell readings immediately after reload.

11. Unload the system.

12. Record deflection readings.

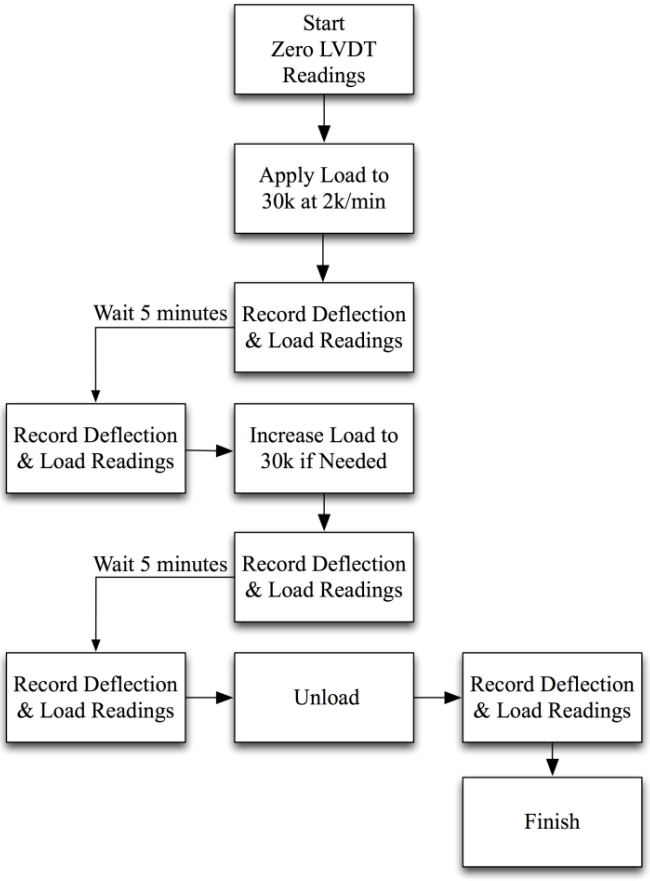

Figure 58 Static load test procedure

Results for load and deflection readings for all pavement panels at load application location (LVDT 1) are shown in Table 14. Test Pavement I and Test Pavement II have the same slab and beam thicknesses. As expected, the deflections between these two test panels are

similar. It is worth noting, however, that Pavement II is subjected to higher prestress force as per the pavement design. Test Pavement III is thicker by two inches than the other two test panels, and the resulting stiffness is reflected in the deflection measurements.

Note that the repeated test loads deflections for measurements were not reset after each cycle and this causes the results to look different but in fact the results are similar if one measures the deflections as the difference when the load is zero and when the load is fully applied. For example, Table 13 shows that Panel III-B1 (load location 3) deflected --0.0004 in before the last 27k was removed but the deflection before unload was -0.0118 and this gives total deflection of -0.0114 in. Furthermore, Pavement III was reloaded with 50k load at all load locations prior to the actual tests here. The reload was necessary to test the load frame and equipment and might have increased the stiffness of the subgrade causing inconsistent results.

As indicated in the testing procedures and with the instrumentation plans, seven LVDT measurements of pavement deformation were made and recorded during each test. The results indicate that the deformation response effectively decays, or diminishes with distance from the point of loading. Figure 59 shows the deflection readings for all LVDTs over the duration of the test for Pavement I Panel A. The graph indicates uniform deflection in at given distances from the load in both directions. Other static load tests at the other testing locations showed similar patterns.

The arrayed LVDT's allowed us to construct deflection profiles during each of the tests. We are interested in seeing the panel deformations as a function of distance from loading, plus the deflection data can provide a snapshot of the effectiveness of load transfer across the panel joints. As noted in Table 14, the maximum measured deflection at LVDT 1 for Panel I-A was 0.0321 in. Other LVDTs measured deflections at transverse distances of zero, 12 in., 36 in., and 60 in. from the loading point (Locations of the LVDTs are shown in Figure 48). The actual deflections in Figure 59 indicate the maximum deflection of 0.0321 in. near the load point with

deflections decreasing with distance from the load point. At LVDT 4, the surface deflection is about 0.008 in.

Load (kips)	Pavement I			Pavement II			Pavement III		
	Panel A	Panel B1	Panel B2	Panel A	Panel B1	Panel B2	Panel A	Panel B1	Panel B2
0	0.0000	0.0000	0.0000	0.0000	0.0000	0.0000	0.0000	0.0000	0.0000
30	0.0321	0.0234	0.0547	0.0349	0.0207	0.0524	0.0163	0.0063	0.0377
0	-0.0035	0.0009	0.0090	0.0040	0.0010	0.0016	0.0018	-0.0116	0.0047

Table 14 Static load test deflections for LVDT 1 (inches)

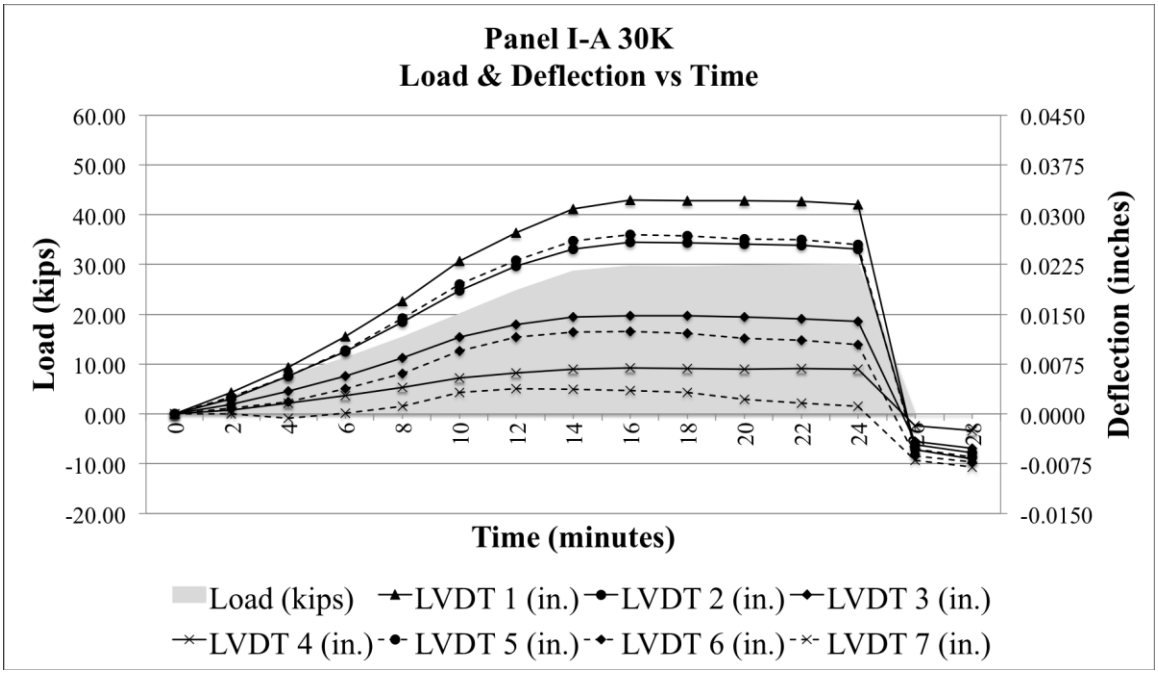

Figure 59 Static load & deflections plotted against time for Pavement I Panel A

Figure 60 shows the deflections readings for the static test to 30,000 lbs performed on test Panel I-A (Panel I-A at Test Location 1) at the load location (LVDT 1). The data was taken from the physical measurements during the testing. The coefficient of determination, R^2, was calculated to be 0.99825 for this test. The coefficient of determination shows how well a

regression model fits the data with value closer to 1.0 indicating better fit. Figure 61 and Figure 62 also show deflections for the 30k static load tests for Panels I-B1 and Panel I-B2, respectively. The coefficients of determination, R^2, for both tests are 0.99982 and 0.98848 for Panel I-B1 and Panel I-B2, respectively. This indicates the data can be represented by a straight line as shown in these figures. The response of the pavements to loads up to 30k remained linear and therefore the supporting subgrade can be modeled as linear springs with accuracy.

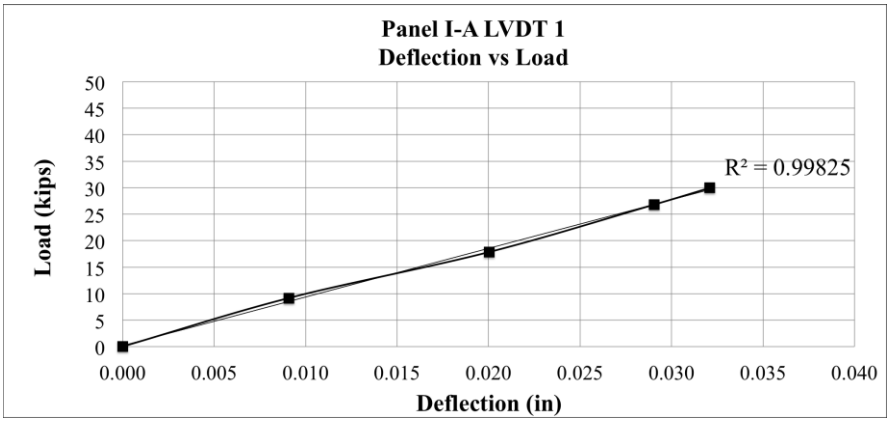

Figure 60 Deflection vs Load for Panel I-A LVDT 1 linear relationship

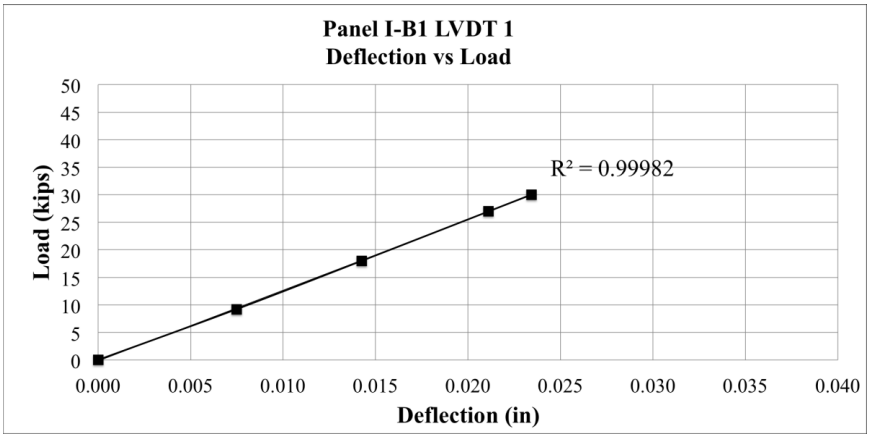

Figure 61 Deflection vs Load for Panel I-B1 LVDT 1 linear relationship

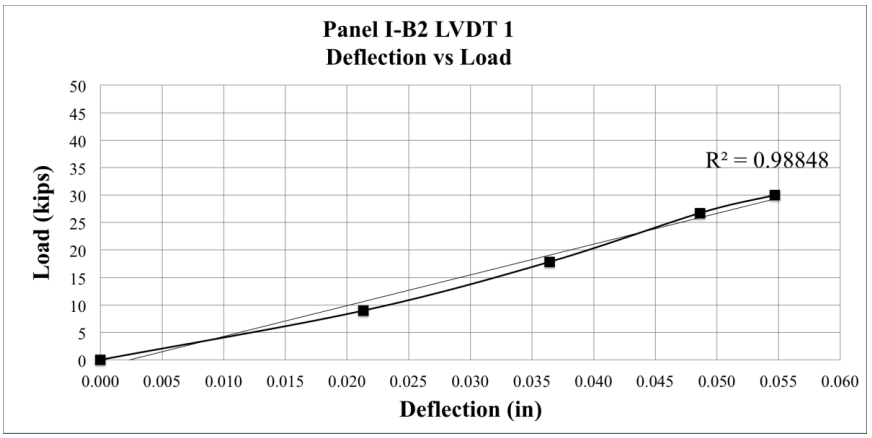

Figure 62 Deflection vs Load for Panel I-B2 LVDT 1 linear relationship

Additionally, Figure 63 and Figure 64 show deflections for the 30k static load tests for Panels II-A and Panel III-A, respectively. The coefficients of determination, R^2, for both tests are 0.9884 and 0.99963 for Panel II-A and Panel III-A, respectively. The figures show that the response remained linear regardless of position, pavement thickness, and prestress magnitude for loads up to 30k and therefore the supporting subgrade can be modeled as linear springs with accuracy. Other tests showed similar linear relationship. See Appendix E

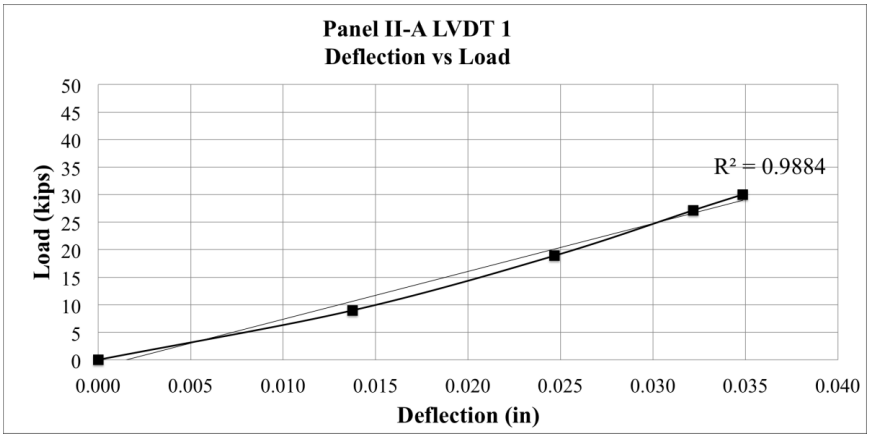

Figure 63 Deflection vs Load for Panel II-A LVDT 1 linear relationship

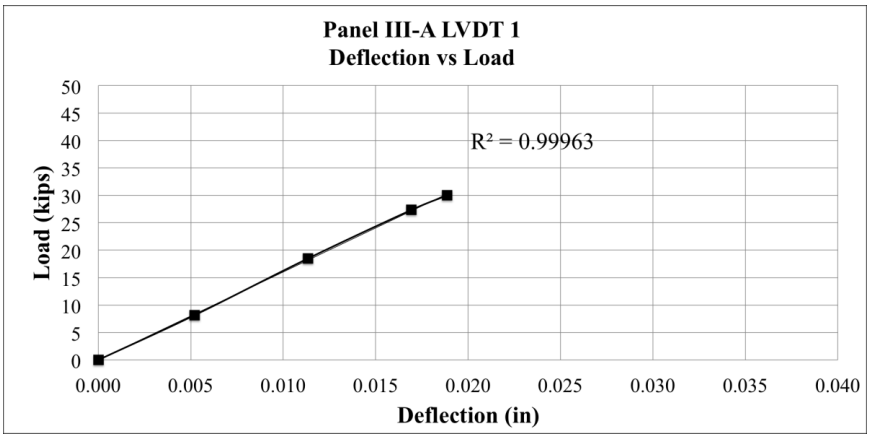

Figure 64 Deflection vs Load for Panel III-A LVDT 1 linear relationship

6.3 SUMMARY

Three Test Pavements were constructed and tested. Each Test Pavement consisted of three pavement panels. Two set of tests were performed on each pavement panel. Repeated load tests were used to measure pavement deflections and observe behavior under repetitive loads of 4,500 lbs., 9,000 lbs., 18,000 lbs., and 27,000 lbs. Static tests were performed at the end of each repeated load test by applying a 30 kips load at the repeated test location.

The repeated and static loads tests provided valuable information related to the analysis and design assumptions. Both test showed that load vs deflection remained linear even loads reaching 30,000 lbs.

CHAPTER VII

RESULTS AND DISCUSSION

This chapter contains results and discussion pertaining to the various structural analysis and test results. Three analysis procedures – finite element analysis (FEA), beam on elastic foundation (BEF) subjected to stationary load, and beam on elastic foundation (BEF) subjected to moving load – are used to determine pavement stresses and deflections. The FEA was used to calculate pavement stresses when the pavement is subjected to non-uniform subbase support and determine whether grouting voids are necessary. The static and dynamic BEF closed for solution will developed and the solution will be used to determine the minimum pavement thickness for pavement with finite and infinite length. The load tests performed on the test pavements will be modeled using FEA and BEF and the results will be compared to determine the viability of using the BEF method as design tool.

7.1 FEA OF PAVEMENT WITH NON-UNIFORM BASE SUPPORT

FEA was also used to analyze various conditions where the PPCP panels were supported by non-uniform bearing. The number of possible variations is without limit and to examine each and every case would be impossible. However, there exist few critical support conditions based on sub base condition and panel response to temperature and moisture changes. The support

conditions are shown in Figure 65 and Figure 68. The pavement is supported in areas shaded with gray color.

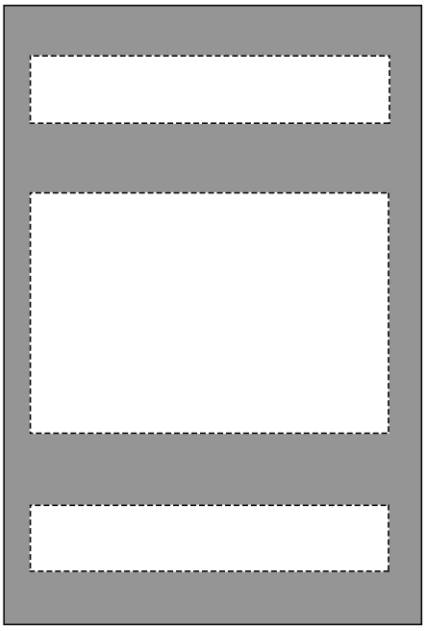

Figure 65 Support Case I Panel is supported only at the thickened beams.

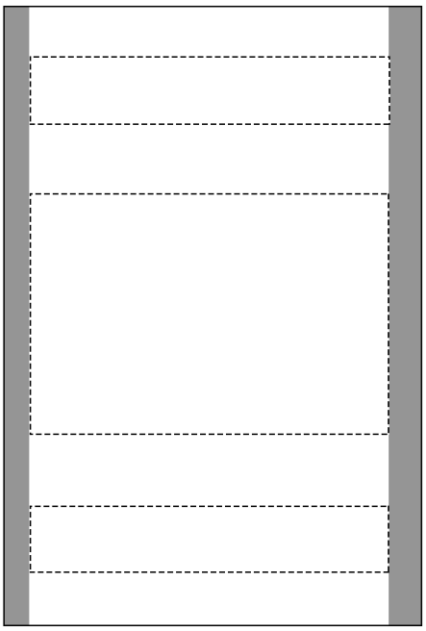

Figure 66 Support Case II Panel is supported at edges, which span the length of the panel or 8’-0.

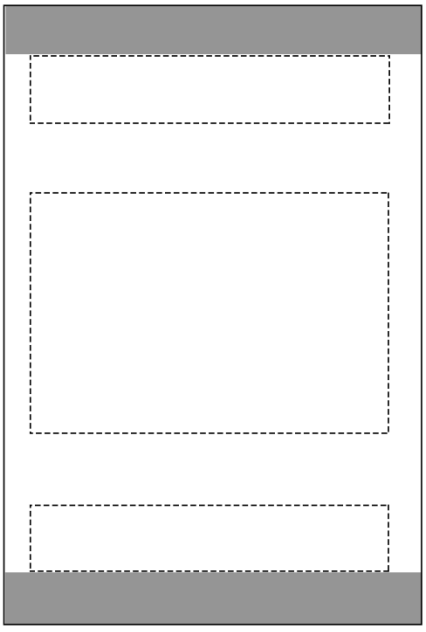

Figure 67 Support Case III Panel is supported at its edges which span the width of the panel or 12’-0.

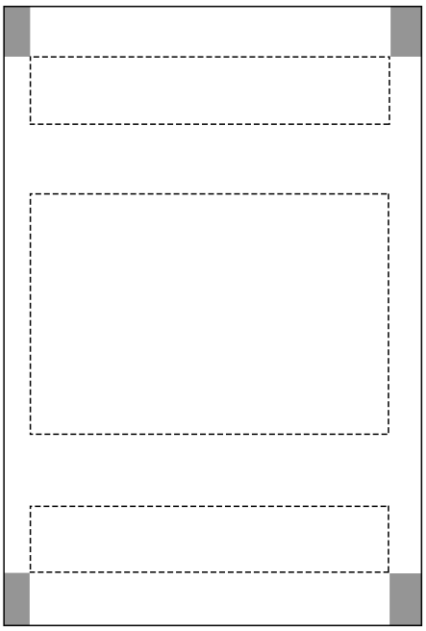

Figure 68 Support Case No. IV The panel is supported only at its corners.

Support conditions shown are considered critical as there is high probability that at least one will actually happens during the pavement life. Support Case I is usually when the pavement is placed on the subbase before grouting. It could also be the result of insufficient grouting. Case II and III are due to uneven support subbase while case number IV could be caused by pavement curling due to temperature or humidity.

The cases above were analyzed using FEM and the same load conditions discussed in CHAPTER IV. As expected, the stress levels were higher than that of uniform subbase support. Table 15 and Table 16 shows a summary of the maximum longitudinal and transverse tensile stresses and compare them to uniform support stresses from Table 4. The maximum tensile stresses in the tables are caused by LC2 where one wheel is at the edge.

Pavement	Maximum Longitudinal Tensile Stress (psi)					
	Uniform Support	Case I	Case II	Case III	Case IV	Maximum Increase in Stresses
I & II	355	449	679	408	742	387
III	232	282	416	248	454	222

Table 15 Maximum longitudinal tensile stresses for non-uniform support compared to uniform subbase support stresses

Pavement	Maximum Transverse Tensile Stress (psi)					
	Uniform Support	Case I	Case II	Case III	Case IV	Maximum Increase in Stresses
I & II	227	283	224	516	500	289
III	120	159	121	307	297	187

Table 16 Maximum transverse tensile stresses for non-uniform support compared to uniform subbase support stresses

The results above indicate an increase in tensile stresses of more than 100 percent over uniform subbase support. Longitudinal tensile stresses for Pavement I & II Case II and Case IV above exceed the design modulus of rupture of concrete (530 psi). However, Case IV is an extreme example of worst case scenario and considering such case for design might not be feasible in design since it required more than twice the prestressing force to achieve the stress levels as the original designs. On the other hand, Case II is more likely to exist and could be problematic in long term. Even with Pavement II post-tensioning (320 psi), the stress in concrete (359 psi) is still above the concrete fatigue endurance limit of 265 psi and could reduce pavement life. The non-uniform support cases have minimum impact on the thicker Pavement III since the

prestress and post-tension stresses will counter the stresses caused by the load and keep such stresses below the concrete fatigue endurance limit.

The results above further confirm that grouting between the pavement and subbase is important. The results also indicate that under pavement grouting is more critical in thinner pavement with Pavement I/II (8 in.) being more critical to stress increase than Pavement III (10 in.). Since thinner pavements are more sensitive to variation in subbase support, it is recommended that higher prestress levels be used as pavement thickness decreased to improve pavement performance and durability.

7.2 BEAM ON ELASTIC FOUNDATION SUBJECTED TO STATIONARY LOAD

One of the objectives of this research is to develop generalized classic solutions for finite and infinite length beam on elastic foundations (BEF) to determine minimum pavement thickness. PPCP are structurally more continuous when compared to jointed pavements. The continuity of post-tensioned PPCP systems lends analysis to that of a BEF. In the mid- to late 19^{th} century, classical methods for BEFs were developed for rail road engineering. These same principles can be applied to any continuous structural element supported at regular intervals by other structures or by soils.

Analyses were performed where PPCP structures were subjected to stationary loads. Stresses and deflections for the pavement structures were analyzed using BEF techniques. The general analysis for BEF is described below. Solutions for deflections of BEF caused by static loads can be compared to that from the FEA and experimental test results. The general solution for BEF follows.

Consider an elastic simply supported beam subjected to arbitrary loading as shown below in Figure 69.

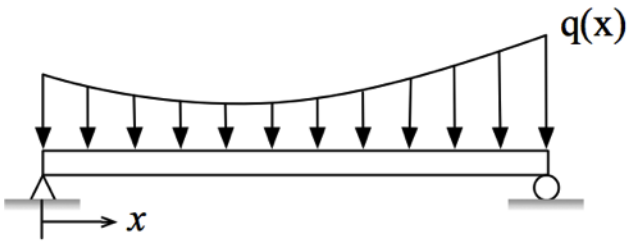

Figure 69 simply supported beam

Using the classical beam theory, the load (q) on the beam can be expressed as the derivative of the shear with respect to the x as in Equation 3. The negative sign of the load indicate that load is acting downward, so the sign convention has positive deflections and forces acting upward.

$$-q = \frac{dV}{dx} \qquad \text{Equation 3}$$

The internal shear can also be expressed as the derivative of the internal bending moment with respect to distance x.

$$V = \frac{dM}{dx} \qquad \text{Equation 4}$$

From Equation 3and Equation 4, the load can be expressed as the second derivative of the bending moment with respect to x as shown in Equation 5. Furthermore, fundamental beam mechanics dictate that the internal bending moment is proportional to beam curvature which is the second derivative of the beam deflection, y, as shown in Equation 6. The constant of integration between moment and curvature is the flexural rigidity, EI.

$$-q = \frac{d^2M}{dx^2} \qquad \text{Equation 5}$$

$$M = -EI\frac{d^2y}{dx^2} \qquad \text{Equation 6}$$

Combining equations Equation 5 and Equation 6, the beam equation can be written as:

$$EI\frac{d^4y}{dx^4} = -q(x) \qquad \text{Equation 7}$$

7.2.1 BEAM ON WINKLER FOUNDATION

The theory of beam on elastic foundation was developed assuming that the beam is supported by foundation system modeled as a series of independent linear springs. The reaction on the springs is assumed to be linearly proportionate to the deflection and constant along the length of the beam (Winkler 1867). The stiffness of the spring is related to the modulus of subgrade reaction, expressed as k_o with units of psi/in. Therefore, the relation between the soil pressure on the beam, p, and the beam deflection, y, can be represented as:

$$p = k_o \cdot b \cdot y = k \cdot y \qquad \text{Equation 8}$$

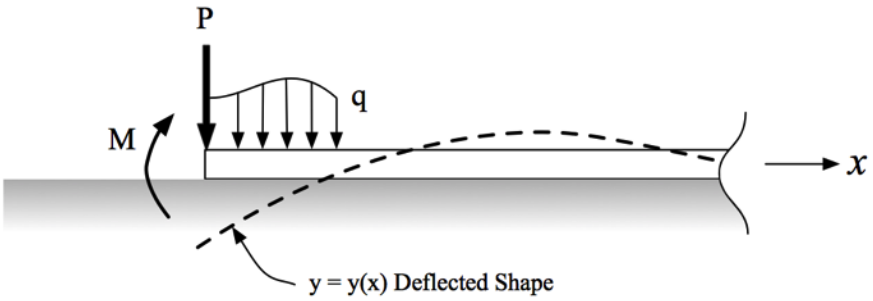

Figure 70 General deflected shape of semi-infinite beam on elastic foundation

The elastic beam Equation 7 becomes:

$$EI\frac{d^4y}{dx^4}+k\cdot y=q(x) \qquad \text{Equation 9}$$

$$\frac{d^4y}{dx^4}+4\frac{k}{4EI}y=\frac{q}{EI} \qquad \text{Equation 10}$$

To solve the differential equation above, a new stiffness term that represents the foundation and beam stiffness is introduced:

$$\beta=\sqrt[4]{\frac{k}{4\,E\,I}} \qquad \text{Equation 11}$$

The general solution for the equation can be written as:

$$y(x)=e^{\beta x}(C_1\sin(\beta x)+C_2\cos(\beta x)) + e^{-\beta x}(C_3\sin(\beta x)+C_4\cos(\beta x)) \qquad \text{Equation 12}$$

The terms C_1, C_2, C_3, and C_4 are constants of integrations that vary depending on boundary conditions. To simplify the process of solving the above equation, classical texts offer the following symbols for certain derivatives that are used to solve for deflections, shears, and bending moments. These symbols and their solutions are used for both infinite and semi-infinite BEF solutions:

$$A = e^{-\beta x}(\cos\beta x+\sin\beta x) \qquad \text{Equation 13}$$

$$B = e^{-\beta x}\sin\beta x \qquad \text{Equation 14}$$

$$C = e^{-\beta x}(\cos\beta x-\sin\beta x) \qquad \text{Equation 15}$$

$$D = e^{-\beta x}\cos\beta x \qquad \text{Equation 16}$$

7.2.2 SEMI-INFINITE BEAM ON ELASTIC FOUNDATION

The equations above can be used to derive the shear, moment, slope, and deflection equations for semi-infinite beam on elastic foundation subjected to point load and moment as shown in Figure 71. The boundary condition for the semi-infinite beam on elastic foundation can be used to determine the constants C_1, C_2, C_3, and C_4 from Equation 12.

Figure 71 Semi-infinite beam on elastic foundation

For the beam shown in Figure 71, two boundary conditions are defined at x = ∞ where both deflections and rotations must be zero. Therefore, $C_1 = C_2 = 0$. Two other boundary conditions can be defined where x = 0 where both Moment and shear must be zero. Therefore, C3 and C4 are derived as follows:

$$C_3 = \frac{3\beta^2 M}{k} \qquad \text{Equation 17}$$

$$C_4 = \frac{2\beta P}{k} - \frac{2\beta^2 M}{k} \qquad \text{Equation 18}$$

As a result, solutions for deflections, rotations, moment and shears for beam on semi-infinite foundation follow:

$$y(x) = \frac{2\beta P}{k} D - \frac{2\beta M}{k} C \qquad \text{Equation 19}$$

$$\theta(x) = \frac{dy}{dx} = -\frac{2\beta^2 P}{k}A + \frac{4\beta^3 M}{k}D \qquad \text{Equation 20}$$

$$M(x) = \frac{d^2y}{dx^2} = -\frac{P}{\beta}B \qquad \text{Equation 21}$$

$$V(x) = \frac{d^3y}{dx^3} = PC \qquad \text{Equation 22}$$

7.2.3 INFINITE BEAM ON ELASTIC FOUNDATION

Consider a finite length beam subjected to a concentrated load as shown in Figure 72. Note that x = 0 at the load location. The boundary condition for the infinite beam is that beam rotations at the load point is zero, $\theta(0) = 0$.

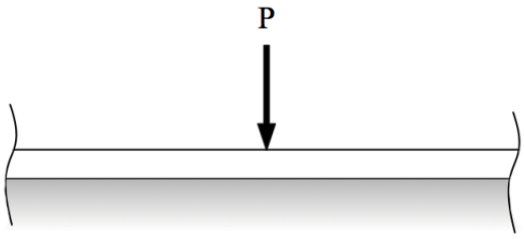

Figure 72 Finite length beam on elastic foundation

By substituting the $\theta(0) = 0$ into Equation 20, we see the following intermediate step (note *P* here is *P/2* since the load is shared by both ends of the beam).

$$\theta(0) = -\frac{2\beta\left(\frac{P}{2}\right)}{k} + \frac{4\beta^3 M}{k} = 0 \qquad \text{Equation 23}$$

Solving for *M* in Equation 23 gives:

$$M(0)= \frac{P}{4\beta} \qquad \text{Equation 24}$$

From these derivations we can obtain equations for deflection, beam rotation, bending moments and shears as follows:

$$y(x) = \frac{\beta P}{2k} A \qquad \text{Equation 25}$$

$$\theta(x) = \frac{\beta^2 P}{k} B \qquad \text{Equation 26}$$

$$M(x) = \frac{P}{4\beta} C \qquad \text{Equation 27}$$

$$V(x) = \frac{P}{2} D \qquad \text{Equation 28}$$

7.2.4 NUMBERICAL RESULTS FOR PAVEMENT AS BEF SUBJECTED TO STATIONARY LOAD

The beam on elastic foundation (BEF) theory discussed earlier was used to calculate deflection and stresses for 8 in. and 10 in. pavement. Material properties assumed for the BEF analysis matched that from the FEA that was performed. The modulus of subgrade reaction was taken as 150 psi/in and the concrete modulus was taken as 4,000 ksi.

In the FEA a pair of 9,000 lbs. point loads was applied to the pavement at the wheels path but in the BEF, the axle is assumed to support a paired point load so the total point load in the BEF is 18,000 lbs. The finite element models used in this section have length of 100 ft and width of 12 ft The length was chosen after many trials which showed that length above 100 ft did not affect the FEA results and the model acted as infinite length pavement. The effective width of the beam was taken as the full pavement width of 144 in.

Figure 73 and Figure 74 show the deflected shape for the 8 in. and 10 in. pavements, respectively. BEF analysis indicates that two paired point loads of 9,000 lbs each will cause a downward deflection under the load point of approximately 0.0089 in. as shown in Table 17. The analysis also shows uplift located from approximately 120 in. to 200 in. from the applied load for the 8 in. and 10 in. pavements, respectively. Please note that the deflected shapes for BEF below do not include the self-weight of the pavement. To overcome the uplift indicated by the analysis, a self-weight equivalent to about four in. of pavement thickness is sufficient to maintain contact with the base materials. In other words, a pavement thickness of 4 in. or more will ensure that deflections are downward over the entire length of pavement.

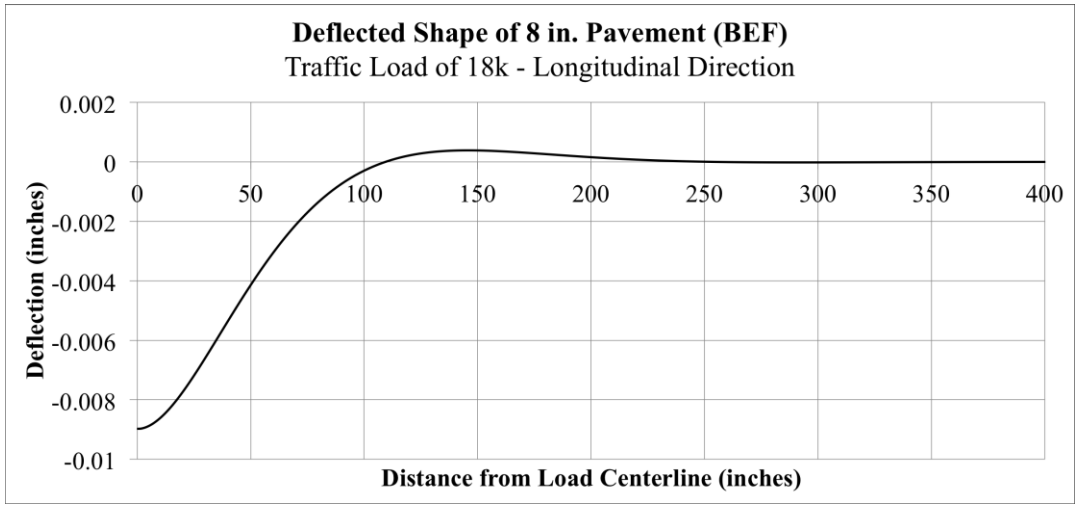

Figure 73 Deflected shape of 8 in. Pavement (self-weight not included)

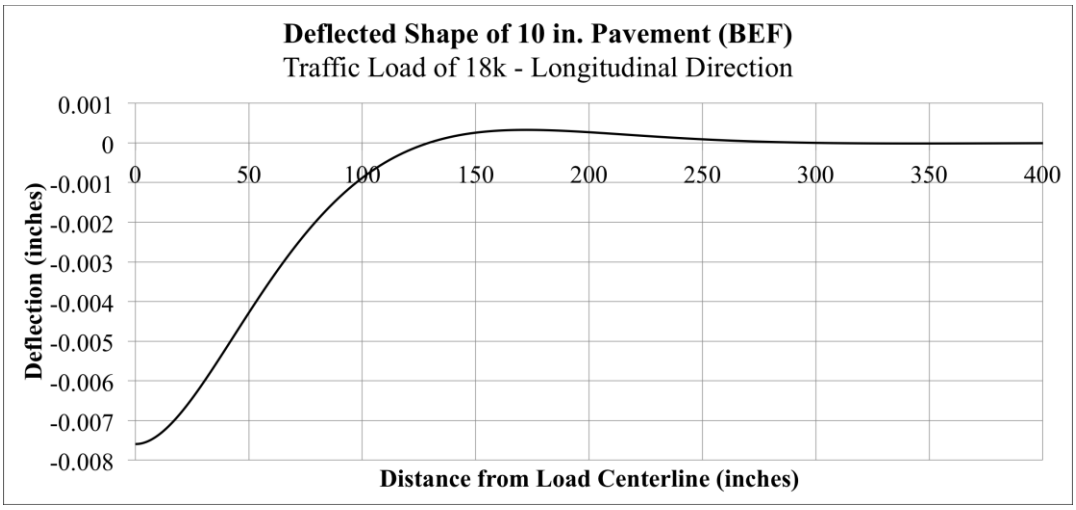

Figure 74 Deflected shape of 10 in. Pavement (self-weight not included)

Table 17 shows comparison of downward and upward deflections and maximum tensile stresses between BEF and FEM. Deflection results of the beam on elastic foundation were relatively close to that from finite element analysis. BEF stresses, on the other hand, are around 25 percent lower than FE stresses. For vehicular traffic loads, the BEF gives reasonable deflection and stresses when compared the more accurate FEM.

Pavement Thickness	Maximum Downward Deflection (in)		Maximum Uplift (in)		Maximum Tensile Stress (psi)	
	BEF	FEM	BEF	FEM	BEF	FEM
8 in.	0.0089	0.0101	0.00039	0.00049	136	183
10 in.	0.0076	0.0083	0.0029	0.00039	103	130

Table 17 Infinite length beam deflection and longitudinal stresses (BEF and FEM)

7.3 BEAM ON ELASTIC FOUNDATION SUBJECTED TO MOVING LOAD

Most pavement designs are based on static loads and ignore the dynamic nature of the vehicular and truck loads. The questions of interest here are (1) how important are dynamics on rigid pavement and (2) how thin can we make the pavement if dynamic effects are important? One of the basic questions to answer with PPCP and other prestressed concrete pavements is whether thinner pavements are possible. Static analysis of the pavement, and design based solely on stresses would suggest that because prestress forces mitigate or eliminate tensile stresses, then the pavement could be thinner. However, one must consider the implications of dynamic loadings, and the stresses and deflections that result from moving loads.

If the pavement is too thin, or in other words if the pavement does not possess adequate mass or ballast to prevent the pavement from separating from the subgrade when traffic loads are applied, the pavement cannot be expected to be durable. Separation between pavement and subgrade would cause other large deflections and vibrations that could be expected to damage the pavement and cause early and pre-mature pavement failures.

For the purposed of this research the following is assumed:

1. Pavements behave as beam on elastic foundation and only longitudinal load movement is considered. Transverse movement is neglected.
2. The foundation supporting the beam is considered damped Winkler foundation. Furthermore, full contact between the beam and foundation is assumed.
3. Beam cross-section and the foundation are assumed to have the same properties along the beam length.

In this section, the theoretical "exact" solution for damped Winkler beam on elastic foundation subjected to moving load will be developed for finite and infinite length beam. The solution will consider a beam subjected to constant load moving at a constant speed and will account for energy dissipation (damping) through the foundation by using dashpots.

7.3.1 DYNAMICS OF FINITE LENGTH BEAM ON ELASTIC FOUNDATION

Consider a beam of length L on uniform continuous support as shown in Figure 75. The beam mass is m, Young's modulus of E, moment of inertia of I, and damping coefficient of c_b. The support is considered to have a spring constant of k and damping coefficient of c_s. The beam and soil properties are expressed per unit length. Furthermore, force $p(t)$ moves along the length of the beam at a constant speed of v.

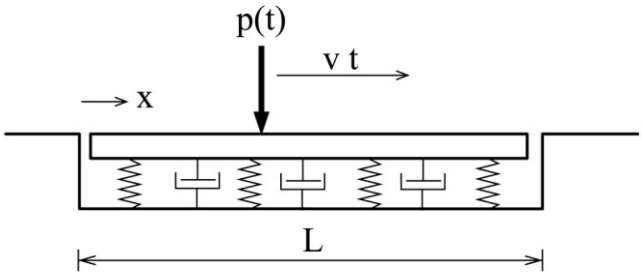

Figure 75 Beam on elastic foundation subjected to moving load

The equation of motion for the beam can be expressed as follow (Frýba 1999) and (Cebon 1985):

$$EI\frac{\partial^4 y}{\partial x^4}+m\frac{\partial^2 y}{\partial t^2}+c\frac{\partial y}{\partial t}+ky=p(t)\delta(x-vt) \qquad \text{Equation 29}$$

Where δ is the Dirac delta function centered at $x = vt$ and is a mathematical representation of the traveling point load. The damping term c in the equation represents beam damping, c_b, and subgrade radiation damping, c_s, with units (*lbf-sec/inch*) per unit length. They can be determined by knowing the radiation damping ratio λ (Chatti 1992)

$$c_b = 2\,\lambda_b\,\beta_1^2\,\sqrt{E\,I} \qquad \text{Equation 30}$$

$$c_s = 2\,\lambda_s\,\sqrt{k\,m} \qquad \text{Equation 31}$$

In Equation 30 and Equation 31 the terms λ_b and λ_s are the beam damping ratio and soils radiation damping ratio, respectively. The parameter β_1 is related to the first eignefunction and will be explained later. The Solving Equation 29 requires separating the variables (Chopra 2007)

$$y(x,t) = \phi(x)\,q(t) \qquad \text{Equation 32}$$

This gives

$$EI\,\frac{\partial^4 y}{\partial x^4} = -m\,\frac{\partial^2 y}{\partial t^2} - c\,\frac{\partial y}{\partial t} - k\,y \qquad \text{Equation 33}$$

$$q(t)\,\frac{1}{m}E\,I\,\frac{d^4\phi(x)}{dx^4} = -\phi(x)\left[\frac{d^2q(t)}{dt^2} + \frac{c}{m}\,\frac{dq(t)}{dt} + \frac{k}{m}\,q(t)\right] \qquad \text{Equation 34}$$

The above equation can be further reduced to

$$\frac{d^4\phi}{dx^4} - \beta^4\,\phi = 0 \qquad \text{Equation 35}$$

The parameter β in Equation 35 is different from β used earlier in deriving the BEF subjected to stationary load. It can be written as

$$\beta^4 = \frac{m\,\omega^2}{E\,I} \qquad \text{Equation 36}$$

The natural frequency of the beam, not to be confused with the constant ω in Equation 36, is

$$\omega_o^2 = \frac{k}{m} \qquad \text{Equation 37}$$

The equation can be written as

$$\frac{d^2q}{dt^2} + \frac{c}{m}\frac{dq}{dt} + \left(\omega_o^2+\omega^2\right) q = 0 \qquad \text{Equation 38}$$

The general solution for Equation 38 can be written as (Chopra 2007)

$$\phi(x) = C_1 \sin\beta x + C_2 \cos\beta x + C_3 \sinh\beta x + C_4 \cosh\beta x \qquad \text{Equation 39}$$

Applying the boundary conditions where M(0) = 0, V(0) = 0, M(L) = 0, and V(L) = 0 and solving the general equation will give the following solution

$$\phi_n(x) = \cos\beta_n x + \cosh\beta_n x - R_n\left(\sin\beta_n x + \sinh\beta_n x\right) \qquad \text{Equation 40}$$

where

$$R_n = \frac{\cosh\beta_n L - \cos\beta_n L}{\sinh\beta_n L - \sin\beta_n L} \qquad \text{Equation 41}$$

and

$$\cosh\beta_n L \cos\beta_n L = 1 \qquad \text{Equation 42}$$

where β_n is the solution for Equation 42. The values for R_n and β_n are given in Table 18.

n	1	2	3	4	≥5
$\beta_n L$	4.73004	7.85320	10.99560	14.13716	$(2n+1)\frac{\pi}{2}$
R_n	0.98250	1.00077	0.99996	1.000000	1.000000

Table 18 Numeric values for Rn and βnL

Since the eigenvalues has been solved for natural frequencies and modes as shown above, the displacement can be expressed in terms of a combination of modes such that

$$y(x,t) = \sum_{n=1}^{\infty} \phi_n(x)\, q_n(t) \qquad \text{Equation 43}$$

The functions $\phi_n(x)$ are the natural eigenfunctions and $q_n(t)$ are the functions to be determined. Using Equation 32 and Equation 43, the equation of motion can be written as

$$\sum_{n=1}^{\infty} \phi_n(x) \left[\frac{d^2 q_n}{dt^2} + \frac{c}{m}\frac{dq_n}{dt} + \left(\omega_o^2 + \omega^2\right) q_n(t) \right] = \frac{1}{m} p_o \delta(x-vt) \qquad \text{Equation 44}$$

Since the load p_o is traveling with velocity v, the time it takes the load to cross the entire beam length is $t_d = L/v$ and the following relationship exists

$$p(x,t) = \begin{cases} p_o \delta(x - vt), & 0 \le t \le t_d \\ 0, & t \ge t_d \end{cases} \qquad \text{Equation 45}$$

$$p(t) = \begin{cases} \int_0^L p_o \delta(x - vt)\phi_n(x)\, dx\,, & 0 \le t \le t_d \\ 0, & t \ge t_d \end{cases}$$ Equation 46

When the load is traveling within the beam length

$$p(t) = p_o\, \phi_n\, (v\, t) = p_o\, h(t)$$ Equation 47

therefore,

$$\frac{d^2 q_n}{dt^2} + \frac{c}{m}\frac{dq_n}{dt} + \left(\omega_o^2 + \omega_n^2\right) q_n(t) = \frac{p_o}{m\, L} h(t)$$ Equation 48

Assuming zero initial conditions and taking the Laplace Transform for Equation 48

$$\mathcal{L}(q_n) = \mathcal{L}\left(\frac{p_o}{mL} h(t)\right)\left[\frac{1}{s^2 + \frac{c}{m} s + (\omega_o^2 + \omega_n^2)}\right]$$ Equation 49

where the expression that needs to be solved is

$$s^2 + \frac{c}{m} s + \left(\omega_o^2 + \omega_n^2\right) = 0$$ Equation 50

the solution for Equation 50 is

$$s_1 = \frac{1}{2}\left(-\frac{c}{m} + \sqrt{\frac{c^2}{m^2} - 4(\omega_o^2 + \omega_n^2)}\right)$$ Equation 51

$$s_2=\frac{1}{2}\left(-\frac{c}{m}-\sqrt{\frac{c^2}{m^2}-4(\omega_o^2+\omega_n^2)}\right) \quad \text{Equation 52}$$

The roots above can be either real or complex. For the case when the roots are real, where $c^2>4m^2(\omega_o^2+\omega_n^2)$, the roots, s_1 and s_2, can be determined using Equation 51 and Equation 52, respectively. The time function can be then expressed as

$$Q_n(t)=\frac{p_o}{m\,L(s_1-s_2)}\int_0^t h(\tau)\left(e^{s_1(t-\tau)}-e^{s_2(t-\tau)}\right)d\tau \quad \text{Equation 53}$$

The final solution for the case when both roots are real can be written as

$$Q_n(t)=\frac{p_o}{2\,m\,L(s_1-s_2)}\sum_{i=1}^{8} B_{i,n} \quad \text{Equation 54}$$

where

$$B_{1,n}=\frac{(1-R_n)}{(\beta_n v-s_1)}\left(e^{\beta_n v t}-e^{s_1 t}\right) \quad \text{Equation 55}$$

$$B_{2,n}=\frac{(1+R_n)}{(-\beta_n v-s_1)}\left(e^{-\beta_n v t}-e^{s_1 t}\right) \quad \text{Equation 56}$$

$$B_{3,n}=\frac{(1+iR_n)}{(i\beta_n v-s_1)}\left(e^{i\beta_n v t}-e^{s_1 t}\right) \quad \text{Equation 57}$$

$$B_{4,n}=\frac{(1-iR_n)}{(-i\beta_n v-s_1)}\left(e^{-i\beta_n v t}-e^{s_1 t}\right) \quad \text{Equation 58}$$

$$B_{5,n}=\frac{-(1-R_n)}{(\beta_n v-s_2)}\left(e^{\beta_n v t}-e^{s_2 t}\right) \quad \text{Equation 59}$$

$$B_{6,n}=\frac{-(1+R_n)}{(-\beta_n v-s_2)}\left(e^{-\beta_n v t}-e^{s_2 t}\right) \quad \text{Equation 60}$$

$$B_{7,n} = \frac{-(1+R_n)}{(i\beta_n v - s_2)}\left(e^{\beta_n v t} - e^{s_2 t}\right)$$ Equation 61

$$B_{8,n} = \frac{-(1-R_n)}{(-i\beta_n v - s_2)}\left(e^{-i\beta_n v t} - e^{s_2 t}\right)$$ Equation 62

For the case when the roots are complex, where $c^2 < 4m^2(\omega_o^2 + \omega_n^2)$, the solution can be achieved by rewriting Equation 50 as

$$s^2 + \frac{c}{m}s + \left(\omega_o^2 + \omega_n^2\right) = \left(s + \frac{c}{2m}\right)^2 + \Omega_n^2$$ Equation 63

where

$$\Omega_n^2 = \omega_o^2 + \omega_n^2 - \frac{c^2}{4m^2}$$ Equation 64

Laplace Transform gives the following time function solution

$$Q_n(t) = \frac{p_o}{mL\Omega_n}\int_0^t h(\tau)e^{\frac{-c}{2m}(t-\tau)}\left(\frac{e^{i(t-\tau)\Omega_n} - e^{-i(t-\tau)\Omega_n}}{2i}\right)d\tau$$ Equation 65

The integral for Equation 65 gives the following final solution

$$Q_n(t) = \frac{-ip_o}{2\,m\,L\,\Omega_n}\sum_{i=1}^{8} D_{i,n}$$ Equation 66

where,

$$D_{1,n} = \frac{(1-R_n)}{\left(\beta_n v + \frac{c}{2m} - i\Omega_n\right)}\left[e^{\beta_n v t} - e^{\left(\frac{-c}{2m} + i\Omega_n\right)t}\right]$$ Equation 67

$$D_{2,n} = \frac{(1+R_n)}{\left(-\beta_n v + \frac{c}{2m} - i\Omega_n\right)}\left[e^{-\beta_n vt} - e^{\left(\frac{-c}{2m}+i\Omega_n\right)t}\right] \quad \text{Equation 68}$$

$$D_{3,n} = \frac{(1+iR_n)}{\left(i\beta_n v + \frac{c}{2m} - i\Omega_n\right)}\left[e^{i\beta_n vt} - e^{\left(\frac{-c}{2m}+i\Omega_n\right)t}\right] \quad \text{Equation 69}$$

$$D_{4,n} = \frac{(1-iR_n)}{\left(-i\beta_n v + \frac{c}{2m} - i\Omega_n\right)}\left[e^{-i\beta_n vt} - e^{\left(\frac{-c}{2m}+i\Omega_n\right)t}\right] \quad \text{Equation 70}$$

$$D_{5,n} = \frac{(1-R_n)}{\left(\beta_n v + \frac{c}{2m} + i\Omega_n\right)}\left[e^{\beta_n vt} - e^{\left(\frac{-c}{2m}-i\Omega_n\right)t}\right] \quad \text{Equation 71}$$

$$D_{6,n} = \frac{(1+R_n)}{\left(-\beta_n v + \frac{c}{2m} + i\Omega_n\right)}\left[e^{-\beta_n vt} - e^{\left(\frac{-c}{2m}-i\Omega_n\right)t}\right] \quad \text{Equation 72}$$

$$D_{7,n} = \frac{(1+iR_n)}{\left(i\beta_n v + \frac{c}{2m} + i\Omega_n\right)}\left[e^{i\beta_n vt} - e^{\left(\frac{-c}{2m}-i\Omega_n\right)t}\right] \quad \text{Equation 73}$$

$$D_{8,n} = \frac{(1-iR_n)}{\left(-\beta_n v + \frac{c}{2m} + i\Omega_n\right)}\left[e^{-i\beta_n vt} - e^{\left(\frac{-c}{2m}-i\Omega_n\right)t}\right] \quad \text{Equation 74}$$

7.3.2 DYNAMICS OF INFINITE LENGTH BEAM ON ELASTIC FOUNDATION

The problem of a force moving along infinite beam on elastic foundation was first solved by Timoshenko (Timoshenko 1926). The case for a constant force was later refined by Kenney (Kenney 1954). This section will present a detailed solution for a beam on elastic foundation subjected to a constant moving force. The solution presented next is a modification an existing solution by Fryba (Frýba 1999). The modification will allow consistency with the solution presented in the previous section for finite length beam on elastic foundation.

Consider a beam of infinite length similar to the beam shown in Figure 72 but with the load moving at a constant speed, *v*, from left to right. The beam and foundation properties are

similar to that of finite length beam on elastic foundation presented in the previous section. The differential equation of motion is also the same as Equation 29 and is expressed as:

$$EI\frac{\partial^4 y}{\partial x^4}+m\frac{\partial^2 y}{\partial t^2}+c\frac{\partial y}{\partial t}+k\,y = p(t)\;\;\delta(x-vt) \qquad \text{Equation 75}$$

The boundary conditions for infinite length beam are different than that of finite length beam since shear, moment, deflection, and rotation are zero at both ends ($-\infty$ and $+\infty$) such that $y(-\infty)=0$, $y(+\infty)=0$, $V(-\infty)=0$, $V(+\infty)=0$, $M(-\infty)=0$, $M(+\infty)$, $\theta(-\infty)=0$, and $\theta(+\infty)=0$.

The method use to solve finite length beam cannot be used here since infinity is not measurable quantity. Therefore, it is best to consider the quasi-static case where the beam is considered at rest relative to the moving coordinate system. This case comes into consideration after a long period of load travel, therefore eliminating the dependence on time (Frýba 1999). For this purpose a new variable representing the dimensionless length, *s*, is used:

$$s = \beta\,(x-vt) \qquad \text{Equation 76}$$

In this equation, β is given previously in Equation 11 for BEF subjected to stationary load. Equation 76 is a dimensionless expression indicating that the origin of the coordinate system moves along the load. For the quasi-static case, the solution for deflection will be expressed as:

$$y(x,t) = y_o \cdot y(s) \qquad \text{Equation 77}$$

where $y(s)$ is the dimensionless deflection of the beam and y_o is the maximum deflection as derived previously for BEF subjected to stationary load and can be expressed as

$$y_o = \frac{P\,\beta}{2\,k} \qquad \text{Equation 78}$$

Furthermore, the Dirac delta function can be expressed as (Frýba 1999)

$$\delta(s) = \frac{1}{\beta}\,\delta(x) \qquad \text{Equation 79}$$

$$\int_{-\infty}^{+\infty} \delta(s)\,ds = \int_{-\infty}^{+\infty} \frac{1}{\beta}\,\delta(x) = 1 \qquad \text{Equation 80}$$

The differentials for Equation 75 and Equation 76 are

$$\frac{\partial s}{\partial x} = \beta \qquad \text{Equation 81}$$

$$\frac{\partial s}{\partial t} = -\beta\,v \qquad \text{Equation 82}$$

$$\frac{\partial y}{\partial t} = -\beta\,v\,y_o \frac{dy(s)}{ds} \qquad \text{Equation 83}$$

$$\frac{\partial^2 s}{\partial t^2} = -\beta^2\,v^2\,y_o \frac{\partial^2 y(s)}{\partial s^2} \qquad \text{Equation 84}$$

$$\frac{\partial^4 s}{\partial x^4} = \beta^4\,y_o \frac{\partial^4 y(s)}{\partial s^4} \qquad \text{Equation 85}$$

Substituting into the equation of motion will give the following ordinary differential equation

$$\frac{\partial^4 y(s)}{\partial s^4} + 4z_1 \frac{\partial^2 y(s)}{\partial s^2} - 8z_2 \frac{\partial y(s)}{\partial s} + 4y(s) = 8\delta(s) \qquad \text{Equation 86}$$

where

$$z_1 = \frac{m\,\beta^2\,v}{k} \qquad \text{Equation 87}$$

$$z_2 = \frac{c\,\beta\,v}{2\,k} \qquad \text{Equation 88}$$

Using Fourier integral transformation and the boundary conditions give the following

$$q^4\,Y(q) - 4\,z_1 q^2\,Y(q) - 8i\,z_2\,q\,Y(q) + 4\,Y(q) = 8 \qquad \text{Equation 89}$$

Where q is a variable and *Y(q)* is the transform function of *y(s)* as given in the following relationship

$$y(s) = \frac{1}{2\pi}\int_{-\infty}^{+\infty} Y(q)\,e^{isq}\,dq \qquad \text{Equation 90}$$

$$Y(q) = \int_{-\infty}^{+\infty} y(s)\,e^{-isq}\,ds \qquad \text{Equation 91}$$

Equation 89 can be written as

$$Y(q) = \frac{8}{q^4 - 4\,z_1\,q^2 - 8i\,z_2\,q + 4} \qquad \text{Equation 92}$$

$$y(s) = \frac{4}{\pi}\int_{-\infty}^{+\infty} \frac{e^{isq}}{q^4 - 4\,z_1\,q^2 - 8i\,z_2\,q + 4}\,dq \qquad \text{Equation 93}$$

The poles of the function in the equation above will be assumed to be in the form of (Frýba 1999)

$$A_1 = a_1 + i\,b$$
$$A_2 = -\,a_1 + i\,b$$
$$A_3 = a_2 - i\,b$$
$$A_4 = -\,a_2 - i\,b$$

The values for a_1, a_2, and b above can be determined from the following condition

$$Q(q) = q^4 - 4\,z_1\,q^2 - 8i\,z_2\,q + 4 = (q-A_1)\,(q-A_2)\,(q-A_3\,)(q-A_4) \qquad \text{Equation 94}$$

The poles of the functions and Equation 93 will give the following solutions

$$a_1^2 = 2\,z_1 + b^2 + \frac{2\,z_2}{b} \qquad \text{Equation 95}$$

$$a_2^2 = 2\,z_1 + b^2 - \frac{2\,z_2}{b} \qquad \text{Equation 96}$$

$$b^6 + 2\,z_1 b^4 + \left(z_1^2 - 1\right) b^2 - z_2^2 = 0 \qquad \text{Equation 97}$$

The above expressions can be solved by finding the first positive root for *b* in Equation 97. The final solution for the dimensionless deflections is (Frýba 1999)

$$y(s \geq 0) = \frac{2}{a_1(D_1^2 + D_2^2)} e^{-bs}(D_1 \cos a_1 s + D_2 \sin a_1 s) \qquad \text{Equation 98}$$

$$y(s < 0) = \frac{2}{a_2(D_3^2 + D_4^2)} e^{bs}(D_3 \cos a_2 s - D_4 \sin a_2 s) \qquad \text{Equation 99}$$

The dimensionless bending moment can be expressed using the relation $M(x, t)=M_oM(s)$, where $M_o=P/4\beta$ is the static bending moment under the load, and $M(s)=y''(s)/2$. The dimensionless bending moment can be expressed as (Frýba 1999)

$$M(s \geq 0) = \frac{1}{a_1(D_1^2 + D_2^2)} e^{-bs}[(a_1^2 D_1 + 2a_1 b D_2 - b^2 D_1)\cos a_1 s + (a_1^2 D_2 - 2a_1 b D_1 - b^2 D_2)\sin a_1 s] \qquad \text{Equation 100}$$

$$M(s < 0) = \frac{1}{a_2(D_3^2 + D_4^2)} e^{bs}[(a_2^2 D_3 + 2a_2 b D_4 - b^2 D_3)\cos a_2 s + (a_2^2 D_4 - 2a_2 b D_3 - b^2 D_4)\sin a_2 s] \qquad \text{Equation 101}$$

where

$$D_1 = a_1 \, b \qquad \text{Equation 102}$$

$$D_2 = b^2 - \frac{1}{4}\left(a_1^2 - a_2^2 \right) \qquad \text{Equation 103}$$

$$D_3 = a_2 \, b \qquad \text{Equation 104}$$

$$D_4 = b^2 + \frac{1}{4}\left(a_1^2 - a_2^2 \right) \qquad \text{Equation 105}$$

7.4 RESULTS FOR PAVEMENT AS BEF SUBJECTED TO MOVING LOAD

In the previous sections, the theoretical "exact" solution for damped beam on elastic foundation was developed for both finite and infinite length beams. The solution considered a beam subjected to constant load moving at a constant speed and accounted for energy dissipation through the foundation by using dashpots. In developing the solutions, it should be noted by the reader that the solutions for the finite length BEF and for infinite length BEF are developed from the same controlling differential equation (Equation 75). However, the boundary conditions for the infinite length beam are considerably different than the boundary conditions for the finite length beam. In the finite length beam, beam moments and shears are zero at the ends of the pavement. However, in the infinite length beam, deflections and rotations and moments are shears are all zero at infinity. Accordingly, the two solutions are different but can be used to check one another. Importantly, the solutions for Finite length BEF converge with the Infinite length BEF as the length increases for the finite length beam.

The following section will apply the derived solution to the research pavement designs to determine the importance of dynamic response and how thin the pavement can be if dynamic effects are more critical than the static response calculated in the previous section.

7.4.1 FINITE LENGTH PAVEMENT AS BEF SUBJECTED TO MOVING LOAD

Consider pavements with length of 50 ft and thicknesses of 4, 6, 8, and 10 in. The width is taken as 144 in. and the modulus of subgrade reaction, k, is 150 psi/in. The load magnitude is 18,000 lbs (one pair of 9,000 lb loads) and the speed of the load is taken as 65 mph moving from the left to right. The damping ratio, λ_b for the concrete beam is taken as 0.05 (Bachmann 1995) and radiation damping ratio, λ_s is 2.0. These values were determined to be good average values to obtain general reduction in surface displacement with increasing vehicle speed which is confirmed by field test results by (National Research Council (U.S.). Highway Research Board. and American Association of State Highway Officials. 1961), (Cebon 1985), and (Harr 1962).

Figure 76 shows the deflected shape of 6 inch pavement modeled as beam on elastic foundation at the instant the moving load is at mid-span. There are two deflected shapes shown in the figure; one is for the moving load and the other is a static load applied at mid-length. The figure shows that the downward deflection for the moving load at the load location is less than that of the static load case. Also note that the maximum downward deflection does not occur at mid-length for the moving load. This "lag" in deflection is equivalent to a phase angle considering the dynamic analysis. The figure also shows that the moving load will cause in increase in uplift when compared to the static load case, located just ahead the load location. The figures shown for both load cases did not account for the pavements self-weight. For 6 in. pavement, self-weight deflection would be 0.0033 in. which in this example is sufficient to overcome the uplift created by the moving load.

Figure 77 shows the deflected shape for 4, 6, 8, and 10 in. pavements due to moving load of 65 mph. Table 19 shows summary of the peak deflections and uplift for the pavements of the varying thicknesses. The data indicate that the downward deflection at load location decreases as the pavement thickness increases. For example, for the 4 in. thick pavement downward

deflection was 0.0100 in. whereas the maximum downward deflection for the 10 in. pavement was only 0.0048 in.

Similarly, the pavement uplift increases as the pavement thickness decreases. The data show that the maximum uplift on the 4 in. thick pavement was 0.0031 in. whereas the maximum uplift for the 10 in. pavement was only 0.0018 in. These data can be compared to the deflection caused by the pavement self-weight. This indicates that the pavements with thicknesses of 6 in., 8 in., and 10 in. possess sufficient ballast or mass to maintain contact with the sub-base whereas the 4 in. pavement is too light.

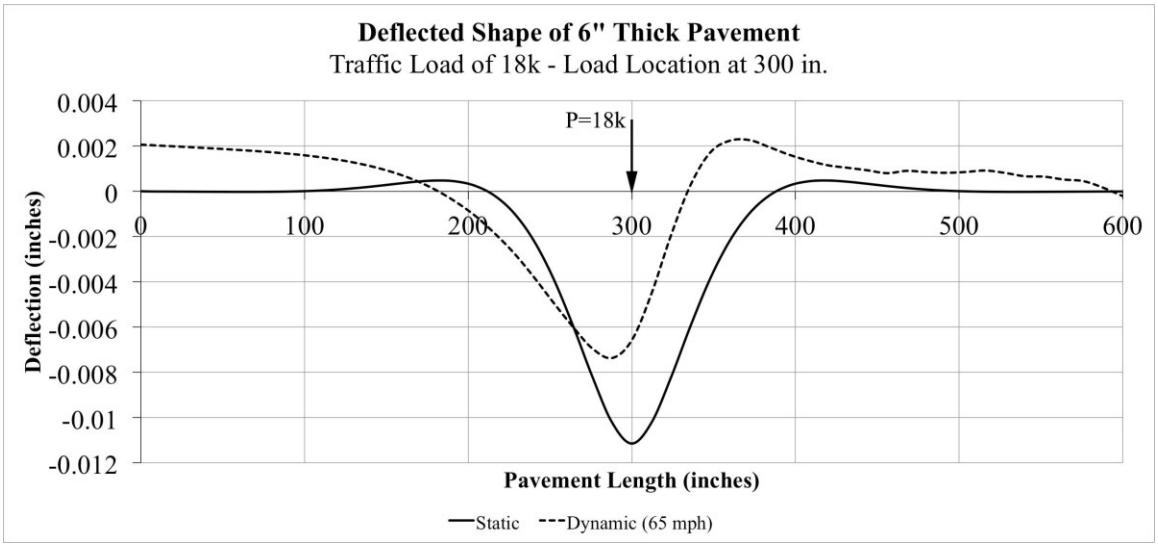

Figure 76 Deflected shape of 6 inch pavement with load moving at 65 mph

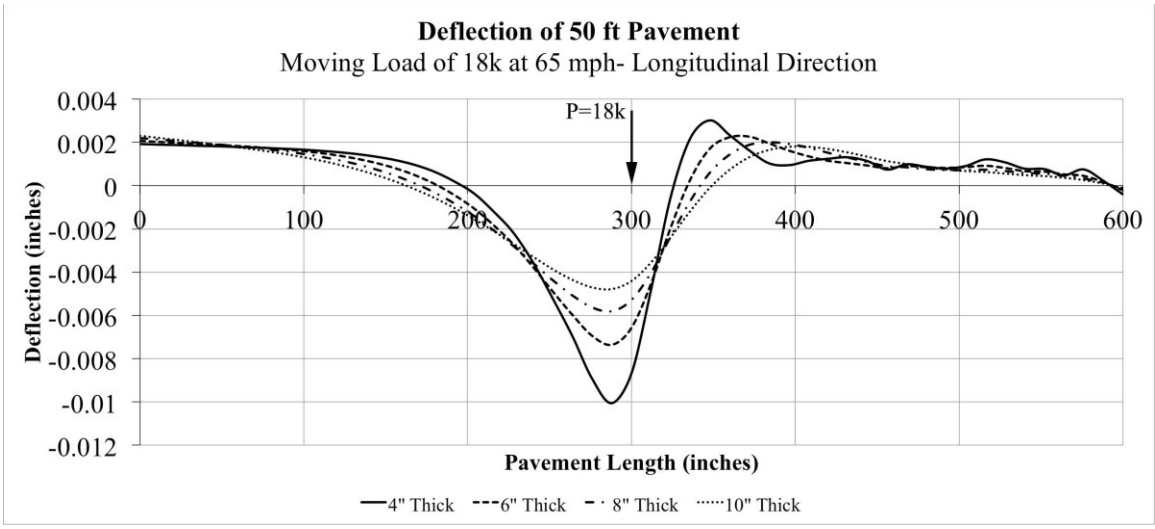

Figure 77 Deflected shape of pavement with different thicknesses subjected to moving load

Pavement Thickness	Deflection Due to self-weight (in.)	Maximum Downward Deflection (in)	Maximum Uplift (in)
4 in.	0.0022	0.0100	0.0031
6 in.	0.0033	0.0074	0.0022
8 in	0.0044	0.0058	0.0020
10 in.	0.0055	0.0048	0.0018

Table 19 Pavement deflections due to 18k load moving at constant speed of 65 mph

Figure 78 charts the bending stresses at the bottom of the pavement for 6 in. pavements at the instant where the moving load is at mid-span. The dashed line represents the bending stresses due to 18,000 lbs load moving at 65 mph while the solid line represents bending stresses due static load of 18,000 lbs. From the general bending stresses profile shape for both static and dynamic, the following observations can be made from Figure 78:

- The tensile stress caused by moving loads is less than that caused by static loads.

- The maximum positive dynamic stress is 56 percent of the maximum positive static stress.
- In both cases, the maximum tensile stresses are at mid-length.
- The compressive stress caused by moving loads is less than that caused by static loads.
- The maximum compressive stress is less than the maximum tensile stress.

Figure 78 shows the bending stress profile for pavement with thicknesses of 4, 6, 8, and 10 in. subjected to18k load moving at speed of 65 mph. Table 20 shows summary of the maximum tensile and compressive stresses for both stationary and moving load (65 mph) for pavements of different thicknesses. Bending stresses decrease as the beam thickness increases. Generally, pavement stresses are not negatively affected by the dynamics of moving load since tensile stresses are reduced when compared to the static response.

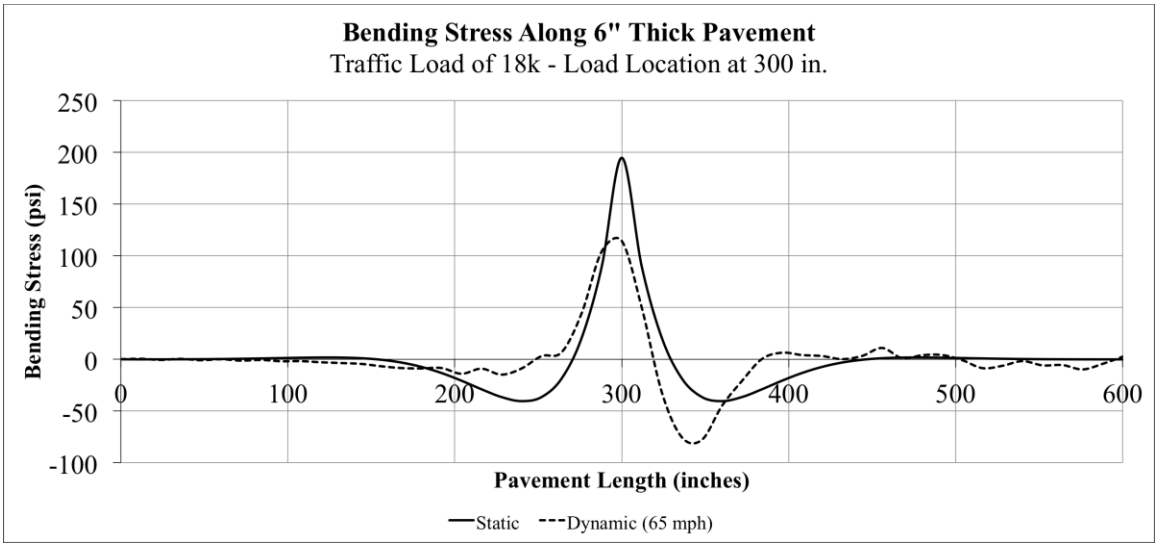

Figure 78 Bottom bending stresses along 6 inch pavement with load moving at 65 mph

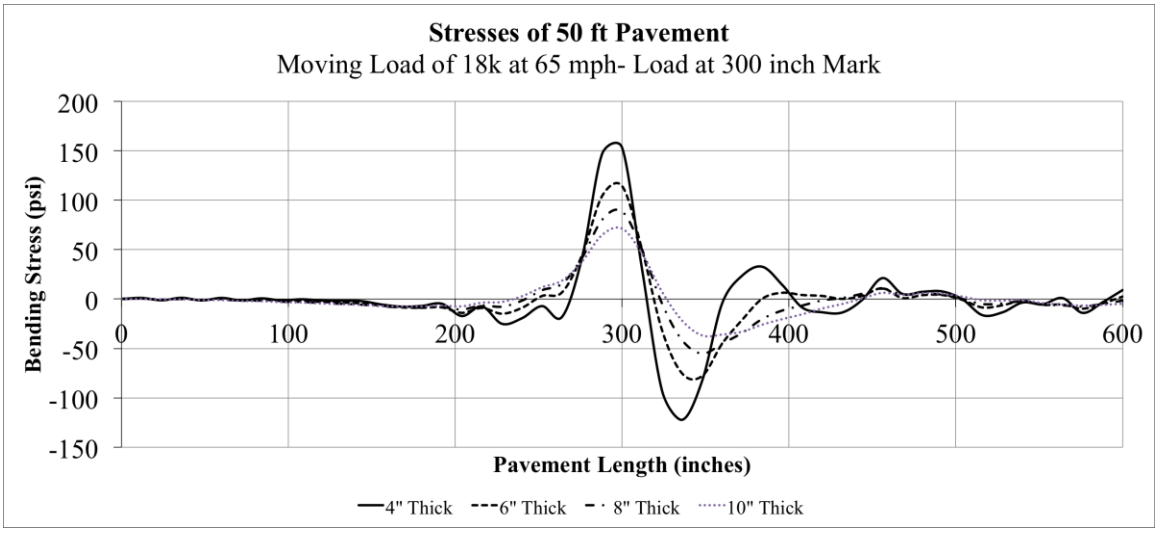

Figure 79 Bottom bending stresses of pavement with different thicknesses subjected to moving load

Pavement Thickness	Maximum Tensile Stress (psi)		Maximum Compressive Stress (psi)	
	Dynamic	Static	Dynamic	Static
4 in.	154	323	123	66
6 in.	115	195	76	41
8 in	86	136	56	29
10 in.	72	103	37	21

Table 20 Maximum tensile and compressive bottom stresses of pavement subjected to static and moving loads

Figure 80 shows the frequency response spectra for 4, 6, 8, and 10 in. thick pavements. The *y*-axis represents the deformation factor, R_d, which is the ratio between the peak dynamic deflection and peak static deflection. The *x*-axis represents the ratio between the frequency of vibration and the natural frequency. The response drops below deformation factor of one since pavement structures are usually overdamped system. The first modes are very important in

obtaining the correct deflection data. In the previous analysis, the dynamic deflection results were obtained using the first 45 mode shapes.

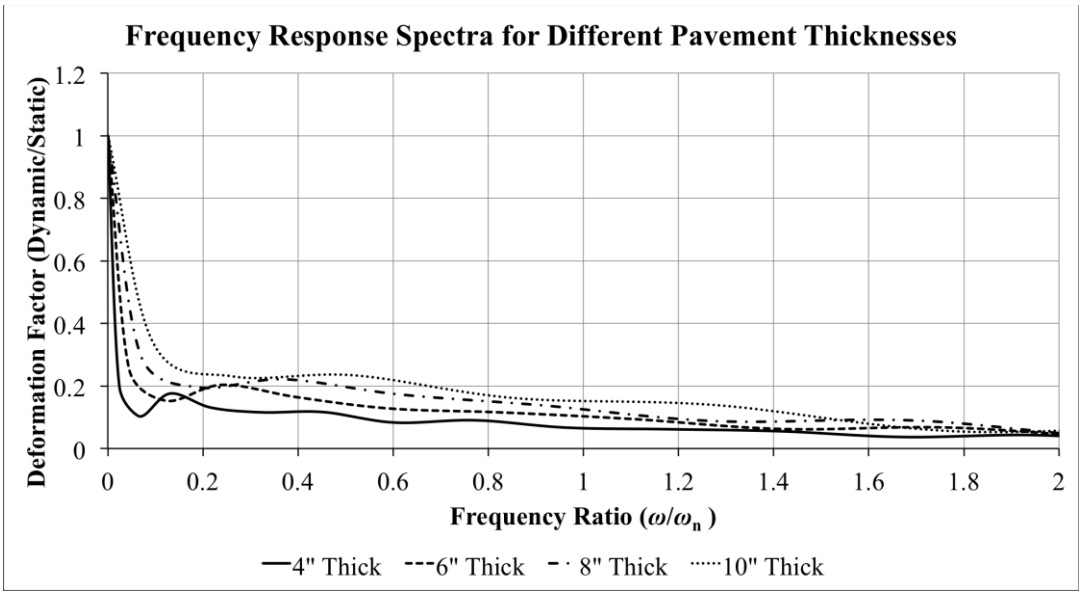

Figure 80 Frequency Response Spectra for various pavement thicknesses

7.4.2 RESPONSE OF PAVEMENT WITH INFINITE LENGTH

Precast prestressed concrete pavement panels are usually prestressed together to form one long pavement that can be several hundred feet long. Consider the previous finite length beam but with infinite length. The pavement dynamic response will be presented here using the same properties from finite length beam and the equations developed in for infinite length BEF subjected to constant moving load.

Figure 81 shows the deflected shape of 6 in. pavement modeled as infinite length beam on elastic foundation at the instant the moving load is at mid-span. The solid line represents the deflected shape due to static load for the same pavement. Similar to finite length pavement, the downward deflection for the moving load at the mid-span is less than that of the static load while the uplift ahead of the load is slightly higher than that of the static case. Figure 82 shows the

deflected shape for 4, 6, 8, and 10 in. pavements due to moving load of 65 mph. Table 19 shows summary of the peak deflections and uplift for the pavements of different thicknesses. The downward deflection at load location decreased as the thickness increased while the uplift almost did not change. The 4, 6, 8, and 10 in. pavements did have enough ballast to maintain contact with the subbase. Further analysis indicated that infinite length pavements will have enough ballast to prevent uplift as long as the thickness is above 2 in.

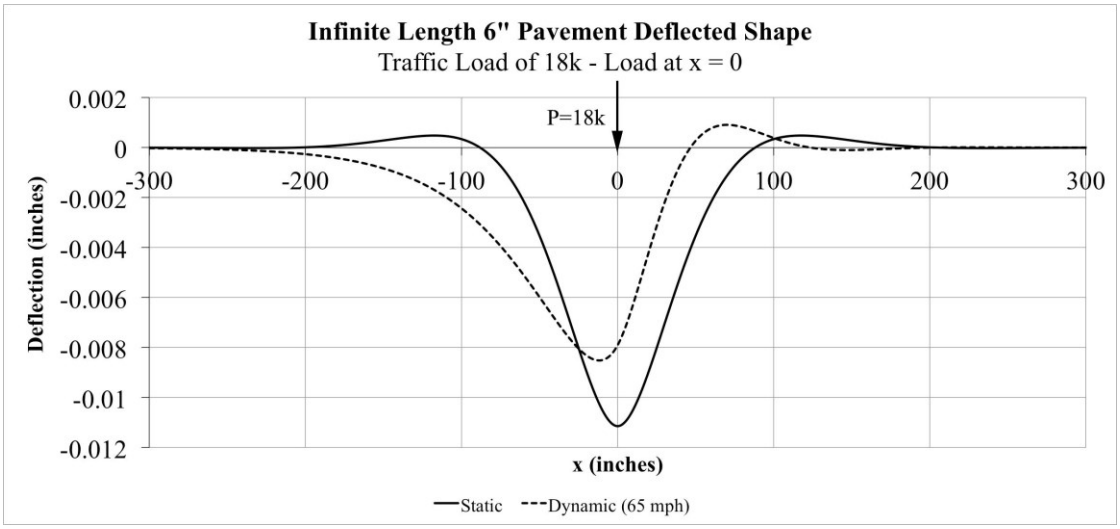

Figure 81 Deflected shape of 6 inch pavement with load moving at 65 mph (infinite length)

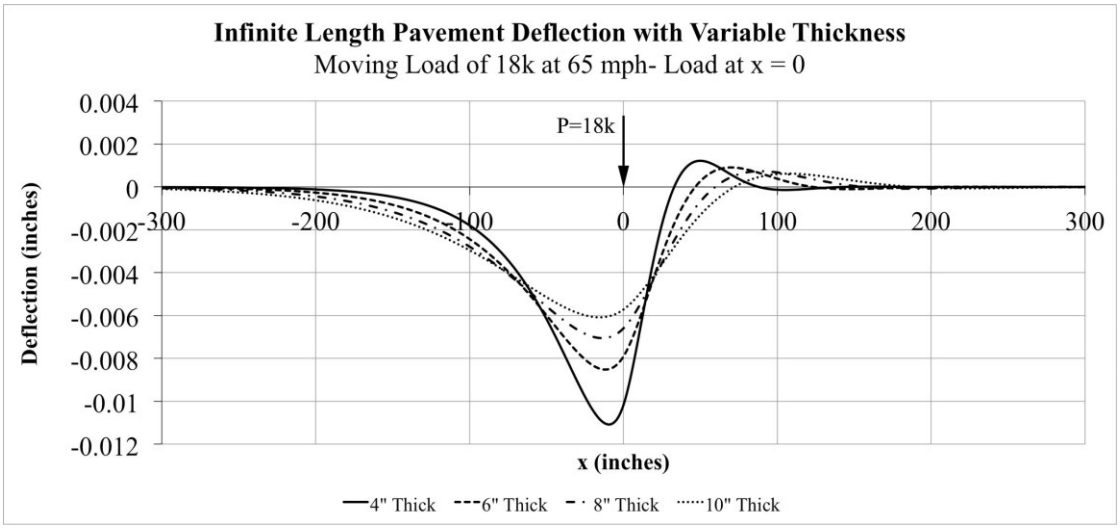

Figure 82 Deflected shape of pavement with different thicknesses (infinite length)

Figure 83 shows the bottom bending stress diagram along partial length of the infinite length pavement at an instant where the moving load is at mid-span. The dashed line represents the dynamic stresses while the solid line represents static stresses. The general bending stresses profile shape for both static and dynamic are similar with the maximum tensile dynamic stress being 75 percent of the maximum positive static stress. Figure 84 shows the bending stress profile for pavement with thicknesses of 4, 6, 8, and 10 inches subjected to18k load moving at speed of 65 mph. Table 21 shows summary of the maximum tensile and compressive stresses for both stationary and moving load (65 mph) for pavements of different thicknesses.

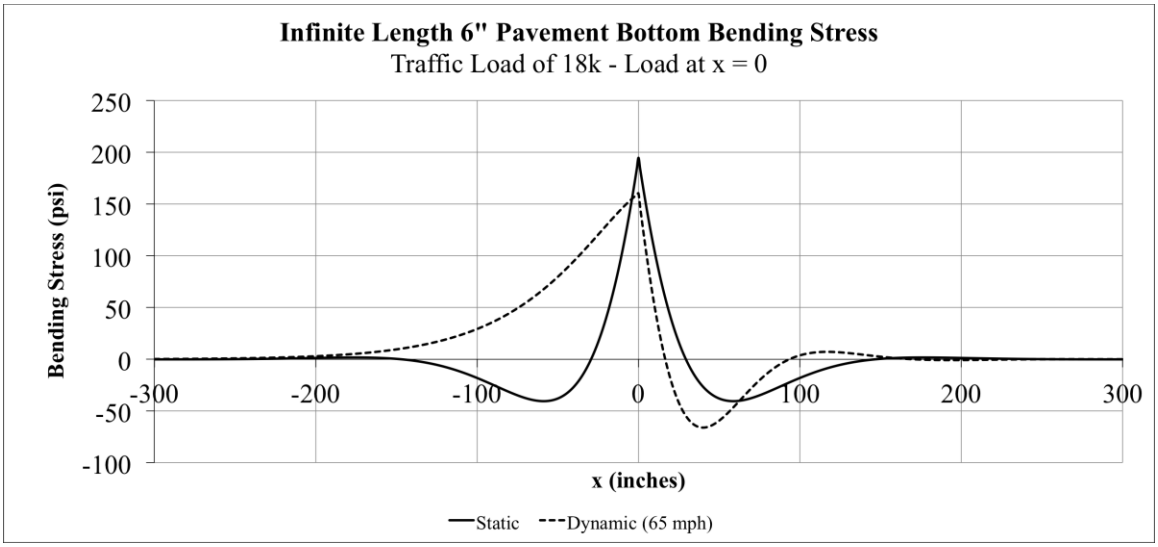

Figure 83 Bottom bending stresses along 6 inch pavement with load moving at 65 mph (infinite length)

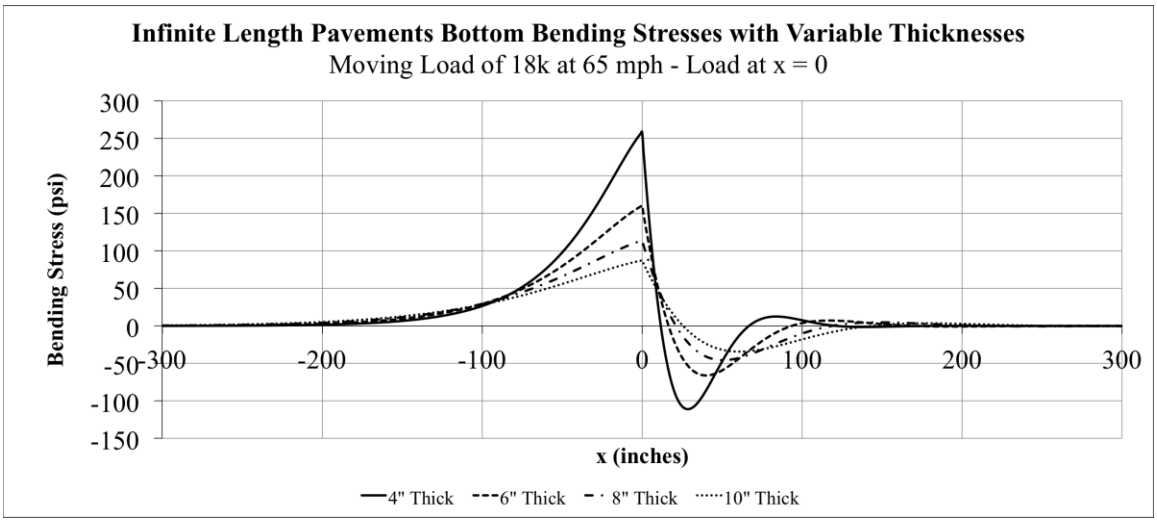

Figure 84 Bottom bending stress of pavement with different thicknesses (infinite length)

Pavement Thickness	Maximum Tensile Stress (psi)		Maximum Compressive Stress (psi)	
	Dynamic	Static	Dynamic	Static
4 in.	259	323	111	66
6 in.	162	195	67	41
8 in	114	136	46	29
10 in.	88	103	35	21

Table 21 Maximum tensile and compressive bottom stresses of pavement subjected to static and moving loads (infinite length)

7.4.3 EFFECTS OF VEHICLE SPEED ON PAVEMENT RESPONSE

Whether the velocity of the load at traffic speeds affects the performance of the pavement in any significant way is a question that needs an answer. The exact solution developed in this research is an excellent tool in answering this question. Using the same pavement properties from the previous analysis, the response of the pavement at different speeds will be calculated and

presented. The traffic speeds that will be shown are 50 mph and 75 mph. Furthermore, higher velocity of 100 mph is only shown for the purpose of illustration.

Figure 85 shows the deflection of 6 inch pavement at speeds of 50, 75, and 100 mph as the instant the load at mid-span. The figure also shows the deflection due to static load of the same magnitude. Figure 86 shows the bending stress for same pavement at the same speed range. Several observations can be made from both figures:

- The location of the maximum deflection moves further past mid-span as the speed increases
- The peak downward deflection and bending stress decrease as velocity increases
- The speed effect is negligible for normal highway speeds (less than 75 mph).

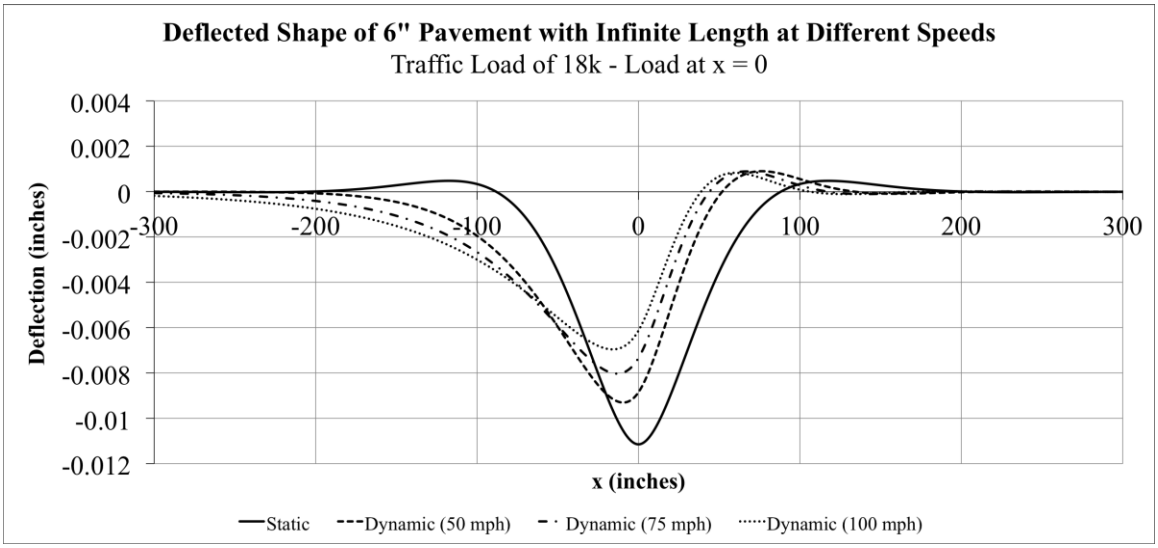

Figure 85 Deflected shape of 6 inch pavement at different load speeds (infinite length)

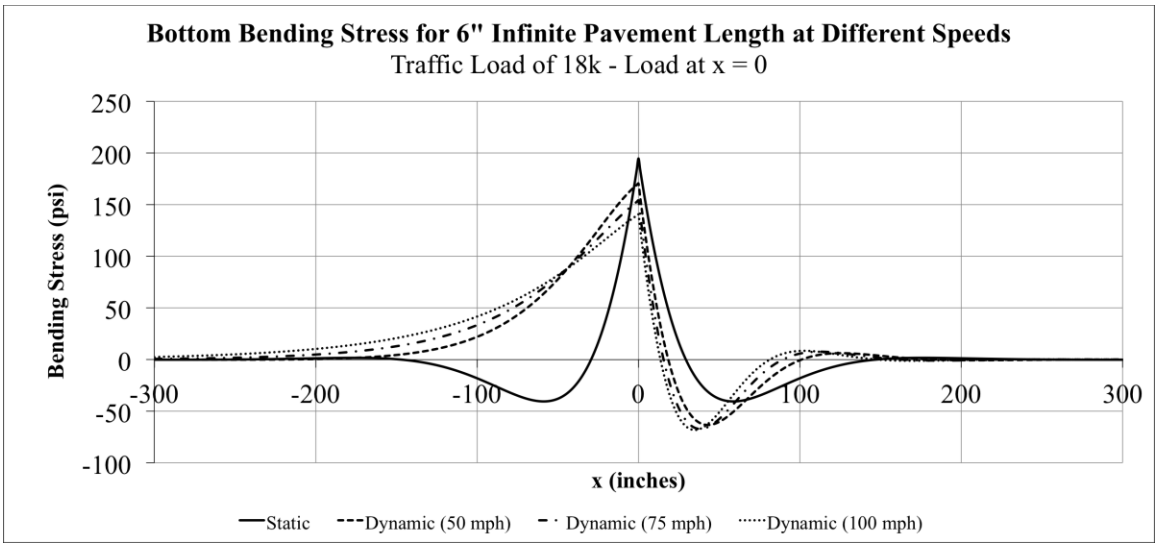

Figure 86 Bending stresses of 6" pavement at different load speeds (infinite length)

7.4.4 MINIMUM PAVEMENT THICKNESS

The results from dynamic analysis discussed earlier indicated that 50 ft long pavement requires a minimum thickness of 6 in. to prevent uplift. Further, very long pavements with the same properties require minimum thickness of 4 in. to achieve the same result. Further analysis of different pavement lengths indicated that minimum pavements thicknesses are a function of pavement length. This could be important factor in pavement design since it pavement thickness becomes a controlling factor in joint spacing. Figure 87 gives minimum pavement thickness required as pavement length increases. Note that once the pavement length exceeds 200 ft the length pavement act as pavement with infinite length. The figure is specific for the pavement dimensions and subbase properties used in this research.

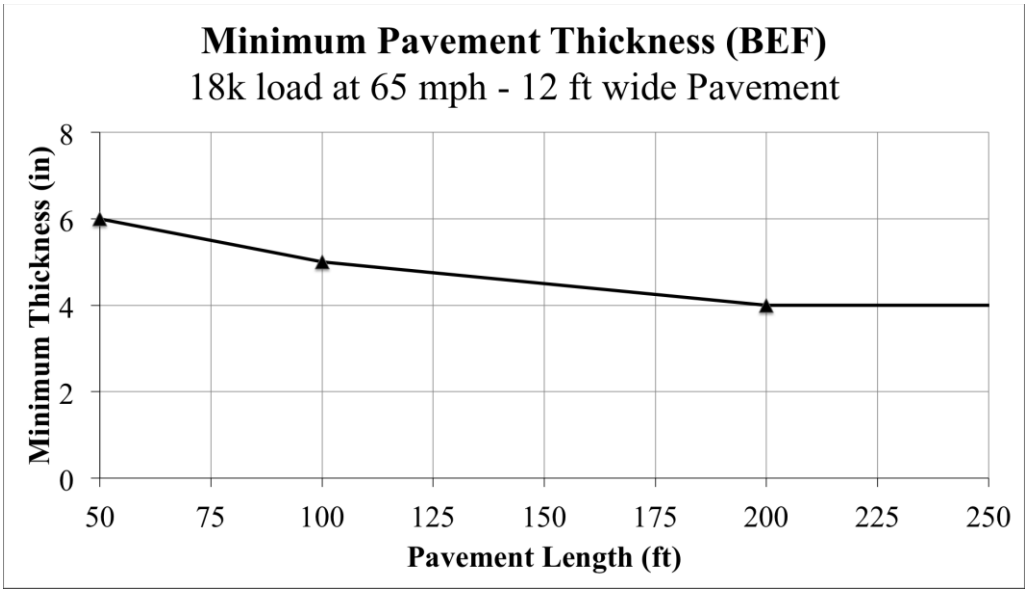

Figure 87 Minimum pavement thickness as function of pavement length based on dynamic response

7.5 COMPARISON OF TEST RESULTS

The tests were modeled using finite method and beam on elastic foundation theory discussed earlier. The deflections from 9k, 18k, 27k, and 30k loads were compared to determine the accuracy of each method. The modulus of subgrade reaction for analysis is taken as 150 psi/in and the concrete modulus of elasticity as 4,000 ksi for FEA and BEF. For the BEF method, the beam width was taken as the test panel full width (12 ft) and the thickness as the actual panel thickness under the load. The deflections shown in this section are measured at the load locations. For test results, this deflection is recorded from LVDT 1.

7.5.1 DEFLECTED SHAPE COMPARISON

The deflected shape of the test pavement was constructed from the test data deflections at distances of 0, 12, 36, and 60 in. from the point load. The corresponding deflections from the

finite element model and beam on elastic foundation were used to draw the deflected shapes. Line smoothing was used in drawing the deflected shapes presented next. Figure 88 shows the longitudinal deflected shape of Panel I-A under 30k point load placed at the center of the panel. The figure compares results from actual 30k static load test deflections with results from finite element analysis and beam on elastic foundation. The analysis models were assumed to have modulus of subgrade reaction of 150 psi/in and concrete modulus of elasticity of 4,000 ksi. It can be seen that the finite element method predicted the panel behavior more accurately than BEF method. The figure shows that the actual deflection is slightly greater than the FEA model, which suggests that the actual modulus of subgrade reaction is less than the assumed 150 psi/in for this particular test location.

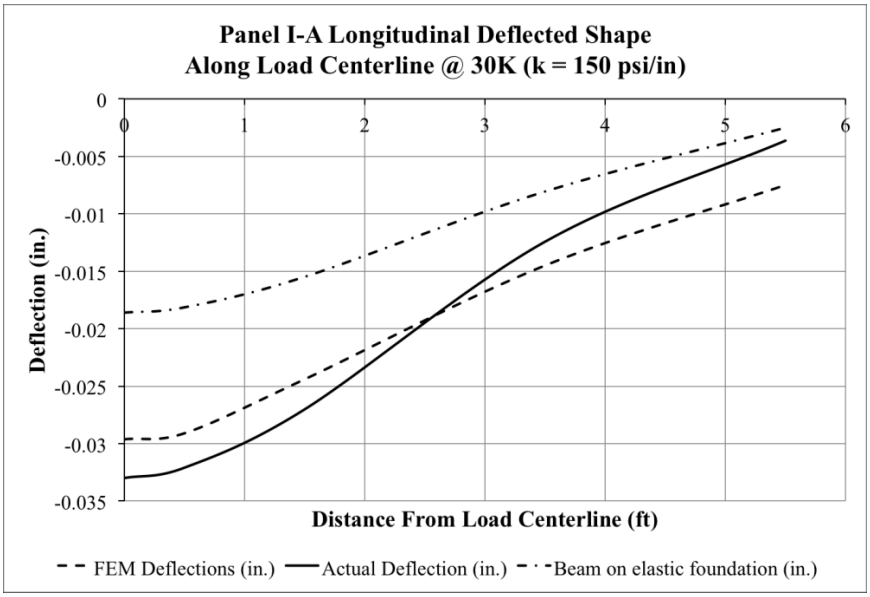

Figure 88 Panel I-A Actual/FEA/BEF Longitudinal Deflected Shape (k = 150 psi/in)

Figure 89 and Figure 90 shows longitudinal deflected shape of Panel I-B1 and Panel I-B2 under 30k, respectively. Panel I-B1 was loaded at the wheel path where the thickness is 8 in. The general deflected profile for actual, FEA, and BEF are matching. However, the actual test

deflection is less than that obtain from FEA indicating that the actual subgrade stiffness is greater than 150 psi/in used in the analysis. Figure 90 results are for Panel I-B2 where the load was placed at the edge of the pavement. The BEF results were not representing the deflection accurately because the BEF does not account for the edge discontinuity.

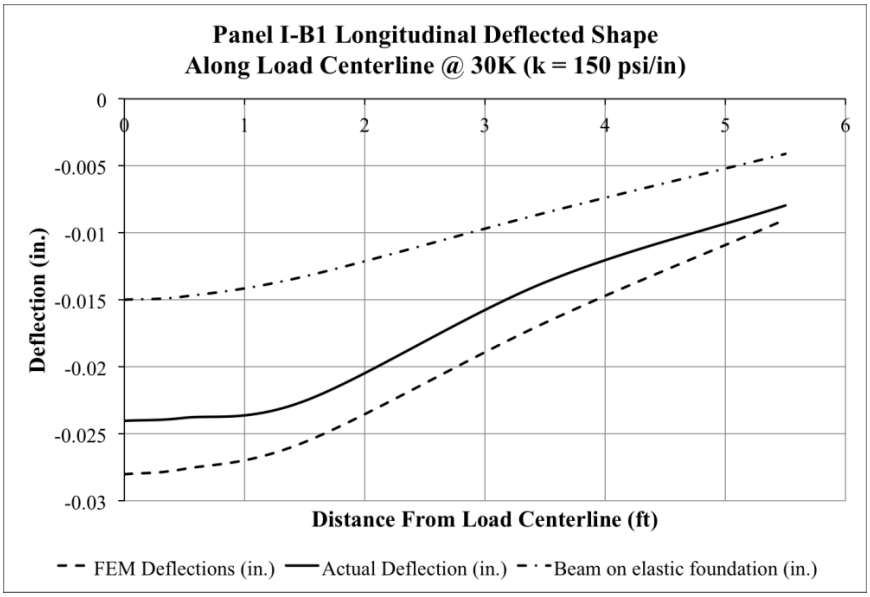

Figure 89 Panel I-B1 Actual/FEA/BEF Longitudinal Deflected Shape (k = 150 psi/in)

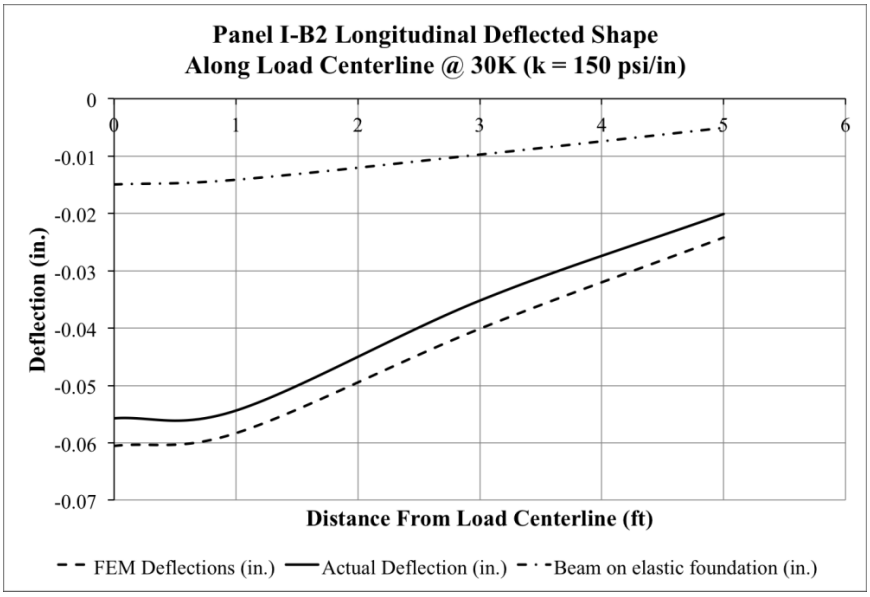

Figure 90 Panel I-B2 Actual/FEA/BEF Longitudinal Deflected Shape (k = 150 psi/in)

Figure 91 shows longitudinal deflected shape of Panel II-A when 30k is applied at the center of the panel. Similar to previous figures, the general deflected shapes are similar with FEA deflections being closer to the actual deflections than the BEF. The actual deflection for Panel II-A is larger than FEA deflections, which indicate that the actual k-value is less than 150 psi/in used in the FEA. Figure 92 shows longitudinal deflected shape of Panel III-A where the 30k is applied at the edge of the panel. Unlike Panel II-A, the actual deflection for Panel III-A is less than that of FEA. This indicate higher subgrade stiffness and therefore a larger k-value larger than 150 psi/in.

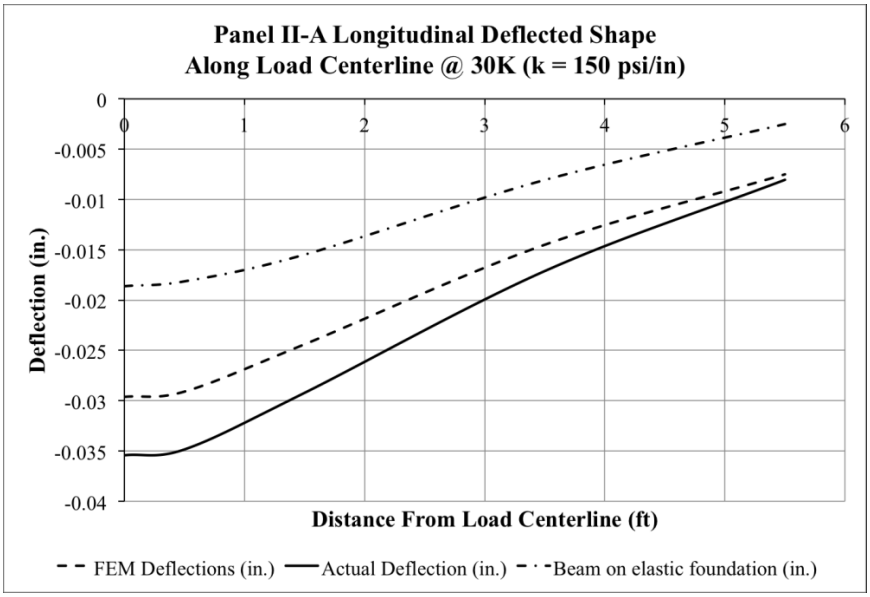

Figure 91 Panel II-A Actual/FEA/BEF Longitudinal Deflected Shape (k = 150 psi/in)

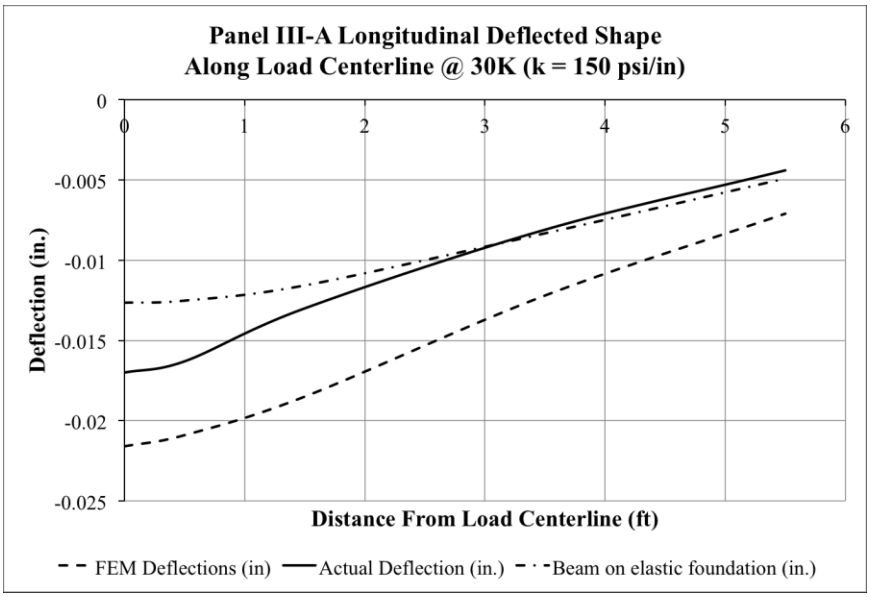

Figure 92 Panel III-A Actual/FEA/BEF Longitudinal Deflected Shape (k = 150 psi/in)

7.5.2 MAXIMUM DEFLECTION COMPARISON

The tests were modeled using finite method and beam on elastic foundation theory discussed earlier. The deflections from 9k, 18k, 27k, and 30k loads were compared to determine the accuracy of each method. The modulus of subgrade reaction for analysis is taken as 150 psi/in and the concrete modulus of elasticity as 4,000 ksi for FEA and BEF. For the BEF method, the beam width was taken as the test panel full width (12 ft) and the thickness as the actual panel thickness under the load. The deflections shown in this section are measured at the load locations. For test results, this deflection is recorded from LVDT 1.

Table 22 and Table 23 compare results from Panel I-A and II-A, respectively. The test results show linear relation between load and deflection. The FEA show strong correlation with test deflections. The small difference between FEA and test results is due to the differences between the analysis and actual modulus of subgrade reaction and materials stiffness. On the

other hand, the beam on elastic foundation method shows results that are almost half of actual deflections. Table 24 compares from Panel III-A test deflections with those from FEA and BEF. The results for Panel III-A show better relation between test and analysis deflections. In fact, the analysis deflections are higher than test deflections. This reduction in test deflection is due to the fact that Panel III-A was loaded to 50,000 earlier during this research to test the equipment and loading frame. During the preload run, the load increased modulus of subgrade reaction by compressing the base. Therefore, the results from Panel III-A is not an accurate representation of the results.

Load (kip)	Test Results Deflections (LVDT 1) (in)	Finite Element Analysis		Beam on Elastic Foundation	
		Deflection (in)	FEA/Actual (%)	Deflection (in)	BEF/Actual (%)
9	0.0088	0.0087	98.9	0.0056	63.6
18	0.0201	0.0175	87.1	0.0112	55.7
27	0.0304	0.0262	86.2	0.0168	55.3
30.	0.0321	0.0291	90.3	0.0186	57.9

Table 22 Comparison of test and analysis deflections at load location for test Panel I-A.

Load (kip)	Test Results Deflections (in) (LVDT 1)	Finite Element Analysis		Beam on Elastic Foundation	
		Deflection (in)	FEA/Actual (%)	Deflection (in)	BEF/Actual (%)
9	0.0088	0.0087	98.9	0.0056	63.6
18	0.0189	0.0175	92.6	0.0112	59.3
27	0.0265	0.0262	98.9	0.0168	63.4
30.	0.0349	0.0291	83.4	0.0186	53.3

Table 23 Comparison of test and analysis deflections at load location for test Panel II-A.

Load (kip)	Test Results Deflections (in) (LVDT 1)	Finite Element Analysis		Beam on Elastic Foundation	
		Deflection (in)	FEA/Actual (%)	Deflection (in)	BEF/Actual (%)
9	0.0044	0.0064	145.5	0.0045	102.3
18	0.0117	0.0128	109.4	0.0090	76.9
27	0.0153	0.0192	125.5	0.0135	88.3
30.	0.0163	0.0214	131.3	0.0150	92.1

Table 24 Comparison of test and analysis deflections at load location for test Panel III-A.

Table 25 and Table 27 compare results from Panel I-B1 and II-B1, respectively. The difference between FEA and test results for Panel B1 is most likely due to variation in modulus of subgrade reaction. Similar to Panel A results, the beam on elastic foundation method show results that are 60 percent of actual deflections. Table 27 compares from Panel III-B1 test deflections with those from FEA and BEF. Actual deflections for Panel III-B1 are much lower than FEA and BEF deflections. Similar to Panel III-A, the panel was loaded to 50,000 lbs earlier during this research to test the equipment and loading frame and the load must have increased modulus of subgrade reaction by compressing the base.

Load (kip)	Test Results Deflections (in) (LVDT 1)	Finite Element Analysis		Beam on Elastic Foundation	
		Deflection (in)	FEA/Actual (%)	Deflection (in)	BEF/Actual (%)
9	0.0072	0.0083	115.3	0.0045	63.5
18	0.0146	0.0166	113.7	0.0090	61.6
27	0.0204	0.0249	122.1	0.0135	66.2
30.	0.0234	0.0276	117.9	0.0150	64.1

Table 25 Comparison of test and analysis deflections at load location for test Panel I-B1.

Load (kip)	Test Results Deflections (in) (LVDT 1)	Finite Element Analysis		Beam on Elastic Foundation	
		Deflection (in)	FEA/Actual (%)	Deflection (in)	BEF/Actual (%)
9	0.0036	0.0083	230.5	0.0045	125.0
18	0.0108	0.0166	107.4	0.0090	83.3
27	0.0164	0.0249	151.8	0.0135	82.3
30.	0.0207	0.0276	133.3	0.0150	72.5

Table 26 Comparison of test and analysis deflections at load location for test Panel II-B1.

Load (kip)	Test Results Deflections (in) (LVDT 1)	Finite Element Analysis		Beam on Elastic Foundation	
		Deflection (in)	FEA/Actual (%)	Deflection (in)	BEF/Actual (%)
9	0.0028	0.0065	232.1	0.0038	135/7
18	0.0080	0.0129	161.3	0.0076	95.0
27	0.0110	0.0194	176.4	0.0114	103.6
30.	0.0063	0.0215	241.3	0.0127	201.6

Table 27 Comparison of test and analysis deflections at load location for test Panel III-B1.

Table 28 and Table 29 compare results from Panel I-B2 and II-B2, respectively. Similar to Panel B1, the difference between FEA and test results for Panel B is most likely due to variation in modulus of subgrade reaction. The beam on elastic foundation deflections are 30 percent of actual deflections and almost half defections obtained earlier for loads located at center and wheel path. Unlike Panel B1, Panel B2 load is an edge load and BEF does not account for load location with respect to beams or pavements width. Table 30 compares deflections from Panel III-B2 with those from FEA and BEF. Similar to Panel III-A and B1 , the panel was loaded to 50,000 lbs earlier during this research to test the equipment and loading frame and the load must have increased modulus of subgrade reaction by compressing the base.

Load (kip)	Test Results Deflections (in) (LVDT 1)	Finite Element Analysis		Beam on Elastic Foundation	
		Deflection (in)	FEA/Actual (%)	Deflection (in)	BEF/Actual (%)
9	0.0136	0.0181	133.1	0.0045	33.1
18	0.0275	0.0363	132.0	0.0090	32.7
27	0.0421	0.0544	129.2	0.0135	32.1
30.	0.0547	0.0604	110.4	0.0150	27.4

Table 28 Comparison of test and analysis deflections at load location for test Panel I-B2.

Load (kip)	Test Results Deflections (in) (LVDT 1)	Finite Element Analysis		Beam on Elastic Foundation	
		Deflection (in)	FEA/Actual (%)	Deflection (in)	BEF/Actual (%)
9	0.0138	0.0181	131.1	0.0045	32.6
18	0.0282	0.0363	128.7	0.0090	31.9
27	0.0409	0.0544	133.0	0.0135	33.1
30.	0.0524	0.0604	115.3	0.0150	28.6

Table 29 Comparison of test and analysis deflections at load location for test Panel II-B2.

Load (kip)	Test Results Deflections (in) (LVDT 1)	Finite Element Analysis		Beam on Elastic Foundation	
		Deflection (in)	FEA/Actual (%)	Deflection (in)	BEF/Actual (%)
9	0.0106	0.0139	131.1	0.0038	35.8
18	0.0215	0.0278	129.3	0.0076	35.3
27	0.0337	0.0416	123.4	0.0114	33.8
30.	0.0377	0.0463	122.8	0.0127	33.7

Table 30 Comparison of test and analysis deflections at load location for test Panel III-B2.

7.5.3 TRAFFIC LOADS VS CONCENTRATED LOADS

Previous tables give only comparisons between tests and analysis. The tables showed that the FEA results were more accurate than BEF in predicting deflections for test pavements with one concentrated point load. However, previous results from Table 17 for 18k axle (two 9,000 tire loads spaced 6 feet apart) showed that the FEA and BEF deflections are within 10 percent difference. Figure 93 shows the transverse deflected shape (cut along 8 ft width) for Pavement I/II. The deflections are for cases when 18k load is located at the middle of the panel compared to when a pair of 9k loads - totaling 18k - are located at the wheel paths. Notice that for the pair of 9k loads the edge deflections are 0.008 in. and the deflections under the loads are 0.011 in. On the other hand, the edge deflections for 18k single point load are 0.0025 in. while the deflection under the point load is 0.018 in. The figure shows that single concentrated loads at the middle of the pavement act more like a plate. On the other hand, a pair of 9k loads used in pavement designs causes more uniform deflection across the pavement width. This indicates that BEF can accurately predict pavement deflections and possibly stresses for traffic load.

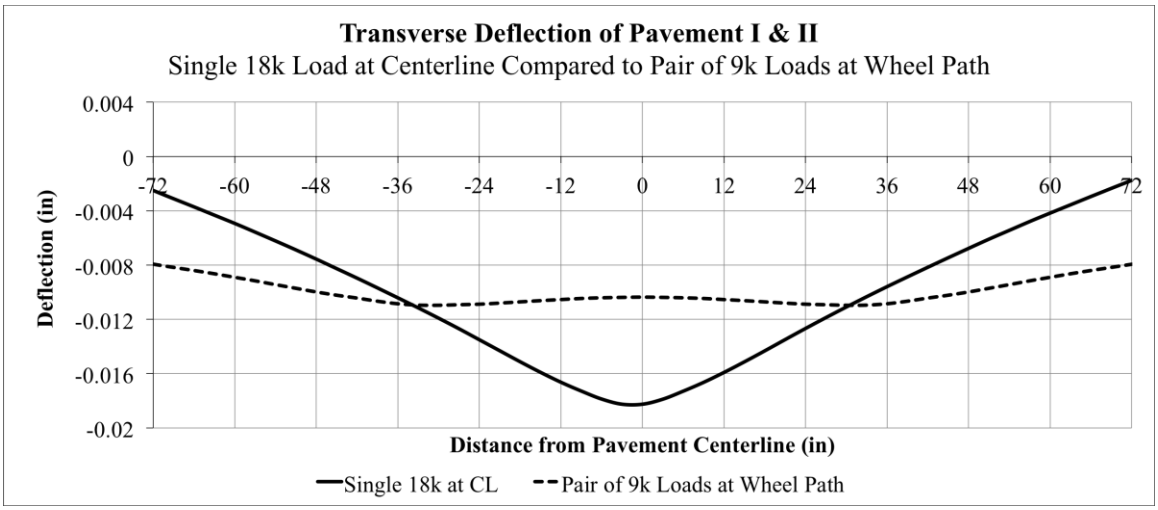

Figure 93 Transverse deflection of 12 ft wide Pavement I & II due to single 18k load at centerline compared to pair of 9k loads at wheel path

7.6 MODULUS OF SUBGRADE REACTION

The deflection data were also used to estimate the modulus of subgrade reaction (k) using methods outlined by Supplement to the AASHTO Guide For Design of Pavement Structures Part II (AASHTO 1998). The method uses deflection data at distances of 0, 8, 12, 18, 24, 36, and 60 in. from the load center to establish deflection basin and calculate the modulus of subgrade reaction. The method requires that the deflection be measured at the wheel path and away from the edge. The deflection data for Panels I-A, II-A, and III-A were used for k-value calculations. The test pavement deflections at 8, 18, 36, and 60 in. where not measured by instruments. Therefore, the data were interpolated from the deflection profile in Figure 88, Figure 91, and Figure 92.

Actual and calculated k-values are reported in Table 31 using deflection data from 30k static load test. The calculated k-value for Pavement I and II are 139 psi/in and 121 psi/in, respectively. These values are lower than the design 150 psi/in k-value but still within the estimated 130 psi/in to 200 psi/in range reported in section 4.1 under design assumptions. On the other hand, Pavement III reported high k-value of 235 psi/in which is predicted since the pavement was preloaded with 50,000 lbs point loads for extended period of time before the actual tests were performed.

	Pavement I	Pavement II	Pavement III
Actual Calculated k-value (psi/in.)	139	121	235
Design k-value (psi/in)	150	150	150

Table 31 Calculated and analysis modulus of subgrade reaction, k-value

7.7 SUMMARY

In this chapter finite element analysis (FEA) for non-uniform subgrade reaction illustrated how the formation of void or weak support conditions under the pavement can result in substantial increase in stresses. Result from the FEA show that pavement stresses can increase 100 percent or more due to non-uniform bearing conditions. The technique of grouting under the precast pavement segments helps to mitigate these variations in stresses, and should prolong the lifespan of the pavement structure.

The use of dynamic analysis illustrated how variation in pavement thickness and traffic affect the pavement performance. It has been shown that pavements with short spans, or short distance between joints, can results in pavement with minimum thickness of 6 inches to provide enough ballast to prevent separation from the subbase as the load moves along the pavement. Further investigation and analysis showed that for this research pavement, pavement with the length less than 200 feet should be analyzed as finite length pavement. On the other hand, pavement with larger spans, or distance between joints, exceeding 200 ft should have minimum thickness of 4 inches to provide enough ballast.

It was also shown that FEA results were more accurate than BEF for pavement with single point load. However, the BEF did predict deflections with accuracy for loads that are

paired and spaced evenly over the width of the pavement. Additionally, deflection results were used to calculate the modulus of subgrade reaction. The calculated modulus of subgrade reaction was within the predicted k-value range based on subgrade soil type and aggregate based thickness.

CHAPTER VIII

CONCLUSIONS AND RECOMMENDATIONS

8.1 CONCLUSIONS

Precast, prestressed concrete pavement offers many advantages over conventional rigid pavements whether plain jointed concrete pavements or continuously reinforced concrete pavements. By using precast concrete, one can expect a better quality concrete product due to plant-cast conditions, improved concrete durability, pavement that is not subject to early age temperature fluctuations that can result in cracking and distress, pavement that is not subject to early age curing issues such as adverse effects from temperature, wind, humidity or moisture. Using precast concrete one can expect faster construction and subsequent reduction in user costs and fewer traffic delays. There are also economies to be expected with repetition in the product.

The principal disadvantage is the need for more specialized and often-times non-standard construction equipment. Since the system is not widely used as yet, the hardware and construction methods are still in development, as well as the "learning curve" among the transportation contractors to understand the best methods for constructing precast concrete pavements. Also, there can be an overall decrease in ride quality, or the need to diamond grind pavements after completion in order to attain a smooth ride. For smaller projects, one can expect higher costs.

Even so two of the primary benefits, reduced user costs through more rapid construction and thinner pavement, are particularly compelling in rehabilitation of urban pavements and increasing the clearance for bridges underpasses.

One of the objectives of this research is to improve the performance and efficiency of PPCP. The designs from this research incorporate the use of aggregate base material without asphalt leveling base to decrease construction time and reduce the overall pavement thickness. The designs also incorporating large grout voids into the precast panels to decrease the area of pavement requiring prestress and to improve the transfer of load from the pavement to the base material. To achieve the objectives of this research full scale test pavements were fabricated, assembled, and tested to verify the proposed design improvements.

One of the major concerns regarding the use of aggregate base is the formation of gaps and weak supports between the pavement panels and aggregate base due to uneven base surface grading. This research demonstrates that precast prestressed concrete pavements can be successfully built atop compacted granular base material as long as under panel grouting is performed to fill spaces between the pavement panels and the granular base. There were no issues related to panel leveling and elevation matching during assembly. The use of granular base did not adversely affect the predicted structural performance of the pavement since the calculated modulus of subgrade reactions in Table 31 were within the expected range (130 psi/in to 200 psi/in).

Incorporating grouted voids within the panel helped reduced the precast pavement mass by 20 percent. The reduction of mass meant that more panels can be hauled from the fabrication plant to the job site per truck. Additionally, the reduction in the panel cross-sectional area results in an increase in the panel prestress. The use of grouting proved to be effective in achieving uniform pavement support.

One of the most important finding in this research is that the pavement load tests showed the pavement response to load remained linear even when the applied loads reached 30k as shown previously in Figure 60, Figure 61, Figure 62, Figure 63, and Figure 64. This finding is important as it validates the use of linear springs as support for the finite elements model and the static and dynamic analysis. Comparison of the measured load vs. deflection to a perfectly linear system indicates R^2 values very nearly 1.00. The coefficient of determination, R^2 is reported in each of the figures referenced above.

This conclusion is also supported by using finite element analysis to obtain deflections using calculated k-values. Calculated k-values were obtained from AASHTO Guide for Design of Pavement Structures Part II (AASHTO 1998) and described earlier in Section 7.6. Table 31 then compares measured deflections to deflections computed from FEA with the adjusted k-values. The results are shown in Figure 94, Figure 95, and show the actual deflections from the 30 kip static load tests to deflections predicted using the FEA and adjusting the modulus of subgrade reaction, k from the data collected in testing. The figures show that the finite element deflections are nearly identical to those from pavement testing. Again, note that the plots for Actual Load vs. Deflection are smoothed curves. Since pavement support was assumed to be uniform in the finite element model then this indicates uniform base support for the test pavement.

Furthermore, the figures show continuity in longitudinal deflection across the internal keyed joints beyond four feet from the load indicating an efficient moment transfer. Note that in the finite element model the panels were assumed to be continuous across the joints; effectively the joints do not exist in the analysis. Results indicate that the approximations are reasonably accurate and that effective load transfer does occur.

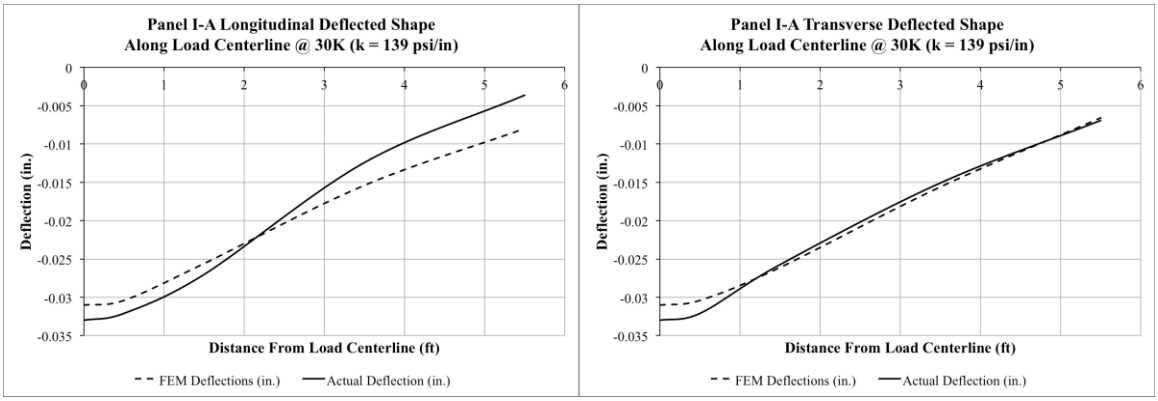

Figure 94 Panel I-A Longitudinal and Transverse Deflected Shape (k = 139 psi/in)

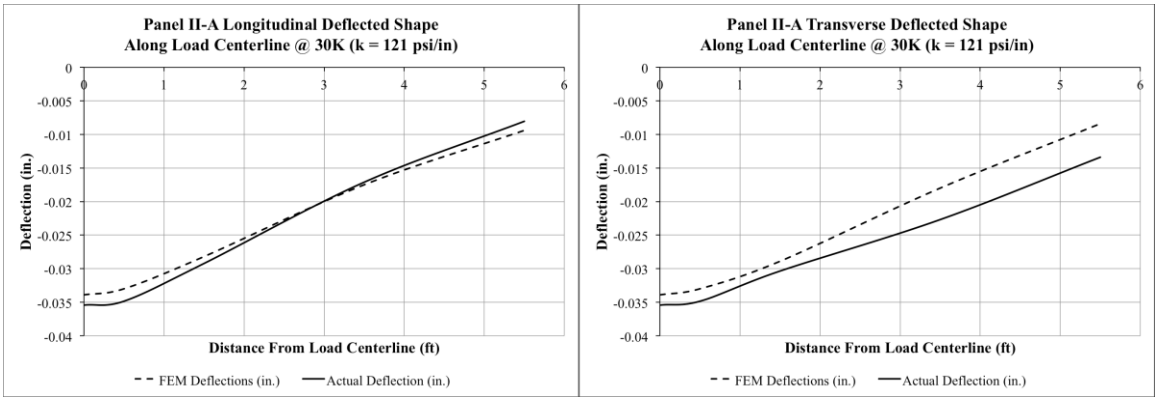

Figure 95 Panel II-A Longitudinal and Transverse Deflected Shape (k = 121 psi/in)

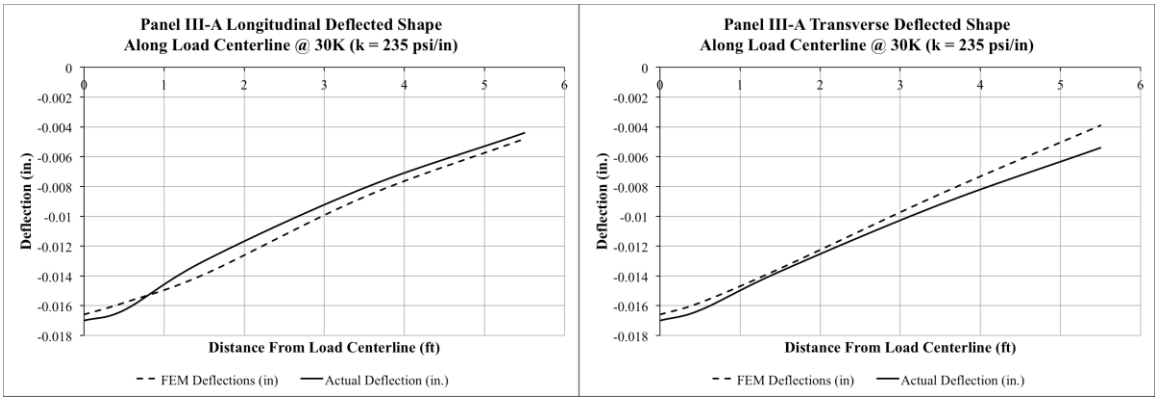

Figure 96 Panel III-A Longitudinal and Transverse Deflected Shape (k = 235 psi/in)

Dynamic analysis was also performed on the precast, prestressed concrete pavement system. This research performed to study the pavement response to stationary and moving traffic

loads. To perform these analyses, the pavement was modeled as beams on elastic foundation. The analyses were used to estimate pavement deflections and internal stresses and to establish minimum pavement thickness. Figure 77 shows that pavement deflections increase as pavement thickness decreases. Figure 85 shows that increasing velocity of the moving load decreases the pavement downward deflections but does not affect uplift cause by the "wave" ahead of the load. Deflections in Table 19 indicated that 50 ft long pavement with thickness of four inches did not possess enough mass to counter the uplift caused by a load moving at 65 mph. On the other hand, pavements with length exceeding 200 ft with four inches thickness did not possess enough mass to maintain contact with the base as shown in Figure 82. Further analyses established minimum pavement thickness based on pavement length or distance between expansion joints as shown in Figure 87. From these analyses, the minimum pavement thickness should be 6 in for short segments and four inches for longer pavements.

Results from pavement tests, FEA, and BEF were compared. Figure 94, Figure 95, and Figure 96 showed that FEA results were very accurate in predicting deflections when using accurate k-value. On the other hand, the BEF results for single point load were not accurate due to plate action as. However, Table 17 shows that the BEF method deflections and stresses were 25 percent lower for paired tire loads spaced at evenly over the width of the pavement.

8.2 RECOMMENDATIONS FOR FURTHER RESEARCH

- Future research is needed on PPCP fatigue caused by repeated loads. Pavements are subjected to millions of loads during its design life and PPCP design life should match or surpass that of conventional cast in-situ concrete pavement. The effect of thousands of repeated loads on the pavement performance and the post-tensioning hardware is critical in determining the effectiveness and durability of PPCP.

- Future research on the effects of moving loads on thin PPCP cross sections. This research focused on the theoretical response of the pavement when subjected to moving load. Future research is needed to study the actual response of test pavement structures moving loads and the extent of damage caused by separation of pavement and sub-base.

8.3 RECOMMENDATIONS FOR THE INDUSTRY

- Multi-strand post-tensioning system is a viable alternative and could reduce construction time. However, special hardware will be required for thinner pavement panels. The 4-strand post-tensioning anchors used in this research required a minimum thickness of 8 in.
- Ducts are precast into the pavement segments. To facilitate placement of the tendons and grouting, hardware for joining ducts between panels could be developed that would marginally ease installation of the tendons, post-tensioning, and grouting. It would be useful for grouting if the connections for ducts would be made air tight.
- The material used in sealing the joints and around the base of the pavement was not suitable to prevent grout leaks and in some cases it blocked the ducts. In the literature, there was more success in using neoprene O-Rings and epoxy around the ducts between the joint. For the voids under the panels it is recommended to use a compressible material with a thickness of at least ½ in.

.

REFERENCES

AASHTO (1993). *AASHTO guide for design of pavement structures, 1993*, American Association of of State Highway and Transportation Officials, Washington, D.C.

AASHTO (1998). *Supplement to the AASHTO guide for design of pavement structures. Part II, Rigid pavement design & rigid pavement joint design*, American Association of State Highway and Transportation Officials, Washington, D.C.

ACI (2005). *Building code requirements for structural concrete (ACI 318-05) and commentary (ACI 318R-05)*, American Concrete Institute, Farmington Hills, Mich.

ACI Committee 325 (1988). *Recommendations for Designing Prestressed Concrete Pavements (325.7R-88).* American Concrete Institute, Detroit, Michigan.

Ballinger, C. A. (1971). "Cumulative fatigue damage characteristics of plain concrete." *Highway Research Record*(370), 13.

Beckemeyer, C. A., Khazanovich, L., Yu, H. T., and Trb, T. R. B. (2002). "Determining amount of built-in curling in jointed plain concrete pavement - Case study of Pennsylvania I-80." *Design and Rehabilitation of Pavements 2002 - Pavement Design, Management, and Performance*, Transportation Research Board Natl Research Council, Washington, 85-92.

Cable, N., Burns, N., and McCullough, F. B. (1985). "New Concepts in Prestressed Concrete Pavements." Center for Transportation Research, Austin, Texas.

Cebon, D. (1985). "An investigation of the dynamic interaction between wheeled vehicles and road surfaces." Ph.D. U357096, University of Cambridge (United Kingdom), England.

Chang, L. M., Chen, Y., and Lee, S. (2004). "JTRP 2004 final reports January-June." West Lafayette, IN : Joint Transportation Research Program, School of Civil Engineering, Purdue University, 1 CD-ROM ; 4 3/4 in.

Chatti, K. (1992). "Dynamic analysis of jointed concrete pavements subjected to moving transient loads." The University of California Transportation Center, Berkeley, CA.

Chávez, C. I. M., McCullough, F. B., and Fowler, D. W. (2003). "Design of a post-tensioned prestressed concrete pavement, construction guidelines, and monitoring plan." *CTR research report*, Springfield, Va.

Chia, W. S., McCullough, F. B., and Burns, N. H. (1986). "Field evaluation of subbase friction characteristics." Center for Transportation Research, September 1986.

Chopra, A. K. (2007). *Dynamics of structures : theory and applications to earthquake engineering*, Pearson/Prentice Hall, Upper Saddle River, N.J.

Clemmer, H. F. (1923). "Fatigue of Concrete." *ASTM Proceedings*, 22(II), 408-419.

Diaz, A. M. (1986). "Behavior of long prestressed pavement slabs and design methodology." Ph.D. Dissertation, The University of Texas at Austin, Austin, Texas.

Diaz, A. M., McCullough, F. B., and Burns, N. H. (1986). *Design of the Texas prestressed concrete pavement overlays in Cooke and McLennan counties and construction of the McLennan County Project*, Springfield, Va., Austin, Tex. : The Center.

Frýba, L. (1999). *Vibration of solids and structures under moving loads*, Thomas Telford, London.

Goldbeck, A. T. (1919). "Thickness of concrete slabs." *Public Roads*, 34-38.

Hanna, A. N. (1976). *Technological review of prestressed pavements : interim report*, Federal Highway Administration, Washington Springfield, Va.

Harr, M. E. (1962). "Influence of Vehicle Speed on Pavement Deflections." *Highway Research Board Preceedings*, 41, 77-82.

Huang, Y. H. 2004. Pavement analysis and design, version 2ndUpper Saddle River, NJ : Pearson/Prentice Hall.

Kenney, J. T. (1954). "Steady-State Vibrations of Beams on Elastic Foundation for Moving Load." *Journal of Applied Mechanics*, 21(4), 359-364.

Klunker, F. "Status and Developments in the Construction of Prestressed Concrete Runways in European Airports." *Proc., Proceedings of the 2nd International Conference on Concrete Pavement Design*.

Lane, B., and Kazmierowski, T. (2006). "Precast Concrete Slab Repair Methods." *Concrete International*, 28(11), 29-35.

Merritt, D. K., McCullough, B. F., and Burns, N. H. (2001). "Construction and preliminary monitoring of the Georgetown, Texas precast prestressed concrete pavement." *Implementation report*, Center for Transportation Research, the University of Texas at Austin.

Merritt, D. K., McCullough, B. F., and Burns, N. H. (2001). "Feasibility of using precast concrete panels to expedite construction of Portland cement concrete pavements." *Transportation research record. No.*, 1259379.

Merritt, D. K., McCullough, B. F., Burns, N. H., and Schindler, A. K. (2000). "The feasibility of using precast concrete panels to expedite highway pavement construction." *Research report*, Springfield, Va.

Merritt, D. K., Miron, A. J., Rogers, R. B., and Rasmussen, R. O. (2007). "Construction of the Iowa Highway 60 precast prestressed concrete pavement bridge approach slab demonstration project." Iowa Highway Research Board.

National Research Council (U.S.). Highway Research Board., and American Association of State Highway Officials. (1961). *The AASHO road test : report*, National Academy of Sciences-National Research Council, Washington.

OKDOT (1999). "1999 standard specifications for highway construction." [Oklahoma City] : Oklahoma Dept. of Transportation, 1 v. (various pagings) ; 21 cm. + 21 computer optical disc (24 23/24 in.).

PCA (1951). "Concrete Pavement Design." Portland Cement Association.

PCA (1966). "Thickness design for concrete pavement." Portland Cement Association.

Pickett, G., Raville, M. E., Janes, W. C., and McCormick, F. J. (1951). "Deflections, moments, and reactive pressure for concrete pavement." *Bulletin No 65.* Engineering Experiment Station, Kansas State College.

Snell, L. M., and Snell, B. G. (2002). "Oldest concrete Street in the United States." *Concrete International*, 72-74.

Tayabji, S. D., Barenberg, E. J., Gramling, W., and Teng, P. "Prestressed Concrete Pavement Technology Update." *Proc., 7th International Conference on Concrete Pavements*.

Timoshenko, S. P. "Statical and Dynamical Stresses in Rails." *Proc., Proc. Intern. Congr. Appl. Mech.*, 407-418.

Winkler, E. (1867). *Theory of Elasticity and Strength*, Dominicus Prague, Czechoslavakia.

APPENDIX A

RIGID PAVEMENT AASHTO DESIGN OUTPUT

Rigid Pavement Design - Based on AASHTO Supplemental Guide

Reference: *LTPP DATA ANALYSIS - Phase I: Validation of Guidelines for k-Value Selection and Concrete Pavement Performance Prediction*

Results

Project # FHWA PPCP
Description:

Location:

Slab Thickness Design

Pavement Type	CRCP	
18-kip ESALs Over Initial Performance Period (million)	10.00	million
Initial Serviceability	4	
Terminal Serviceability	2.5	
28-day Mean PCC Modulus of Rupture	530	psi
Elastic Modulus of Slab	4,000,000	psi
Elastic Modulus of Base	15,000	psi
Base Thickness	6.0	in.
Mean Effective k-Value	150	psi/in
Reliability Level	95	%
Overall Standard Deviation	0.2	
Calculated Design Thickness	**12.84**	in

Temperature Differential

Mean Annual Wind Speed	12.4	mph
Mean Annual Air Temperature	59.9	°F
Mean Annual Precipitation	30.9	in
Maximum Positive Temperature Differential	**11.89**	°F

Modulus of Subgrade Reaction

Period	Description	Subgrade k-Value, psi
4	1	150
4	2	150
4	3	150
4	4	150

Figure A1. Rigid Pavement Design Based on AASHTO Supplemental Guide calculations sheet

APPENDIX B

PRECAST PRESTRESSED CONCRETE PAVEMENT DESIGN & CONSTRUCTION DRAWINGS

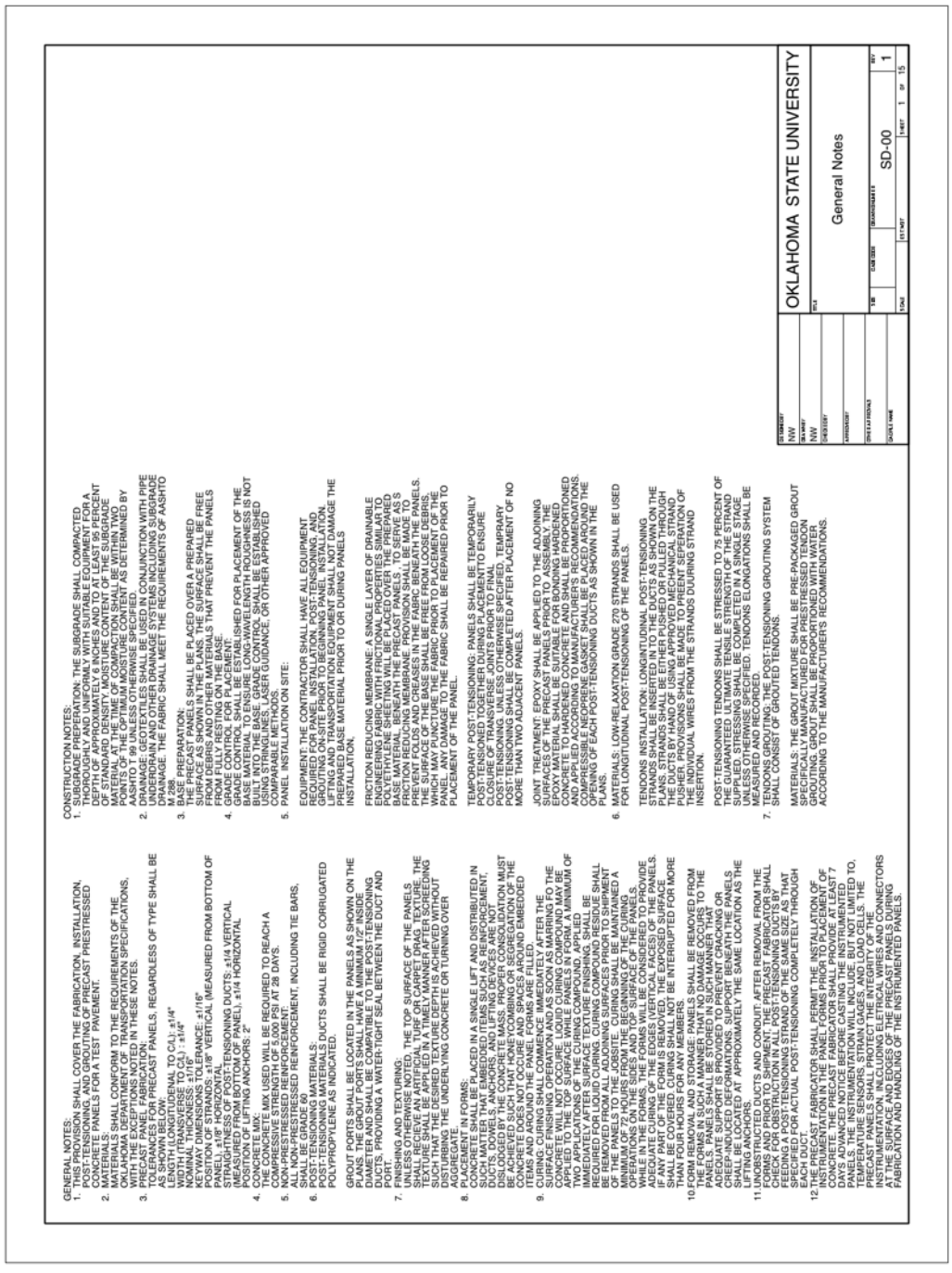

Figure B1 Pavement construction drawings “General Notes”

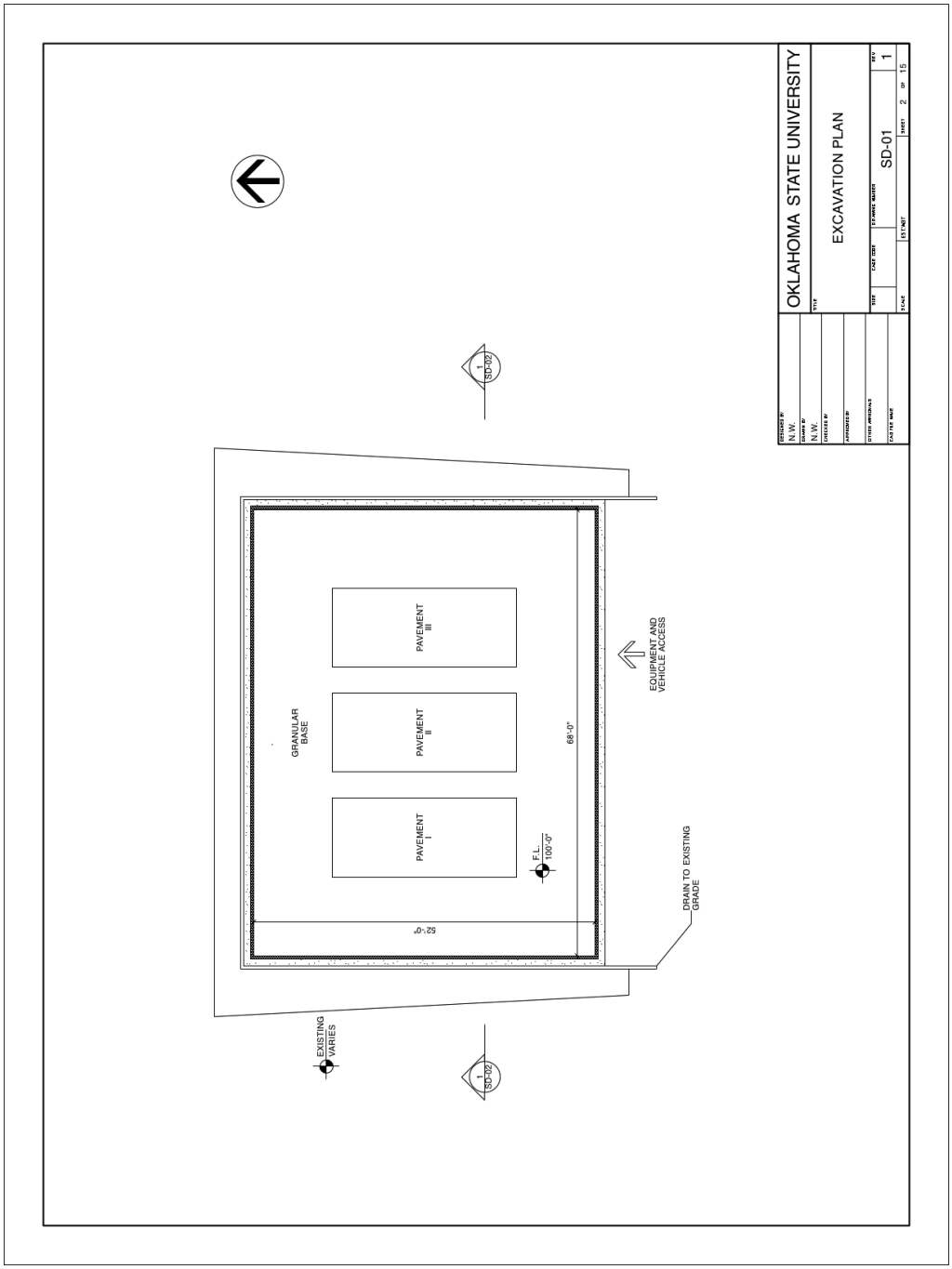

Figure B2 Pavement construction drawings “Excavation Plan”

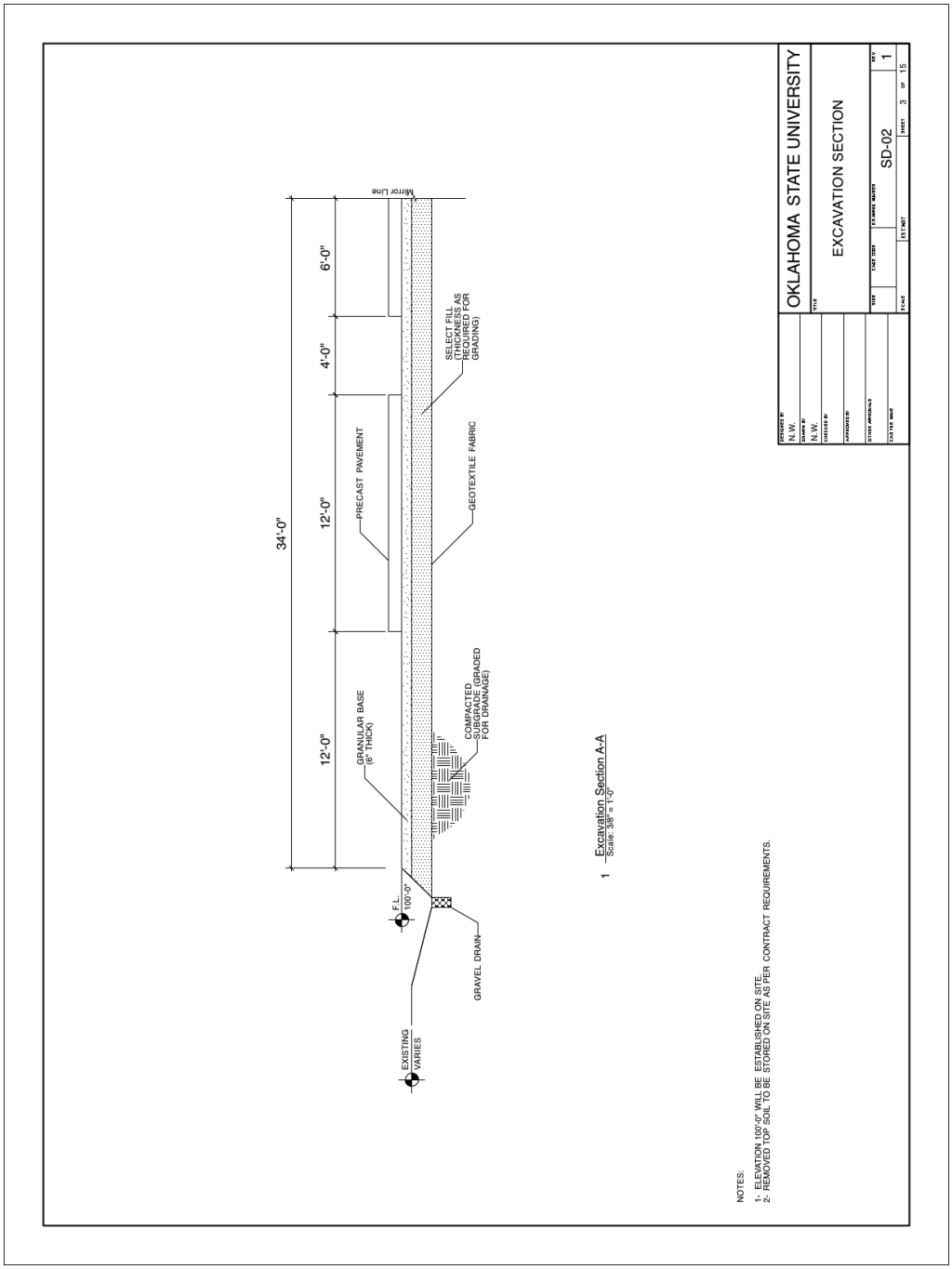

Figure B3 Pavement construction drawings “Excavation Section”

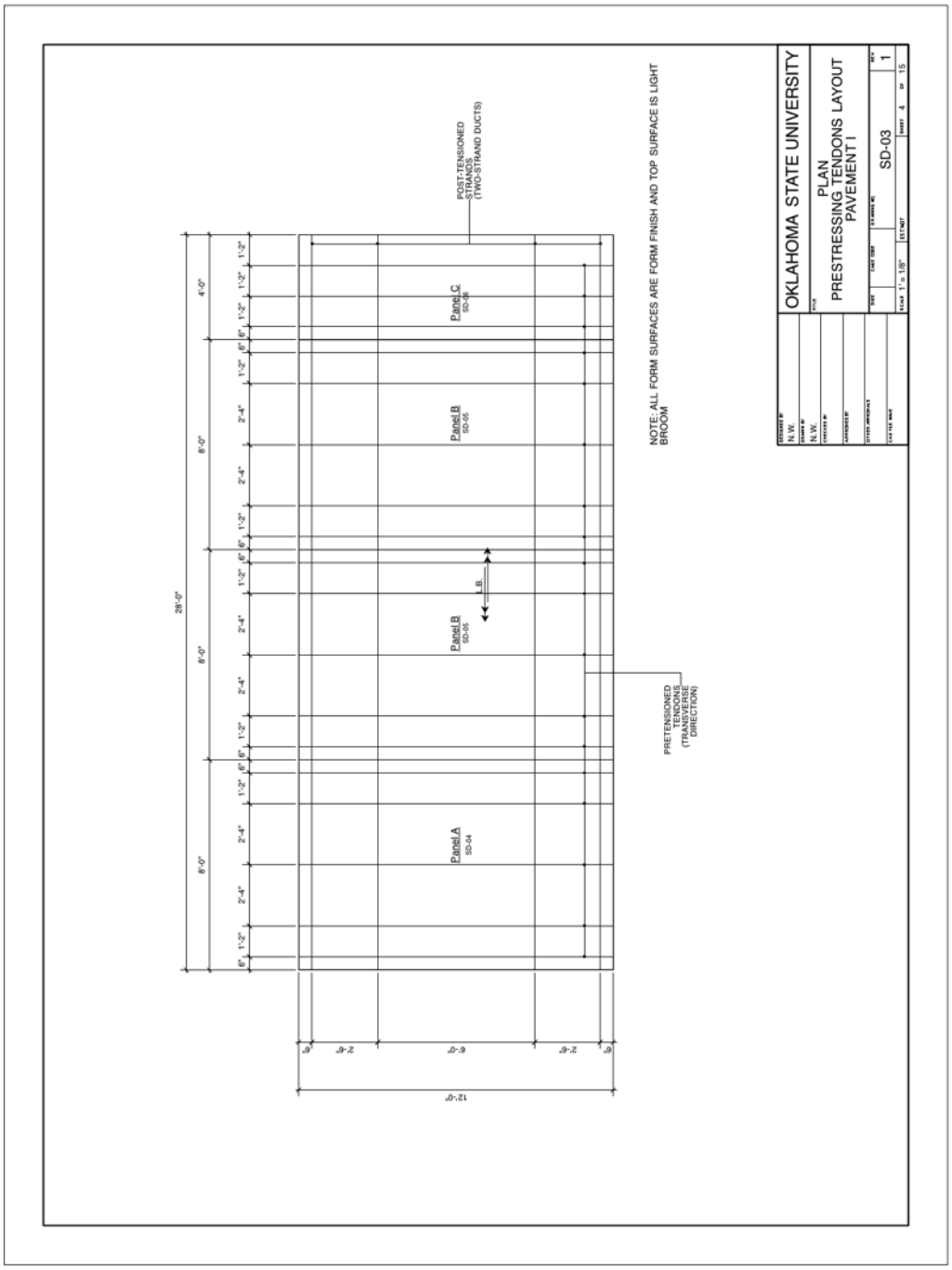

Figure B4 Pavement construction drawings “Prestressing Tendons Layout Pavement I”

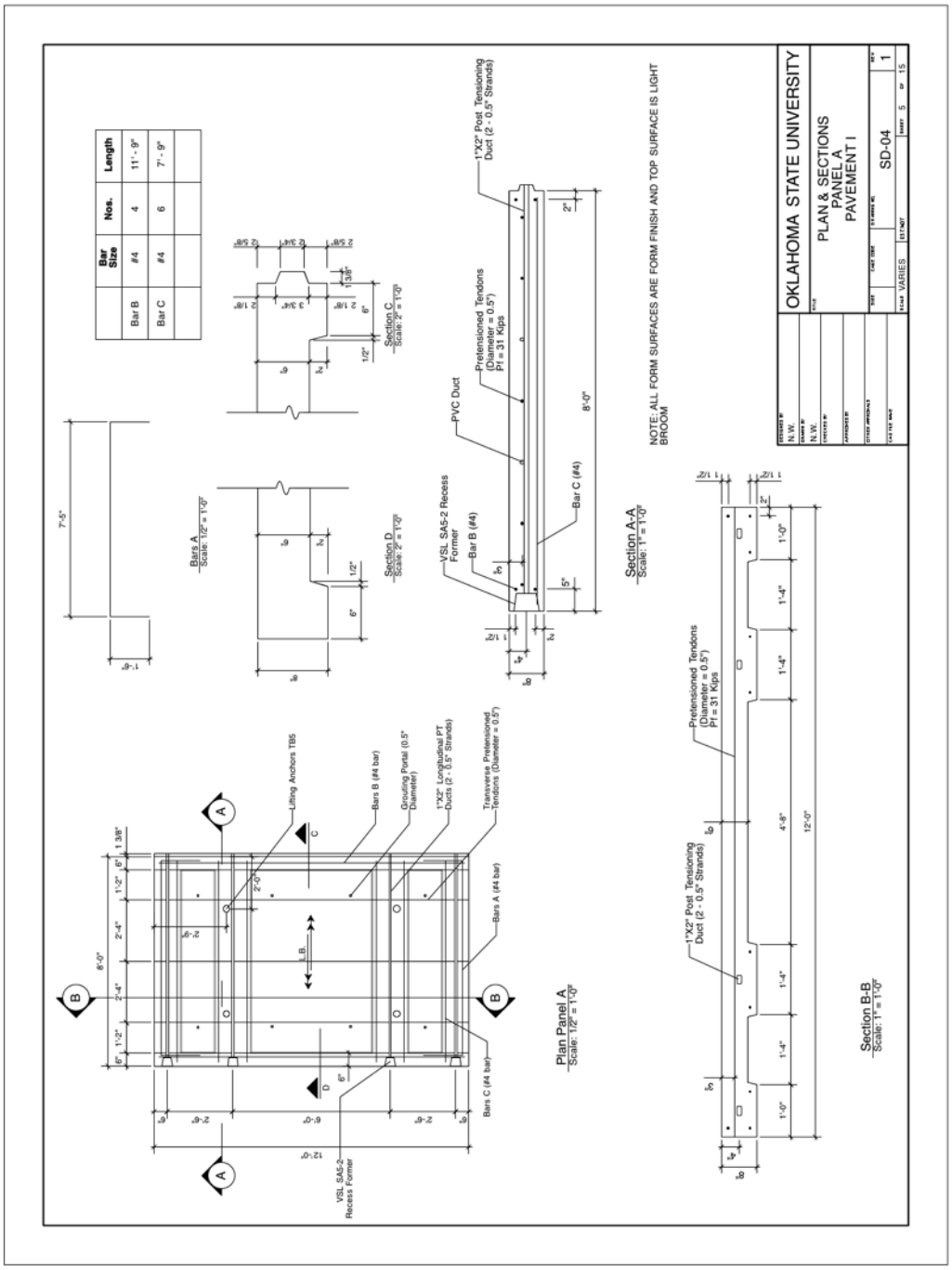

Figure B5 Pavement construction drawings “Plans and Sections Panel A Pavement I”

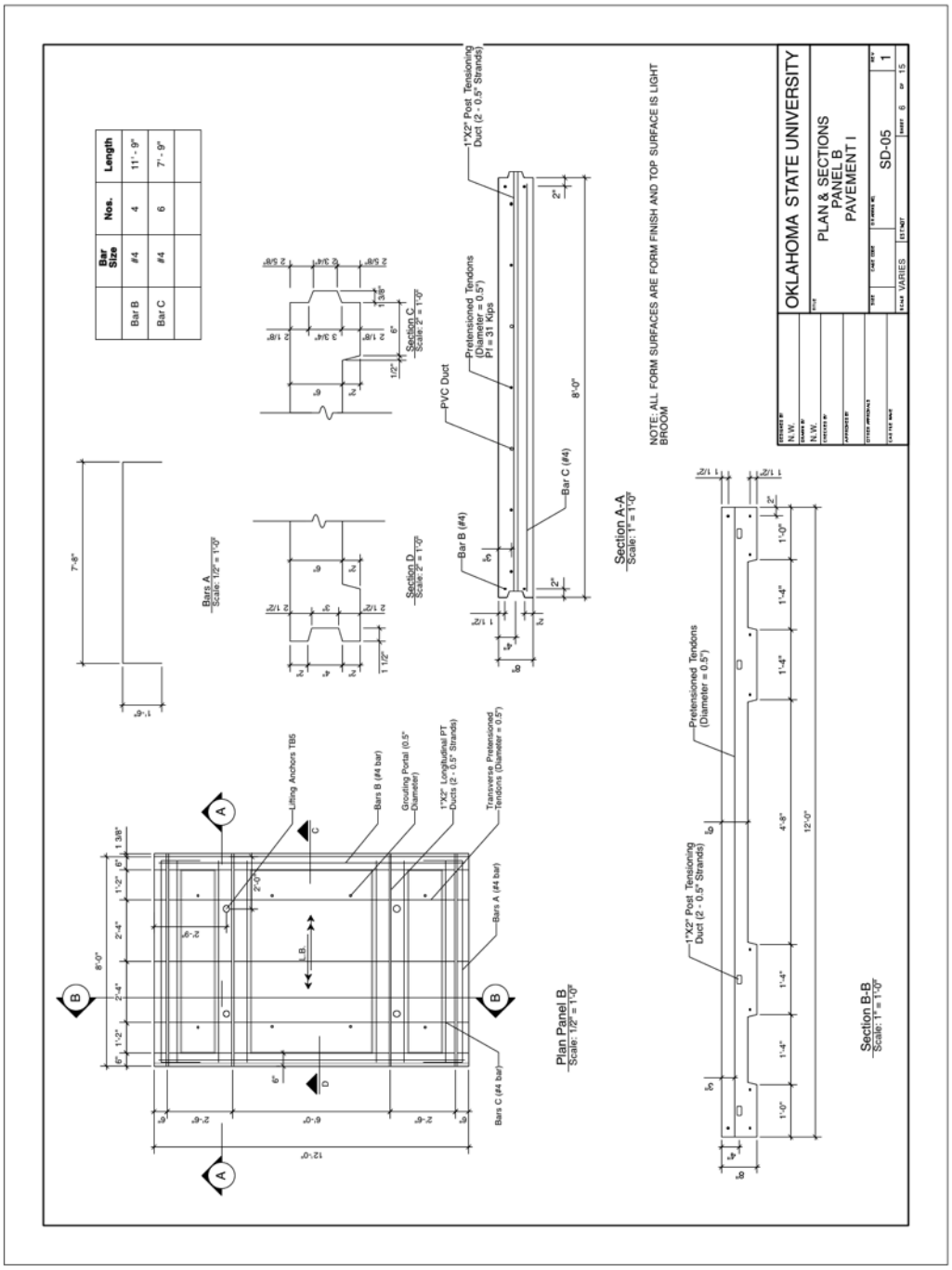

Figure B6 Pavement construction drawings “Plans and Sections Panel B Pavement I”

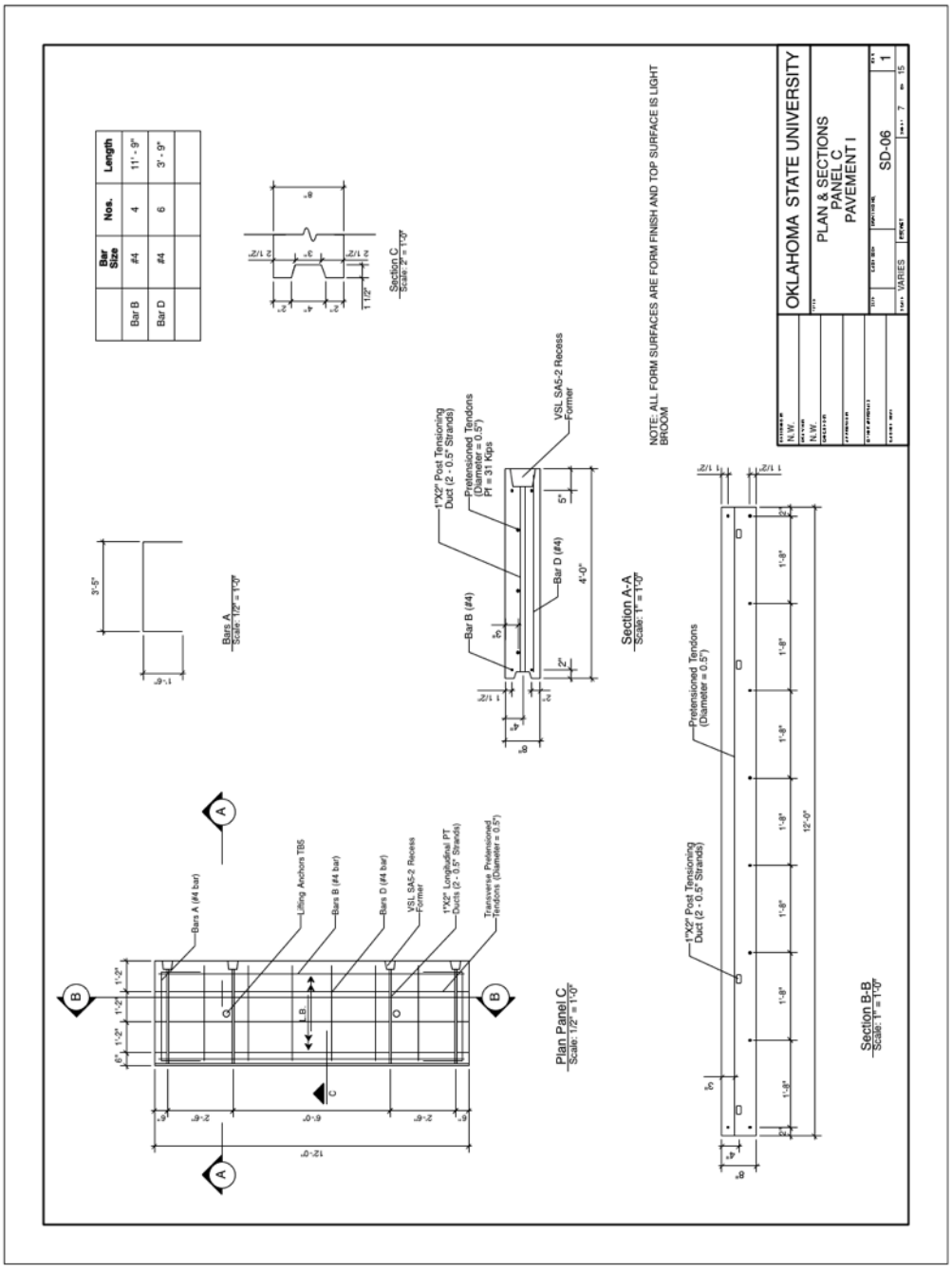

Figure B7 Pavement construction drawings “Plans and Sections Panel C Pavement I”

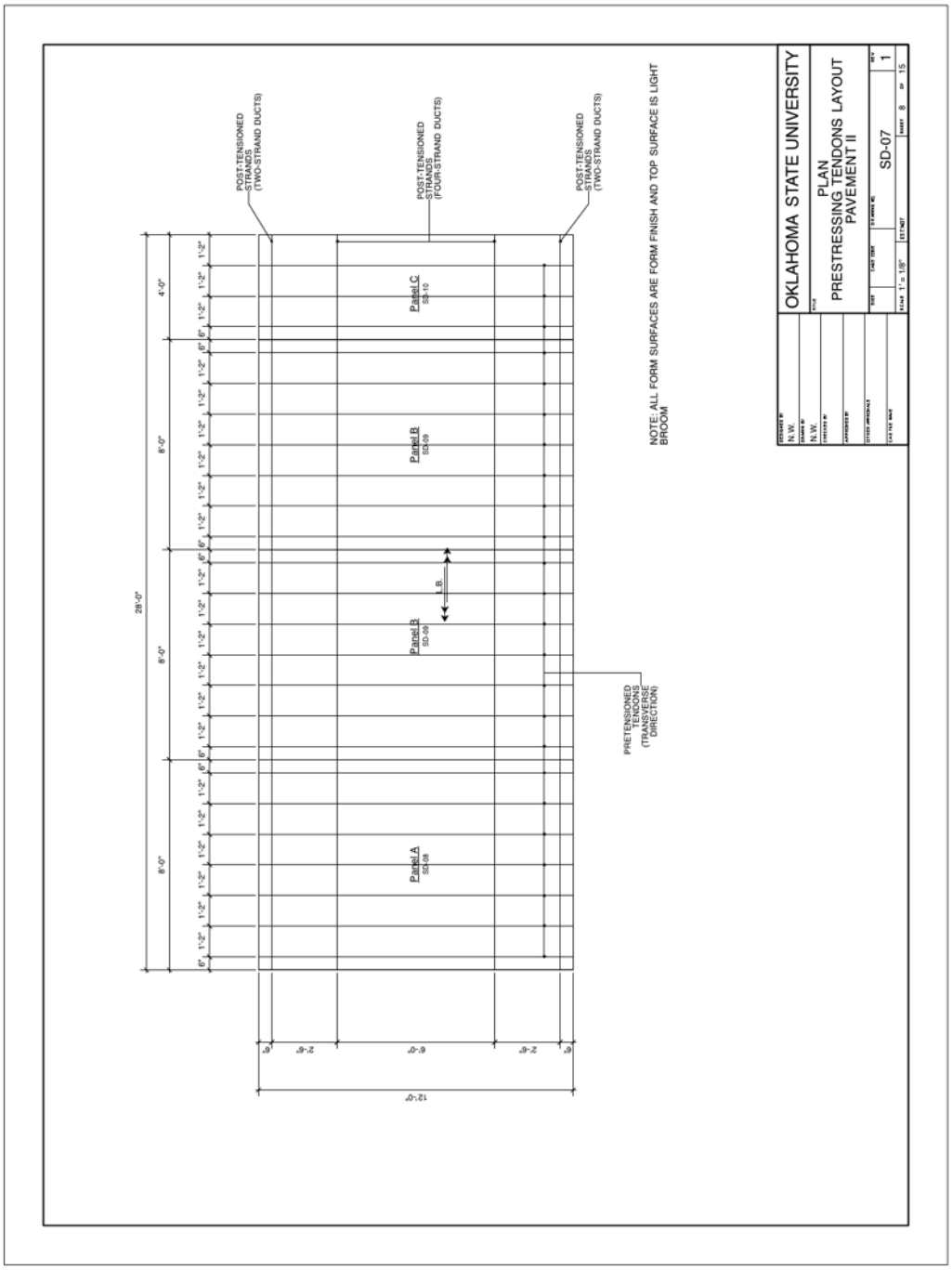

Figure B8 Pavement construction drawings “Prestressing Tendons Layout Pavement II”

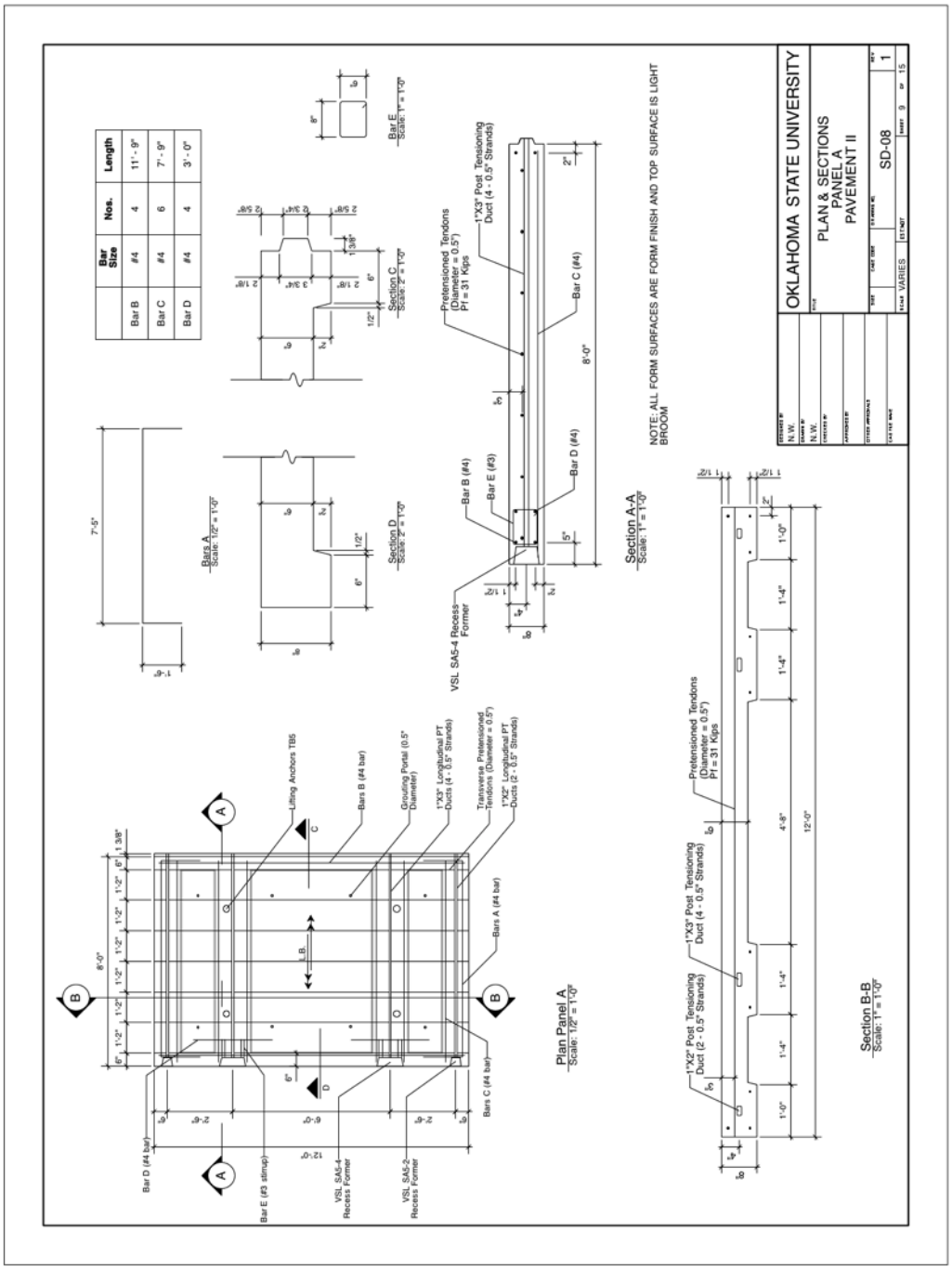

Figure B9 Pavement construction drawings “Plans and Sections Panel A Pavement II”

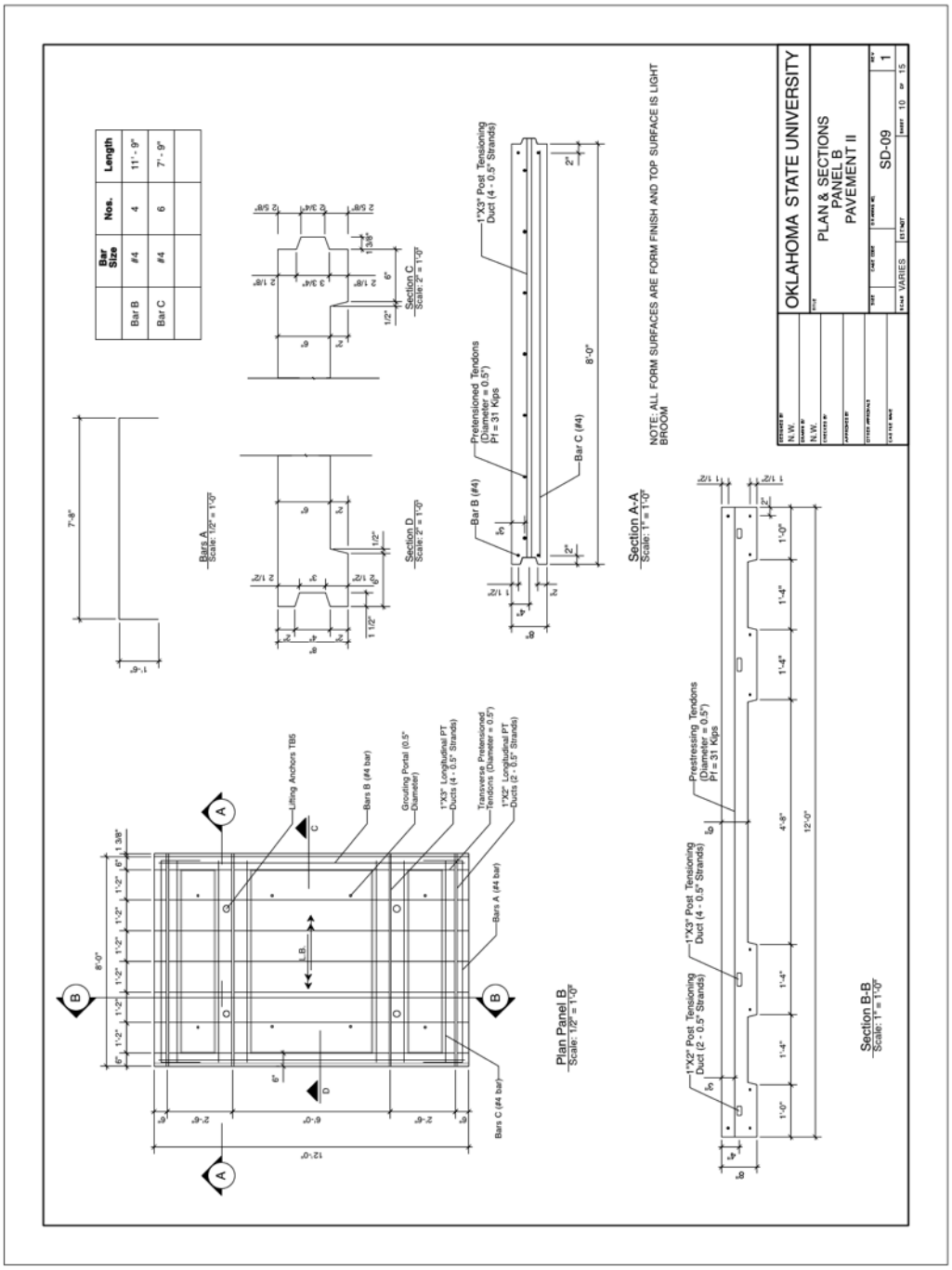

Figure B10 Pavement construction drawings “Plans and Sections Panel B Pavement II”

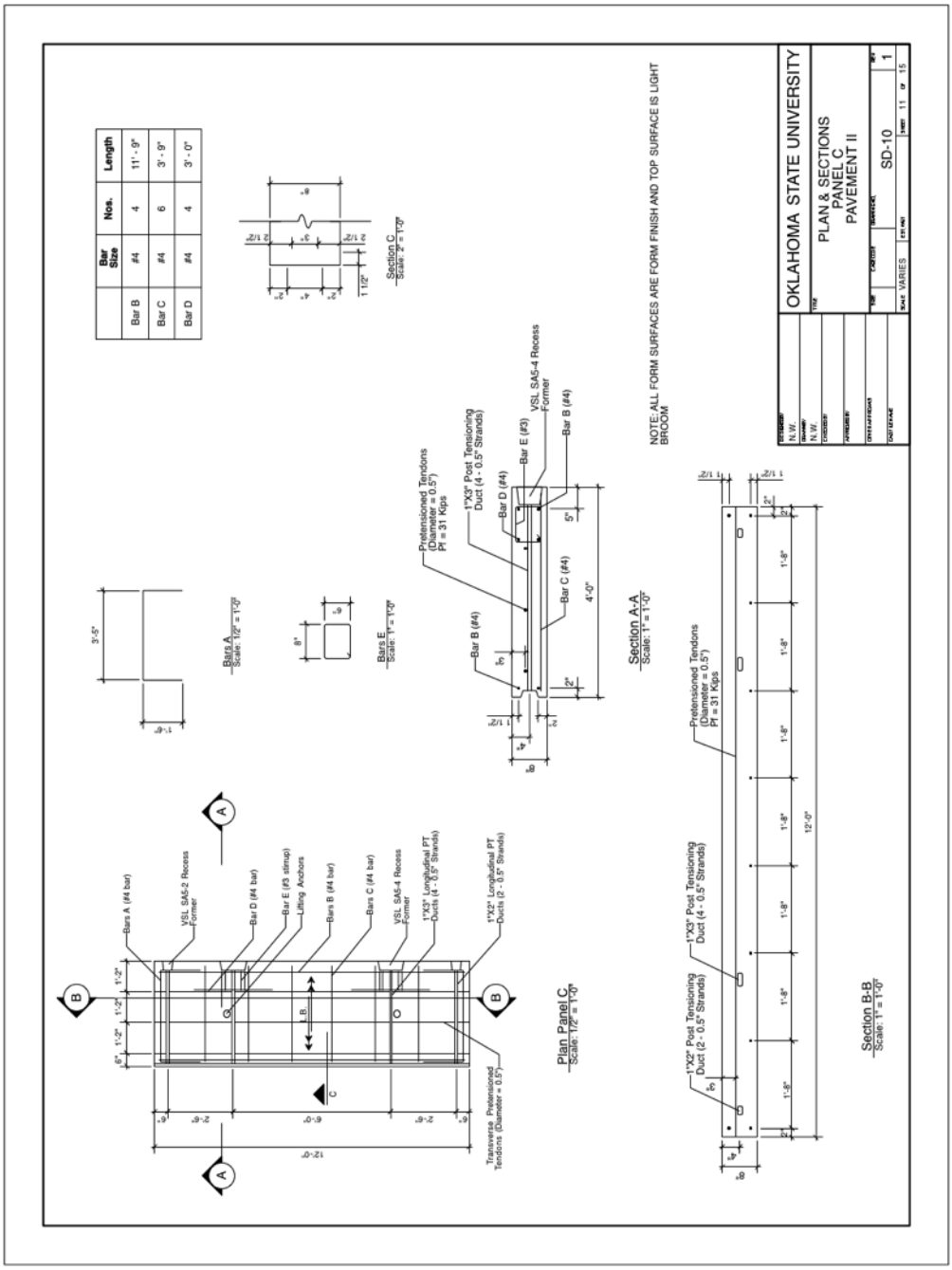

Figure B11 Pavement construction drawings “Plans and Sections Panel C Pavement II”

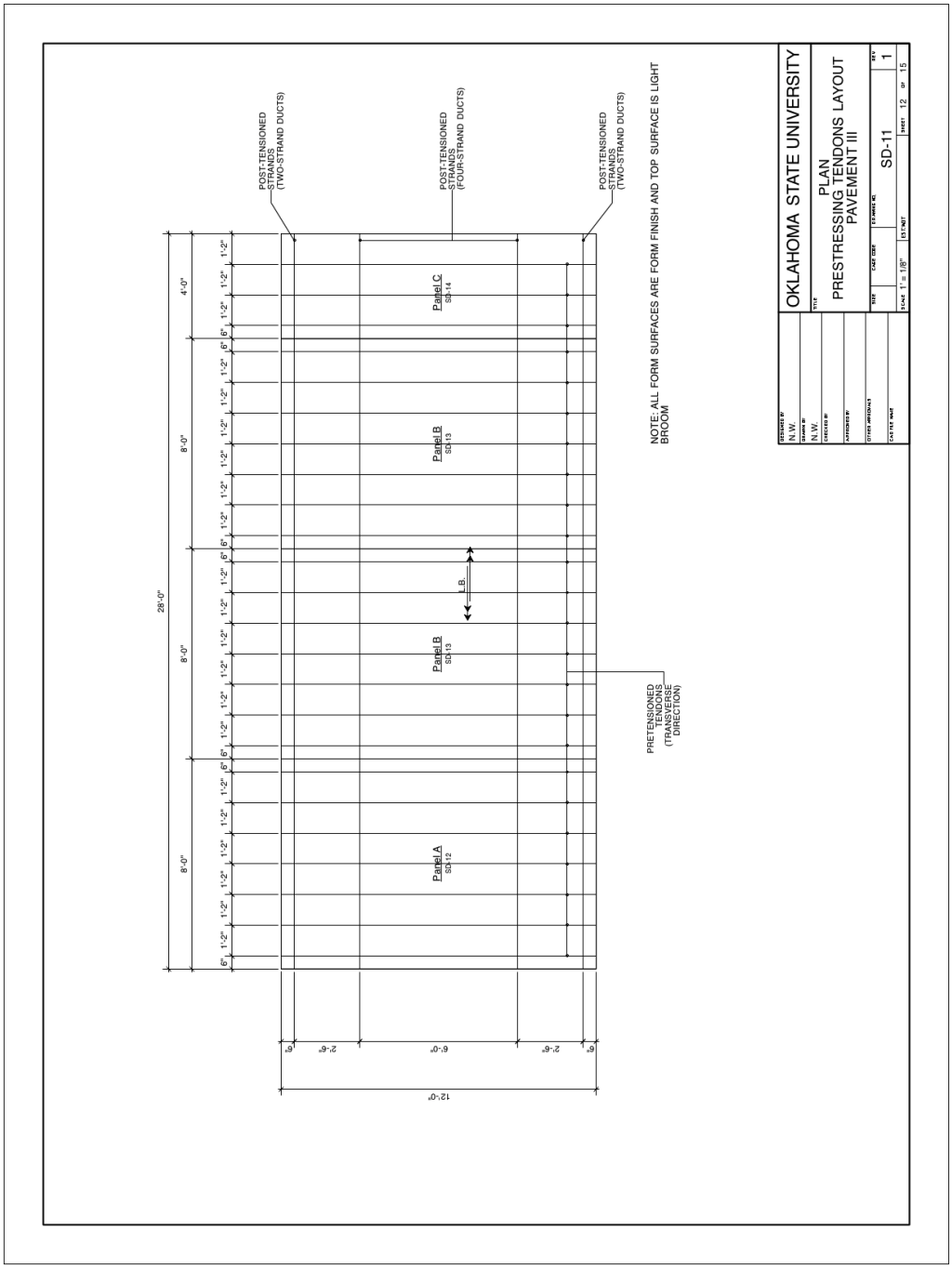

Figure B12 Pavement construction drawings “Prestressing Tendons Layout Pavement III”

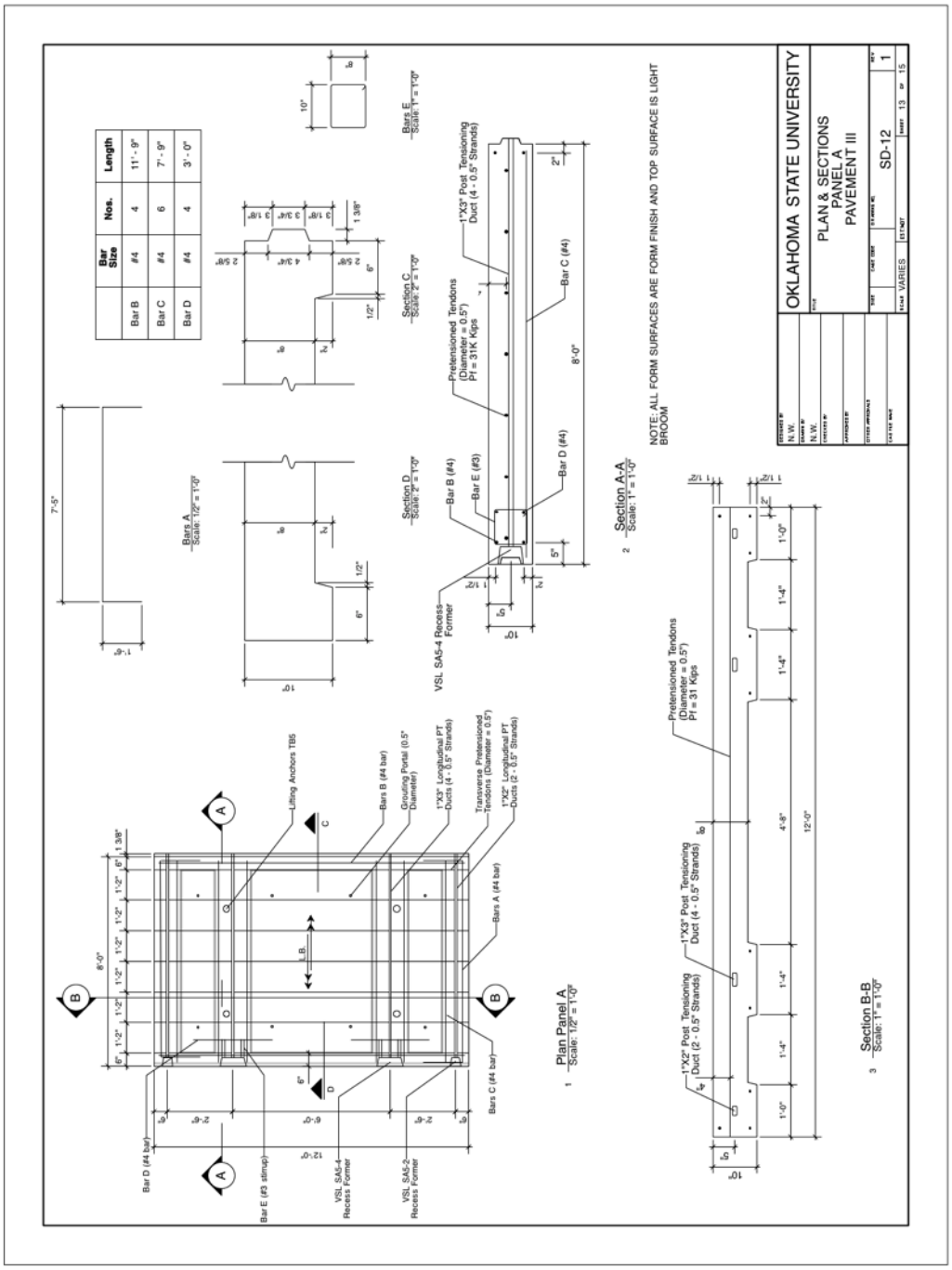

Figure B13 Pavement construction drawings “Plans and Sections Panel A Pavement III”

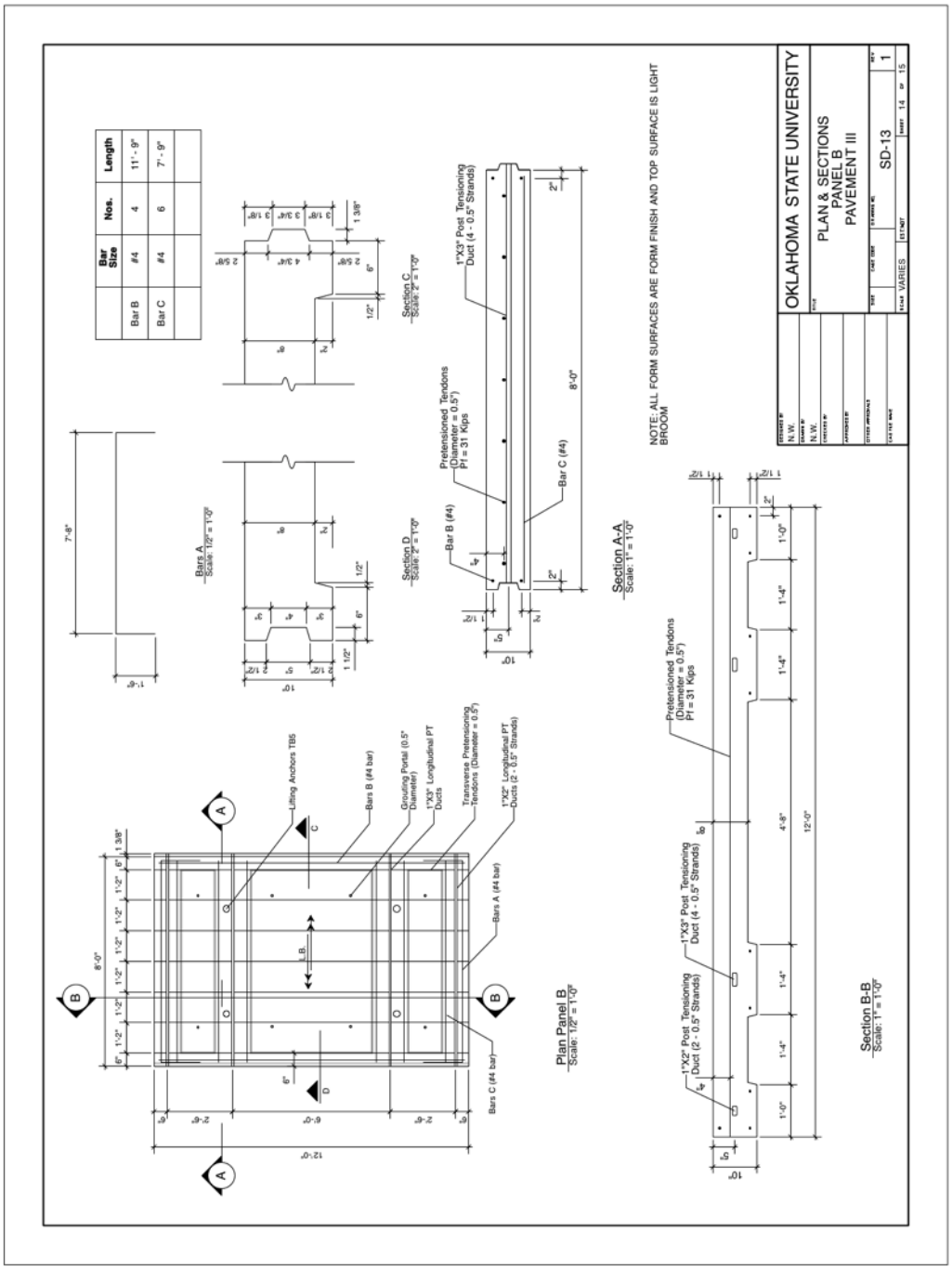

Figure B14 Pavement construction drawings “Plans and Sections Panel B Pavement III”

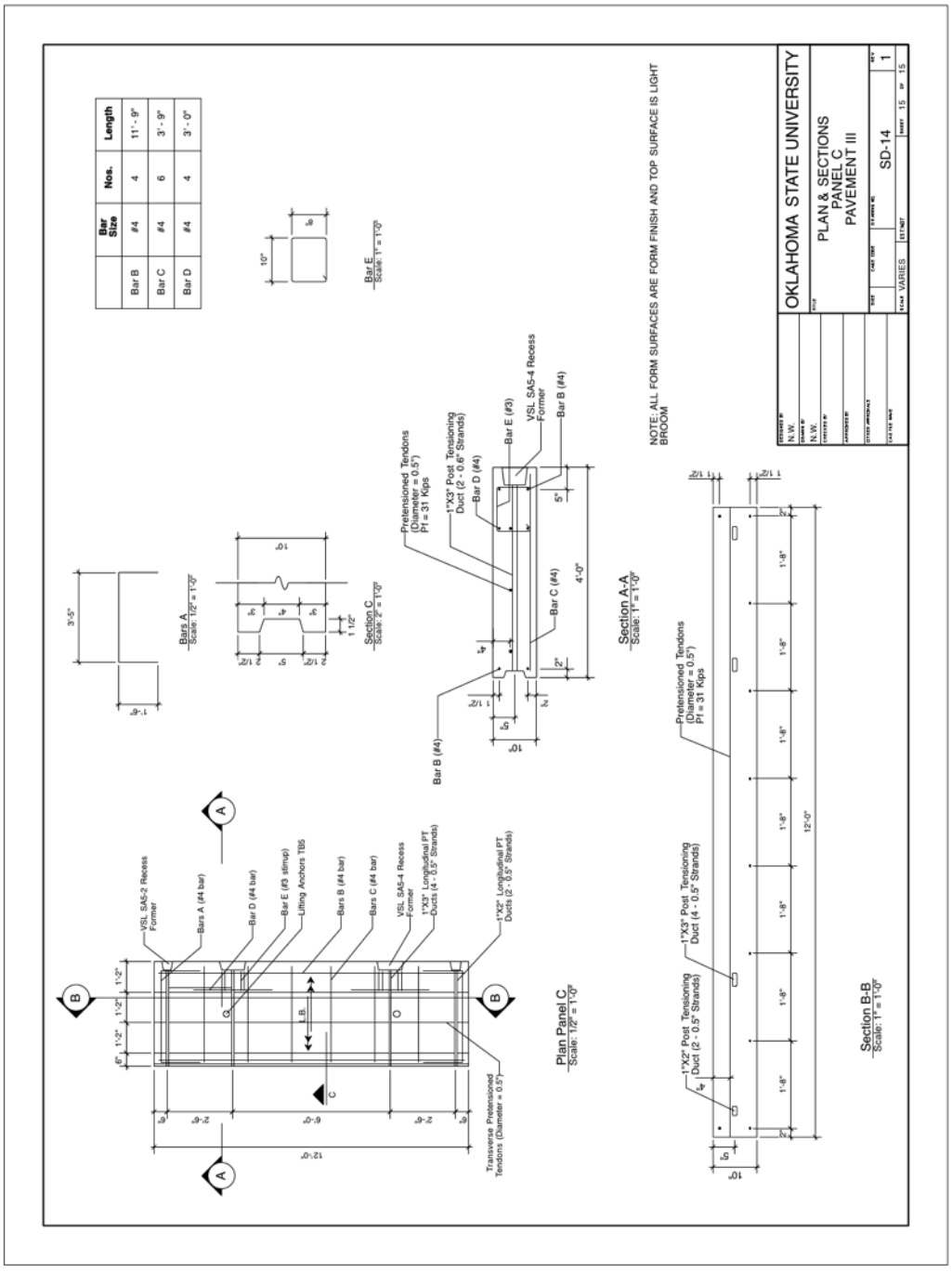

Figure B15 Pavement construction drawings “Plans and Sections Panel C Pavement III”

APPENDIX C

TESTING FRAME DESIGN AND SHOP DRAWING

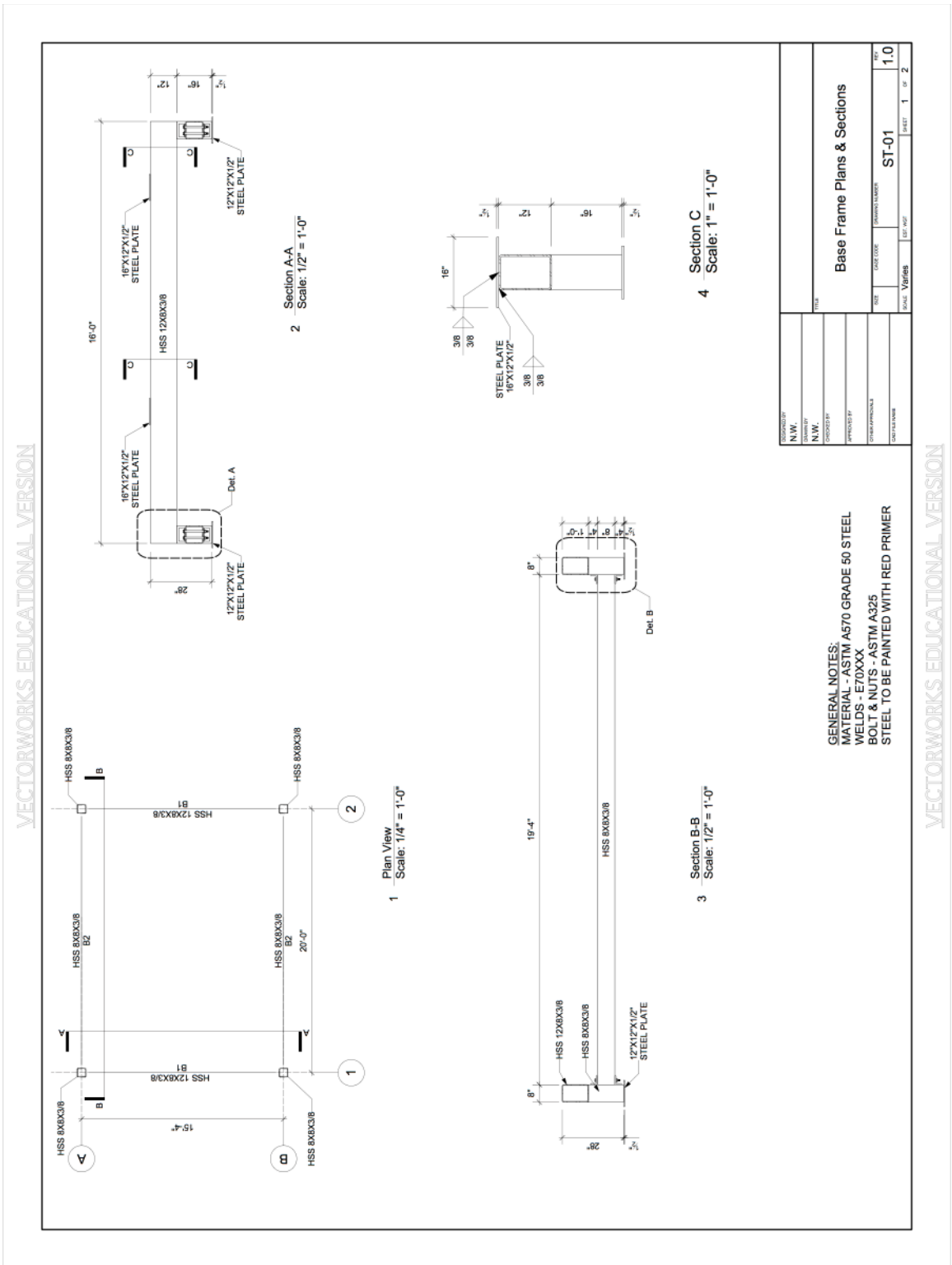

Figure C1 Test frame shop drawings “Base Frame Plans and Sections”

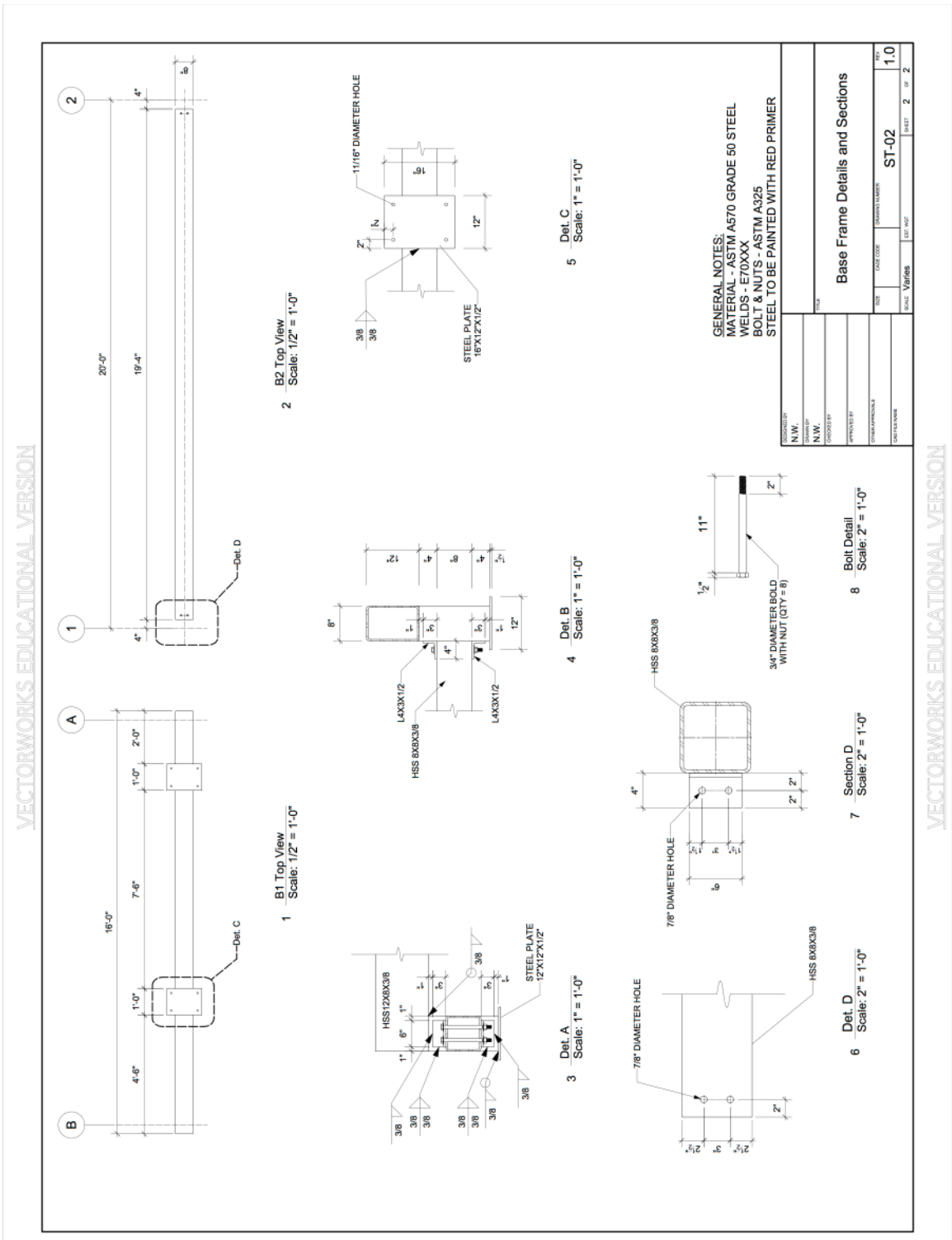

Figure C2 Test frame shop drawings “Base Frame Details and Sections”

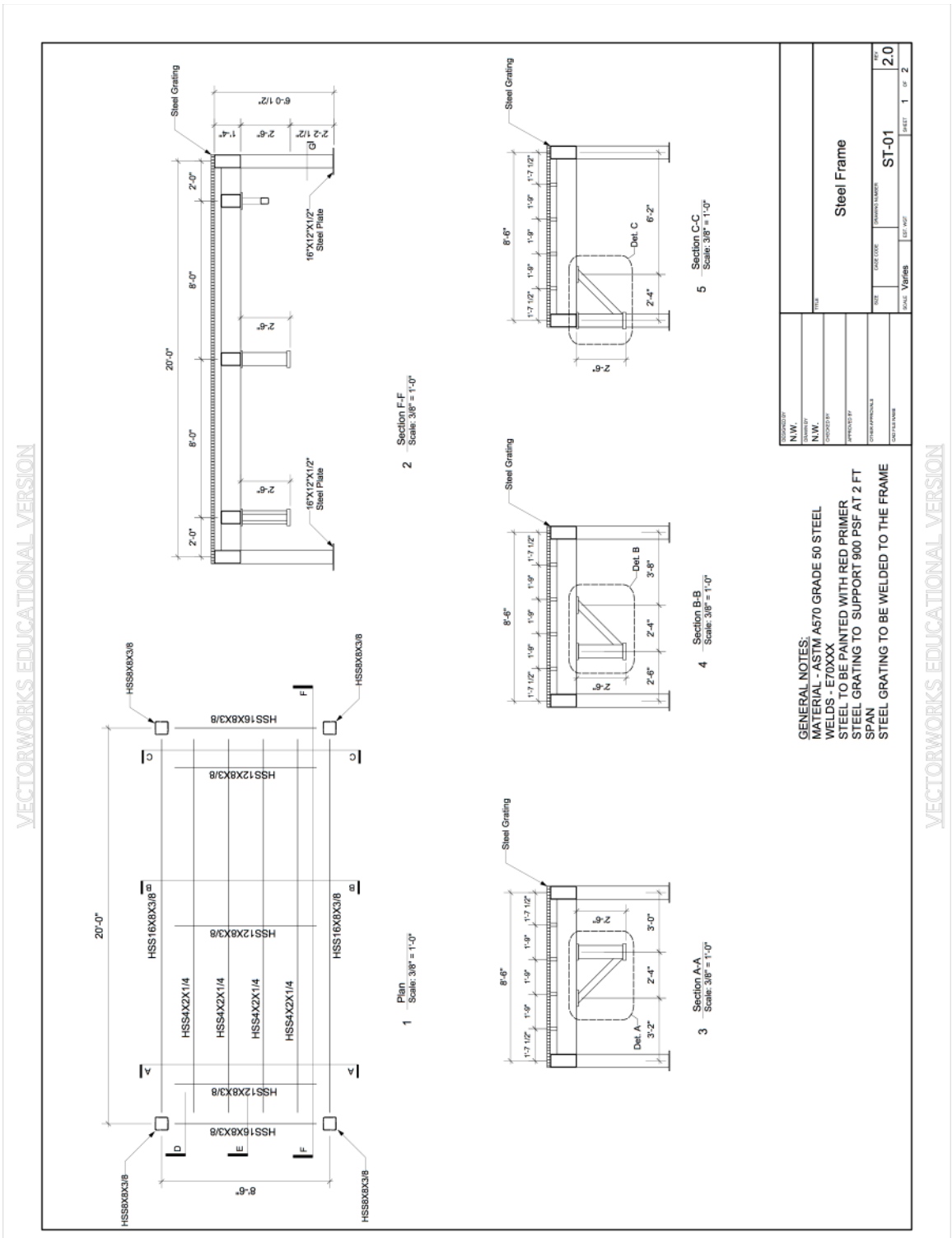

Figure C3 Test frame shop drawings “Steel Frame”

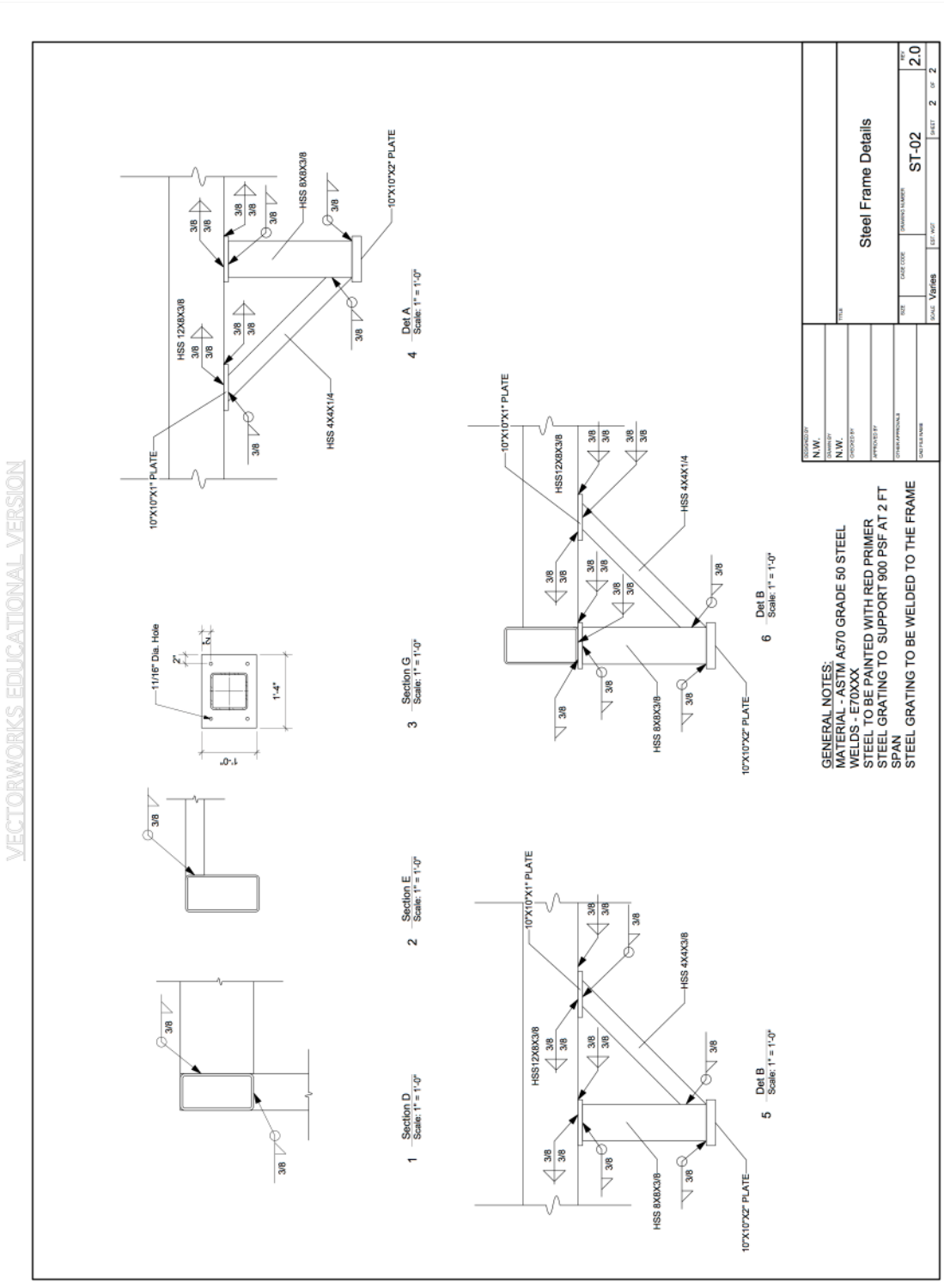

Figure C4 Test frame shop drawings “Steel Frame Details”

APPENDIX D

FINITE ELEMENT ANALYSIS RESULTS

Load Case 1 for 8-inch Panel

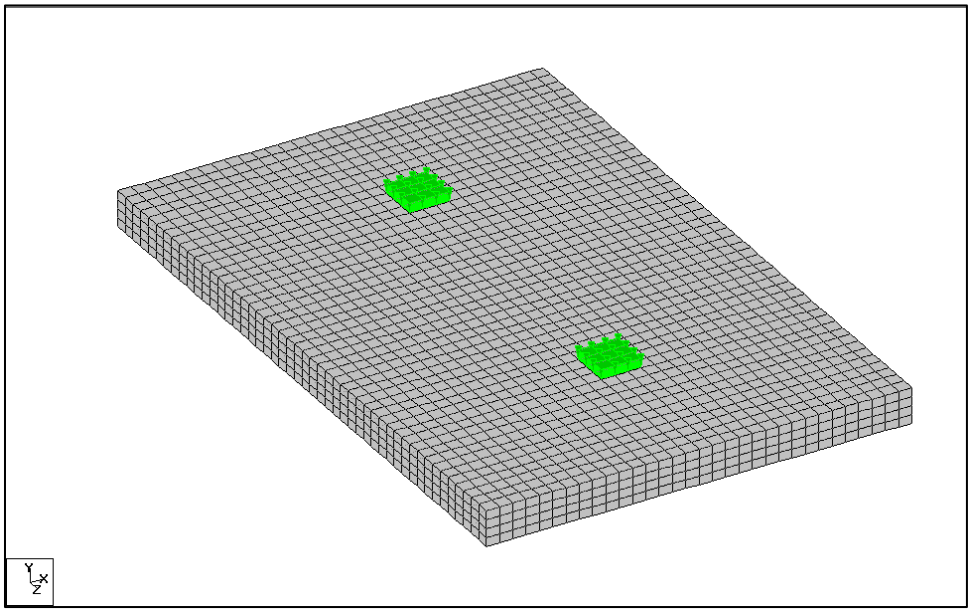

Figure D1 Load Case 1 Locations (LC1-8 inch panel)

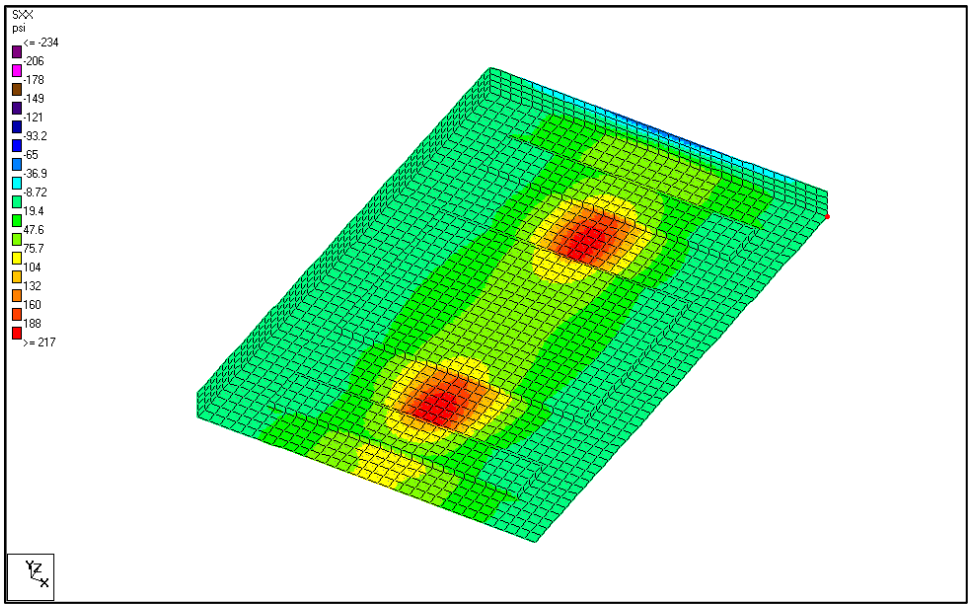

Figure D2 Longitudinal Bottom Stresses (LC1-8 inch panel)

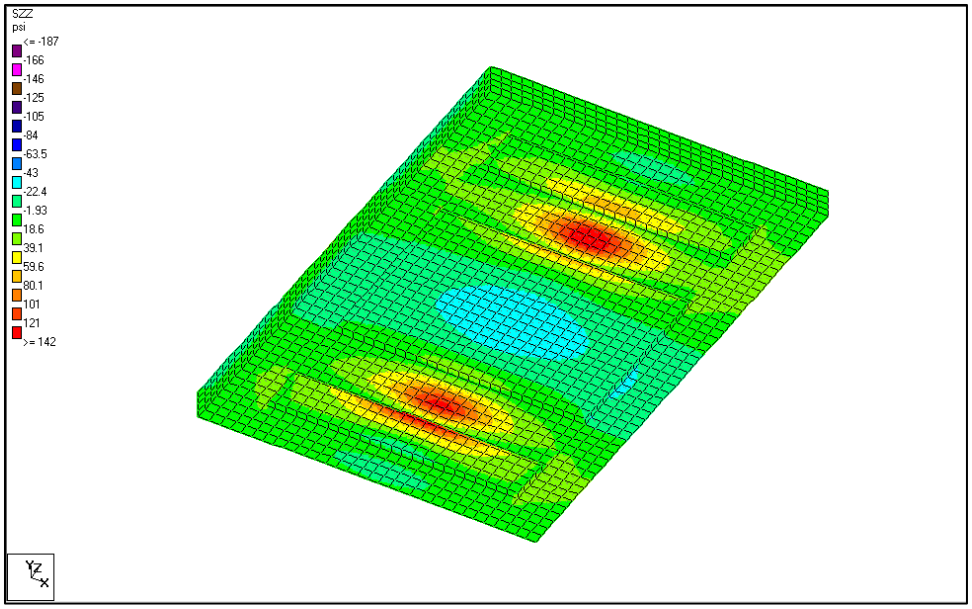

Figure D3 Transverse Bottom Stresses (LC1-8 inch panel)

Load Case 2 for 8-inch Panel

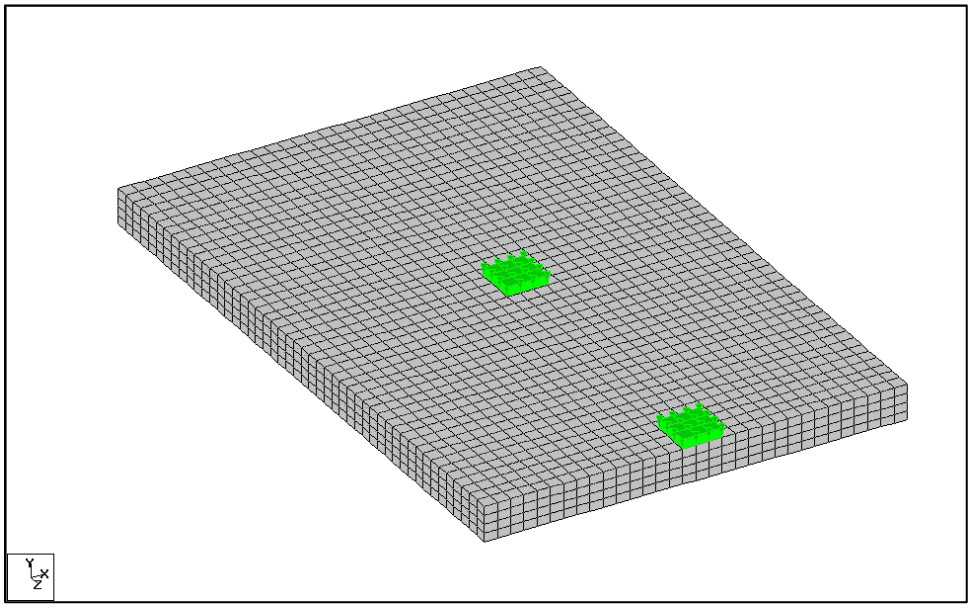

Figure D4 Load Case 2 Locations (LC2-8 inch panel)

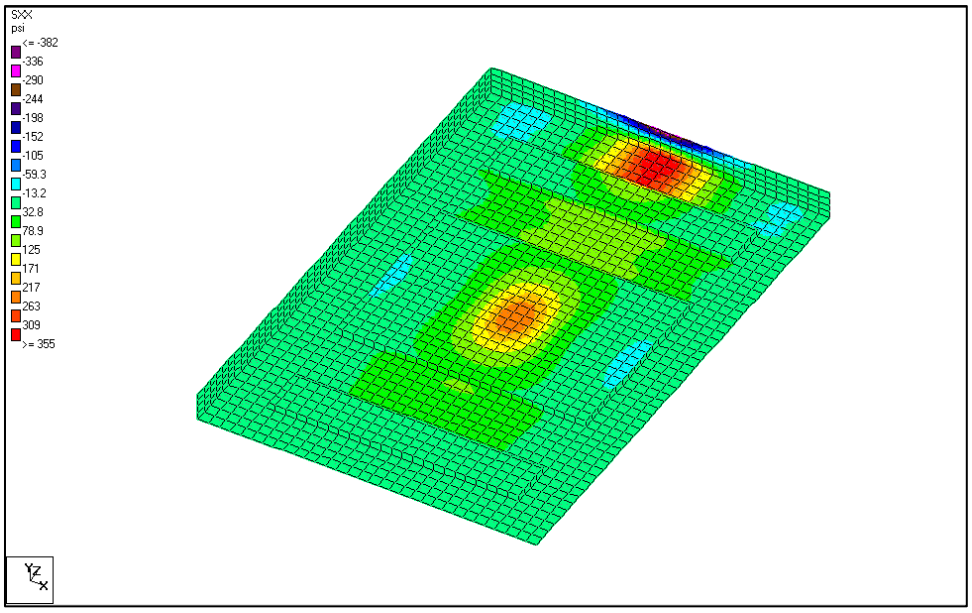

Figure D5 Longitudinal Bottom Stresses (LC2-8 inch panel)

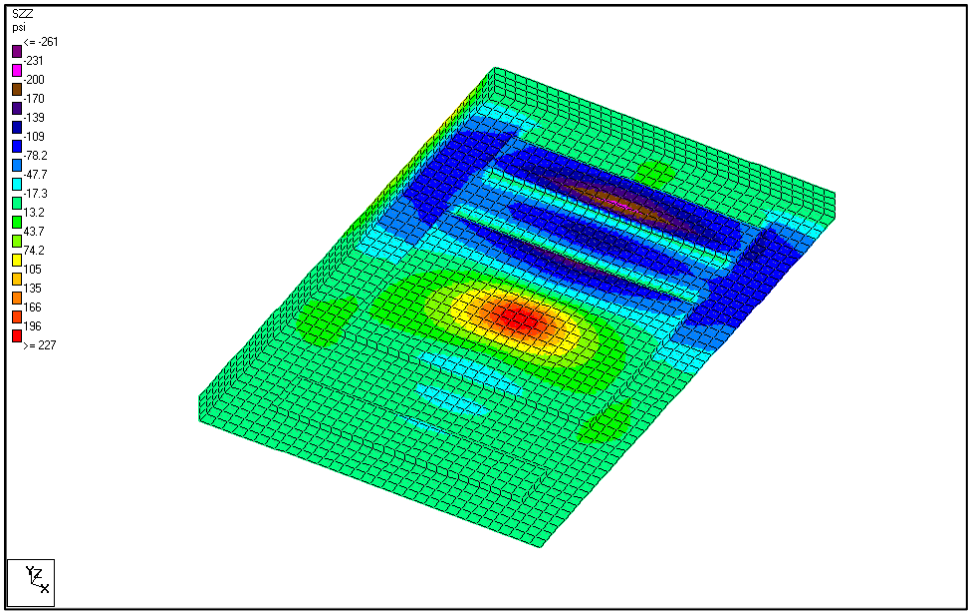

Figure D6 Transverse Bottom Stresses (LC2-8 inch panel)

Load Case 1 for 10-inch Panel

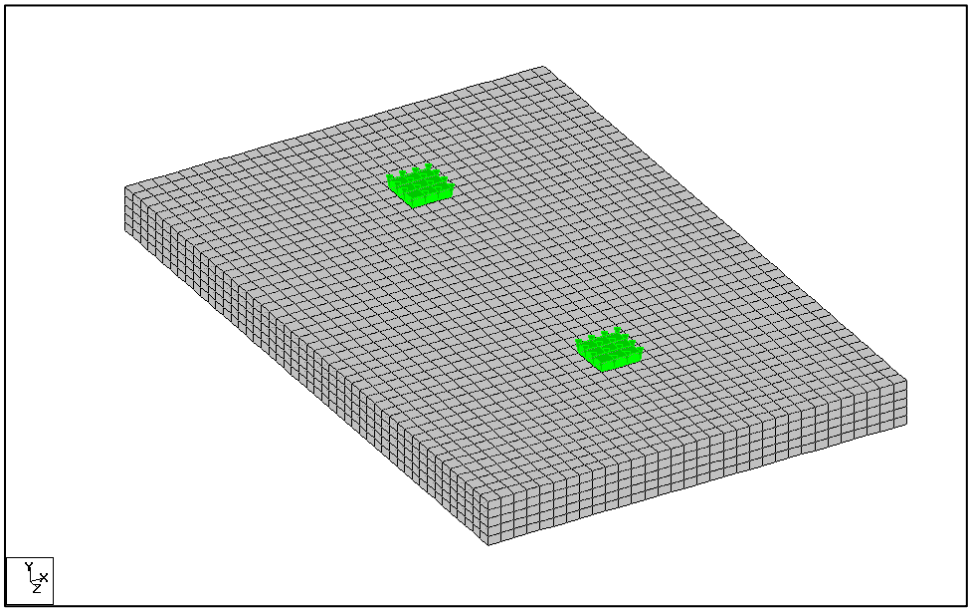

Figure D7 Load Case 1 Locations (LC1-10 inch panel)

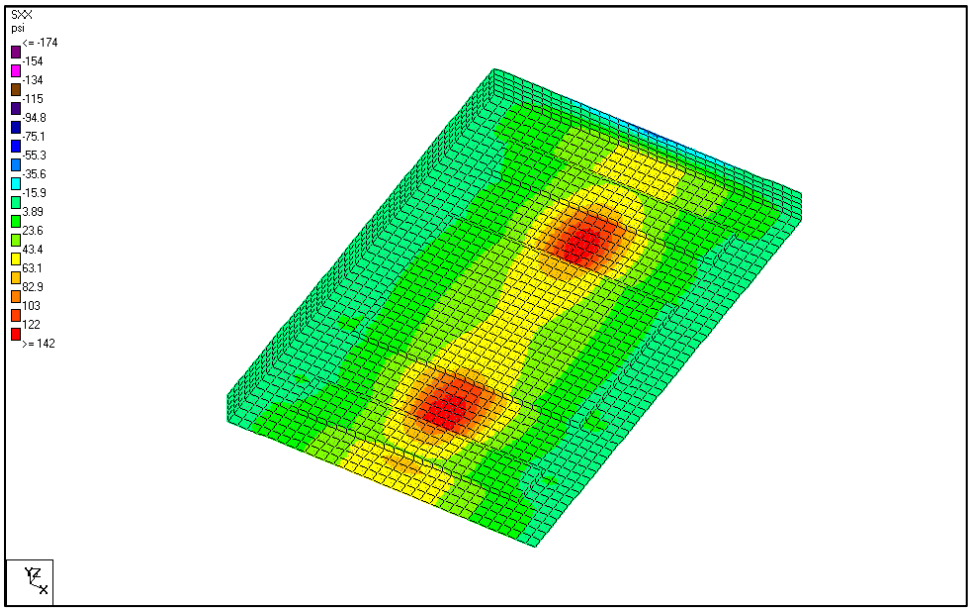

Figure D8 Longitudinal Bottom Stresses (LC1-10 inch panel)

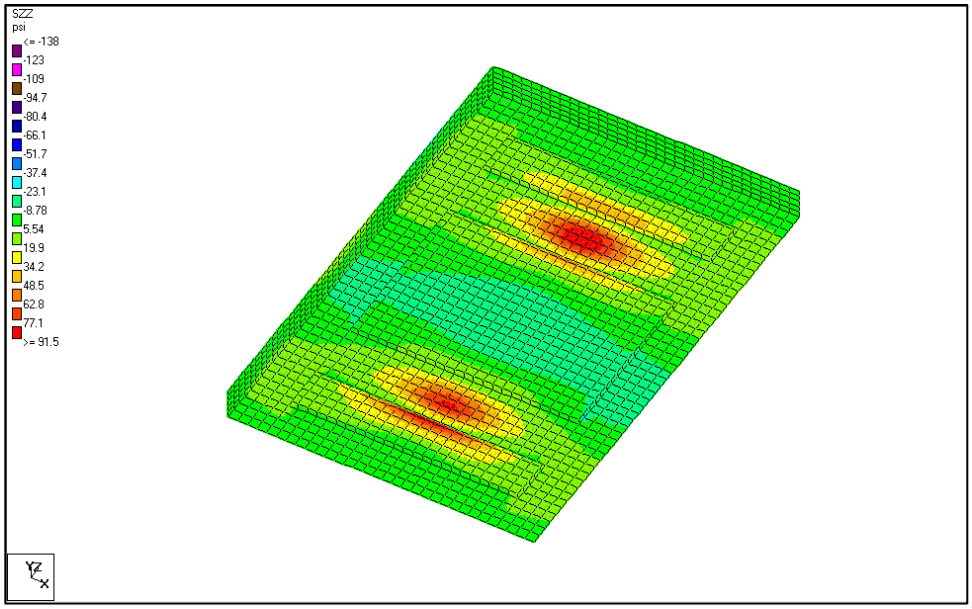

Figure D9 Transverse Bottom Stresses (LC1-10 inch panel)

Load Case 2 for 10-inch Panel

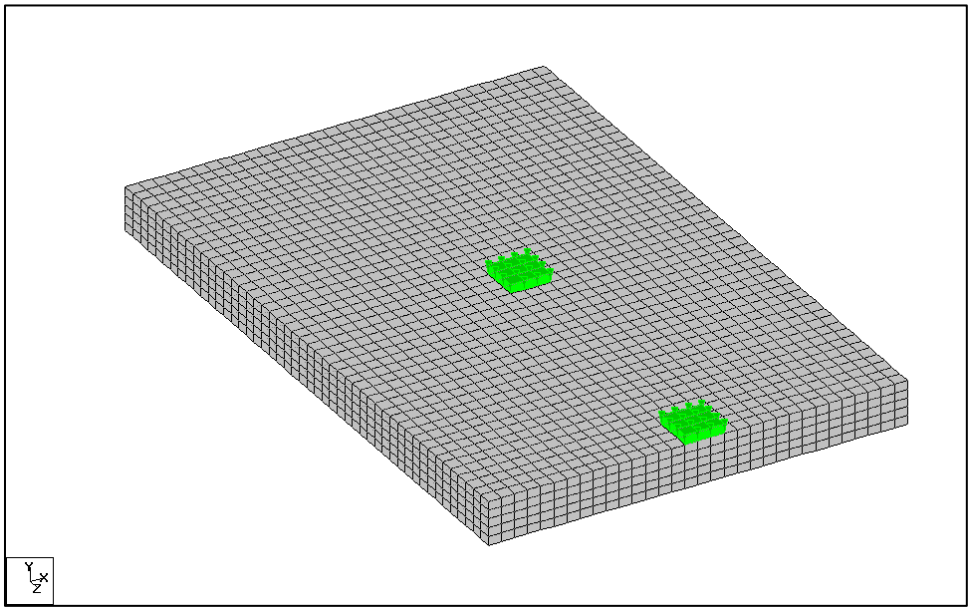

Figure D10 Load Case 2 Locations (LC2-10 inch panel)

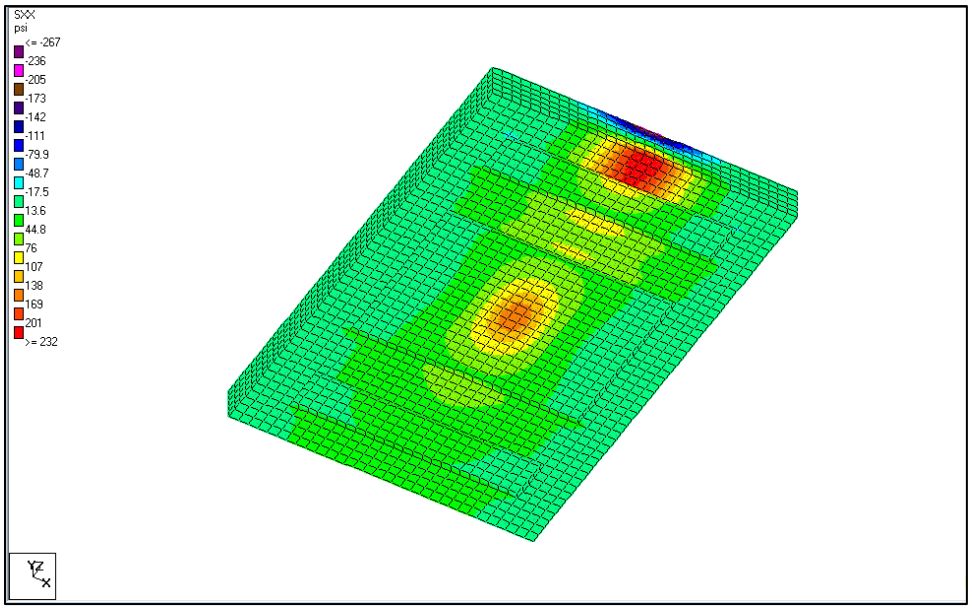

Figure D11 Longitudinal Bottom Stresses (LC2-10 inch panel)

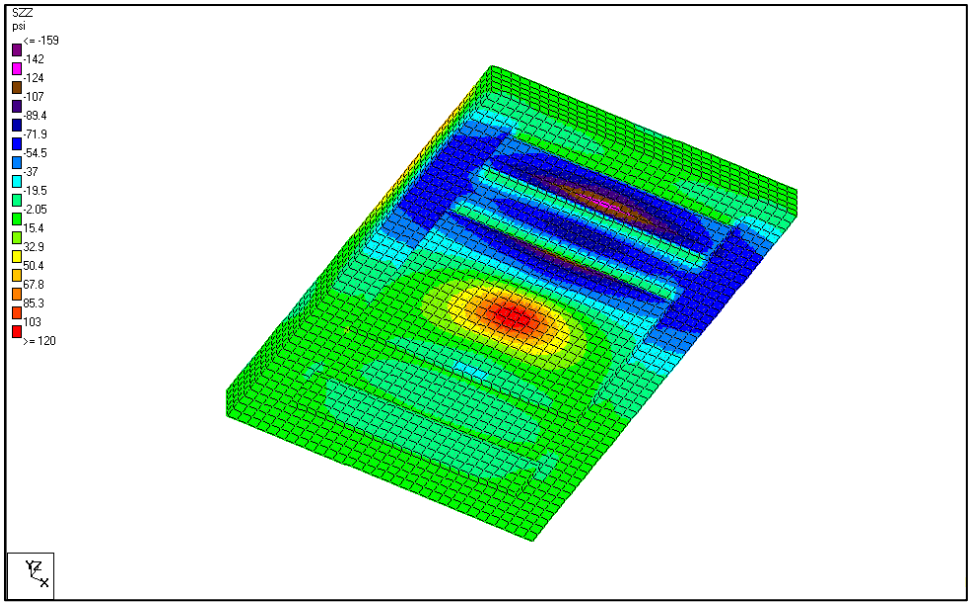

Figure D12 Transverse Bottom Stresses (LC2-10 inch panel)

APPENDIX E

EXPERIEMENTAL WORK AND PAVEMENT TEST RESULTS

Pavement I Panel-A Repeated & Static Load Test Results

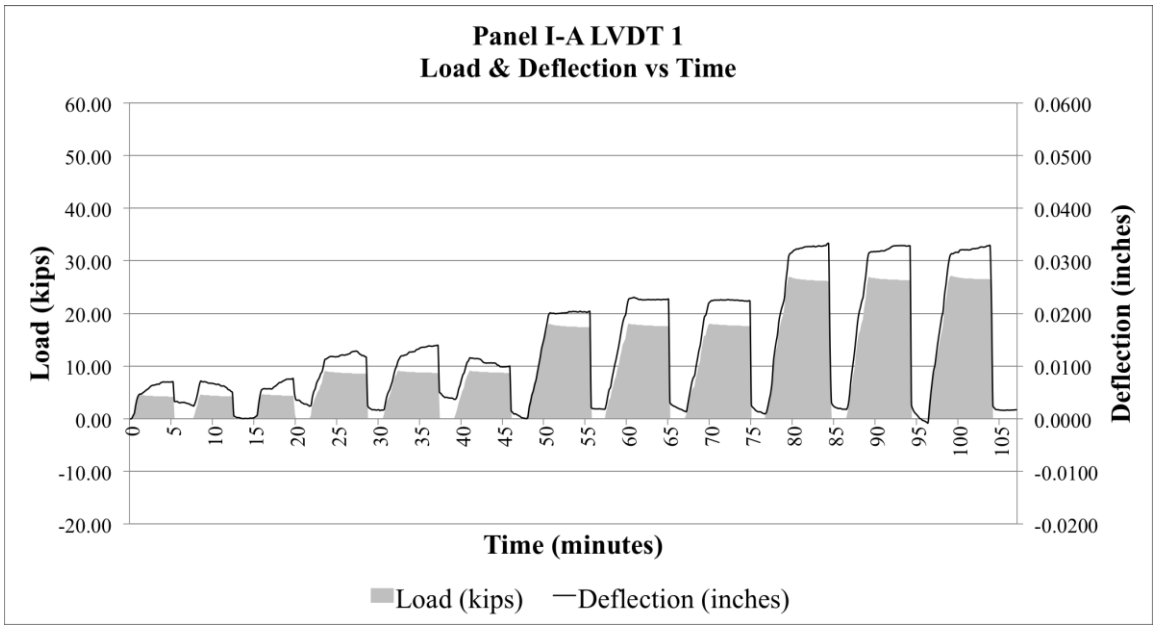

Figure E1 Pavement I Panel-A repeated load deflection and load vs. time for LVDT 1

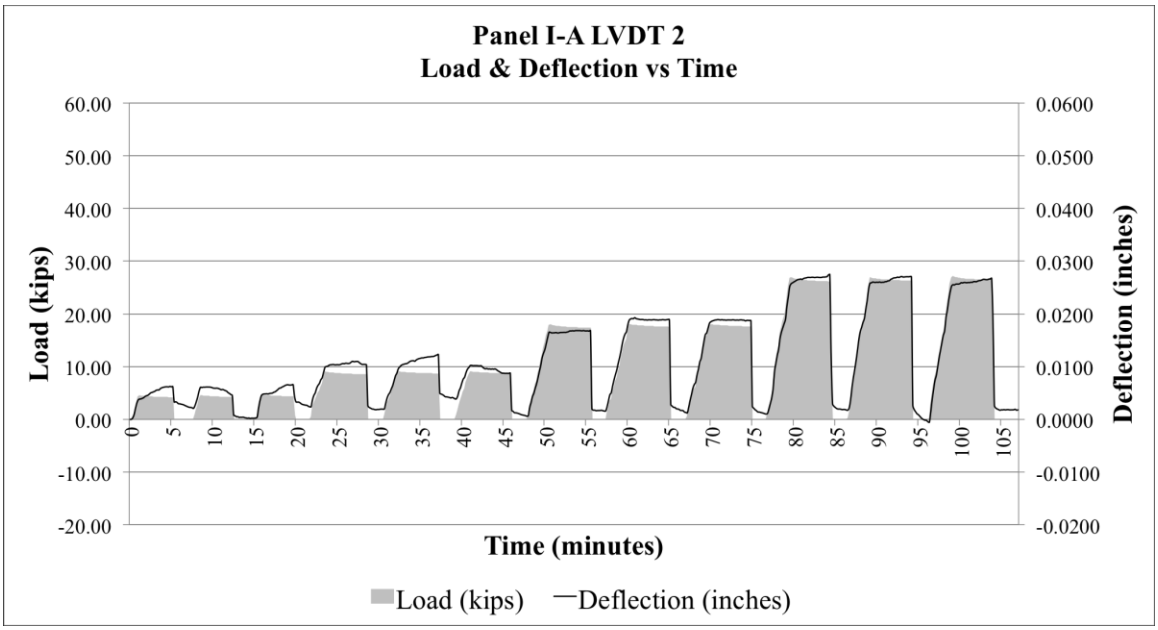

Figure E2 Pavement I Panel-A repeated load deflection and load vs. time for LVDT 2

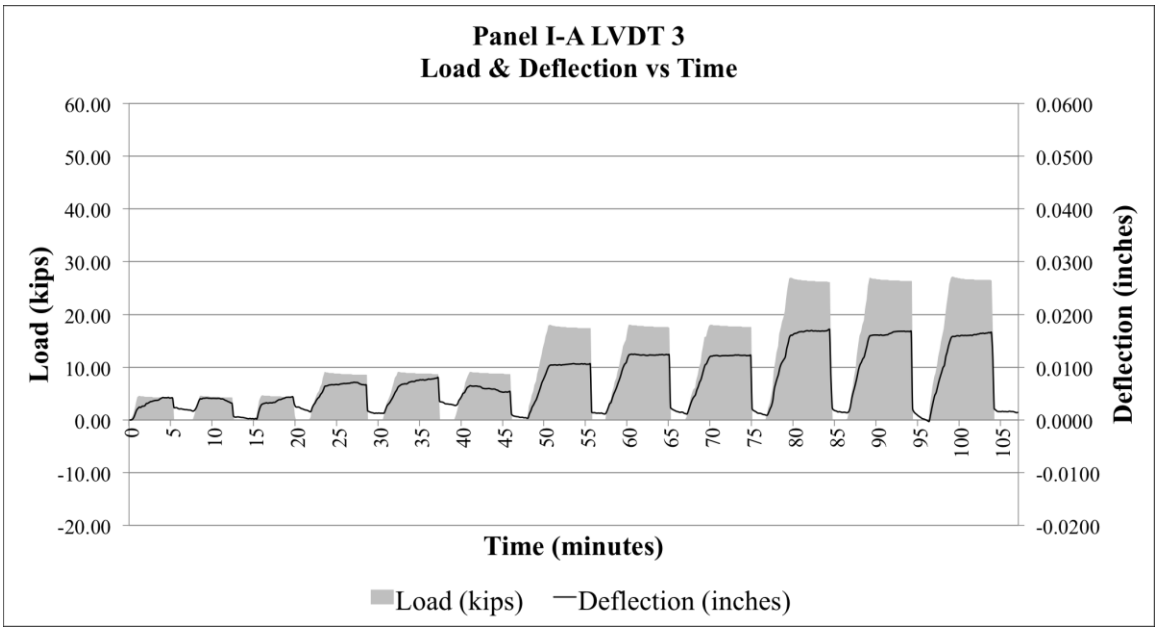

Figure E3 Pavement I Panel-A repeated load deflection and load vs. time for LVDT 3

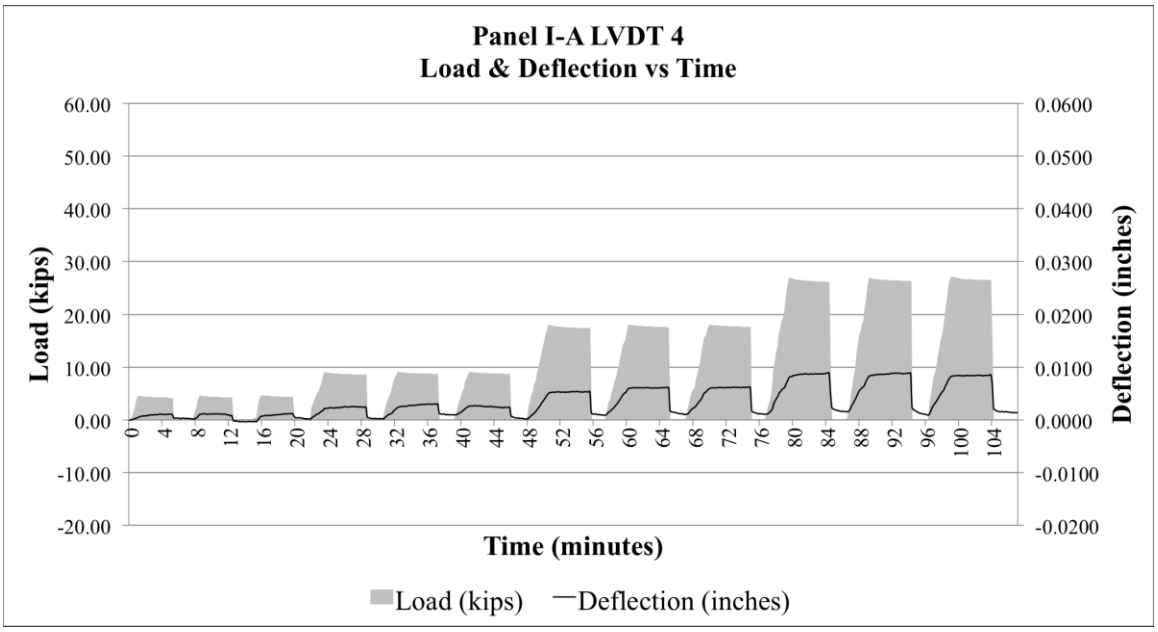

Figure E4 Pavement I Panel-A repeated load deflection and load vs. time for LVDT 4

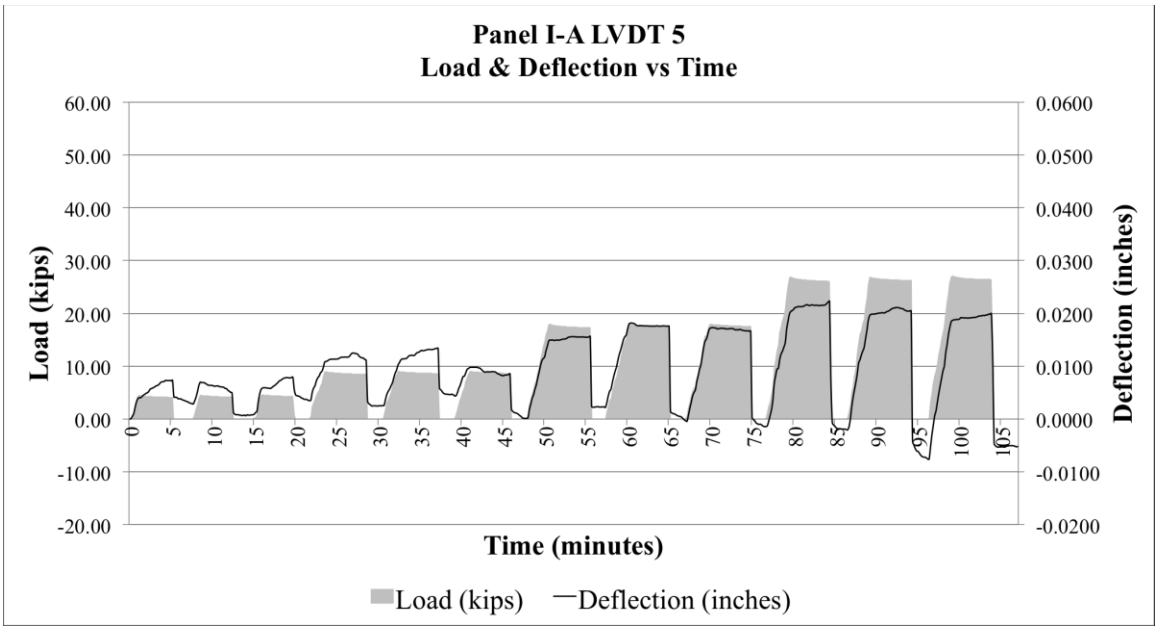

Figure E5 Pavement I Panel-A repeated load deflection and load vs. time for LVDT 5

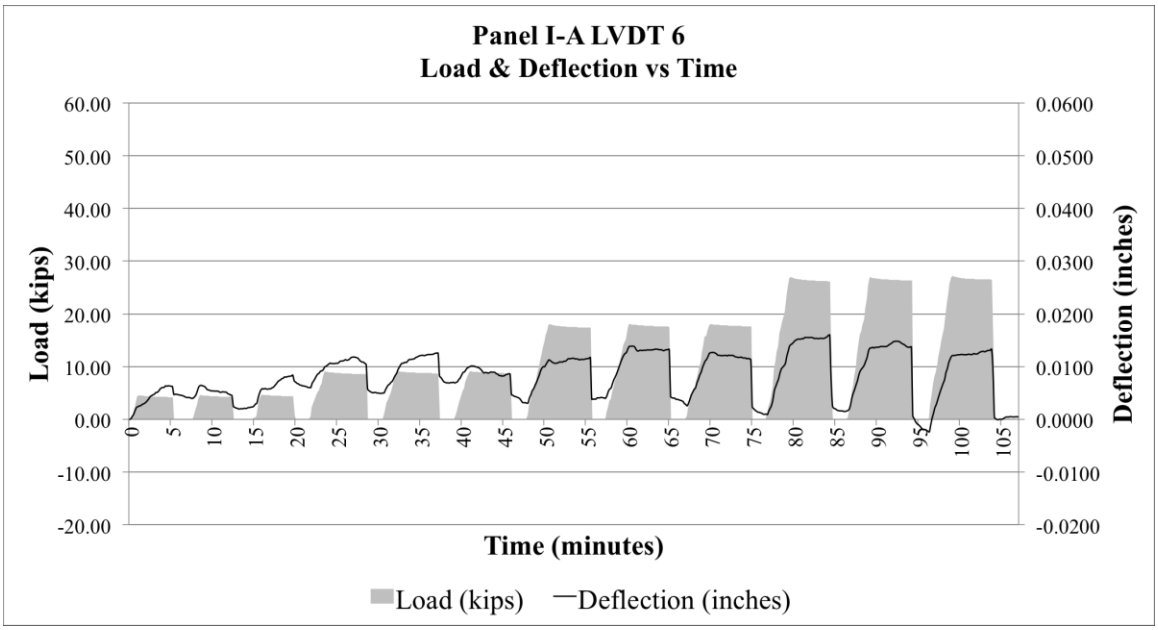

Figure E6 Pavement I Panel-A repeated load deflection and load vs. time for LVDT 6

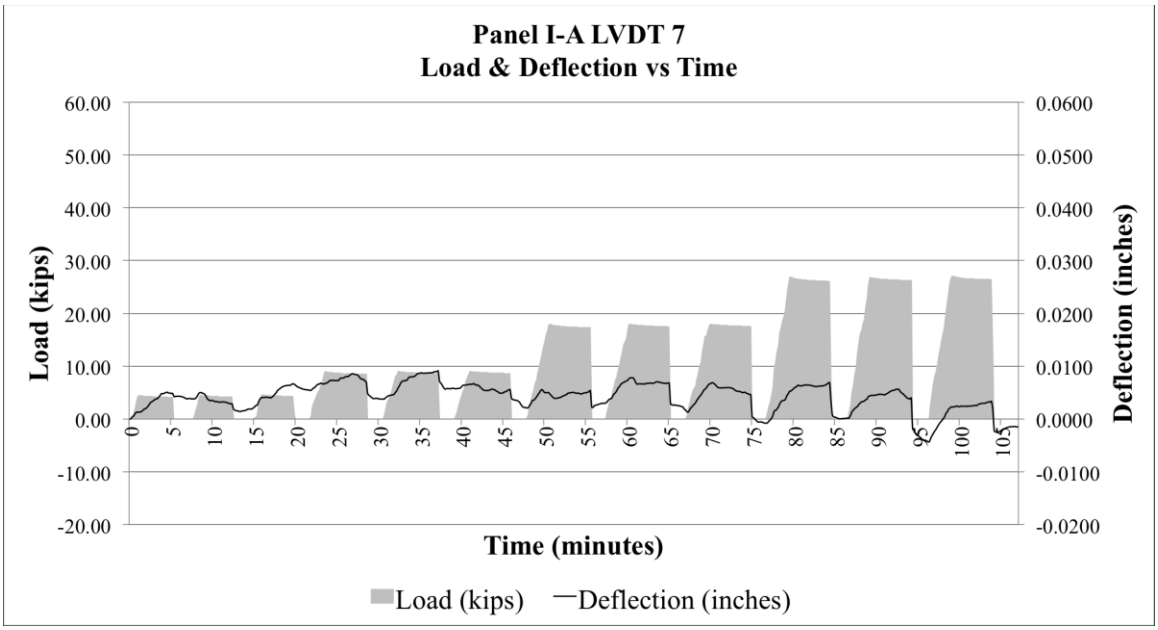

Figure E7 Pavement I Panel-A repeated load deflection and load vs. time for LVDT 7

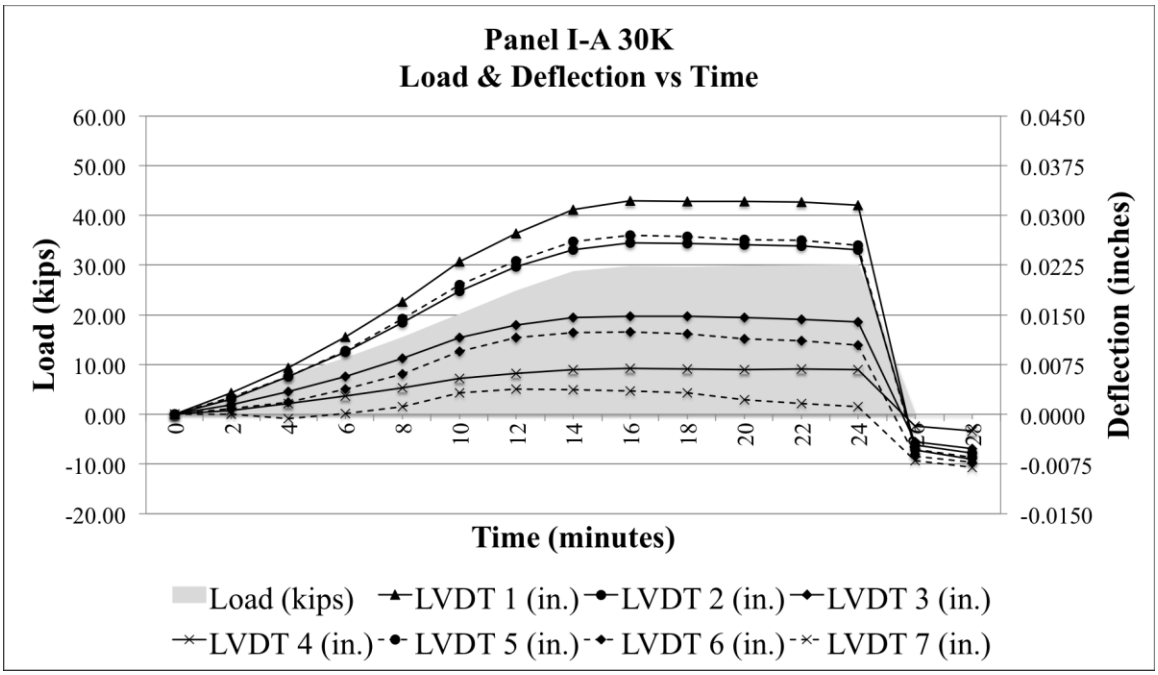

Figure E8 Pavement I Panel-A static load deflection and load vs. time (30,000 lb. Load)

Pavement I Panel-B1 Repeated & Static Load Test Results

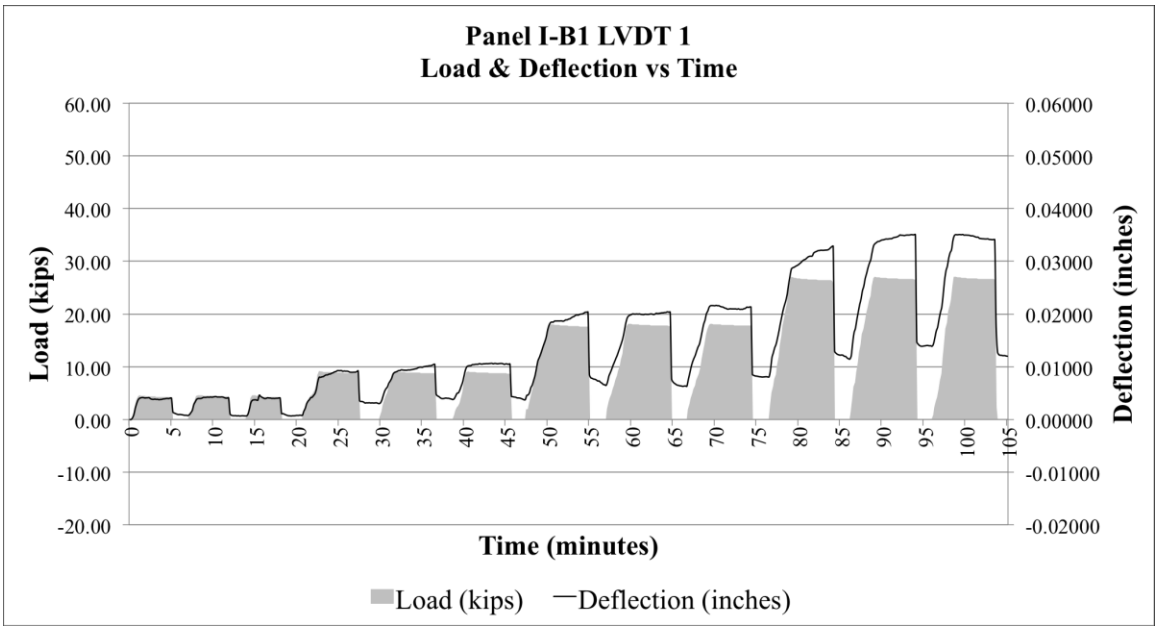

Figure E9 Pavement I Panel-B1 repeated load deflection and load vs. time for LVDT 1

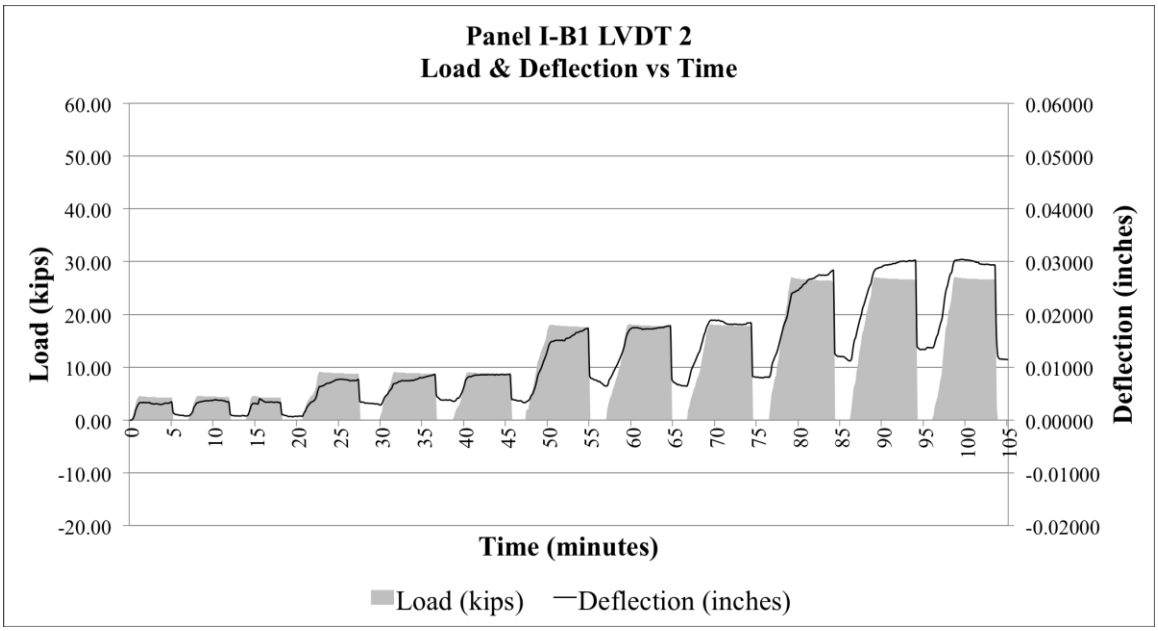

Figure E10 Pavement I Panel-B1 repeated load deflection and load vs. time for LVDT 2

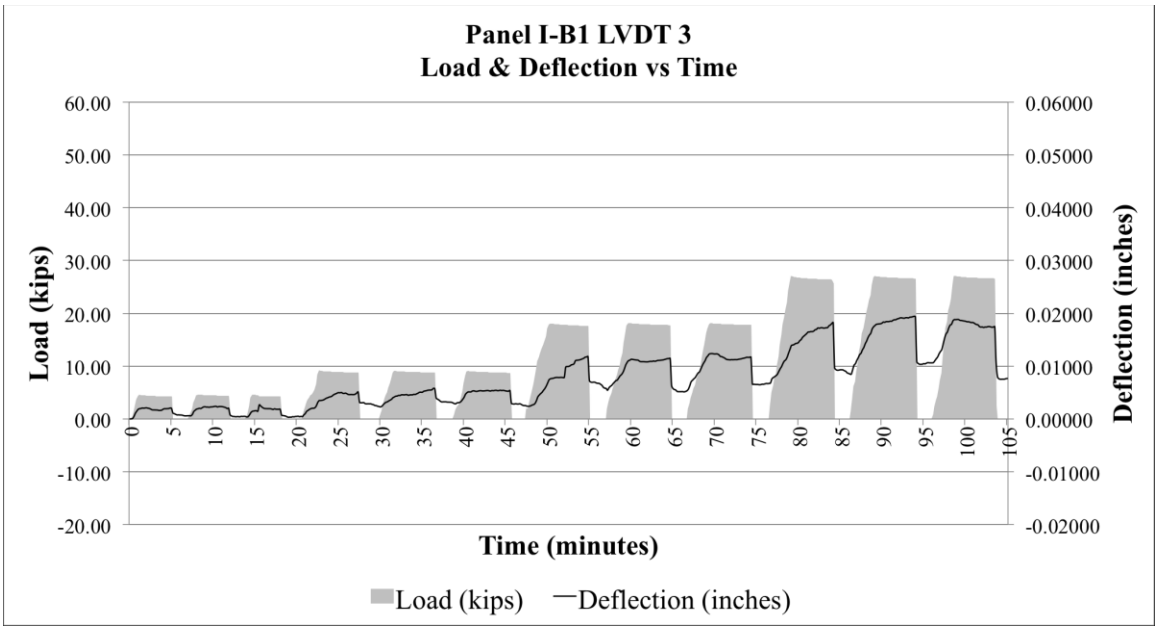

Figure E11 Pavement I Panel-B1 repeated load deflection and load vs. time for LVDT 3

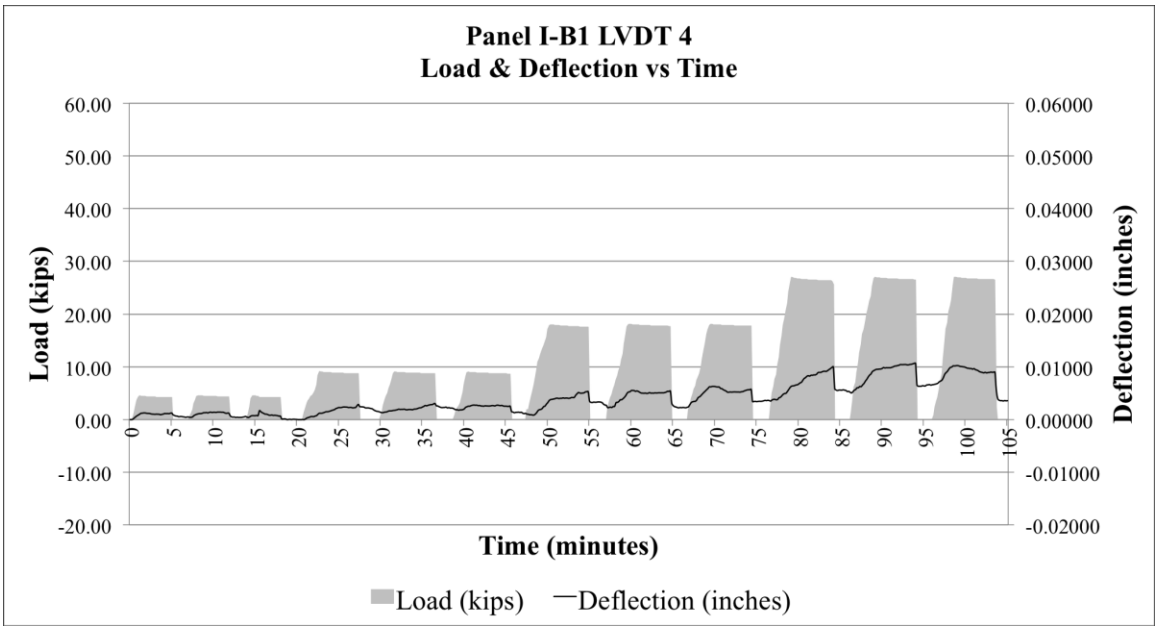

Figure E12 Pavement I Panel-B1 repeated load deflection and load vs. time for LVDT 4

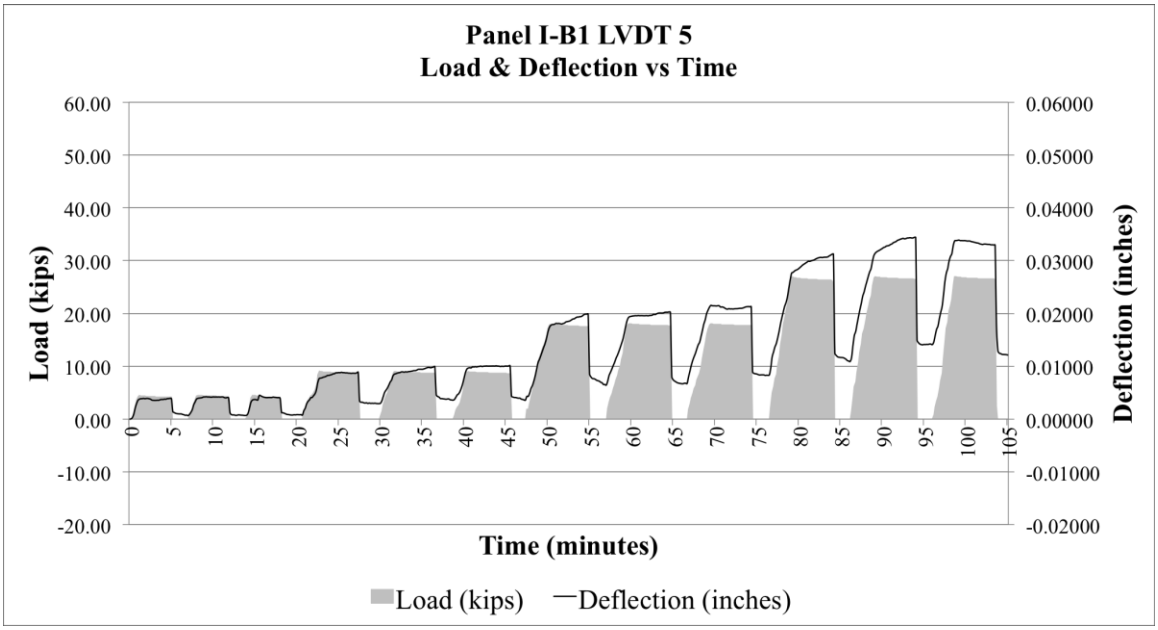

Figure E13 Pavement I Panel-B1 repeated load deflection and load vs. time for LVDT 5

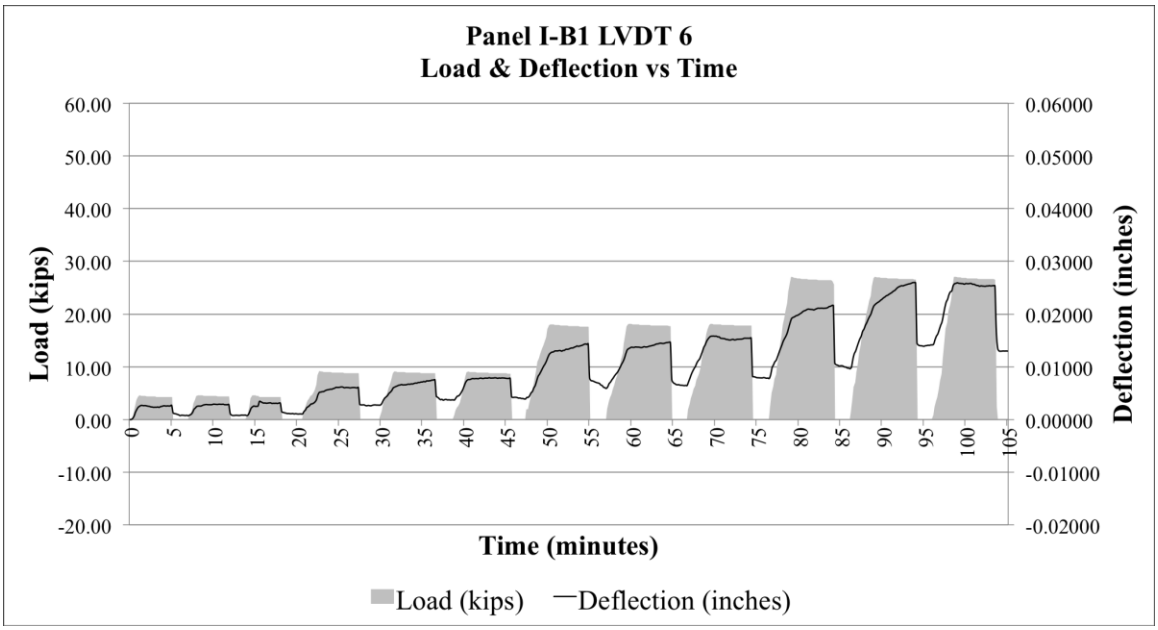

Figure E14 Pavement I Panel-B1 repeated load deflection and load vs. time for LVDT 6

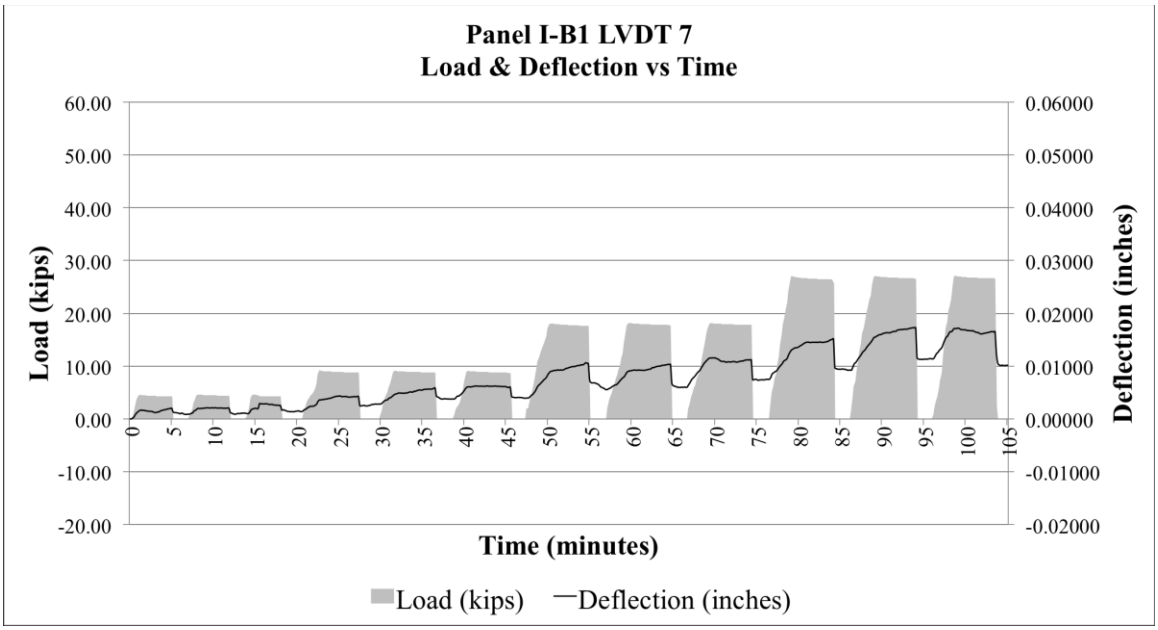

Figure E15 Pavement I Panel-B1 repeated load deflection and load vs. time for LVDT 7

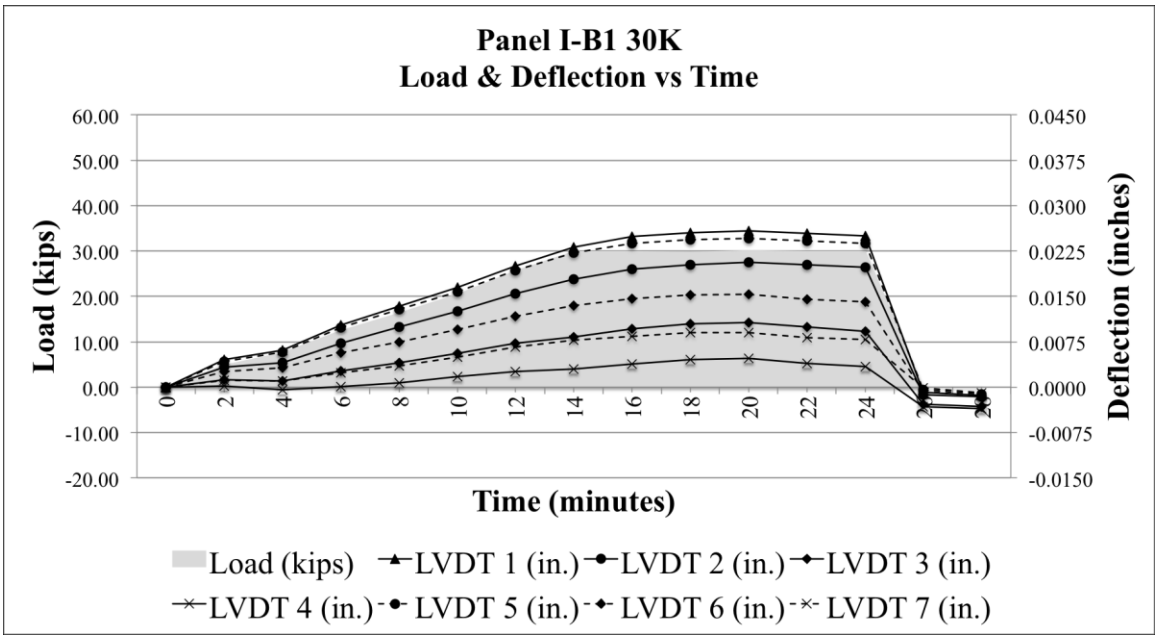

Figure E16 Pavement I Panel-B1 static load deflection and load vs. time (30,000 lb. Load)

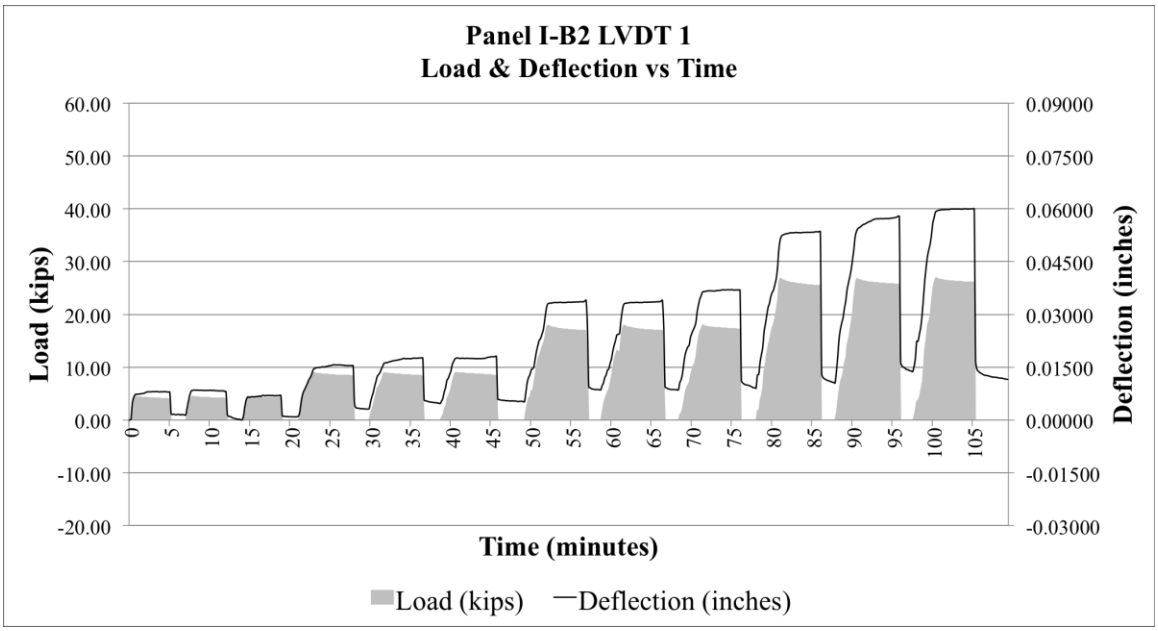

Figure E17 Pavement I Panel-B2 repeated load deflection and load vs. time for LVDT 1

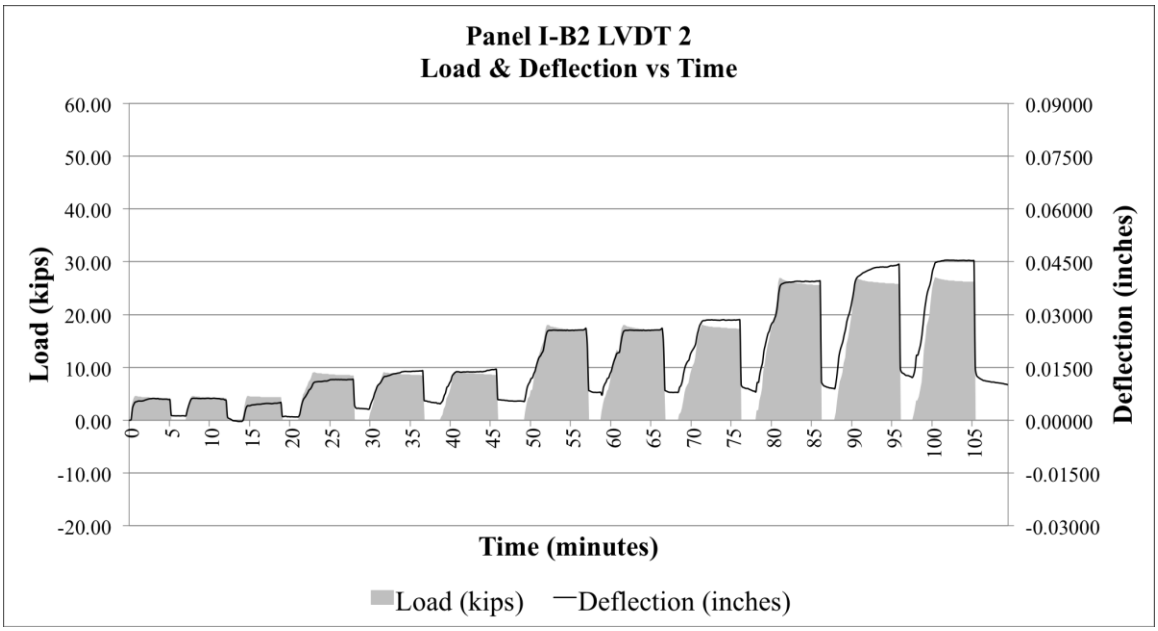

Figure E18 Pavement I Panel-B2 repeated load deflection and load vs. time for LVDT 2

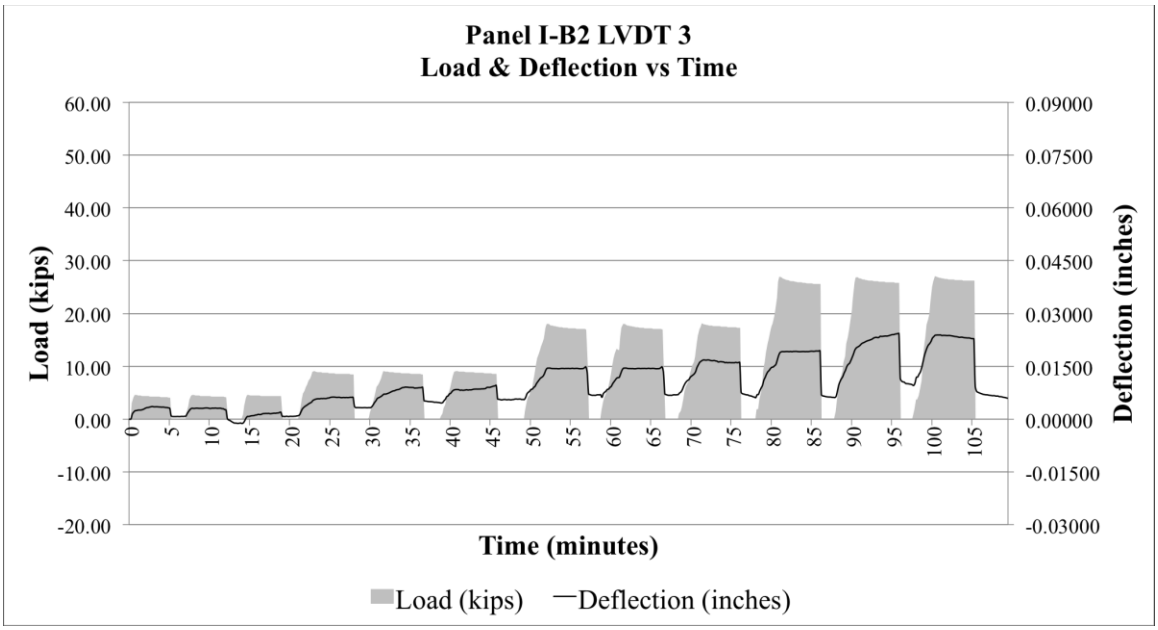

Figure E19 Pavement I Panel-B2 repeated load deflection and load vs. time for LVDT 3

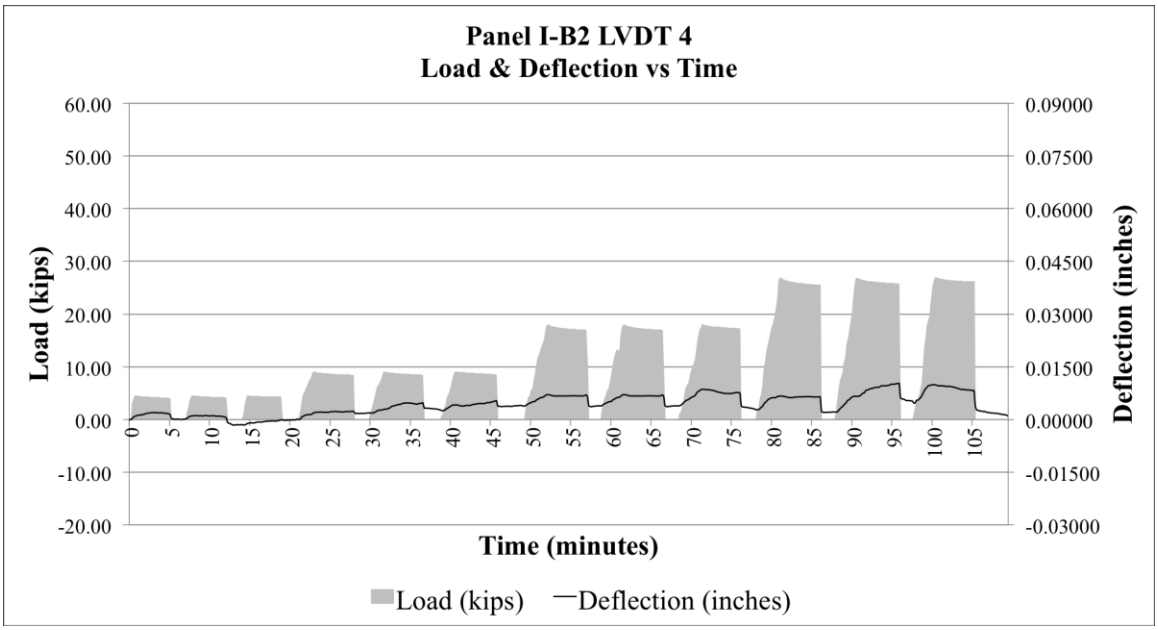

Figure E20 Pavement I Panel-B2 repeated load deflection and load vs. time for LVDT 4

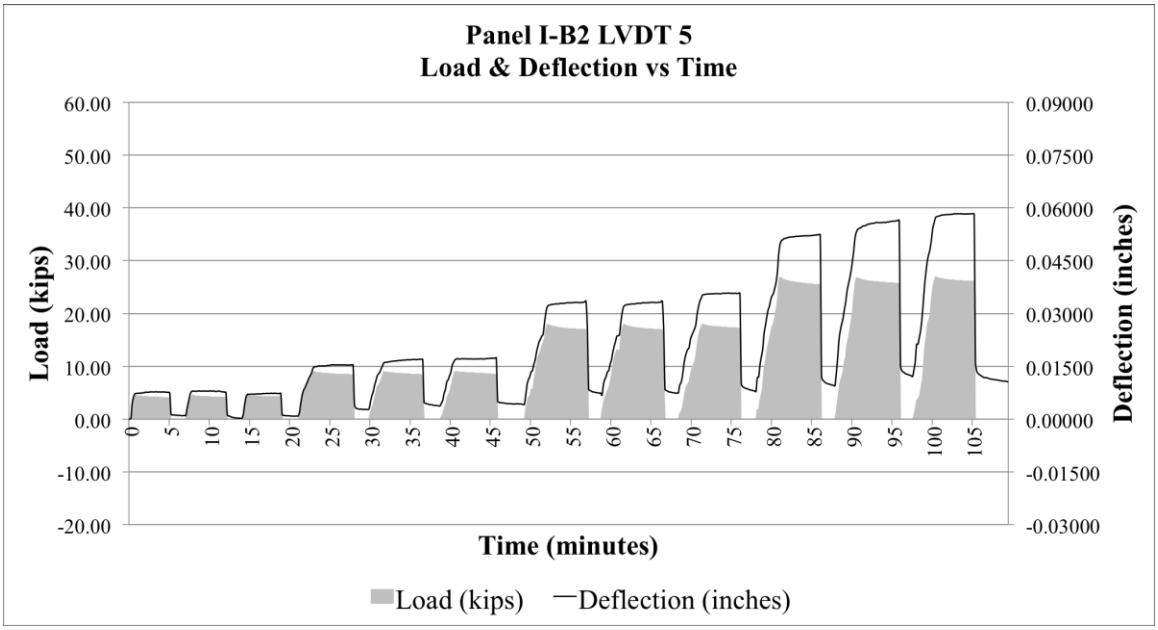

Figure E21 Pavement I Panel-B2 repeated load deflection and load vs. time for LVDT 5

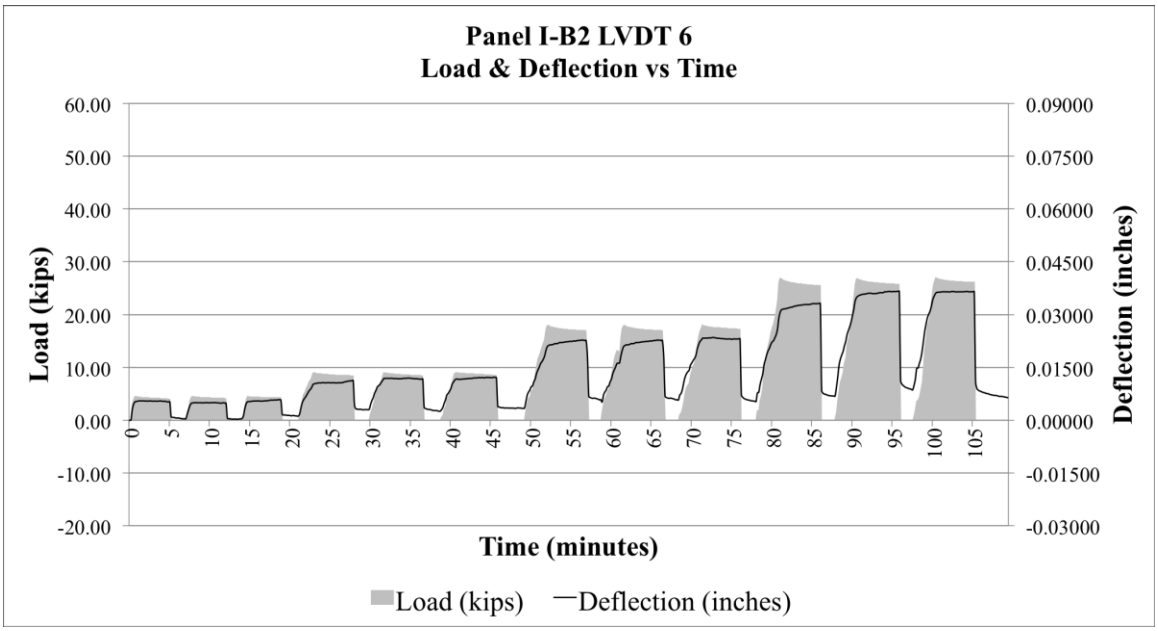

Figure E22 Pavement I Panel-B2 repeated load deflection and load vs. time for LVDT 6

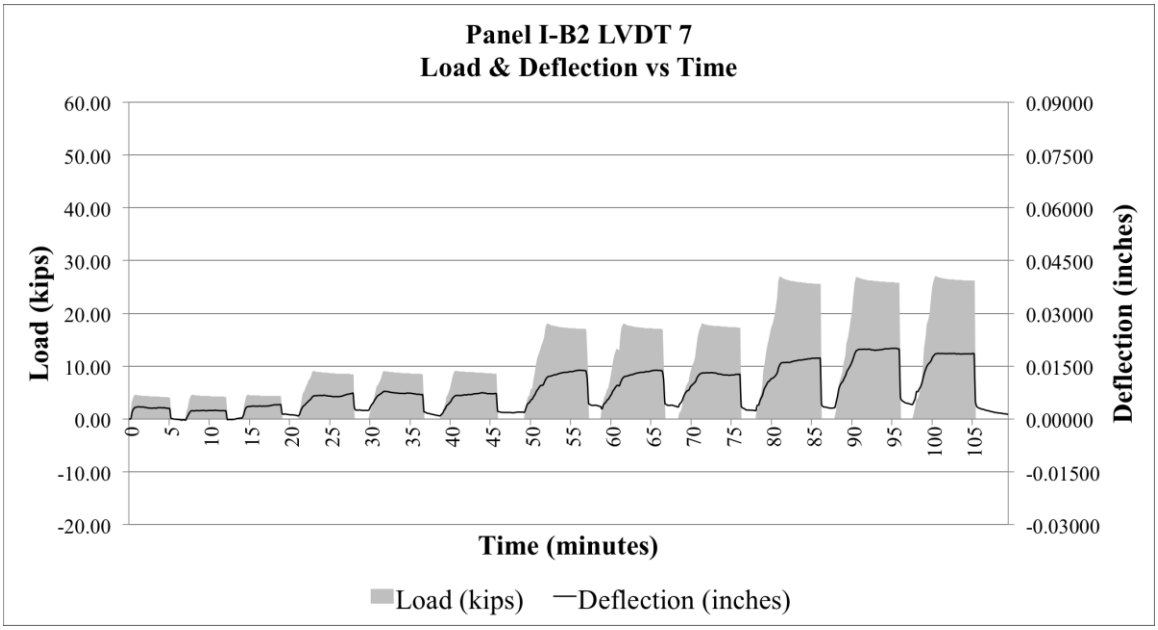

Figure E23 Pavement I Panel-B2 repeated load deflection and load vs. time for LVDT 7

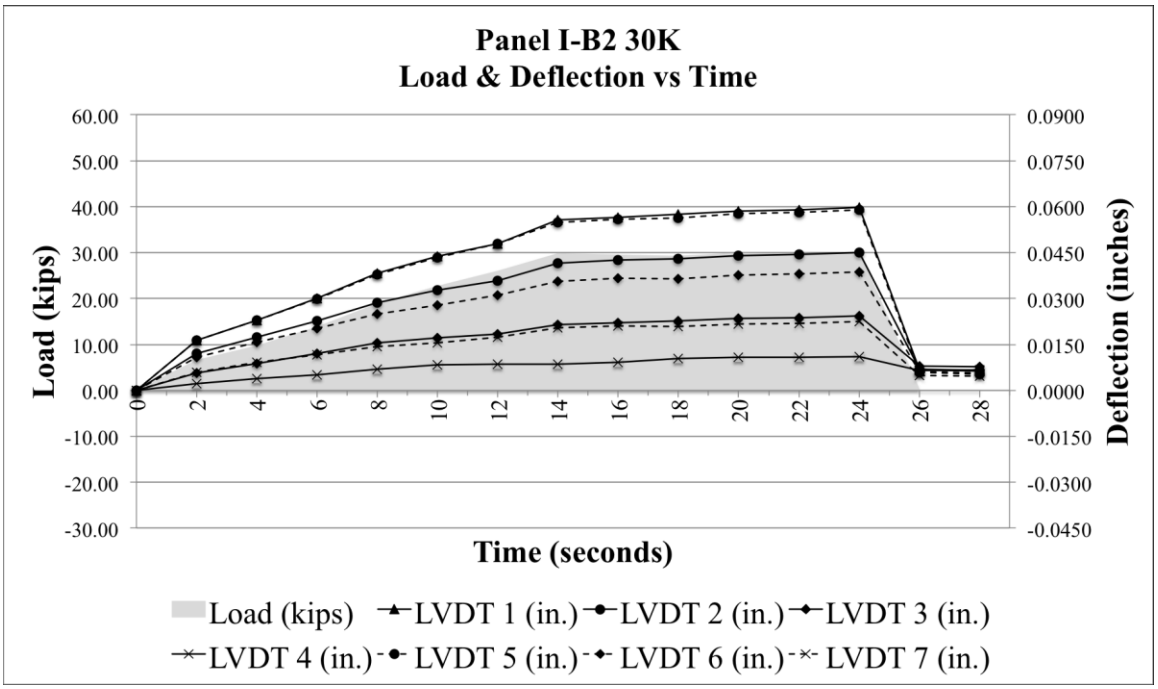

Figure E24 Pavement I Panel-B2 static load deflection and load vs. time (30,000 lb. Load)

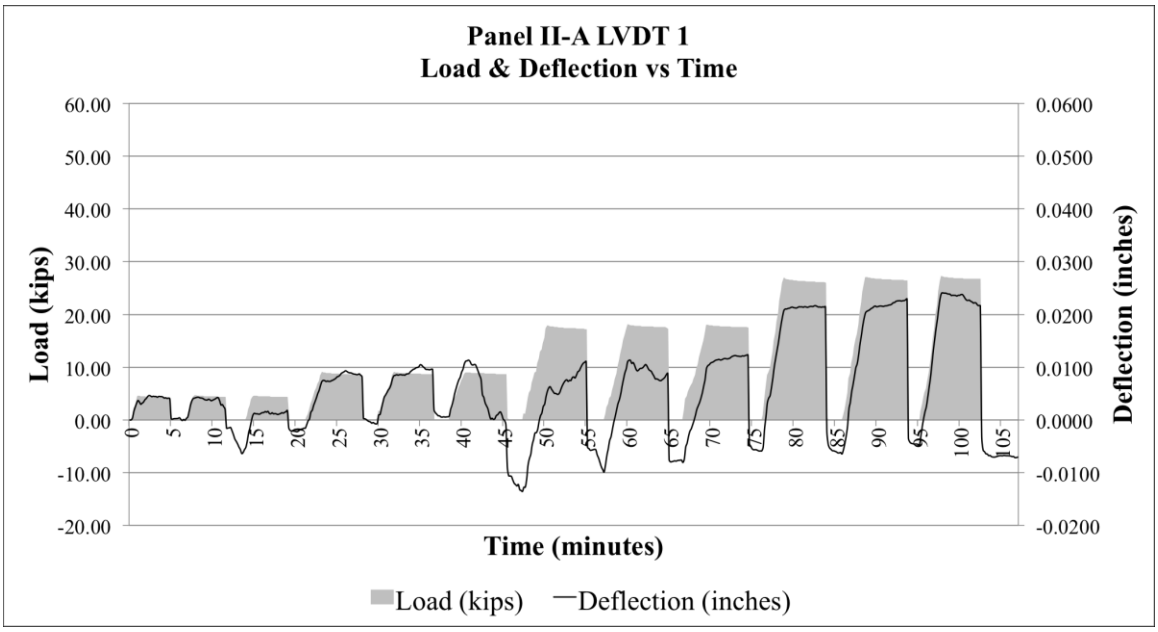

Figure E25 Pavement II Panel-A repeated load deflection and load vs. time for LVDT 1

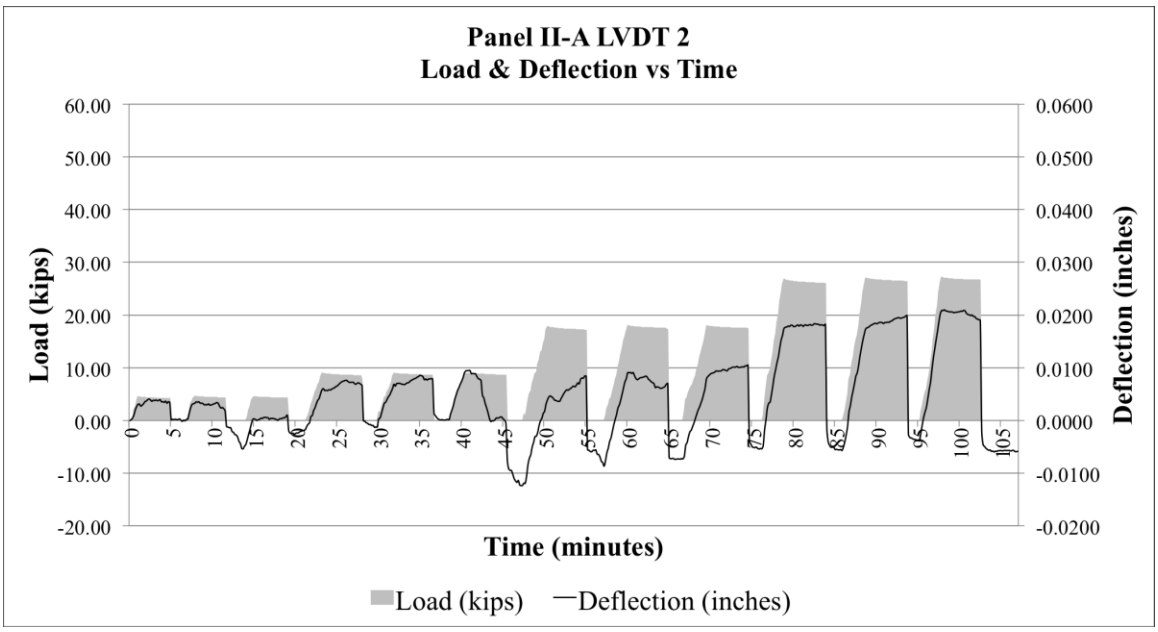

Figure E26 Pavement II Panel-A repeated load deflection and load vs. time for LVDT 2

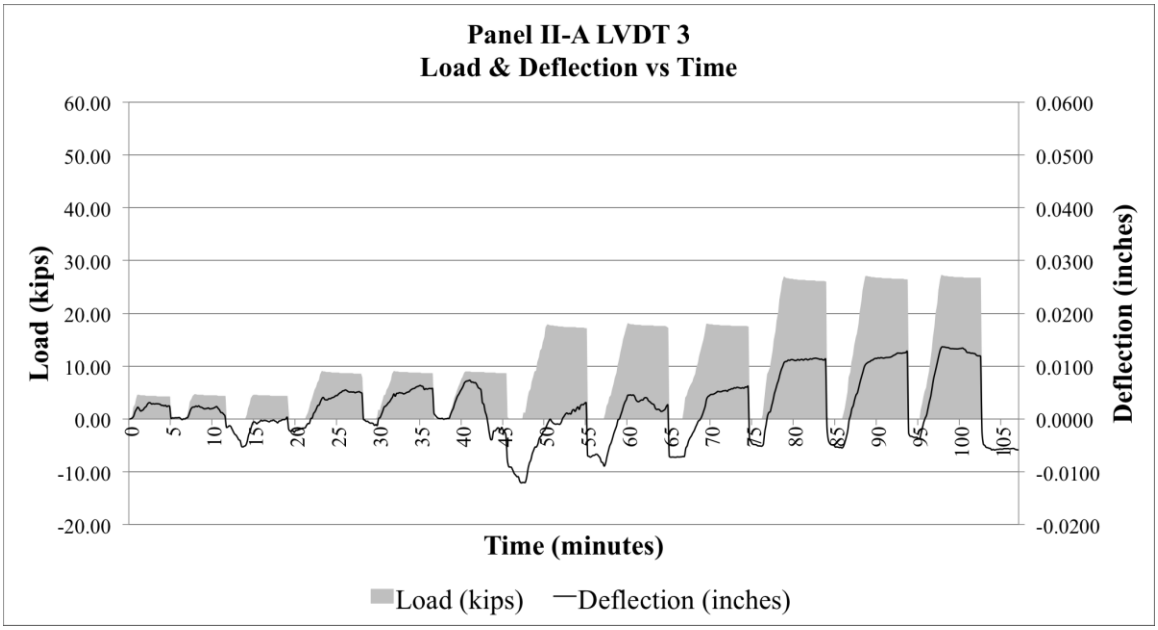

Figure E27 Pavement II Panel-A repeated load deflection and load vs. time for LVDT 3

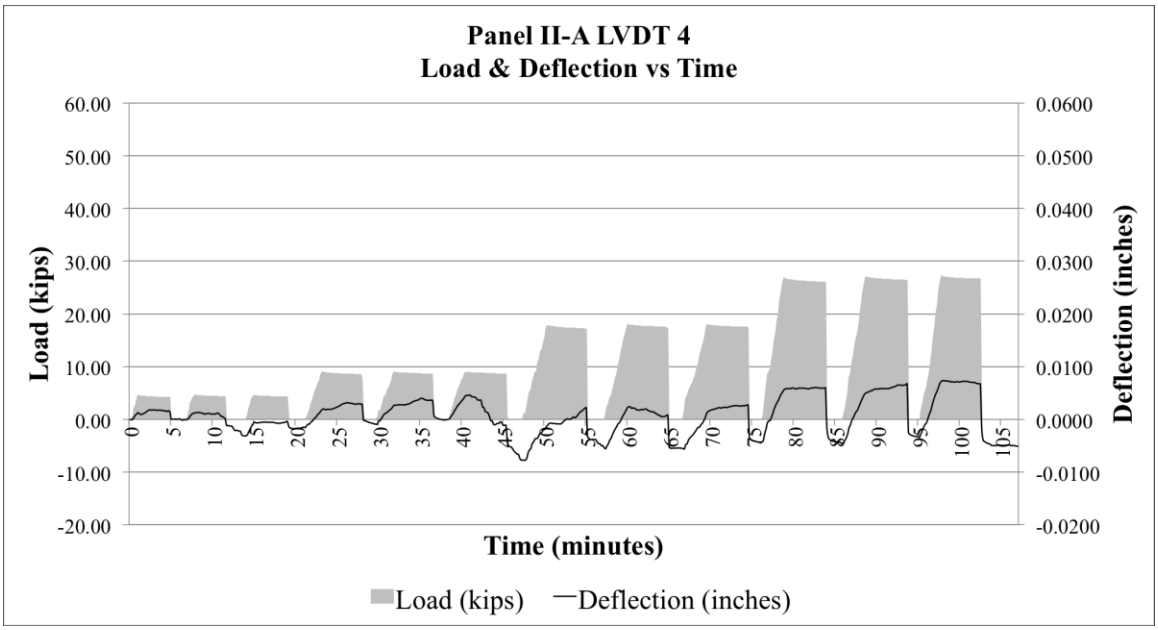

Figure E28 Pavement II Panel-A repeated load deflection and load vs. time for LVDT 4

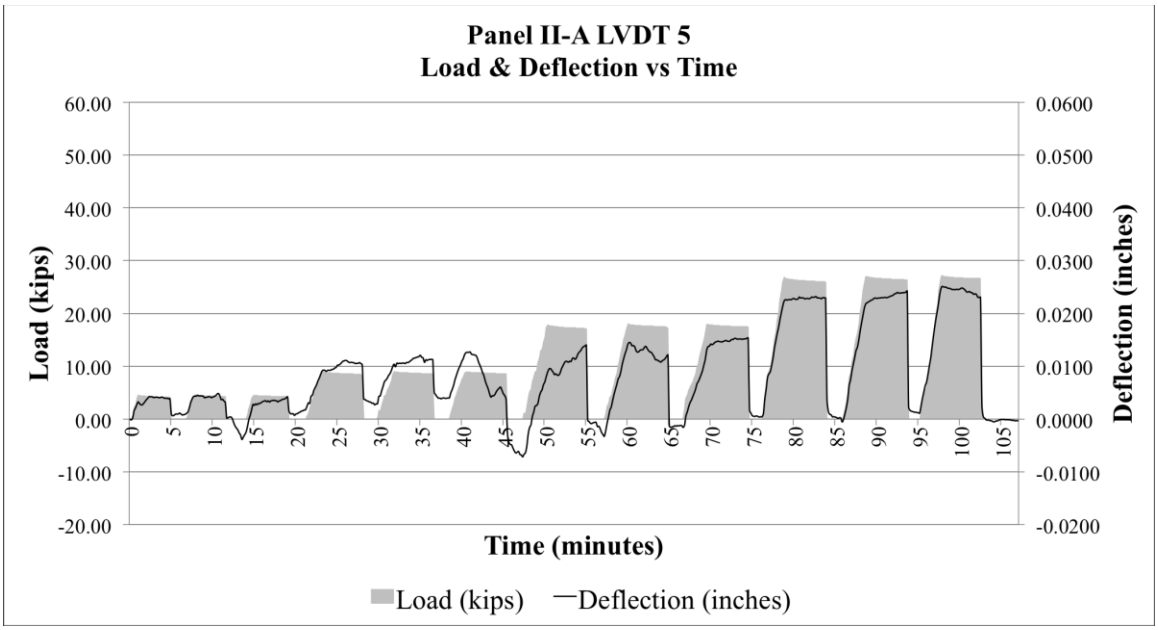

Figure E29 Pavement II Panel-A repeated load deflection and load vs. time for LVDT 5

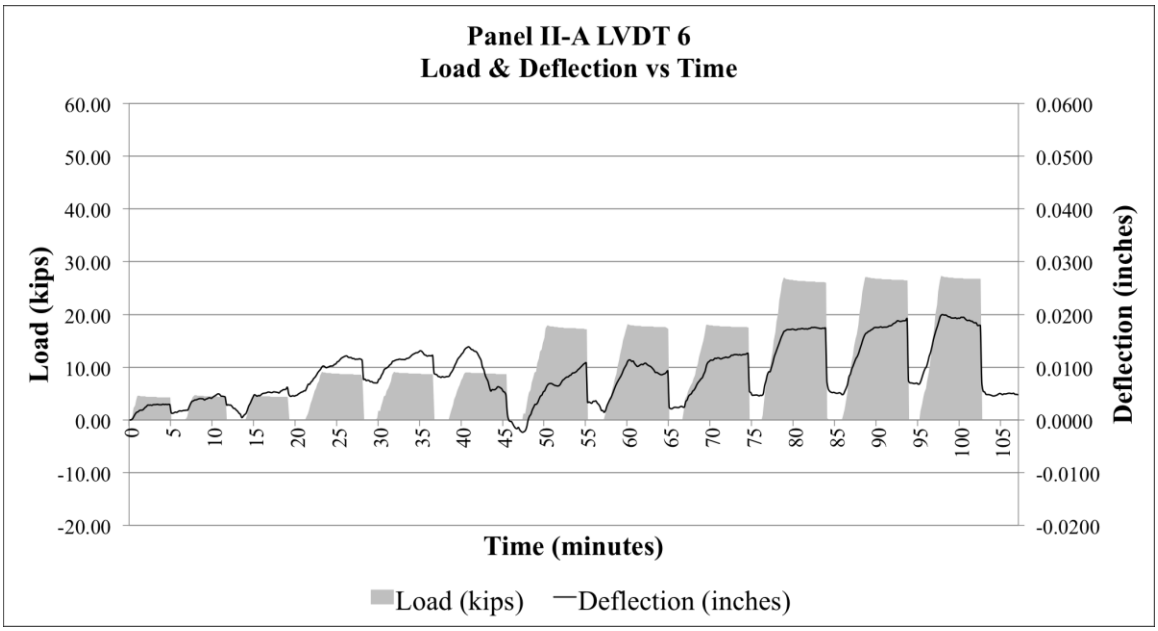

Figure E30 Pavement II Panel-A repeated load deflection and load vs. time for LVDT 6

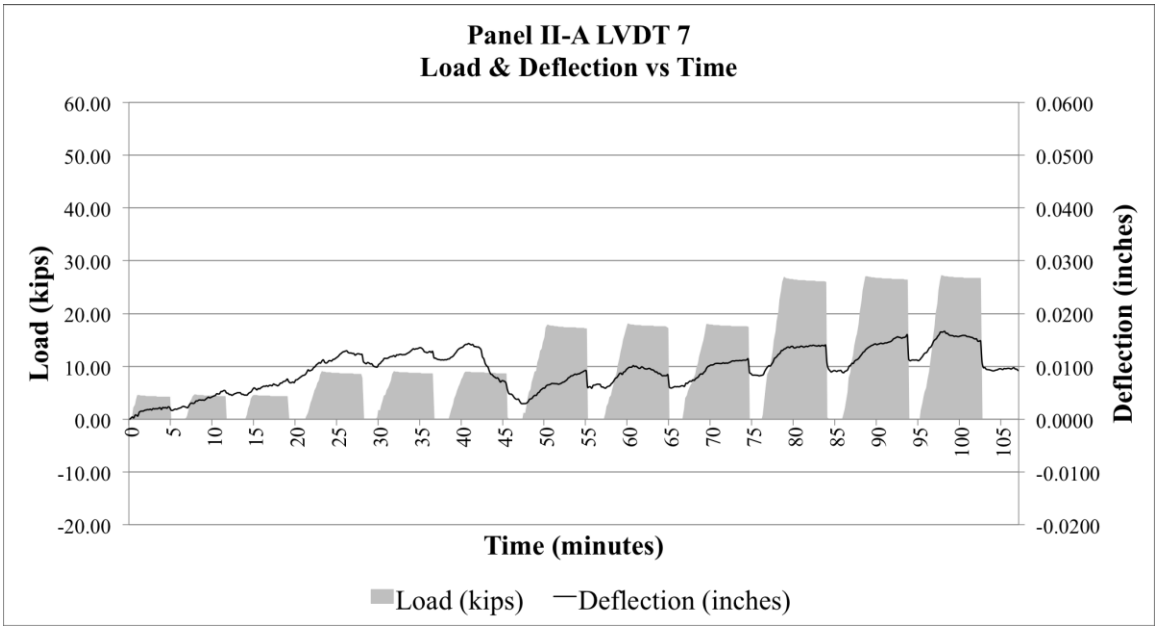

Figure E31 Pavement II Panel-A repeated load deflection and load vs. time for LVDT 7

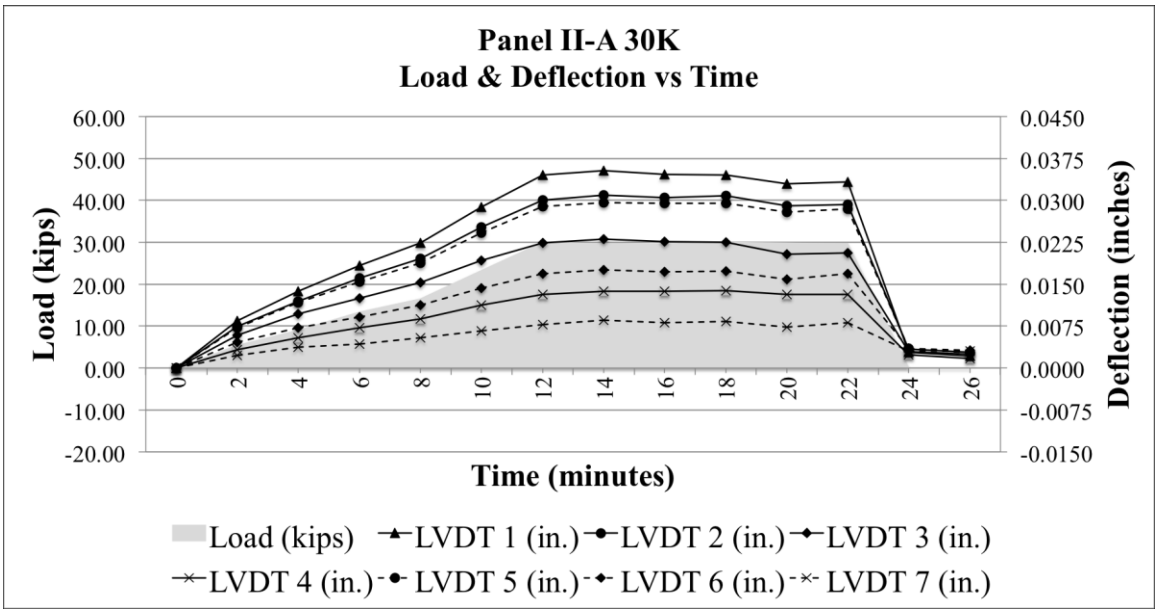

Figure E32 Pavement II Panel-A static load deflection and load vs. time (30,000 lb. Load)

Pavement II Panel-B1 Repeated & Static Load Test Results

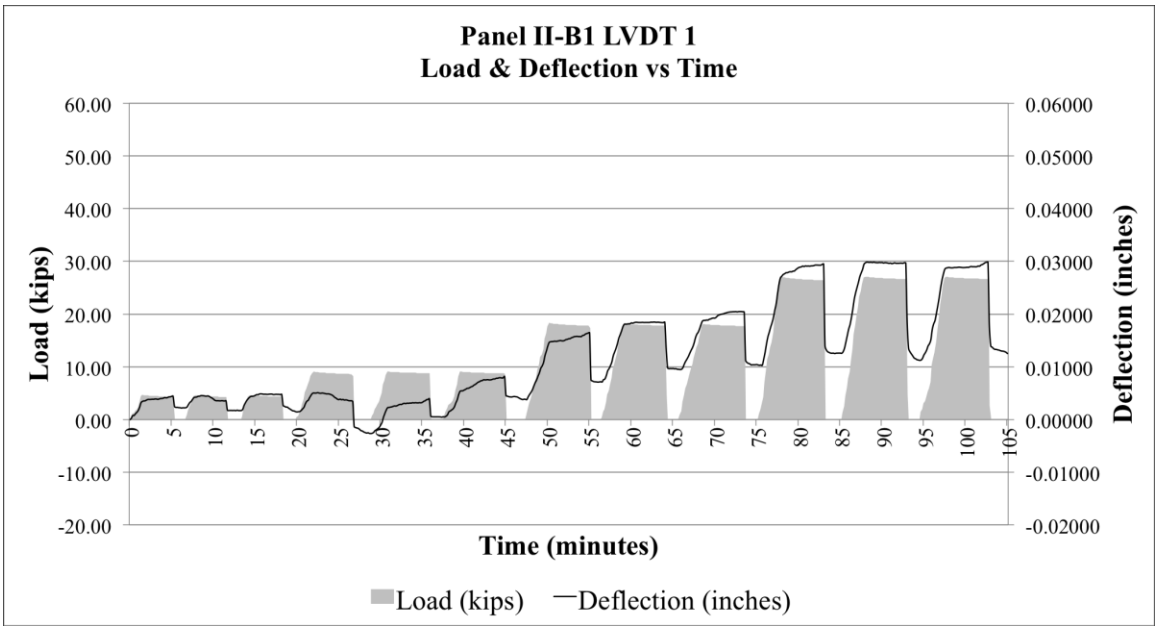

Figure E33 Pavement II Panel-B1 repeated load deflection and load vs. time for LVDT 1

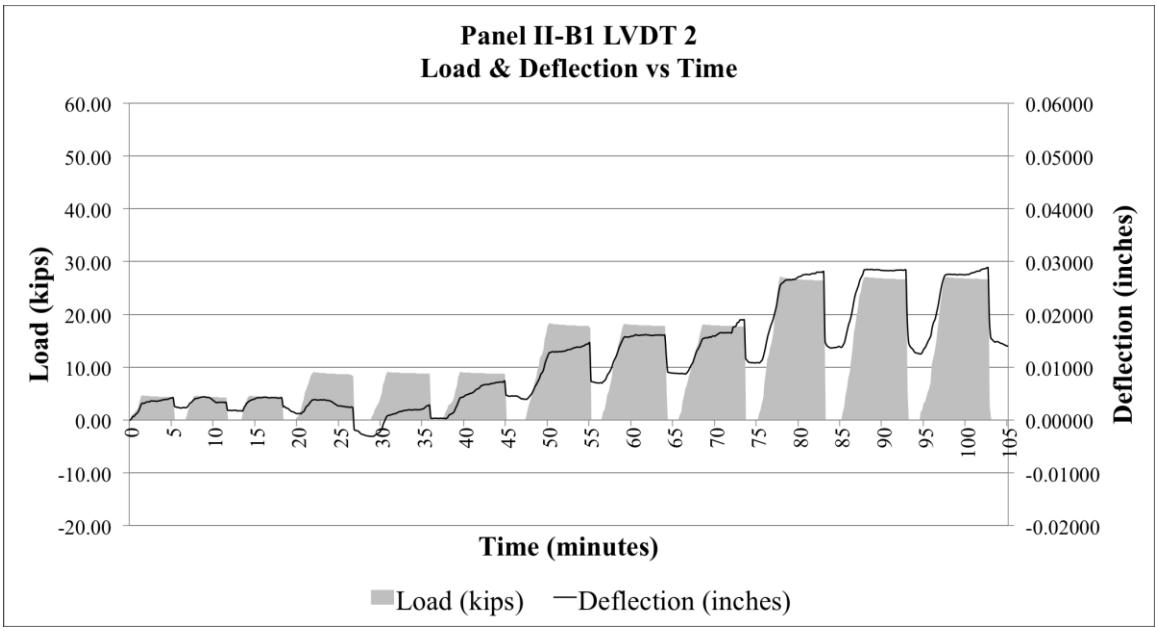

Figure E34 Pavement II Panel-B1 repeated load deflection and load vs. time for LVDT 2

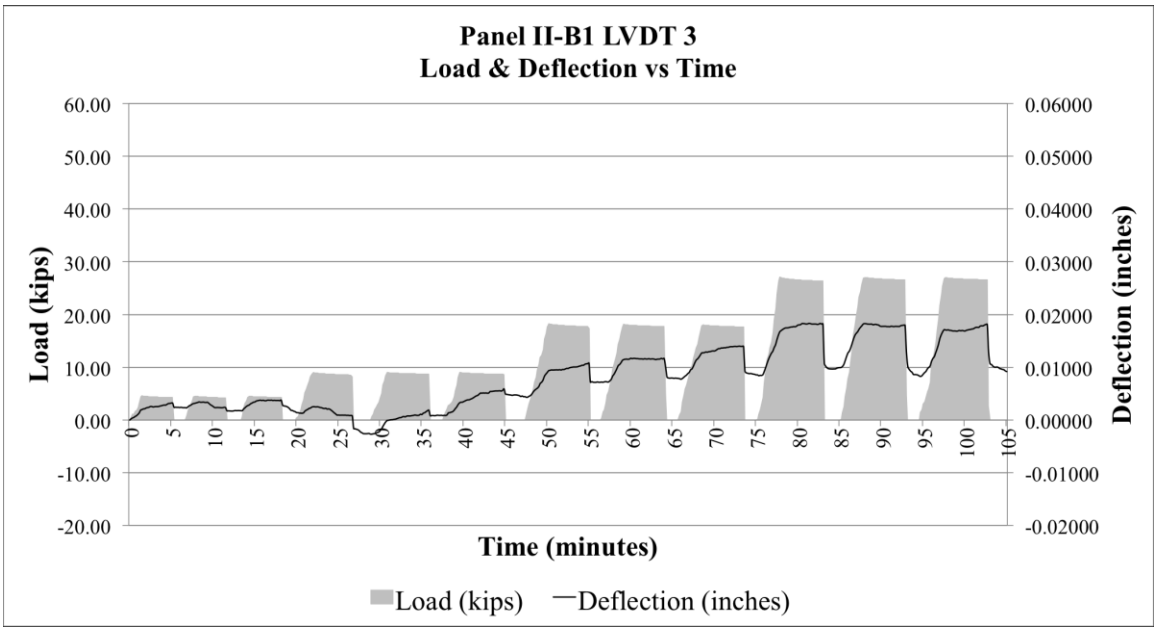

Figure E35 Pavement II Panel-B1 repeated load deflection and load vs. time for LVDT 3

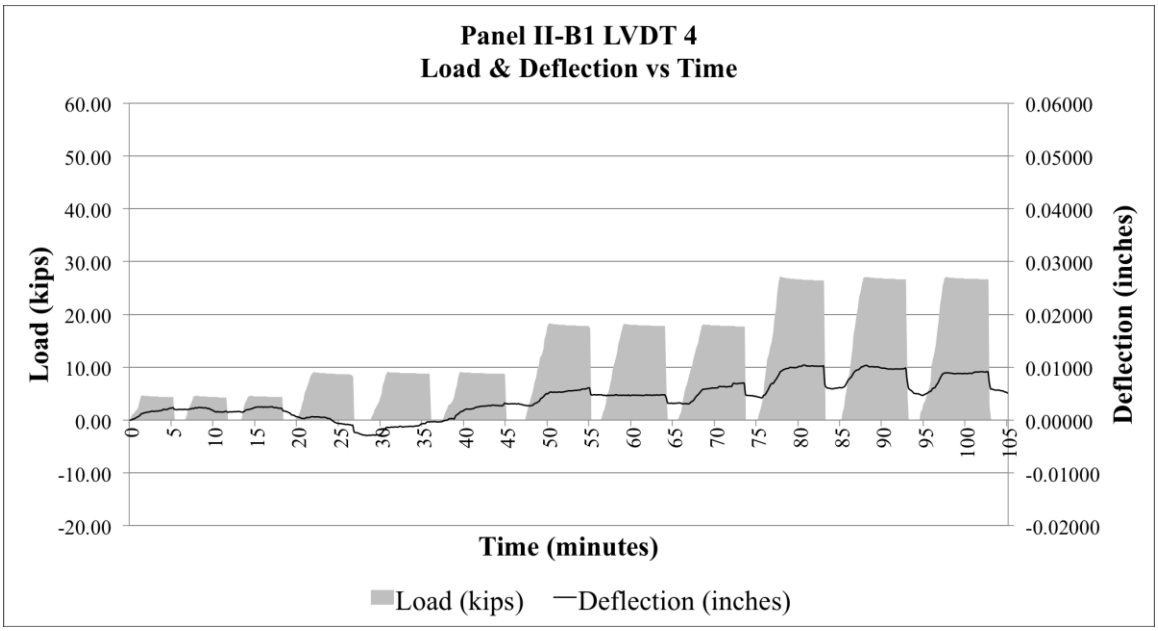

Figure E36 Pavement II Panel-B1 repeated load deflection and load vs. time for LVDT 4

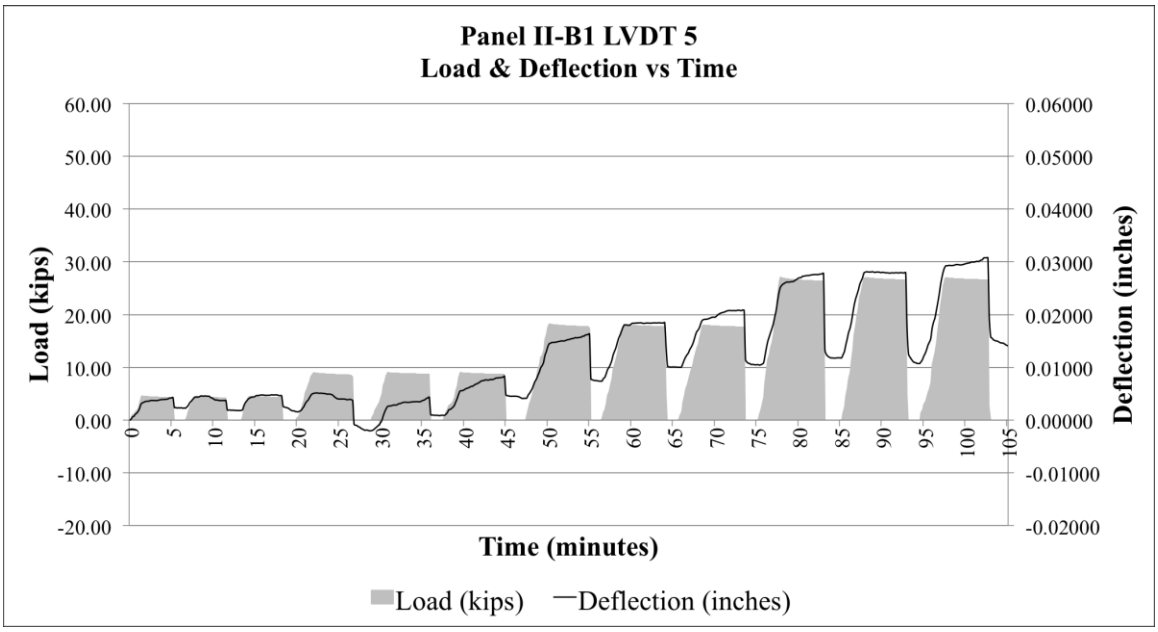

Figure E37 Pavement II Panel-B1 repeated load deflection and load vs. time for LVDT 5

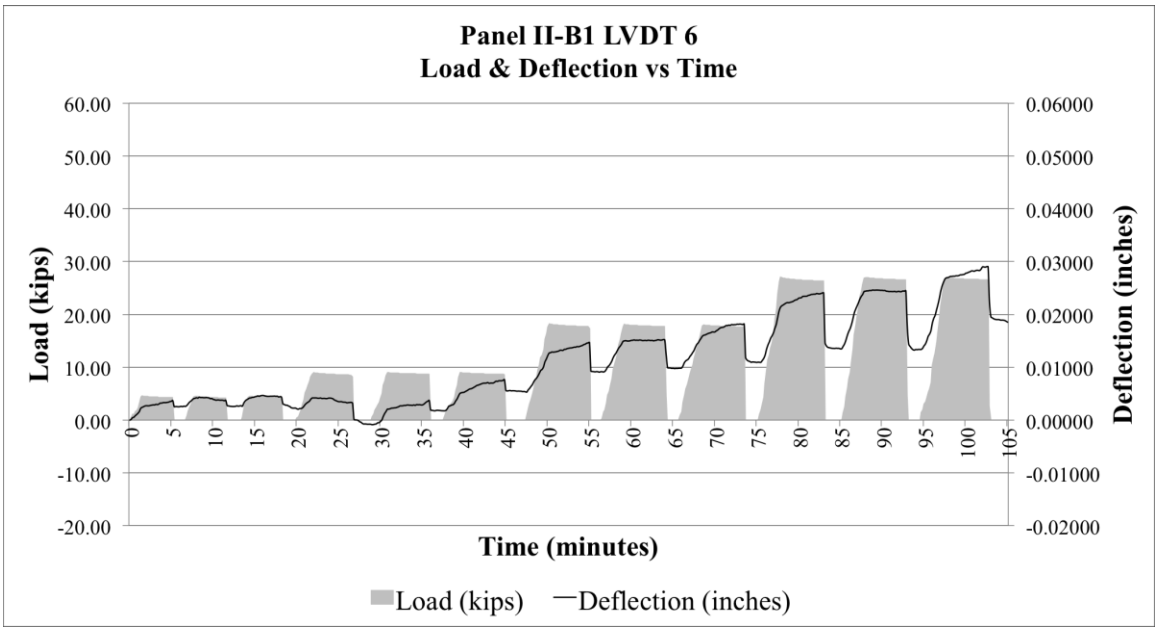

Figure E38 Pavement II Panel-B1 repeated load deflection and load vs. time for LVDT 6

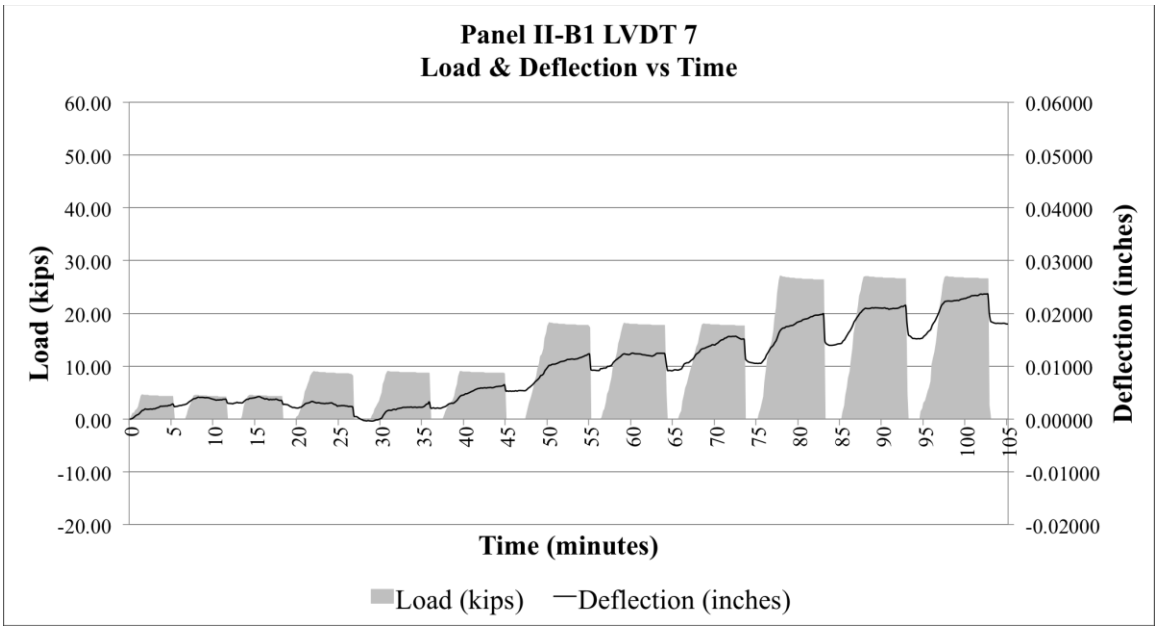

Figure E39 Pavement II Panel-B1 repeated load deflection and load vs. time for LVDT 7

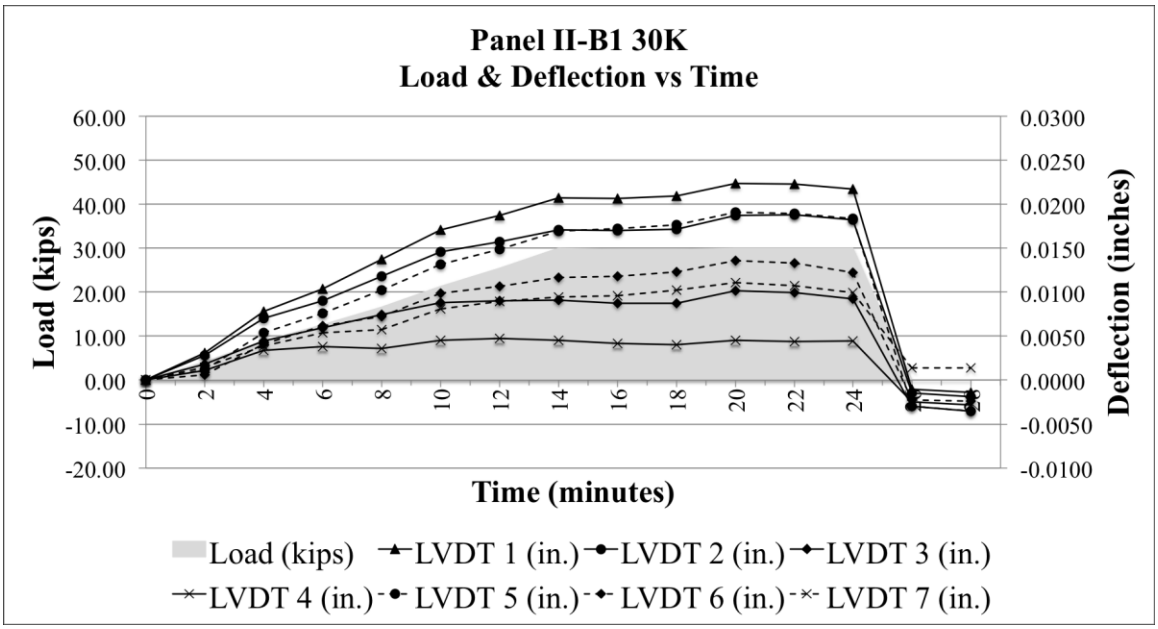

Figure E40 Pavement II Panel-B1 static load deflection and load vs. time (30,000 lb. Load)

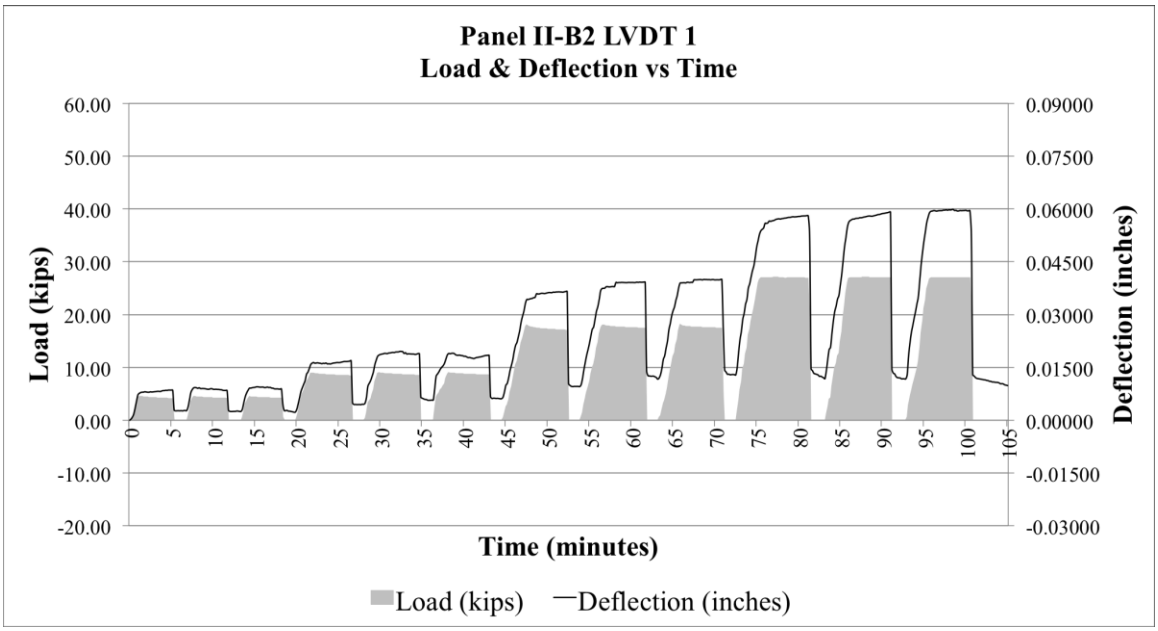

Figure E41 Pavement II Panel-B2 repeated load deflection and load vs. time for LVDT 1

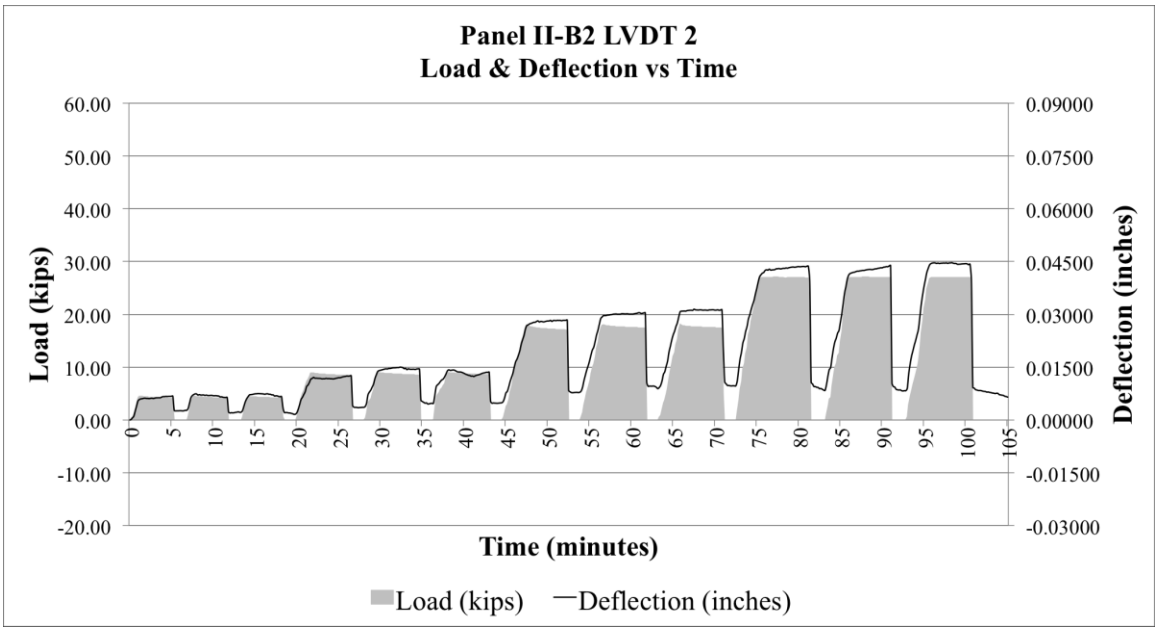

Figure E42 Pavement II Panel-B2 repeated load deflection and load vs. time for LVDT 2

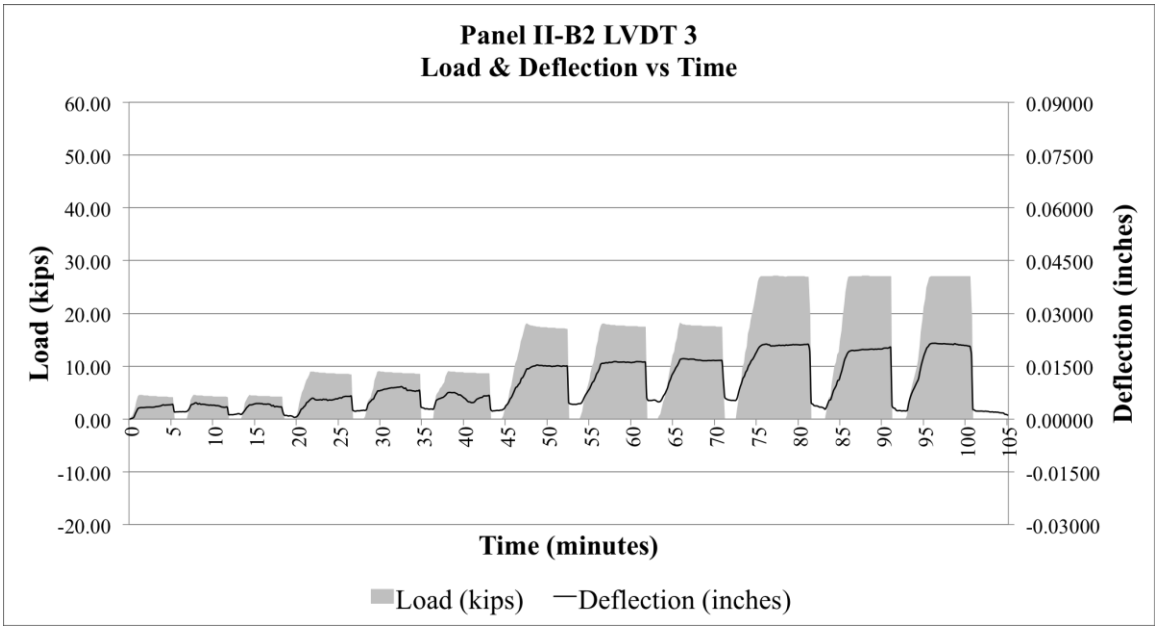

Figure E43 Pavement II Panel-B2 repeated load deflection and load vs. time for LVDT 3

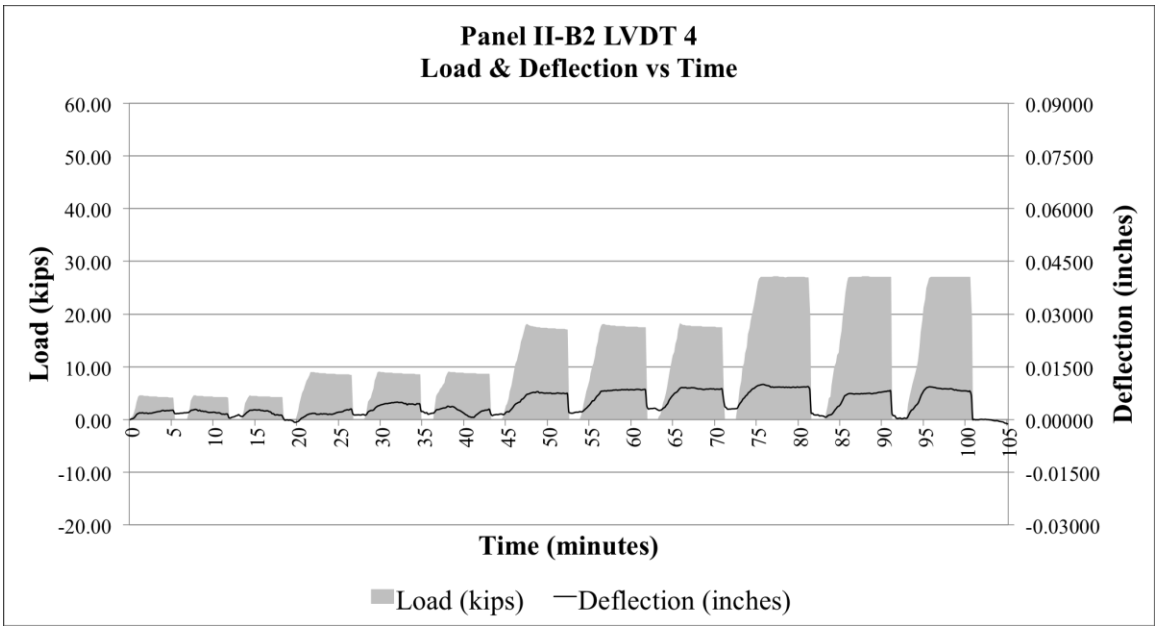

Figure E44 Pavement II Panel-B2 repeated load deflection and load vs. time for LVDT 4

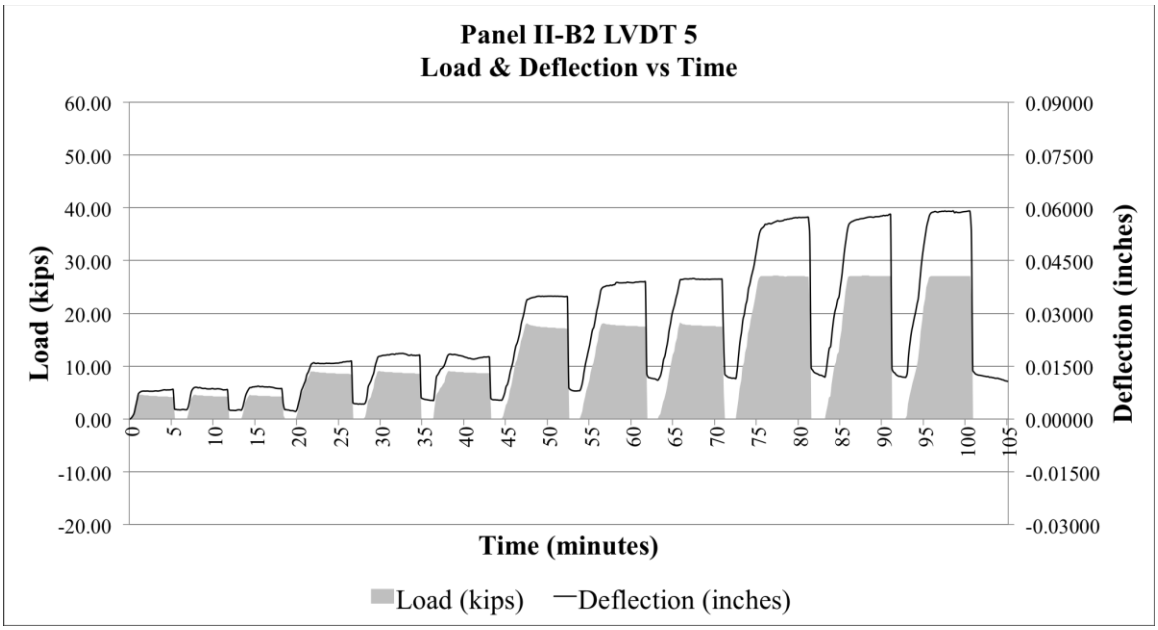

Figure E45 Pavement II Panel-B2 repeated load deflection and load vs. time for LVDT 5

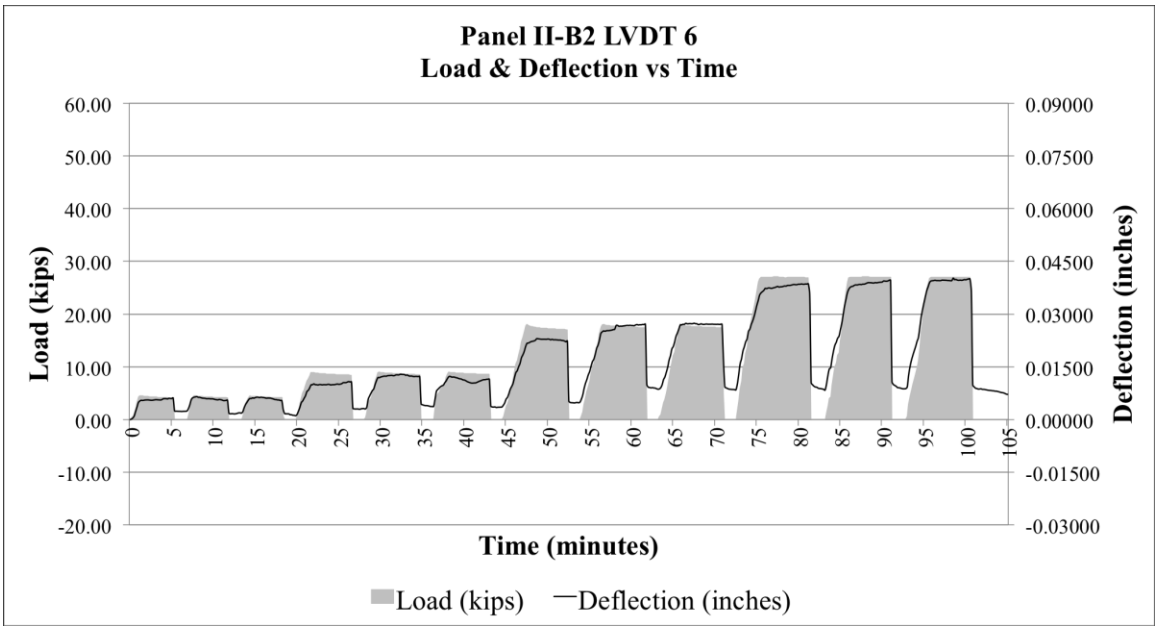

Figure E46 Pavement II Panel-B2 repeated load deflection and load vs. time for LVDT 6

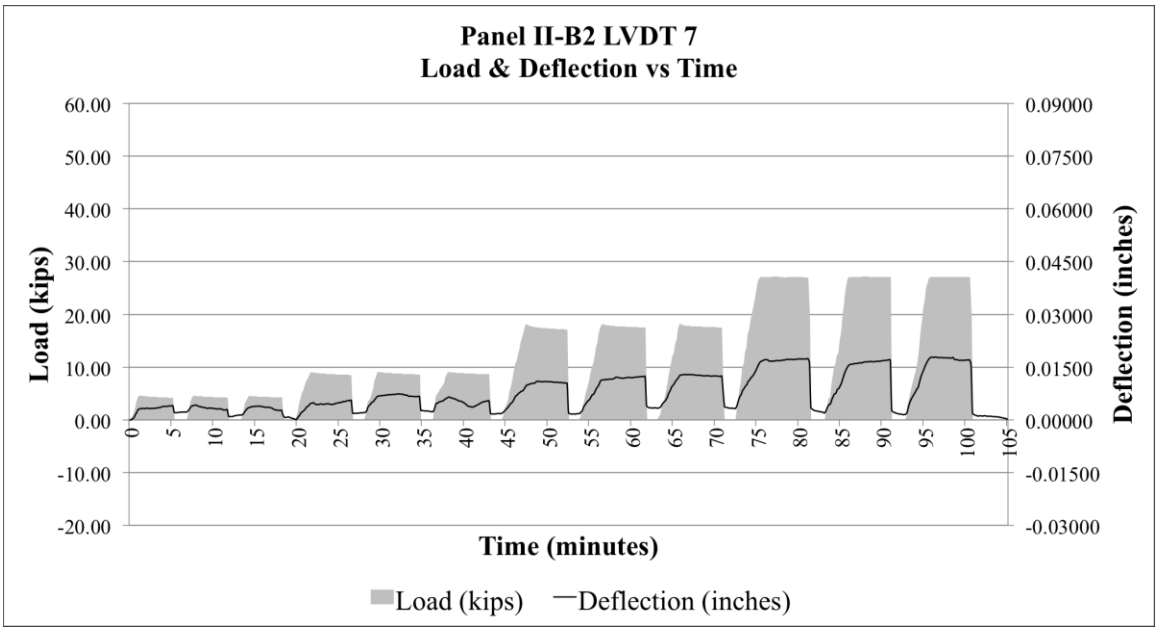

Figure E47 Pavement II Panel-B2 repeated load deflection and load vs. time for LVDT 7

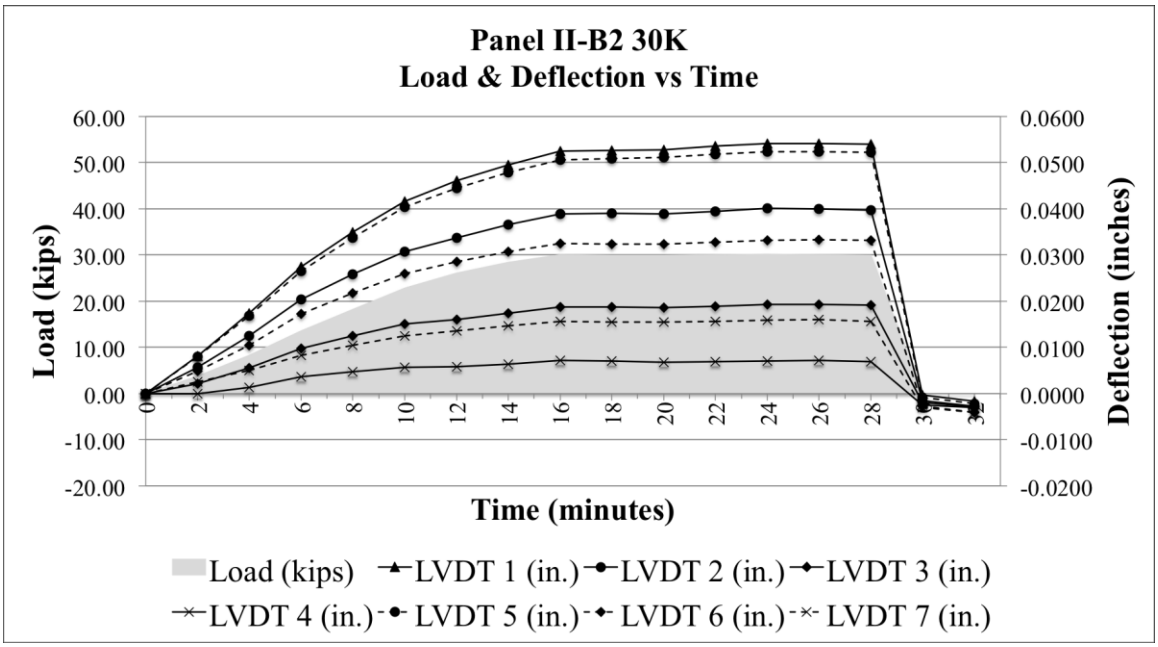

Figure E48 Pavement II Panel-B2 static load deflection and load vs. time (30,000 lb. Load)

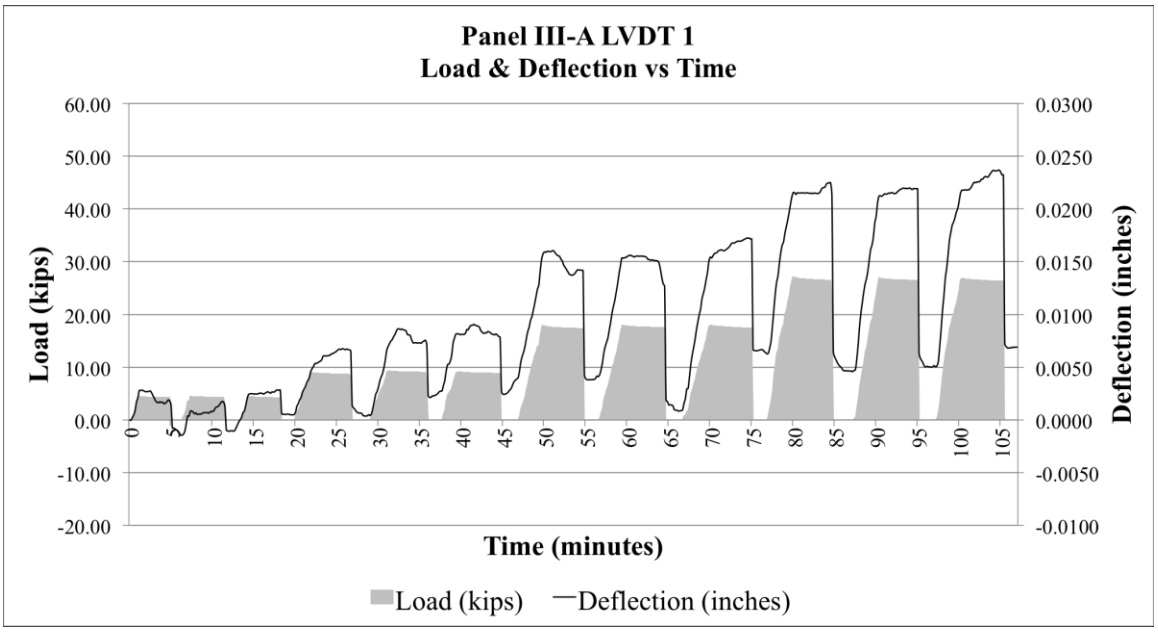

Figure E49 Pavement III Panel-A repeated load deflection and load vs. time for LVDT 1

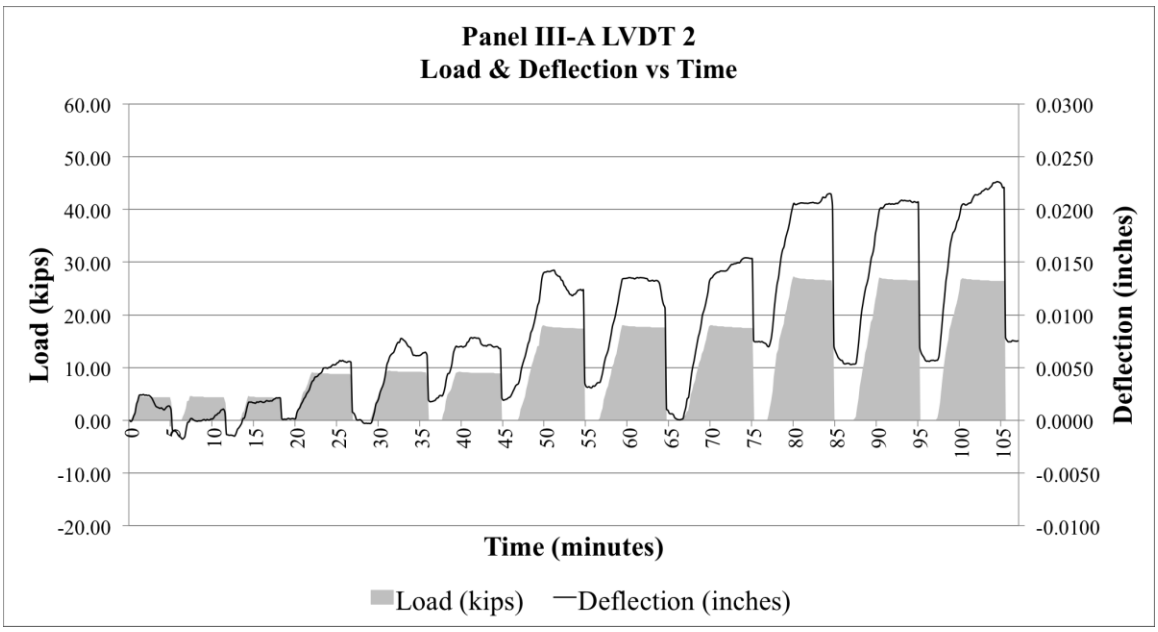

Figure E50 Pavement III Panel-A repeated load deflection and load vs. time for LVDT 2

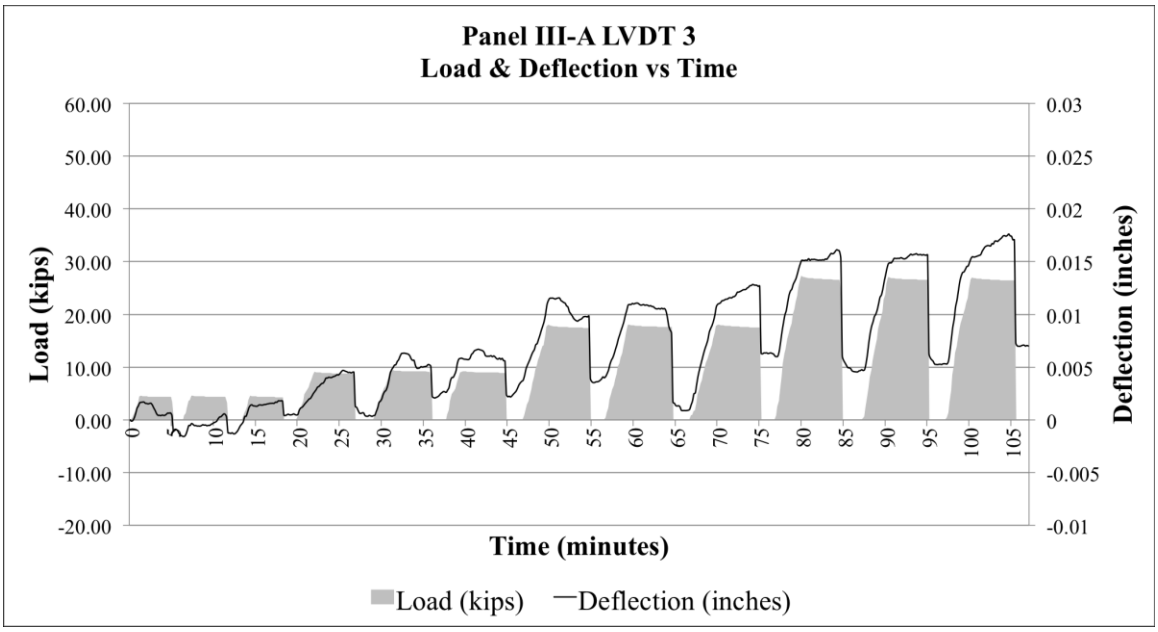

Figure E51 Pavement III Panel-A repeated load deflection and load vs. time for LVDT 3

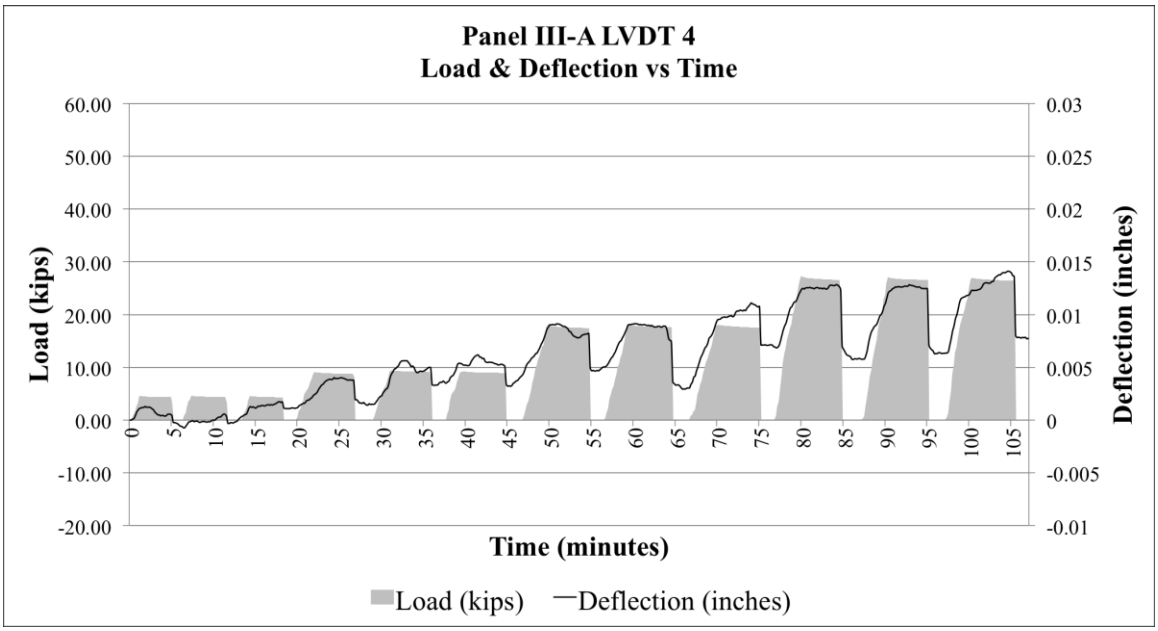

Figure E52 Pavement III Panel-A repeated load deflection and load vs. time for LVDT 4

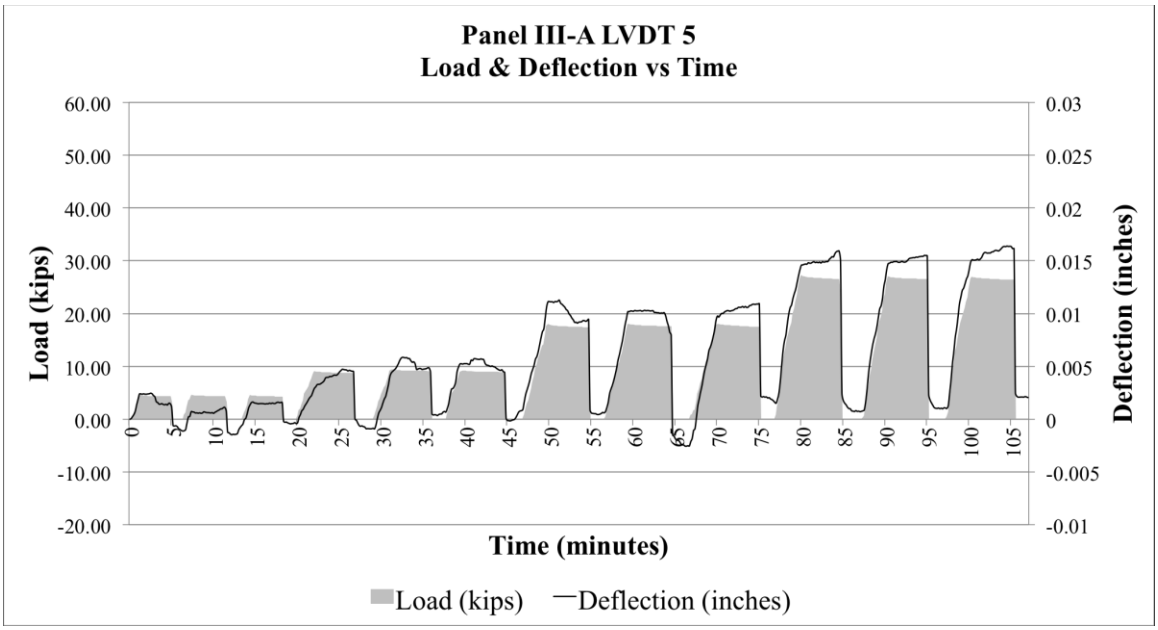

Figure E53 Pavement III Panel-A repeated load deflection and load vs. time for LVDT 5

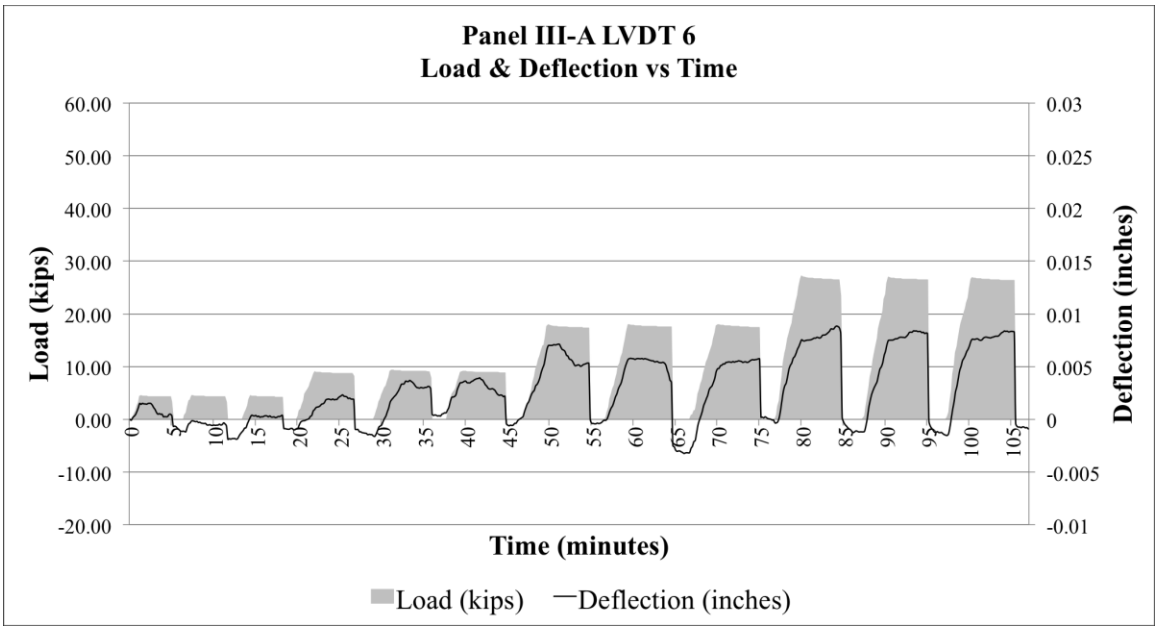

Figure E54 Pavement III Panel-A repeated load deflection and load vs. time for LVDT 6

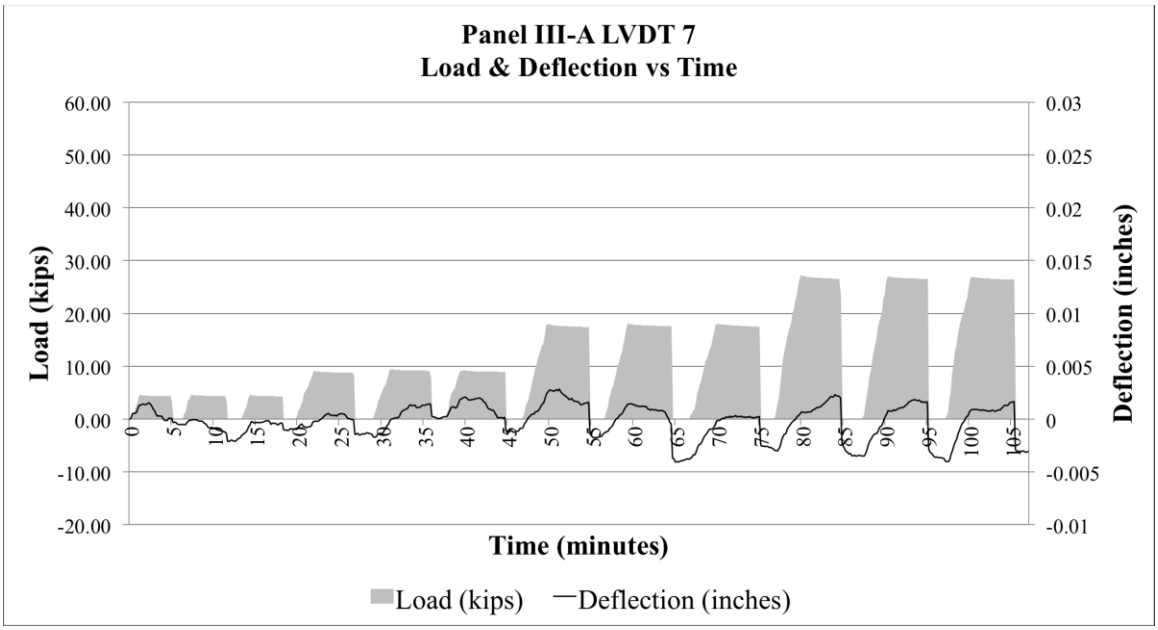

Figure E55 Pavement III Panel-A repeated load deflection and load vs. time for LVDT 7

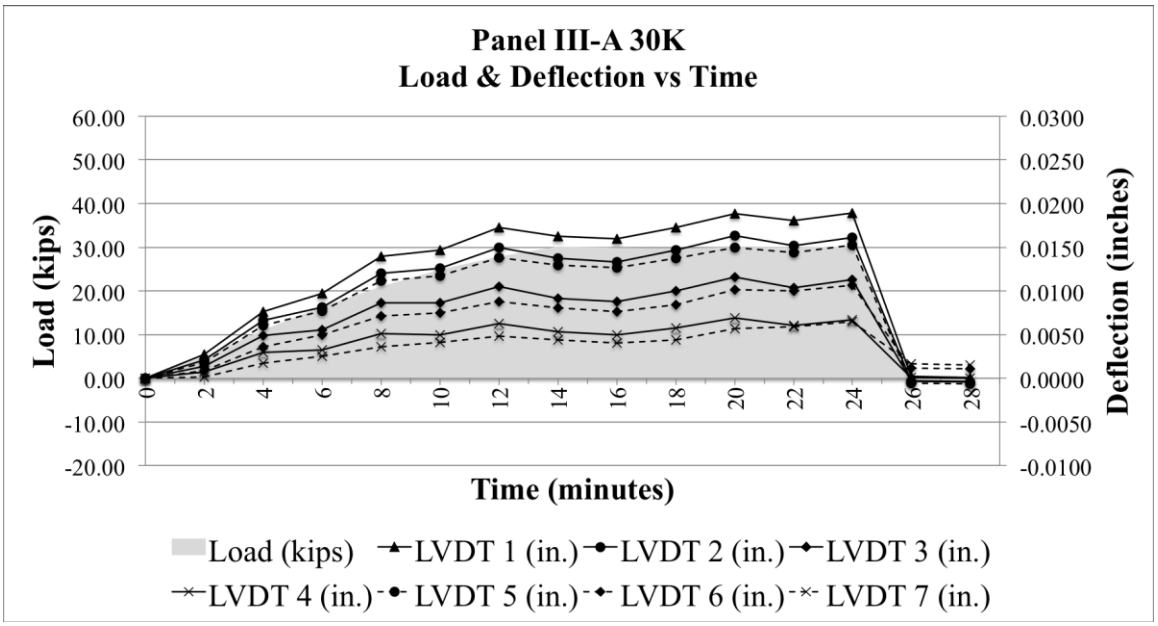

Figure E56 Pavement III Panel-A static load deflection and load vs. time (30,000 lb. Load)

Pavement III Panel-B1 Repeated & Static Load Test Results

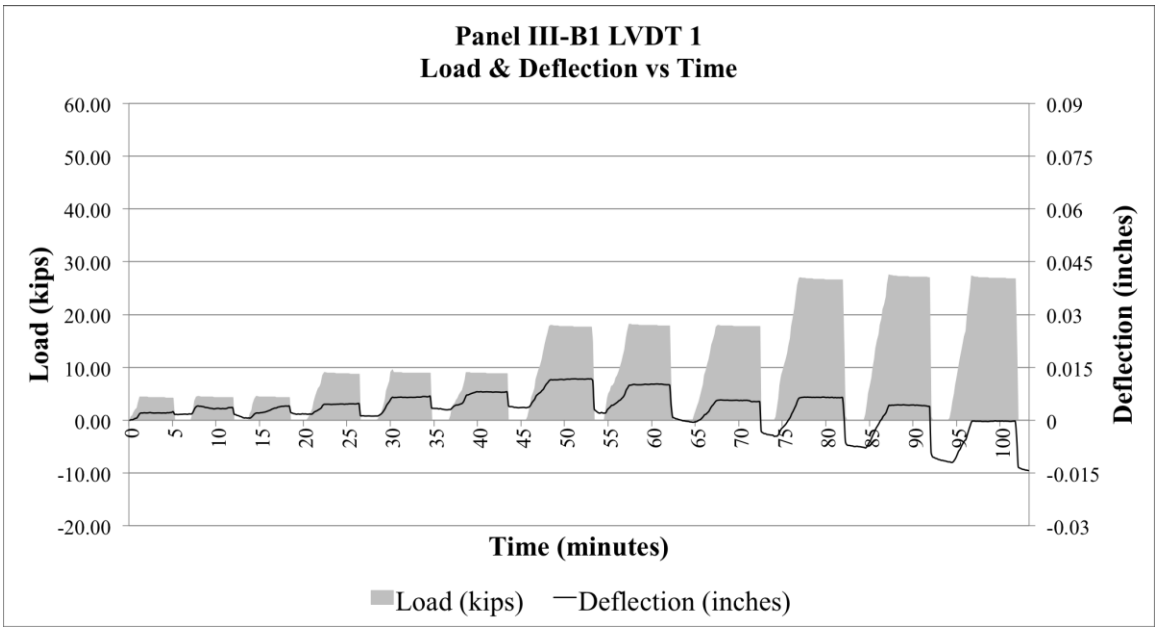

Figure E57 Pavement III Panel-B1 repeated load deflection and load vs. time for LVDT 1

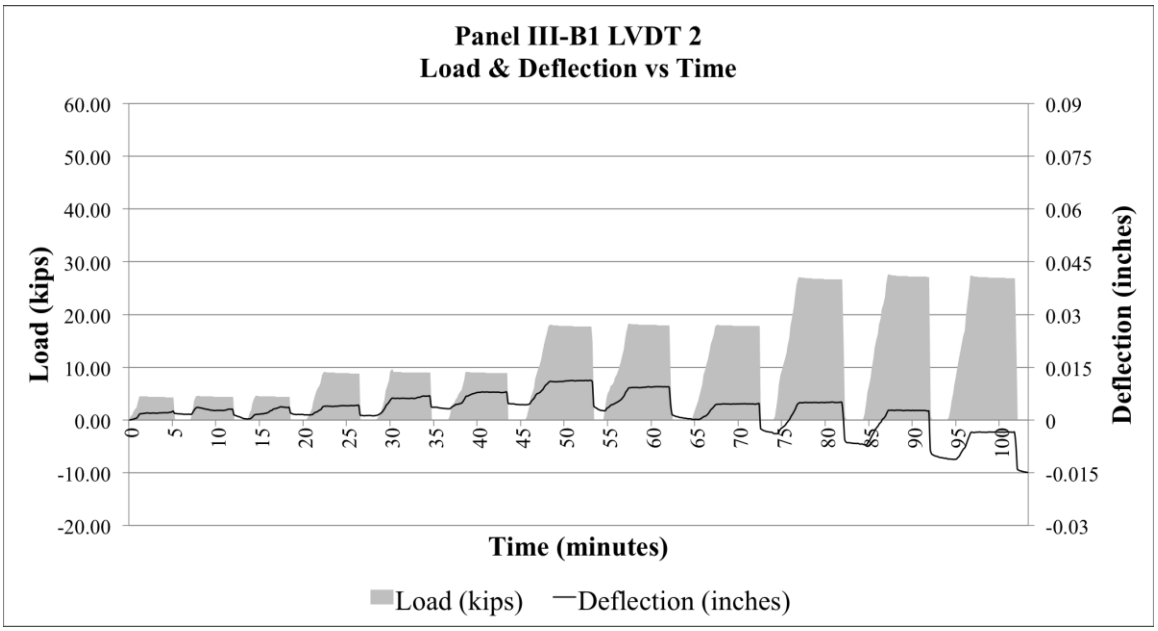

Figure E58 Pavement III Panel-B1 repeated load deflection and load vs. time for LVDT 2

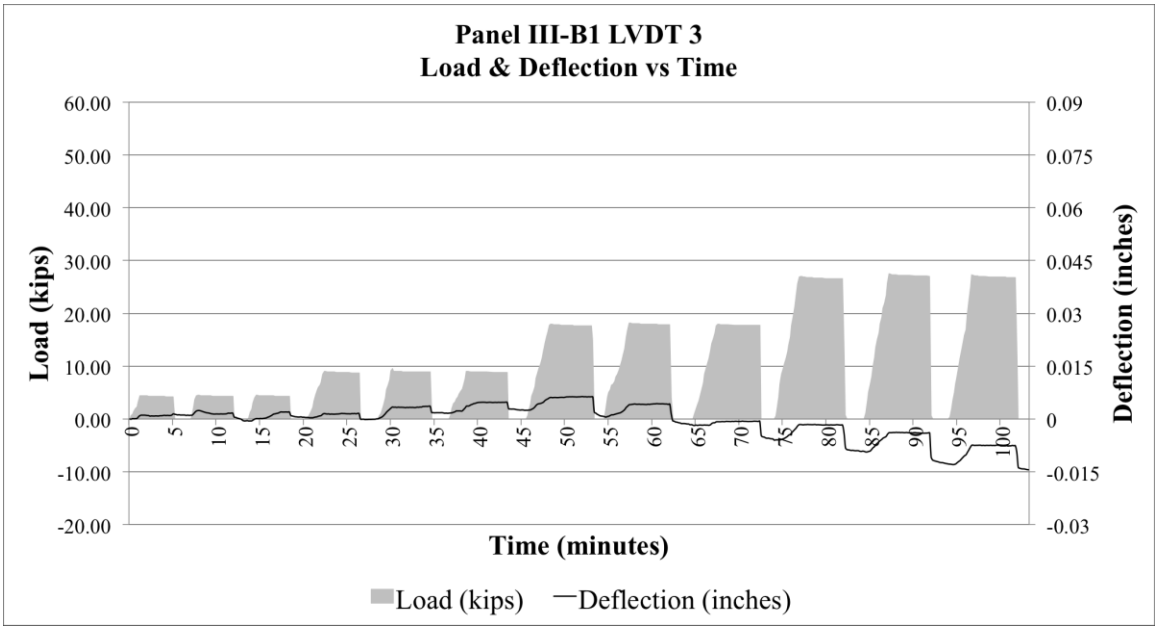

Figure E59 Pavement III Panel-B1 repeated load deflection and load vs. time for LVDT 3

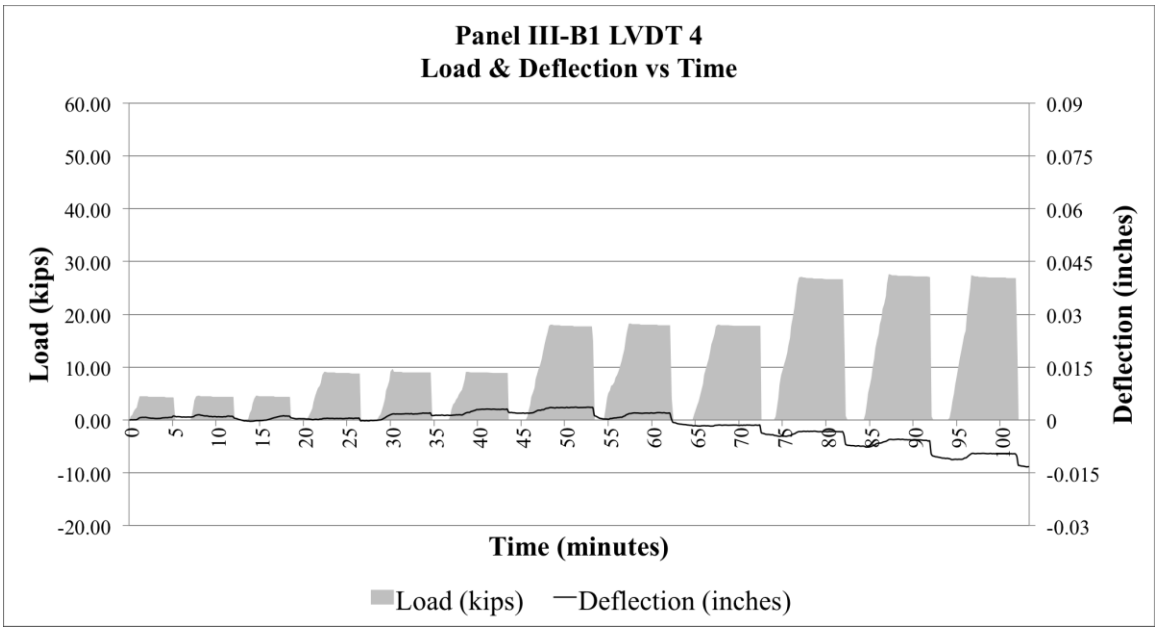

Figure E60 Pavement III Panel-B1 repeated load deflection and load vs. time for LVDT 4

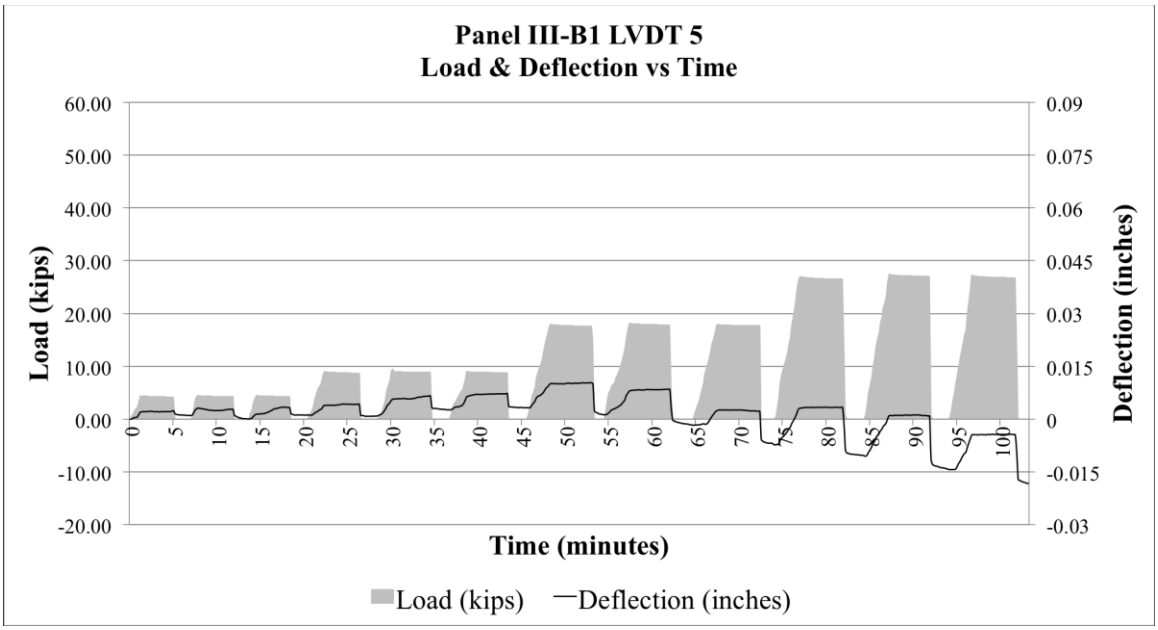

Figure E61 Pavement III Panel-B1 repeated load deflection and load vs. time for LVDT 5

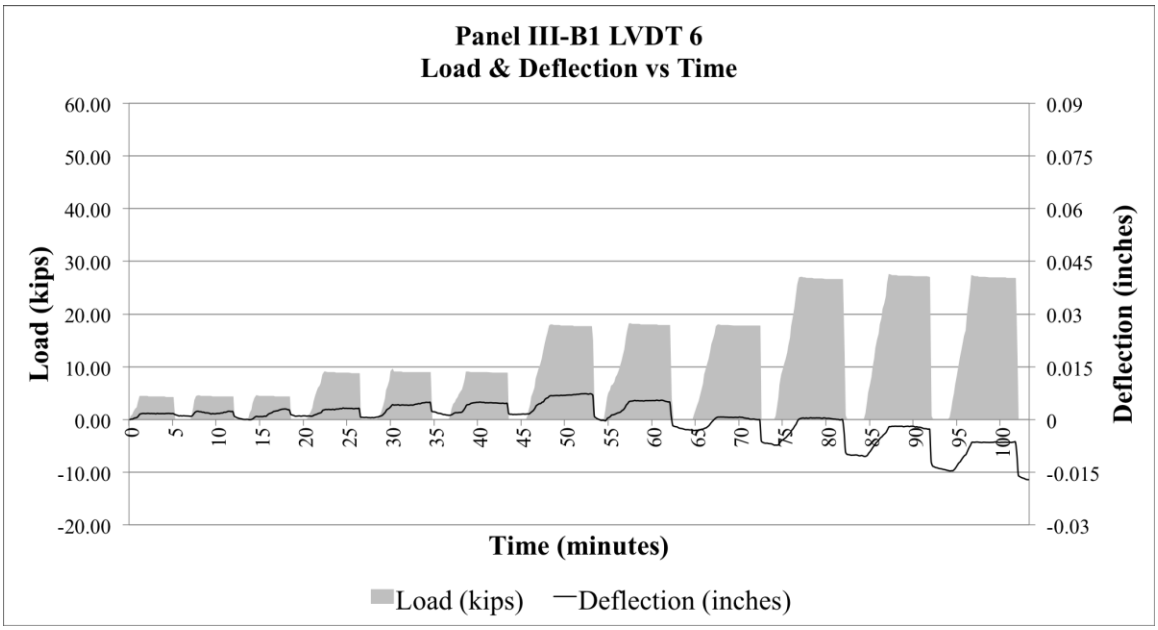

Figure E62 Pavement III Panel-B1 repeated load deflection and load vs. time for LVDT 6

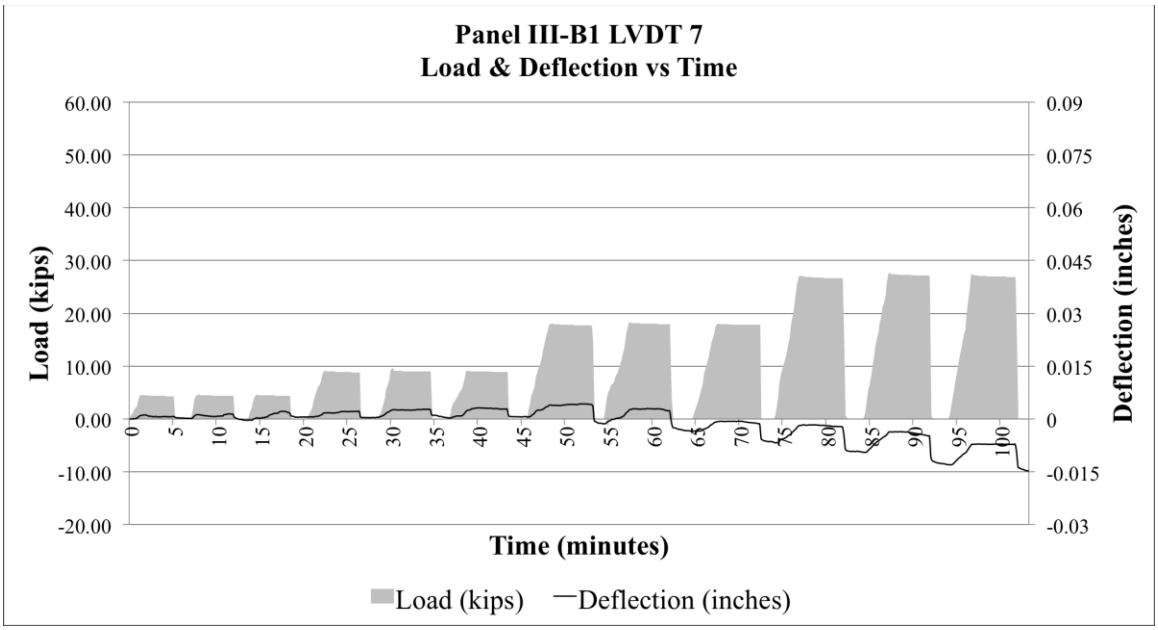

Figure E63 Pavement III Panel-B1 repeated load deflection and load vs. time for LVDT 7

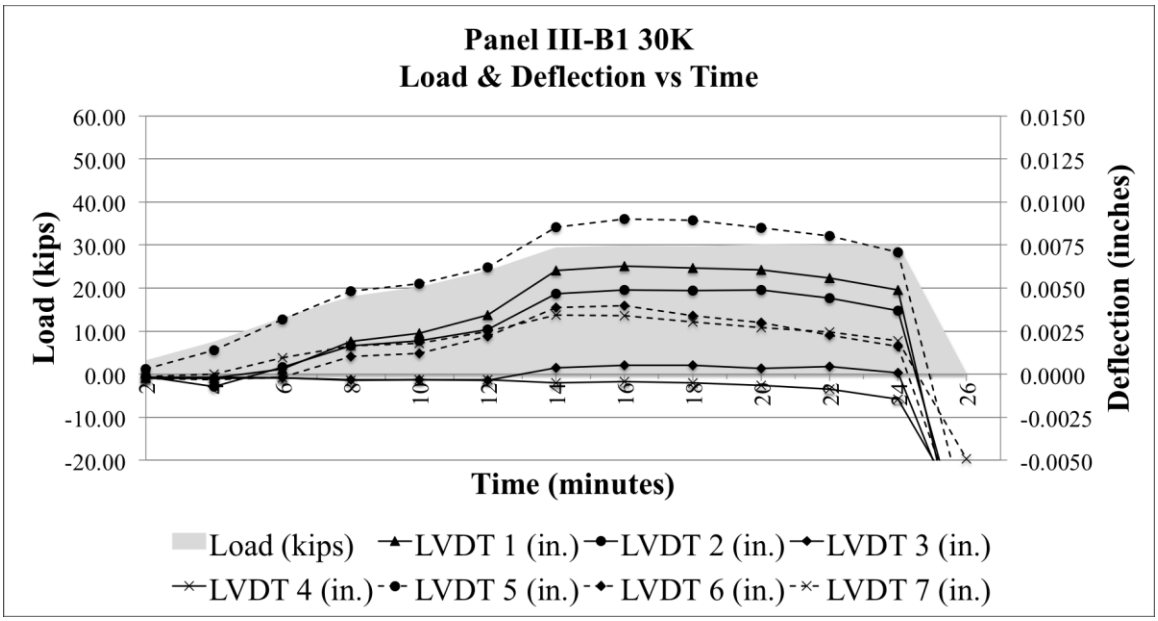

Figure E64 Pavement III Panel-B1 static load deflection and load vs. time (30,000 lb. Load)

Pavement III Panel-B2 Repeated & Static Load Test Results

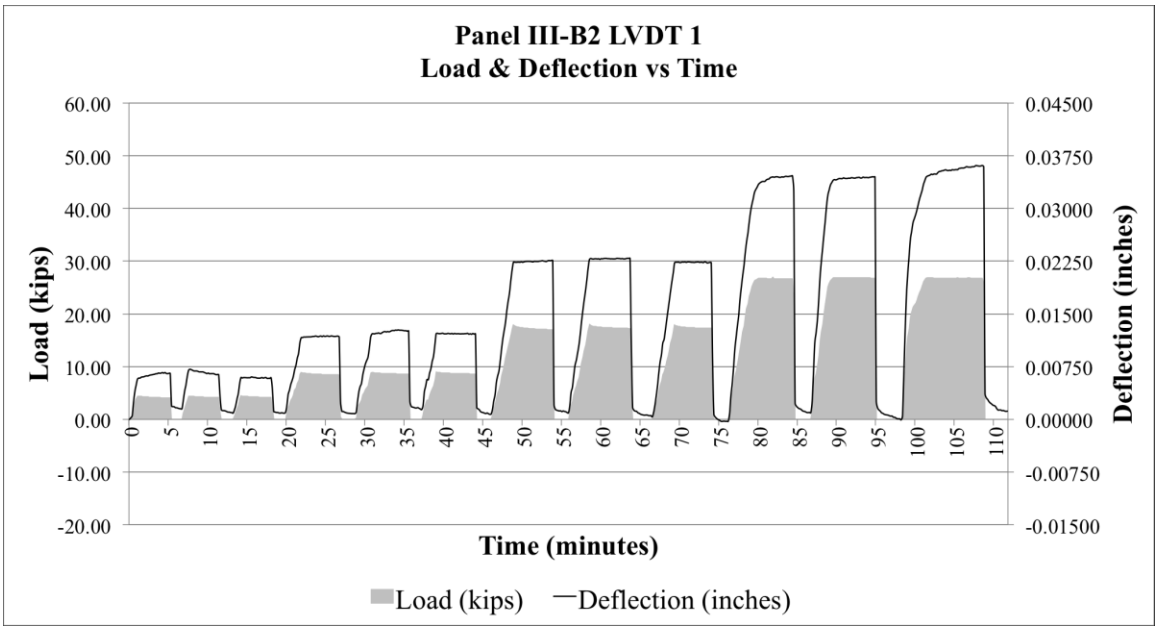

Figure E65 Pavement III Panel-B2 repeated load deflection and load vs. time for LVDT 1

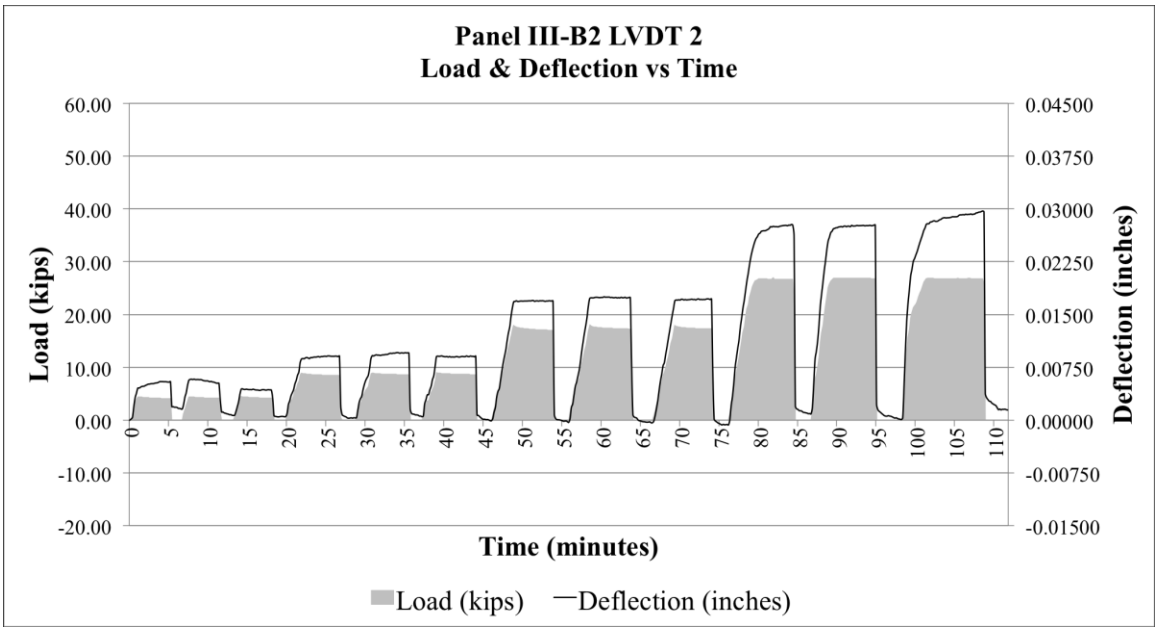

Figure E66 Pavement III Panel-B2 repeated load deflection and load vs. time for LVDT 2

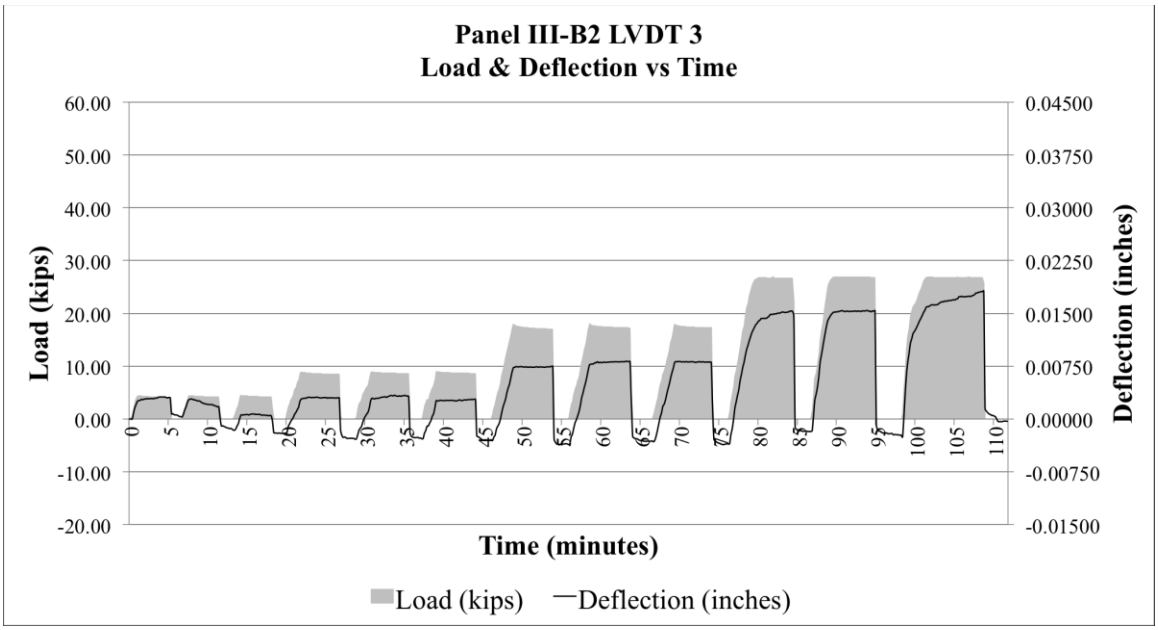

Figure E67 Pavement III Panel-B2 repeated load deflection and load vs. time for LVDT 3

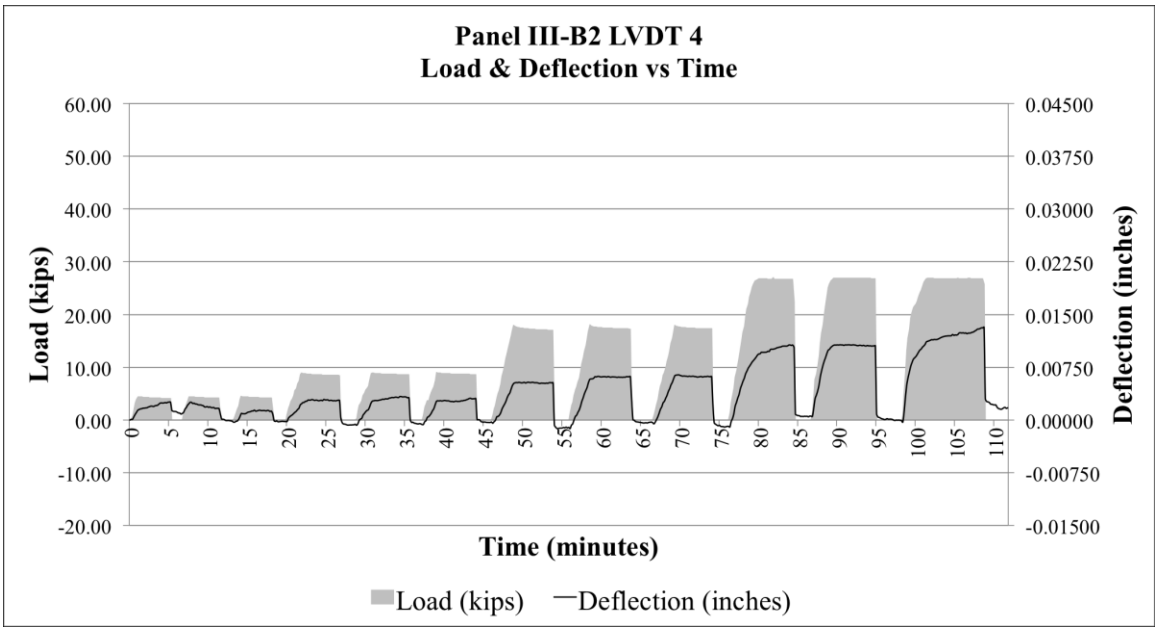

Figure E68 Pavement III Panel-B2 repeated load deflection and load vs. time for LVDT 4

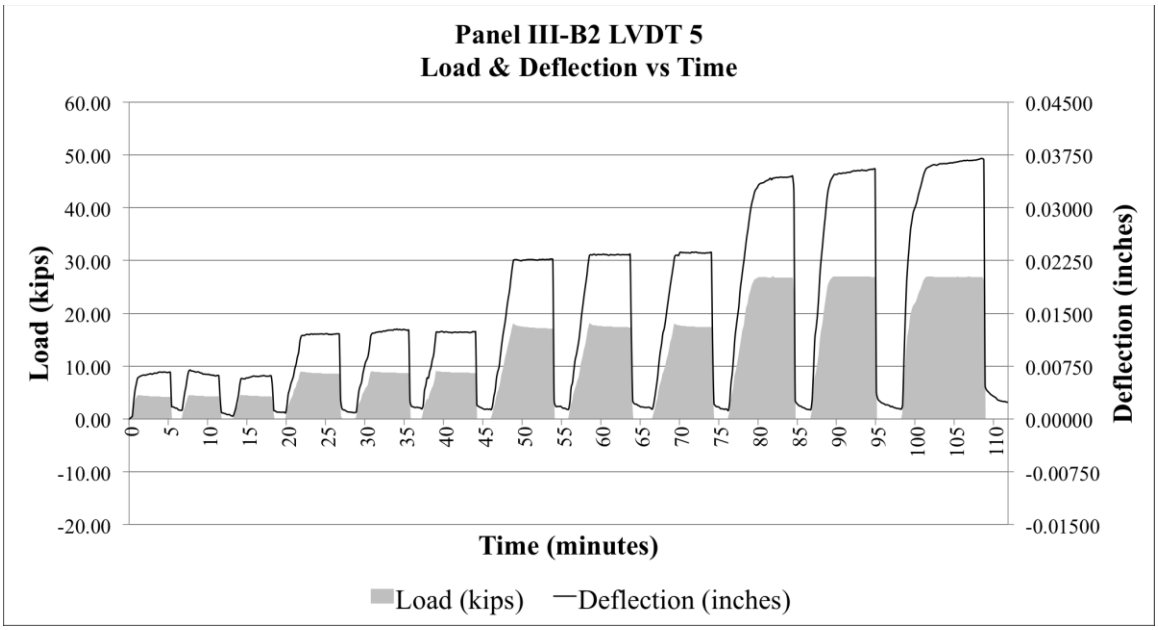

Figure E69 Pavement III Panel-B2 repeated load deflection and load vs. time for LVDT 5

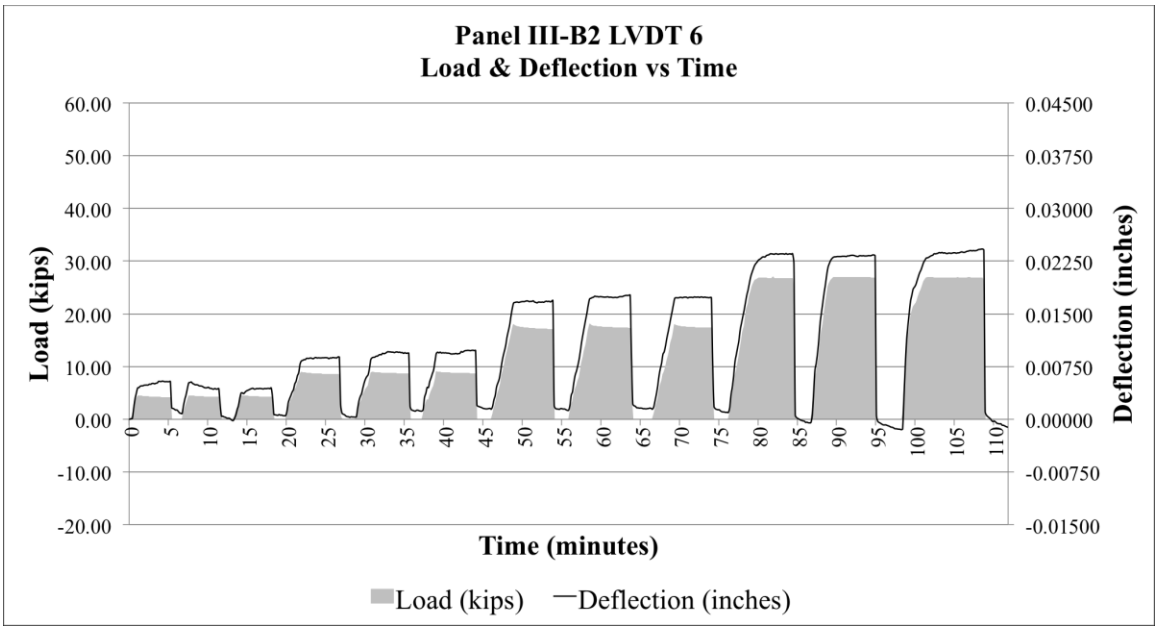

Figure E70 Pavement III Panel-B2 repeated load deflection and load vs. time for LVDT 6

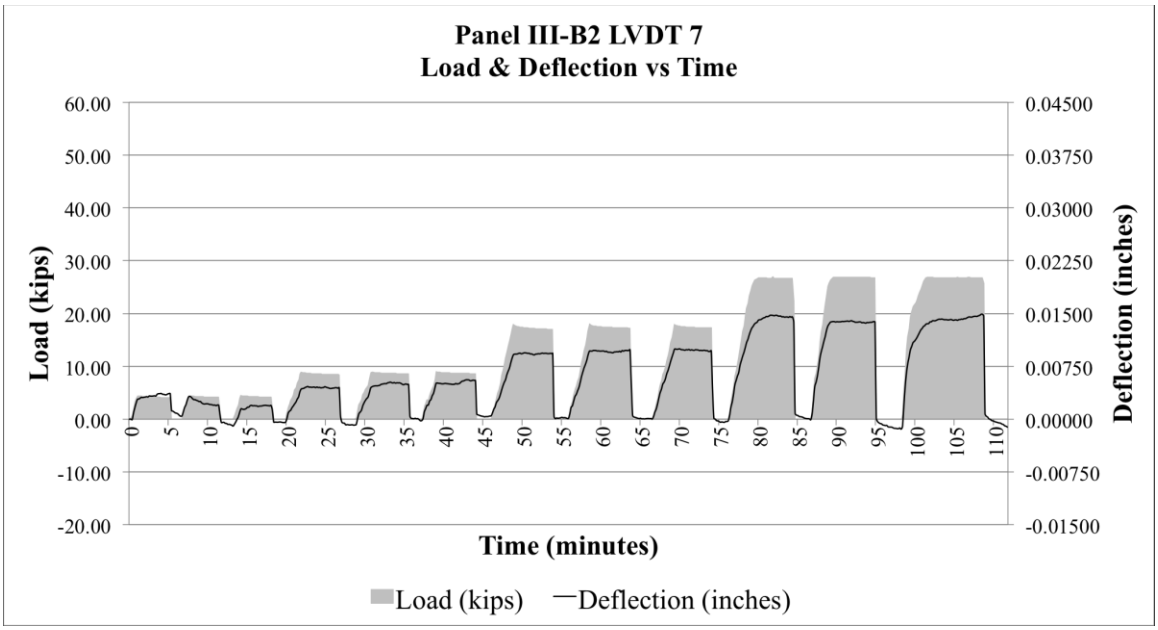

Figure E71 Pavement III Panel-B2 repeated load deflection and load vs. time for LVDT 7

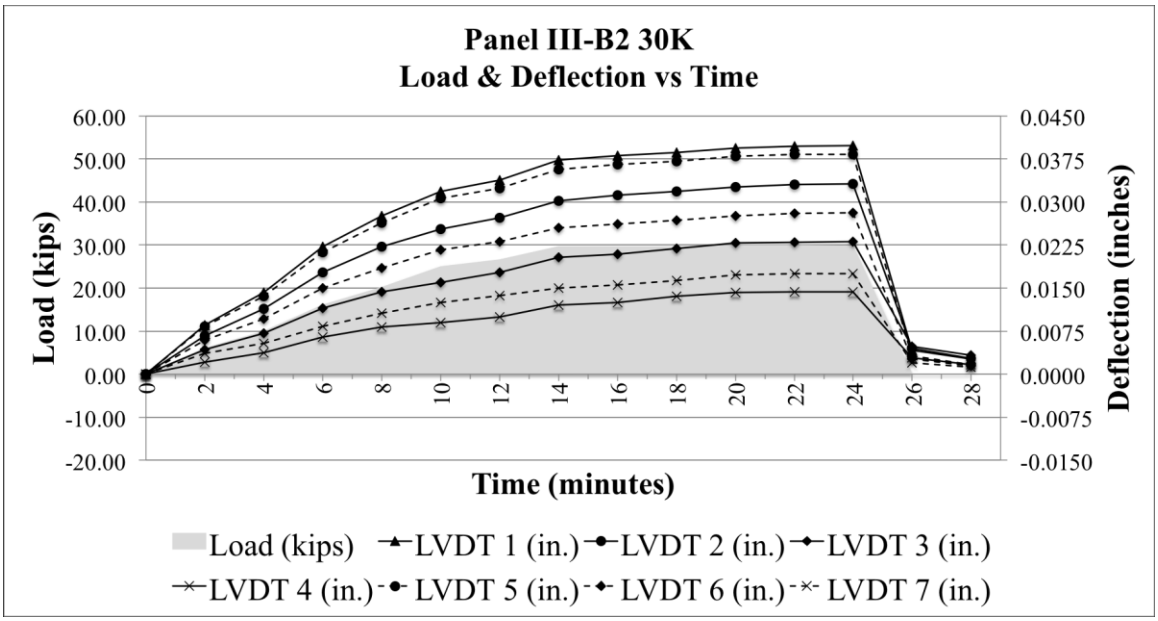

Figure E72 Pavement III Panel-B2 static load deflection and load vs. time (30,000 lb. Load)

Pavement I Deflection vs Load

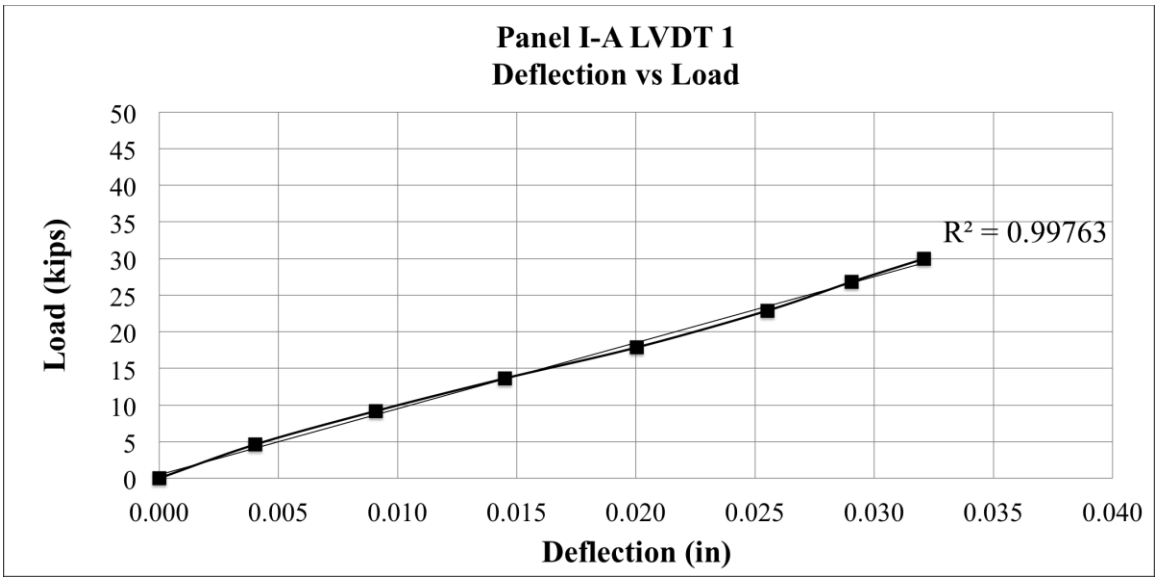

Figure E73 Pavement I Panel-A Deflection vs Load LVDT 1

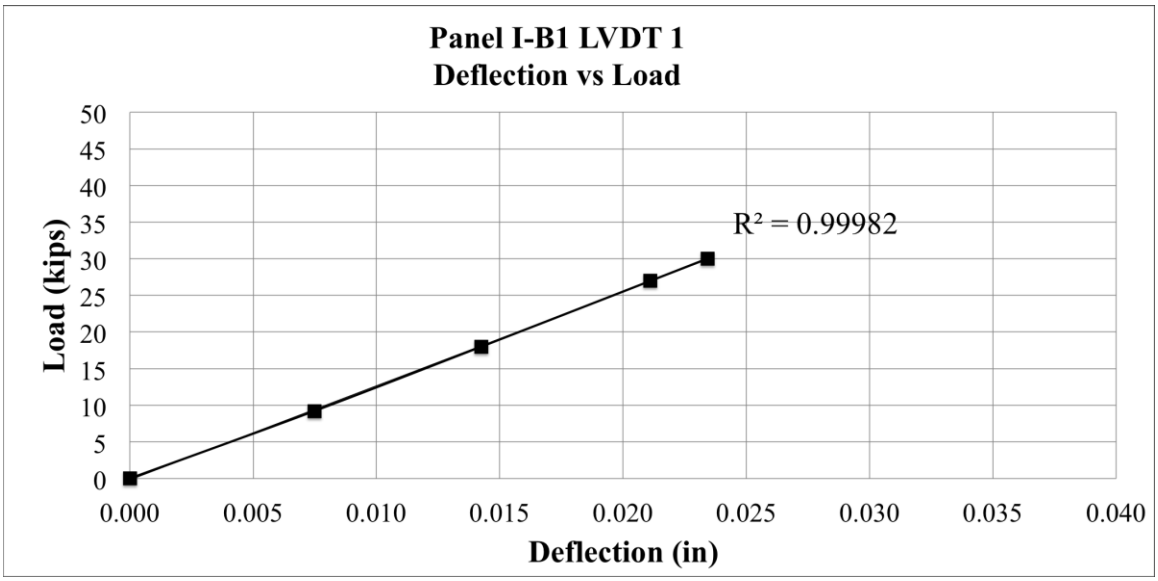

Figure E74 Pavement I Panel-B1 Deflection vs Load LVDT 1

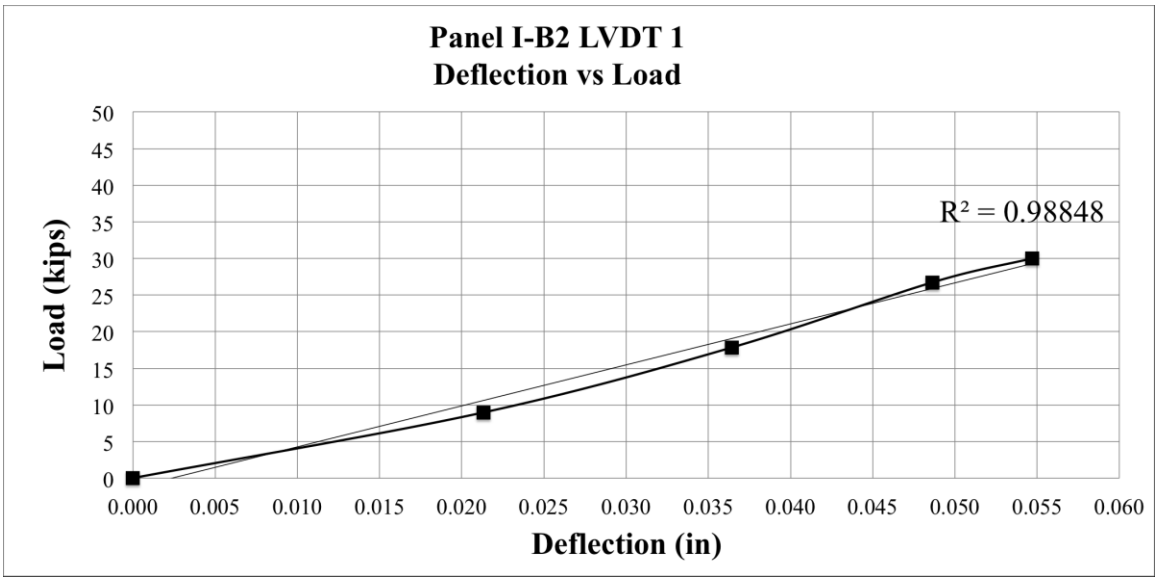

Figure E75 Pavement I Panel-B2 Deflection vs Load LVDT 1

Pavement II Deflection vs Load

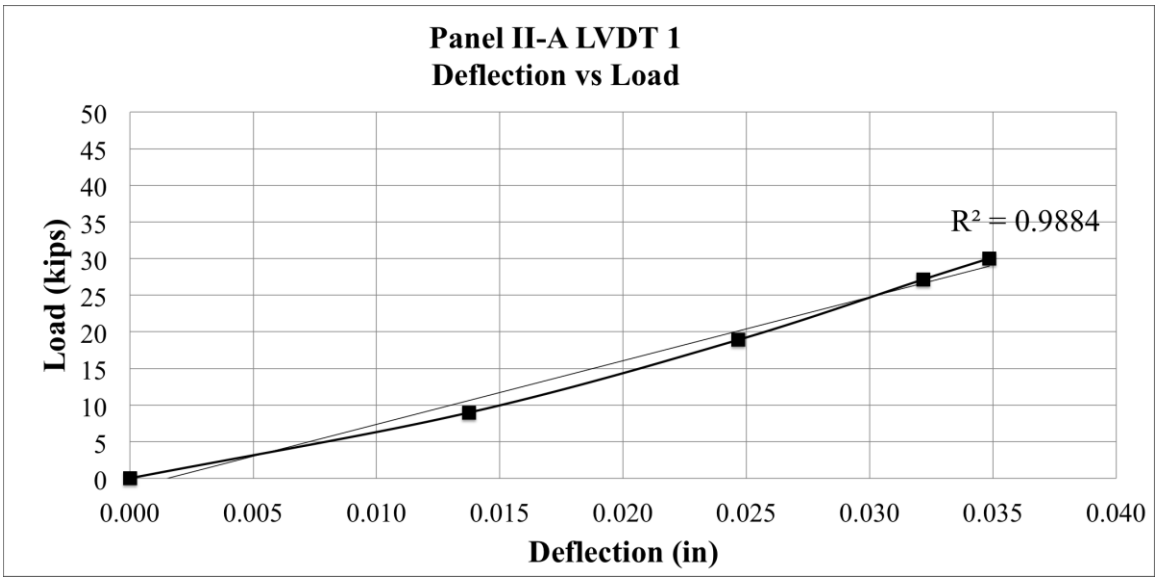

Figure E76 Pavement II Panel-A Deflection vs Load LVDT 1

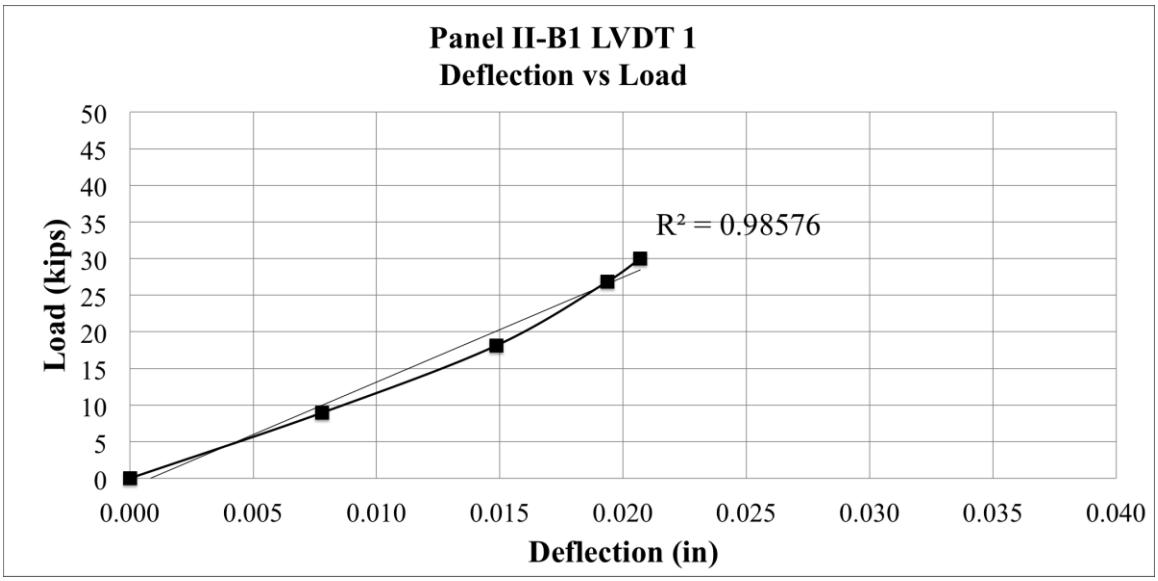

Figure E77 Pavement II Panel-B1 Deflection vs Load LVDT 1

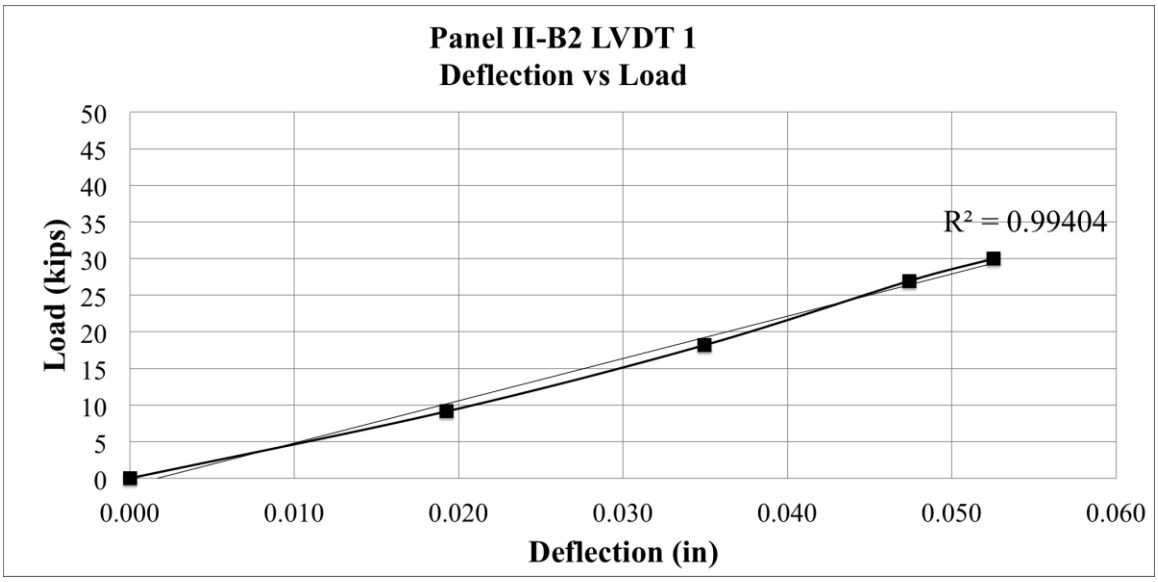

Figure E78 Pavement II Panel-B2 Deflection vs Load LVDT 1

Pavement III Deflection vs Load

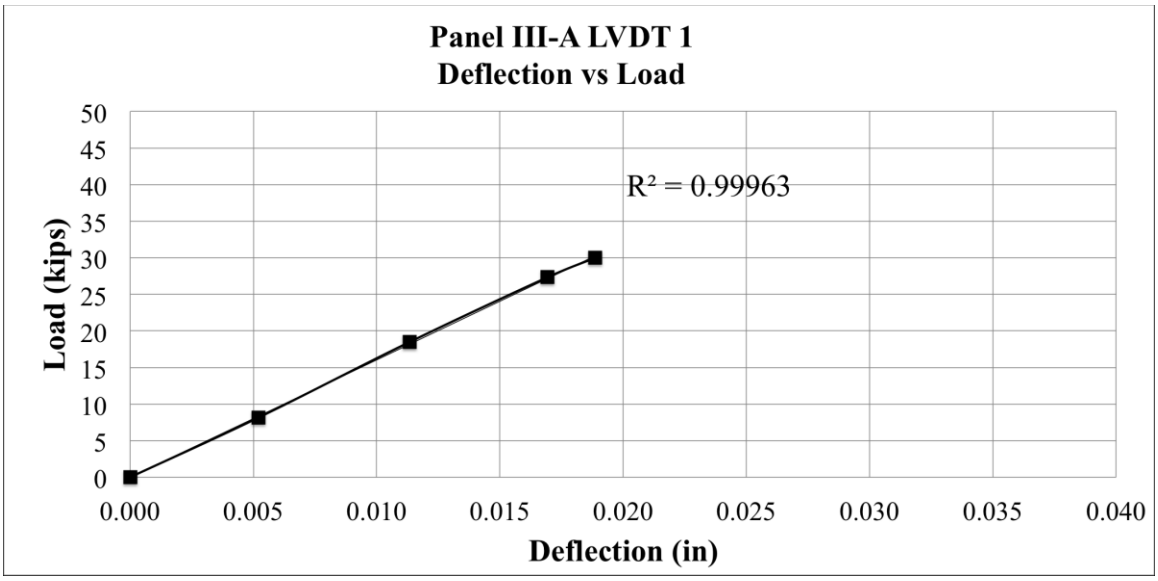

Figure E79 Pavement III Panel-A Deflection vs Load LVDT 1

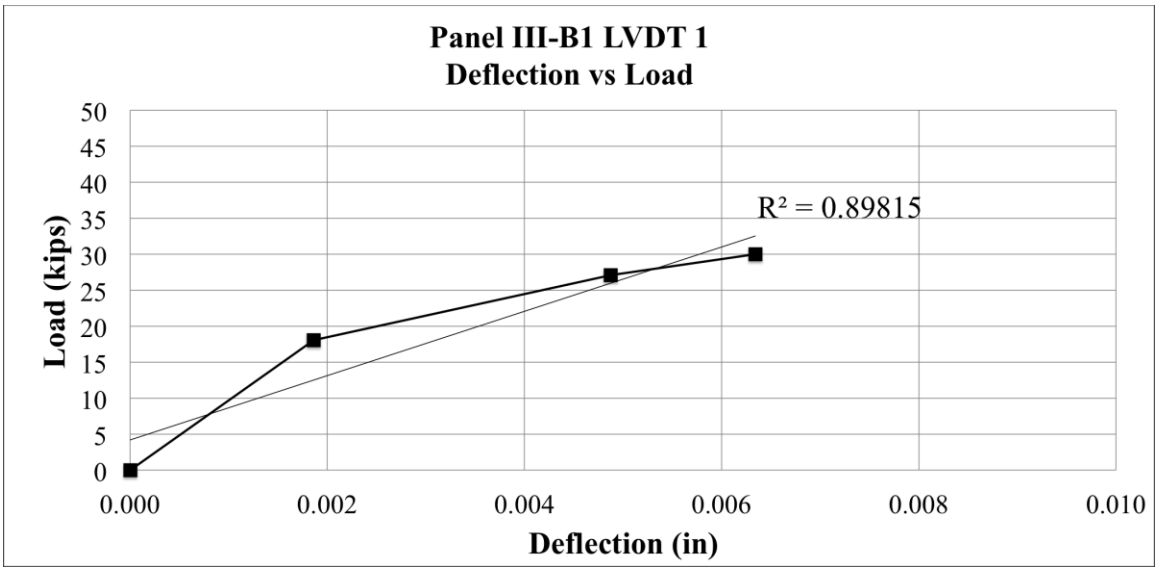

Figure E80 Pavement III Panel-B1 Deflection vs Load LVDT 1

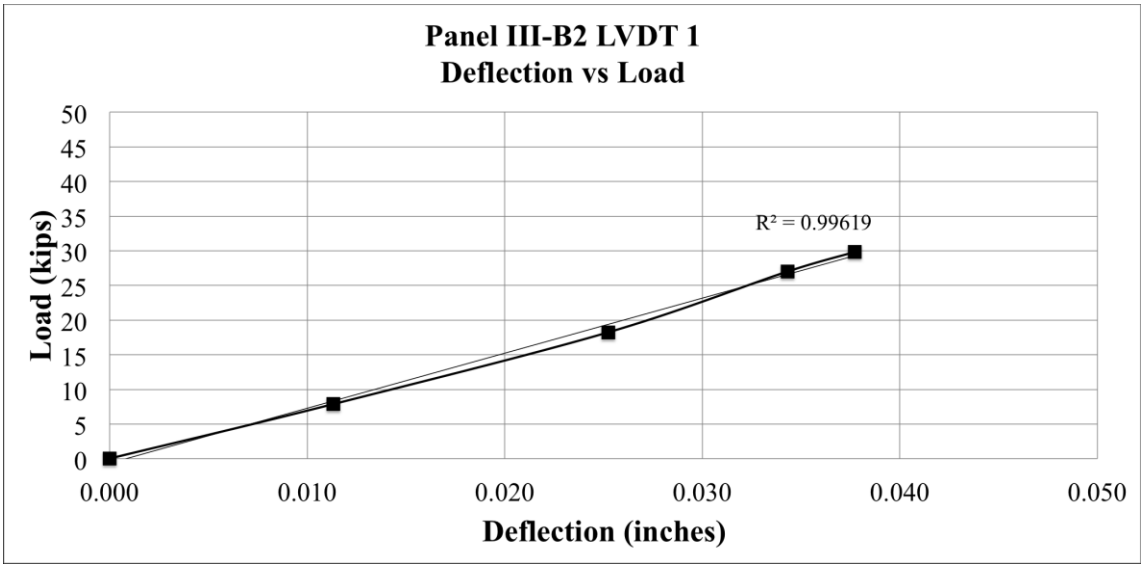

Figure E81 Pavement III Panel-B2 Deflection vs Load LVDT 1

Pavement I Deflection Shape (Actual, FEM, and BEF)

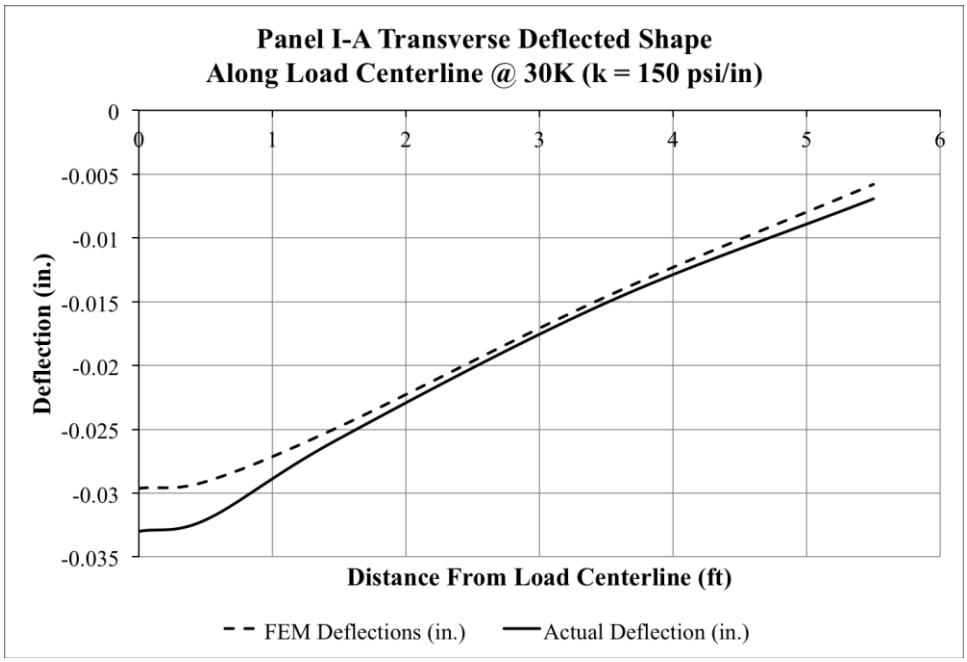

Figure E82 Panel I-A Actual and FEA Transverse Deflected Shape (k = 150 psi/in)

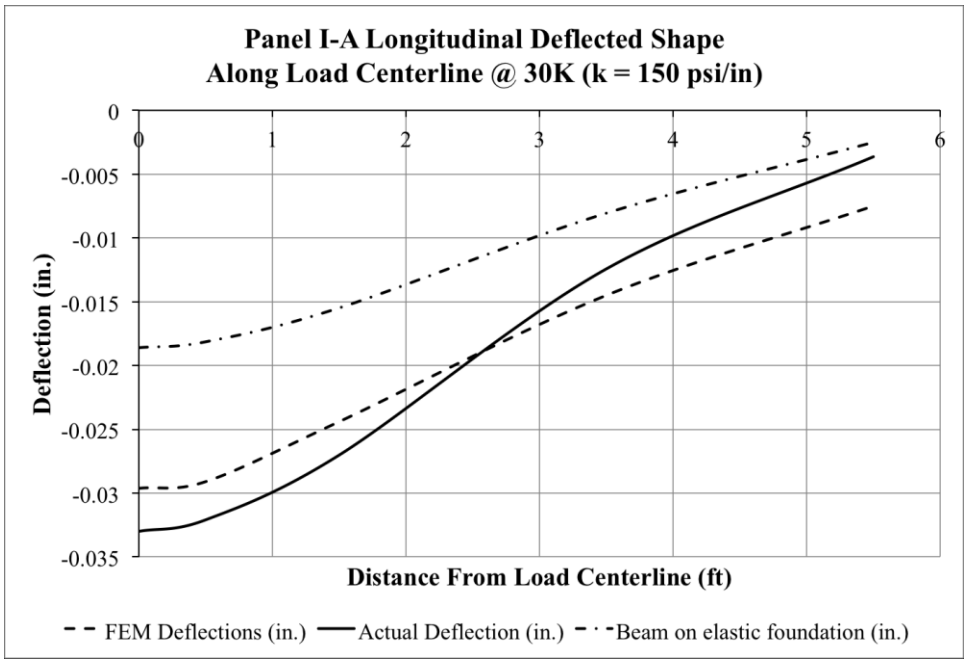

Figure E83 Panel I-A Actual/FEA/BEF Longitudinal Deflected Shape (k = 150 psi/in)

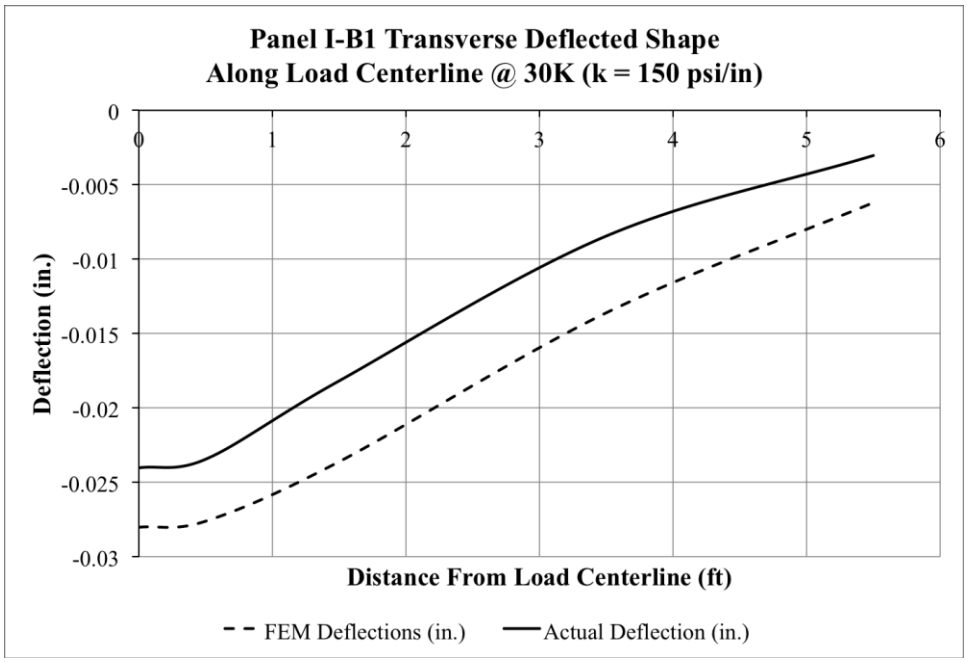

Figure E84 Panel I-B1 Actual and FEA Transverse Deflected Shape (k = 150 psi/in)

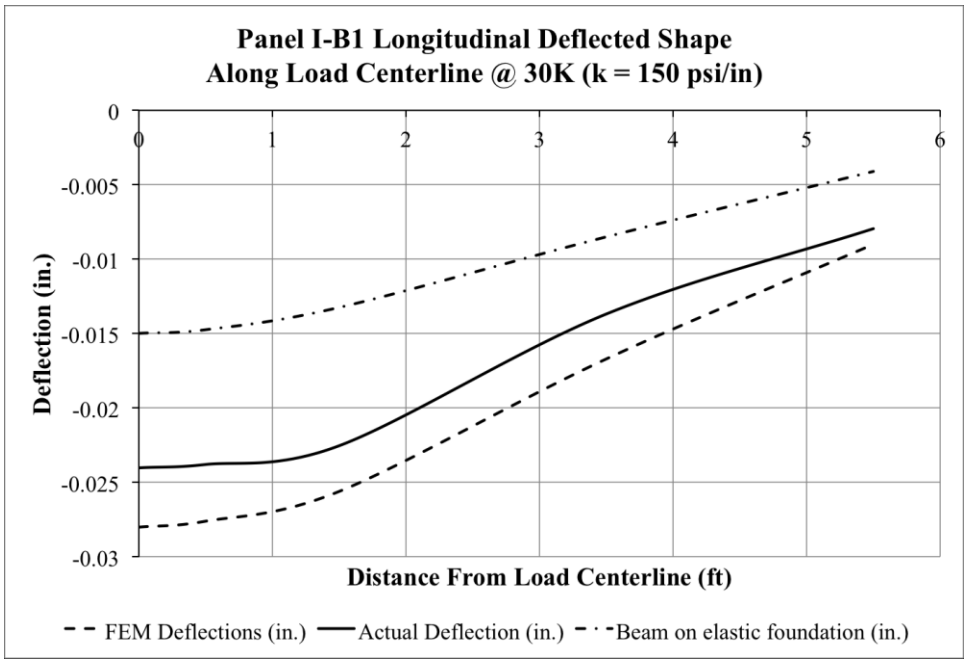

Figure E85 Panel I-B1 Actual/FEA/BEF Longitudinal Deflected Shape (k = 150 psi/in)

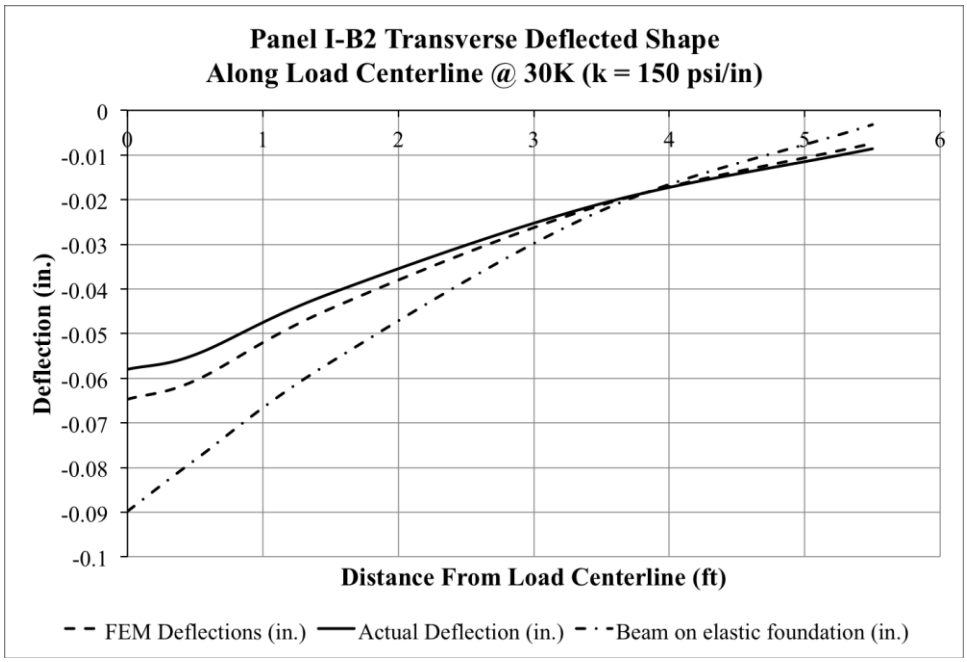

Figure E86 Panel I-B2 Actual/FEA/BEF Transverse Deflected Shape (k = 150 psi/in)

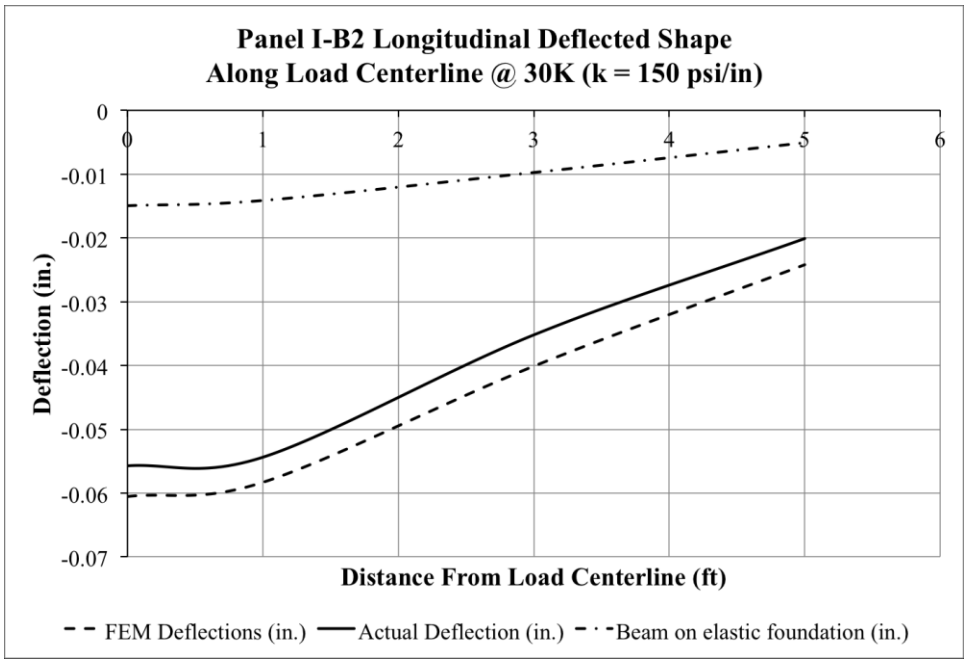

Figure E87 Panel I-B2 Actual/FEA/BEF Longitudinal Deflected Shape (k = 150 psi/in)

Pavement II Deflection Shape (Actual, FEM, and BEF)

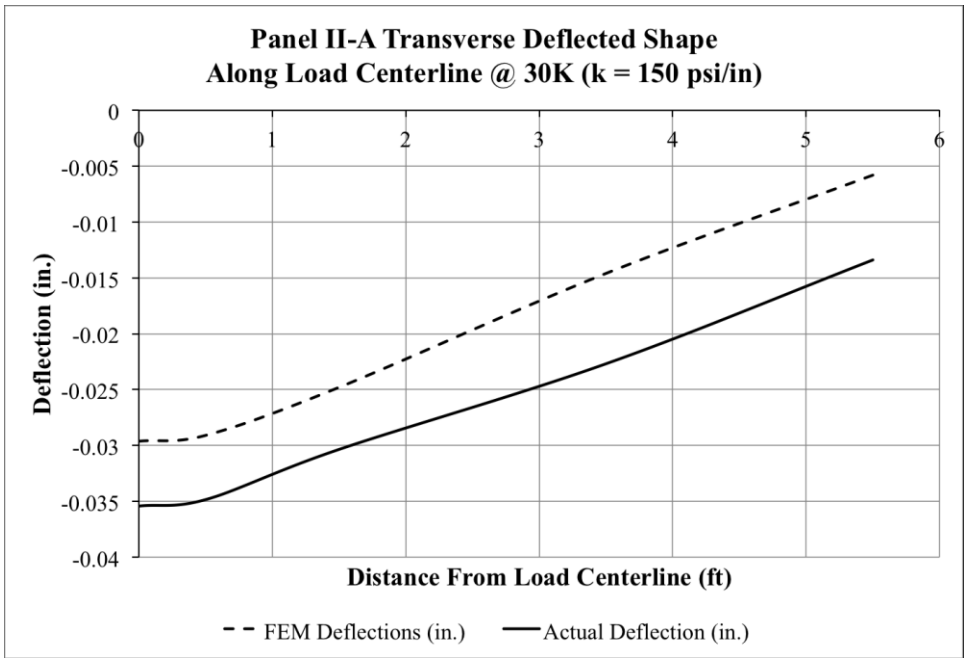

Figure E88 Panel II-A Actual and FEA Transverse Deflected Shape (k = 150 psi/in)

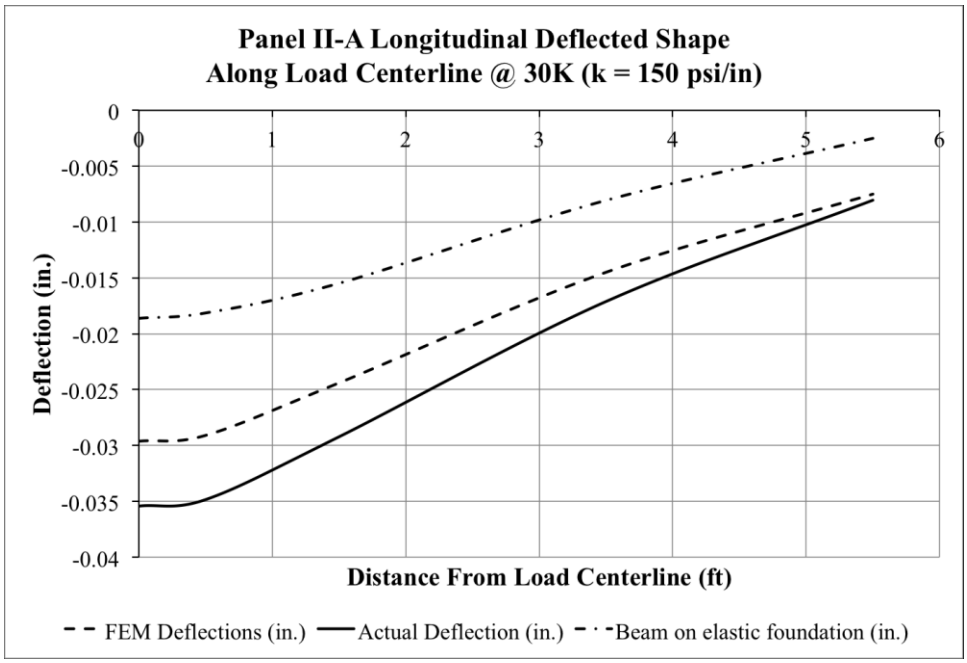

Figure E89 Panel II-A Actual/FEA/BEF Longitudinal Deflected Shape (k = 150 psi/in)

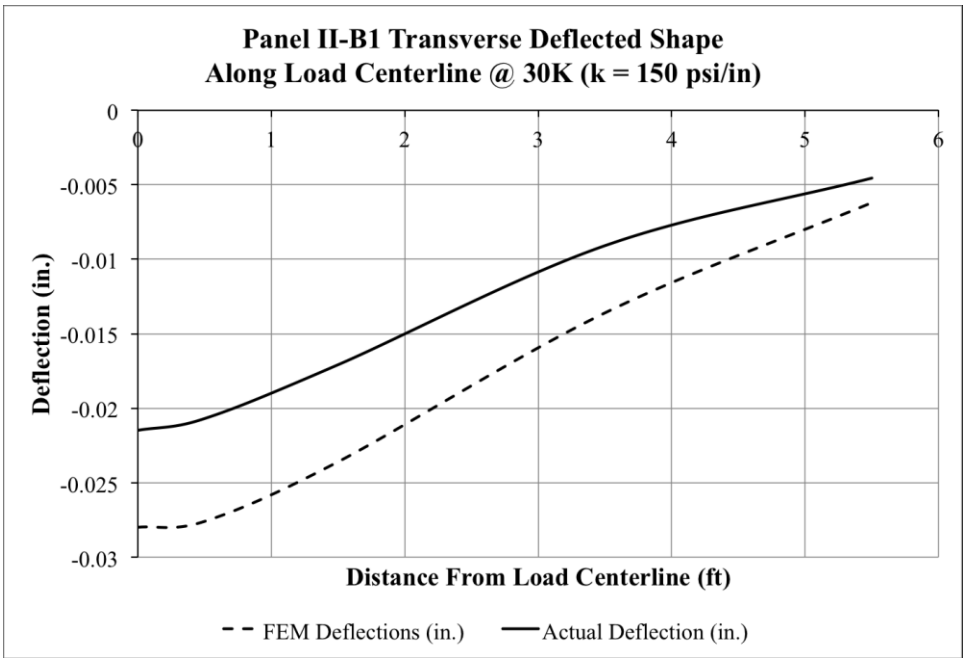

Figure E90 Panel II-B1 Actual and FEA Transverse Deflected Shape (k = 150 psi/in)

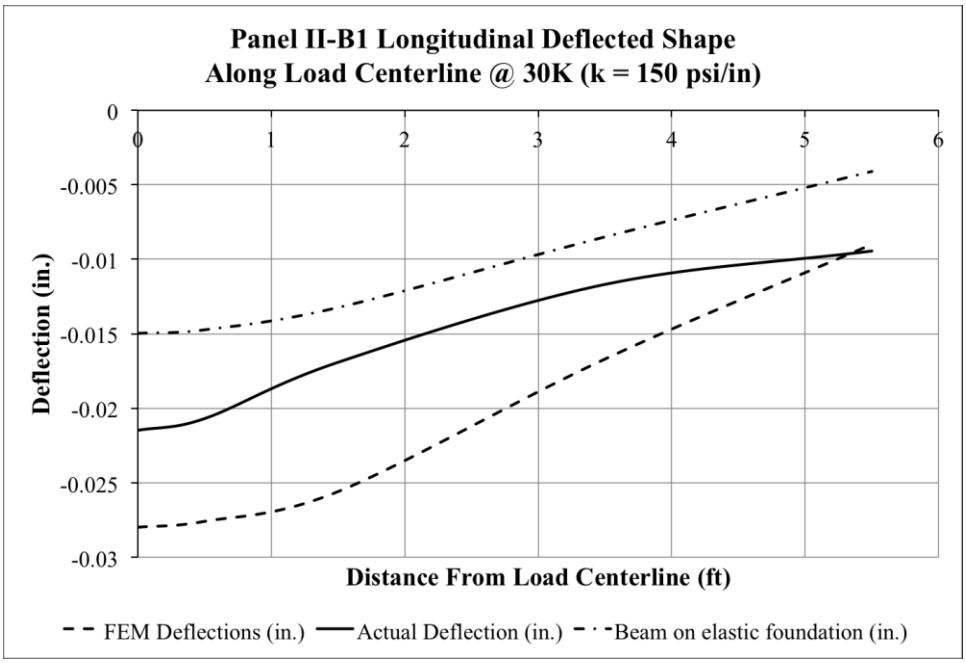

Figure E91 Panel II-B1 Actual/FEA/BEF Longitudinal Deflected Shape (k = 150 psi/in)

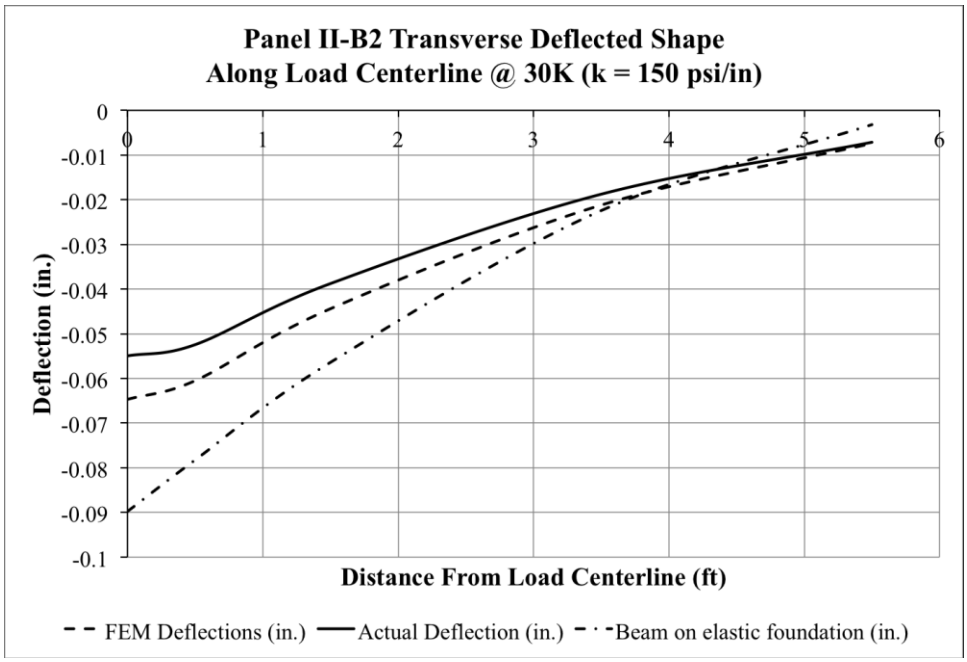

Figure E92 Panel II-B2 Actual/FEA/BEF Transverse Deflected Shape (k = 150 psi/in)

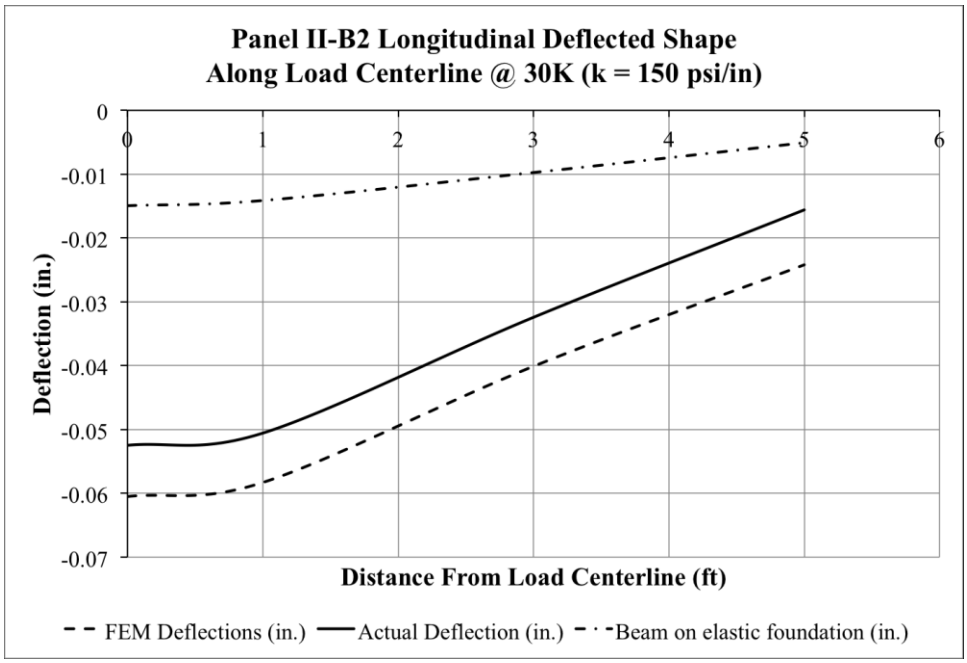

Figure E93 Panel II-B2 Actual/FEA/BEF Longitudinal Deflected Shape (k = 150 psi/in)

Pavement III Deflection Shape (Actual, FEM, and BEF)

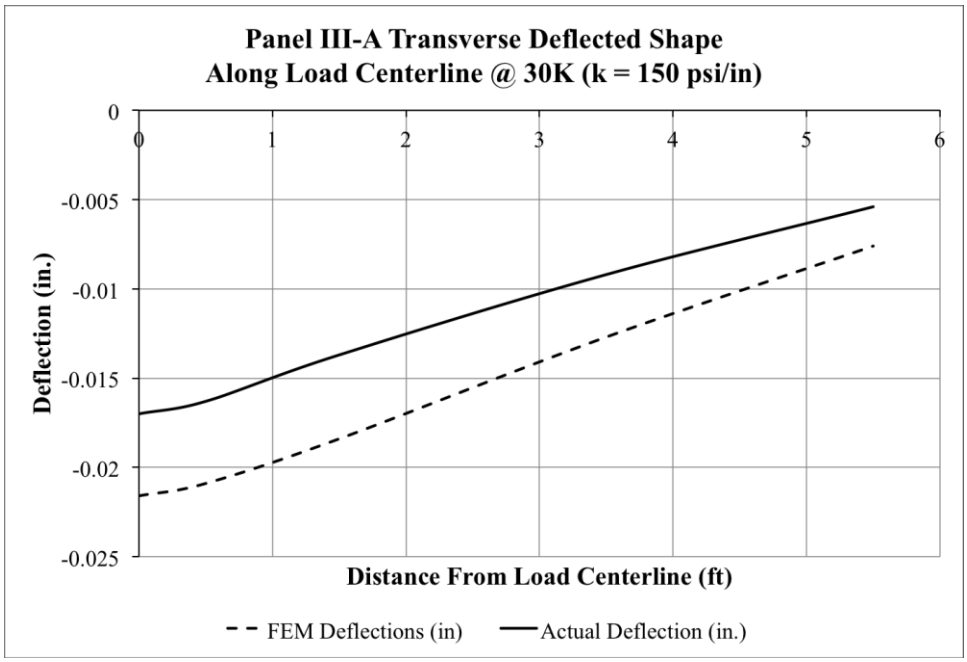

Figure E94 Panel III-A Actual and FEA Transverse Deflected Shape (k = 150 psi/in)

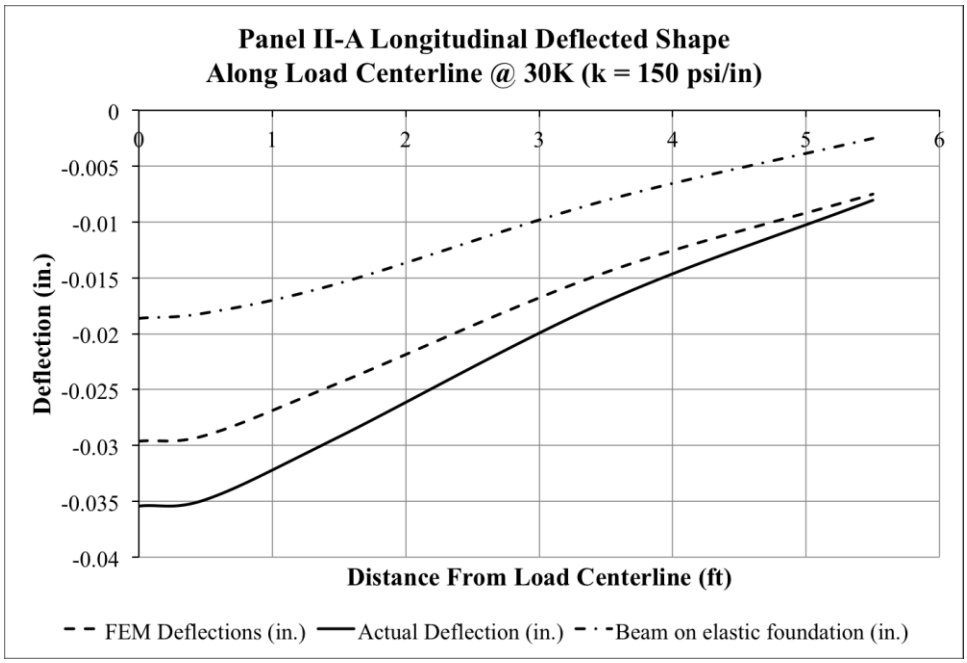

Figure E95 Panel III-A Actual/FEA/BEF Longitudinal Deflected Shape (k = 150 psi/in)

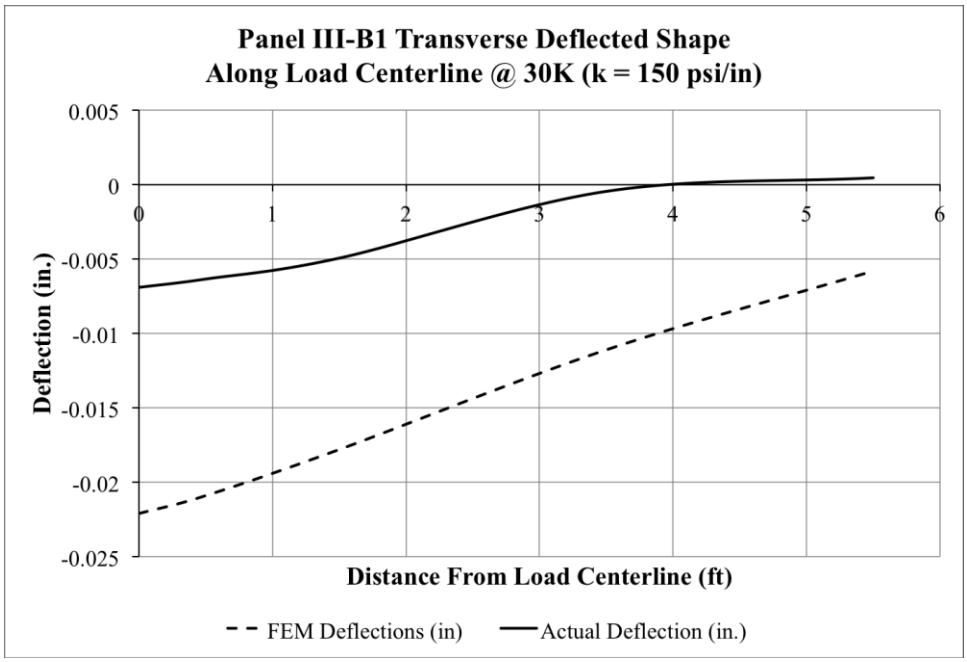

Figure E96 Panel III-B1 Actual and FEA Transverse Deflected Shape (k = 150 psi/in)

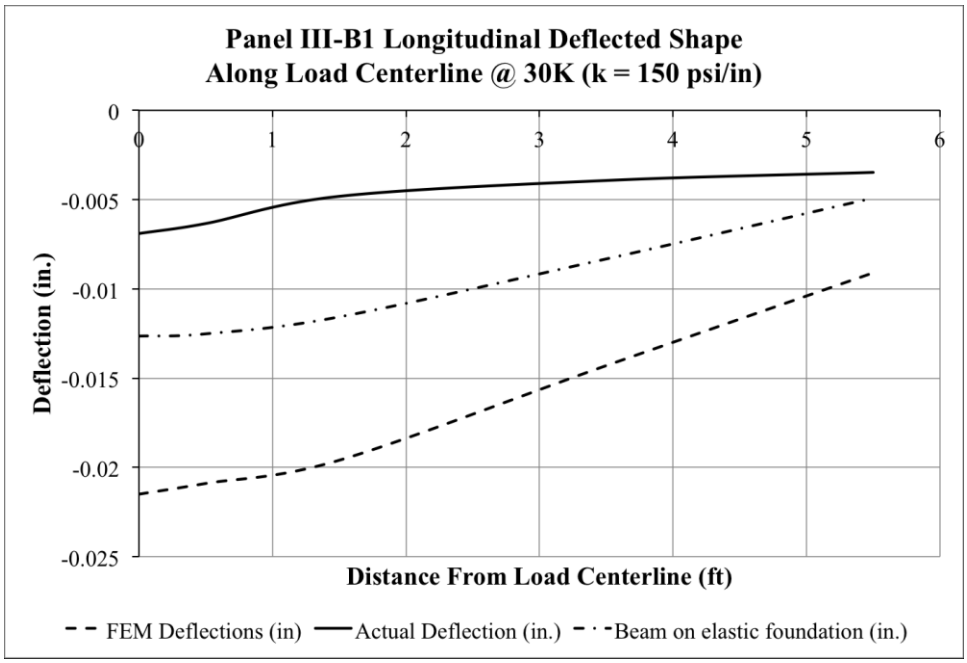

Figure E97 Panel III-B1 Actual/FEA/BEF Longitudinal Deflected Shape (k = 150 psi/in)

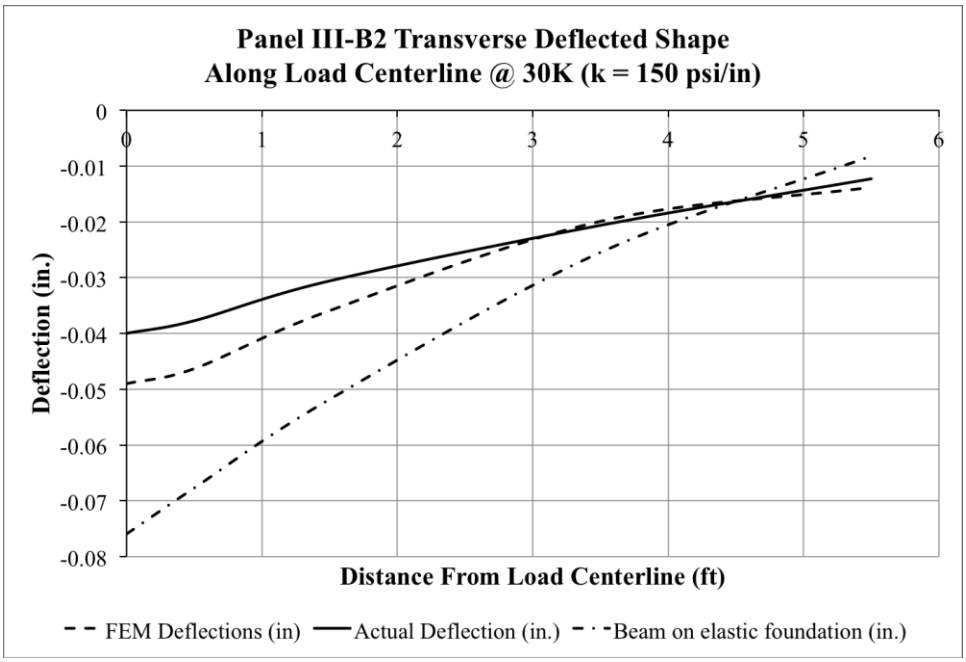

Figure E98 Panel III-B2 Actual/FEA/BEF Transverse Deflected Shape (k = 150 psi/in)

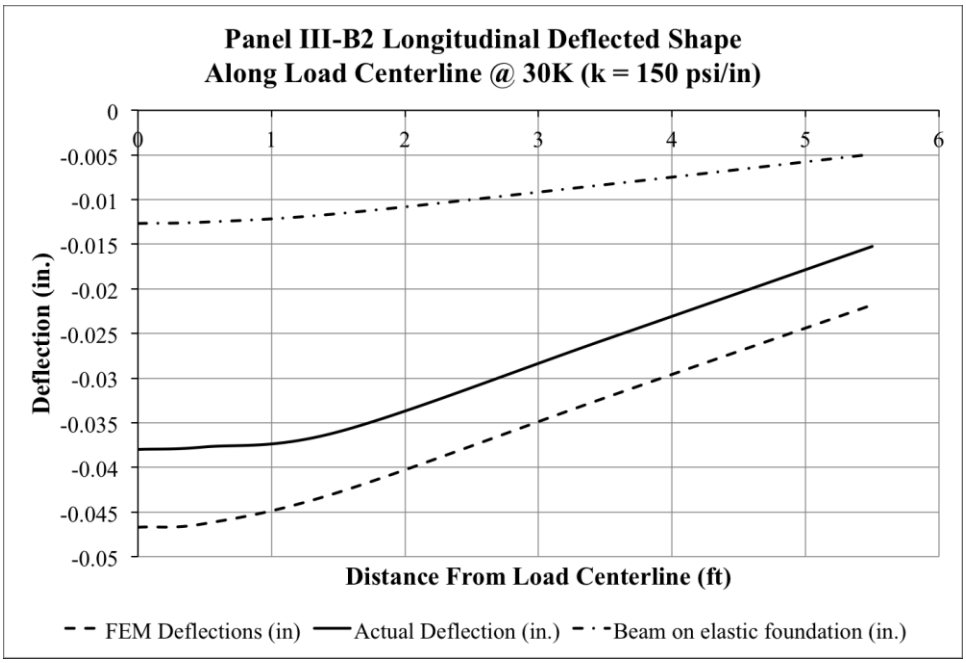

Figure E99 Panel III-B2 Actual/FEA/BEF Longitudinal Deflected Shape (k = 150 psi/in)

VITA

Nasser Mosallam Alwehaidah

Candidate for the Degree of

Doctor of Philosophy

Thesis: DEVELOPMENT OF PRECAST, PRESTRESSED CONCRETE PAVEMENT TECHNOLOGY

Major Field: Civil Engineering

Biographical:

Education:

Completed the requirements for the Doctor of Philosophy in Civil Engineering at Oklahoma State University, Stillwater, Oklahoma in December, 2013.

Completed the requirements for the Master in Architecture Engineering at Oklahoma State University, Stillwater, Oklahoma in December, 2006.

Completed the requirements for the Bachelor in Architectural Engineering at Oklahoma State University, Stillwater, Oklahoma in May, 2002.

Experience:

Pan Arab Consulting Engineers, Hawalli, Kuwait 2002 - 2007

Oklahoma State University, Stillwater, OK 2007 - 2013

Professional Memberships:

Kuwait Society of Engineers
Precast/Prestressed Concrete Institute
American Concrete Institute